

NEW AGE

THIRD EDITION

Lasers and Non-Linear Optics



B.B. Laud



NEW AGE INTERNATIONAL PUBLISHERS

**Lasers
and
Non-Linear Optics**

**This page
intentionally left
blank**

Lasers and Non-Linear Optics

(THIRD EDITION)

B.B. Laud

Professor and Head
Department of Physics
Marathwada University
Aurangabad, Maharashtra



NEW AGE INTERNATIONAL (P) LIMITED, PUBLISHERS

New Delhi • Bangalore • Chennai • Cochin • Guwahati • Hyderabad

Jalandhar • Kolkata • Lucknow • Mumbai • Ranchi

Visit us at www.newagepublishers.com

Copyright © 2011, 1991, 1985, New Age International (P) Ltd., Publishers
Published by New Age International (P) Ltd., Publishers

All rights reserved.

No part of this ebook may be reproduced in any form, by photostat, microfilm, xerography,
or any other means, or incorporated into any information retrieval system, electronic or
mechanical, without the written permission of the publisher. *All inquiries should be
emailed to rights@newagepublishers.com*

ISBN (13) : 978-81-224-3488-0

PUBLISHING FOR ONE WORLD

NEW AGE INTERNATIONAL (P) LIMITED, PUBLISHERS

4835/24, Ansari Road, Daryaganj, New Delhi - 110002

Visit us at www.newagepublishers.com

PREFACE TO THE THIRD EDITION

In this edition of the book, although the headings appear similar (except in a couple of cases), the revision has been extensive. The layout and style pattern have been modified to give an attractive look. A number of alterations have been made and some of the material has been rearranged. Some of the sections have been expanded; while others have been largely rewritten to improve clarity and generality. Mathematical treatment has been simplified wherever possible. A more general discussion on laser pumping and resonators has been provided.

The main change is the extension of the book to cover some important topics such as: coherent state description of the electromagnetic field, hydrogen maser, electroionisation, gas-dynamic lasers, distributed feedback laser, Doppler-free-two photon spectroscopy, laser cooling and trapping of neutral atoms, etc. In all thirteen new sections have been added to take account of the recent developments in the field.

With these additions the book should be suitable for a wider circle of readers. Every effort has been made to make the book error free from the previous edition.

B.B. LAUD

**This page
intentionally left
blank**

PREFACE TO THE FIRST EDITION

The advent of the laser as a primary source of power is one of the most significant events of the century. Since the announcement of the first laser, the subject of laser physics has developed at a rapid rate and lasers of wide variety have been constructed. Amazing advances have been made by applying this new tool in spectroscopy. A new area — nonlinear optics — has now come to the fore and is in a stage of rapid expansion. I have attempted to encompass in this book the wide area joining laser physics and nonlinear optics. It is impossible to give a comprehensive account of the total variety of up-to-date lasers while keeping the book to a reasonable length and, hence a considerable amount of selection has been necessary.

I have endeavoured to introduce all the important physical principles involved in laser devices and tried to give a consistent treatment of each. Original experiments have been described in detail and recent modifications have been discussed briefly. The knowledge of the fundamental processes taking place in laser devices should help the reader to understand the design and operation of newly developed devices.

Throughout the book the treatment has been kept as simple as possible and understandable to readers with variety of backgrounds. Mathematical background that the graduate students usually have is assumed. Some familiarity with the elements of electromagnetic theory and of spectroscopy will be helpful. The general level of the book is such that a graduate student should have no trouble with it and, I hope, they will find much of it digestable and stimulating.

In Chapters 2 (Einstein's theory), 3 (Interaction of radiation with matter) and 5 (Theory of some simple optical processes), I have provided a concise account of the basic physics on which the operation of laser depends. It should prepare the way, by easy stages, for the formal development of lasers.

Attempt has been made to collect in a compact and a unified form, some of the material in nonlinear optics widely scattered in various journals, which

is needed for understanding of the current research work. Papers and articles published up to 1983 and which were accessible, have been taken note of.

In Chapter 16, certain new and somewhat dramatic problems of current interest have been described in detail. It goes without saying that the selection of material to illustrate the achievements in non-linear optics must inevitably be subjective. But I believe that the problems discussed should be of interest to readers who wish to know what is new in non-linear optics. Besides, the ideas and concepts developed in these problems will prove to be of wider, more general, interest for those working in the allied fields.

It is hoped that the approach adopted in the book will help the reader to acquire the new concepts and advanced methods and give him a sort of overall perspective necessary to enable him to continue with confidence further independent research.

The book, therefore, if it fulfills its purpose, should be useful to a wide variety of people; not only to the students in the University, but also to research workers in the field of physics and chemistry and to engineers and scientists working in other disciplines. Some applications of wide interest are discussed in the last chapter.

It is fitting to record here my indebtedness to authors of original papers, books and writers of review articles. I have drawn freely on the original papers and consulted many well-written expositions of laser physics and non-linear optics by celebrated authors. Throughout the book, I have attempted to give full references to all those authors whose work is quoted and full list of references, in alphabetical order, is included at the end of the book.

My thanks are due to a number of friends and former students who took pains to make available to me the literature which would not have been easily accessible.

B.B. LAUD

CONTENTS

<i>Preface to the Third Edition</i>	v
<i>Preface to the First Edition</i>	vii
1. Introduction	1–7
1.1 Directionality	3
1.2 Intensity	4
1.3 Monochromacy	5
1.4 Coherence	6
2. Einstein's Quantum Theory of Radiation	8–15
2.1 Einstein Coefficients	8
2.2 Momentum Transfer	12
2.3 Life-time	13
2.4 Possibility of Amplification	14
3. Interaction of Radiation with Matter	16–44
3.1 Time Dependent Perturbation Theory	17
3.2 Electric Dipole Interaction	20
3.3 Quantum Electrodynamics	26
3.3.1 Creation and Annihilation Operators	26
3.3.2 Fock States	29
3.3.3 Quantization of the Field	29
3.3.4 Zero-point Energy	33
3.3.5 Coherent-state Description of the Electromagnetic Field	34
3.3.6 Interaction of Radiation with Matter	38
4. Masers	45–54
4.1 The Two-level Maser System Ammonia Maser	46
4.2 Hydrogen Maser	50
4.3 The Three-level Maser System	52

5. Theory of Some Simple Optical Processes	55-77
5.1 Waves and Interference	55
5.2 Coherence	57
5.3 Coherence of the Field and the Size of the Source	60
5.4 Visibility and the Size of the Source	62
5.5 Coherence and Monochromacy	64
5.6 Kinetics of Optical Absorption	64
5.7 Shape and Width of Spectral Lines	68
5.8 Line Broadening Mechanisms	69
5.8.1 Natural or Intrinsic Broadening	69
5.8.2 Collision Broadening	72
5.8.3 Doppler Broadening	74
6. Basic Principles of Lasers	78-96
6.1 Population Inversion	78
6.2 Laser Pumping	79
6.2.1 A Two-level System	79
6.2.2 A Three-level System	81
6.3 Resonators	83
6.4 Vibrational Modes of a Resonator	83
6.5 Number of Modes per Unit Volume	85
6.6 Open Resonators	87
6.7 The Confocal Resonator	88
6.8 The Quality Factor Q	89
6.9 Losses inside the Cavity	90
6.10 The Threshold Condition	90
6.11 Quantum Yield	95
7. Solid State Lasers	97-110
7.1 The Ruby Laser—A Three-level System	97
7.2 Pumping Power	101
7.3 Spiking	105
7.4 U ³⁺ in CaF ₂ Laser: A Four-level System	106
7.5 Neodymium Lasers	107
(a) Nd: YAG Laser	107
(b) Neodymium: Glass Laser	108
7.6 Ho ³⁺ : YLF Laser	110
7.7 Other Types of Solid State Lasers	110
8. Gas Lasers	111-134
8.1 Neutral Atom Gas Lasers : Helium-Neon Laser	111
8.2 Copper Vapour Laser	117

8.3	Ion Lasers	119
8.3.1	Argon Ion Laser [Bridges <i>et al.</i> 66]	119
8.3.2	Krypton and Mercury Ion Lasers	121
8.4	Metal Vapour Laser	121
8.4.1	He-Cd Laser	121
8.4.2	He-Se Laser	122
8.5	Molecular Gas Lasers	123
8.5.1	CO ₂ Laser	123
8.5.2	Electroionization Lasers	128
8.5.3	Gas-dynamic Laser	129
8.5.4	Vibronic Lasers	130
8.6	Excimer Lasers	133
9.	Semiconductor Lasers	135–147
9.1	Central Features of Semiconductor Lasers	135
9.2	Intrinsic Semiconductor Lasers	137
9.3	Doped Semiconductors	138
9.4	Condition for Laser Action	140
9.5	Injection Lasers	143
9.6	Injection Laser Threshold Current	144
9.7	Advances in Semiconductor Lasers	145
9.8	C ³ Laser	147
10.	Liquid-, Dye- and Chemical Lasers	148–159
10.1	Liquid Lasers	148
10.2	Dye Lasers	150
10.3	Chemical Lasers	154
10.3.1	HCl Laser	155
10.3.2	HF Laser	156
10.3.3	DF-CO ₂ Laser	157
10.3.4	CO Chemical Laser	158
10.3.5	Brommi Laser	159
11.	Dynamics of the Laser Processes and Advances in Laser Physics	160–182
11.1	Production of a Giant Pulse—Q-Switching	160
11.1.1	Mechanical Shutter	161
11.1.2	Electro-optical Shutters	161
11.1.3	Shutters Using Saturable Dyes	164
11.1.4	Peak Power Emitted During the Pulse	164
11.2	Giant Pulse Dynamics	165
11.3	Laser Amplifiers	169
11.4	Mode Locking	170

11.5 Ultra-short Light Pulses	173
11.6 Mode Pulling	173
11.7 Hole Burning	177
11.8 Distributed Feedback Laser	180
11.9 Gamma-ray Laser	182
12. Holography	183-190
12.1 Principle of Holography	184
12.1.1 Recording of the Hologram	184
12.1.2 Reconstruction of the Image	184
12.2 Theory	185
12.3 Some Distinguishing Characteristics of Holographs	188
12.4 Practical Applications of Holography	189
12.5 Advances in Holography	190
13. Non-linear Optics	191-202
13.1 Harmonic Generation	191
13.2 Second Harmonic Generation	193
13.3 Phase Matching	194
13.4 Third Harmonic Generation	198
13.5 Optical Mixing	198
13.6 Parametric Generation of Light	200
13.7 Self-focussing of Light	200
14. Multiphoton Processes	203-220
14.1 Multiquantum Photoelectric Effect	203
14.2 Two-photon Processes	204
14.3 Theory of Two-photon Processes	205
14.4 Experiments in Two-photon Processes	209
14.4.1 CaF ₂ : Eu ⁺⁺ Crystals	209
14.4.2 Cesium Vapour	210
14.4.3 Anthracene	211
14.4.4 KI	211
14.4.5 Two-photon Effect in a Semiconductor	212
14.4.6 Two-photon Ionization	212
14.5 Violation of the Square Law Dependence	213
14.6 Doppler-free Two-photon Spectroscopy	213
14.7 Multiphoton Processes	213
14.8 Three-photon Processes	214
14.9 Second Harmonic Generation (SHG)	214
14.10 Parametric Generation of Light	215
14.11 Parametric Light Oscillator	216
14.12 Frequency Upconversion	217
14.13 Phase-conjugate Optics	217

15. Laser Spectroscopy	221–239
15.1 Rayleigh and Raman Scattering	221
15.2 Stimulated Raman Effect	223
15.3 Hyper-Raman Effect	225
15.3.1 Classical Treatment	226
15.3.2 Quantum Mechanical Treatment	227
15.4 Coherent Anti-Stokes Raman Scattering (CARS)	228
15.5 Spin-flip Raman Laser	229
15.6 Free-electron Laser (FEL)	230
15.7 Photo-acoustic Raman Spectroscopy (PARS)	232
15.8 Brillouin Scattering	233
15.9 Saturation-absorption Spectroscopy	235
15.10 Doppler-free Two Photon Spectroscopy	238
16. Some Laser Induced Phenomena	240–253
16.1 Modulation of an Electron Wave by a Light Wave	240
16.2 Laser Induced Collision Processes—Pair Excitation	242
16.3 Multi-photon Ionization	247
16.4 Single Atom Detection with Lasers	248
16.4.1 Fluorescence Methods	249
16.4.2 Ionization Methods	249
16.5 Laser Cooling and Trapping of Neutral Atoms	250
17. Applications of Lasers	254–267
17.1 Some Experiments of Fundamental Importance	254
17.2 Ether Drift	255
17.3 Absolute Rotation of the Earth	255
17.4 Counting of Atoms	256
17.5 Isotope Separation	257
17.6 Plasma	259
17.7 Thermonuclear Fusion	259
17.8 Lasers in Chemistry	261
17.9 Communication by Laser	261
17.10 Ranging	264
17.11 Atmospheric Optics	264
17.12 Lasers in Astronomy	265
17.13 Lasers in Biology	265
17.14 Lasers in Medicine	265
17.15 Lasers in Industry	266
Appendix A: Physical Constants	269
Appendix B: Conversion Factors for Energy Units	270
References	271
Index	285

**This page
intentionally left
blank**

INTRODUCTION

1

Spectroscopy held a major position in the forefront of progress in physics in the nineteenth and early twentieth century. Quantum mechanics owes a debt to spectroscopy. Raman spectroscopy was an important tool in molecular analysis. One can cite, in this way, a number of other important disciplines having their origin in spectroscopy or, more generally, in optics. However, there seemed to be a lull prevailing in the field of optics for a couple of decades starting from 1930. All the fundamental problems of resonance radiation seemed to have been solved and, hence, the interest in basic investigation of atomic emission and absorption decayed. Optics was no longer found to be exciting. Hardly any advanced optics was taught at Universities in those days. Nuclear physics and solid state physics became the fashion of the day and optics was left in a peaceful backwater.

This was the state of affairs until 1954 when a certain development fired the imagination of physicists. Their attention was turned to an entirely new area which, within the last twenty-five years, has completely revitalized basic research in spectroscopy. This is the area of coherent optical processes. Laser (the acronym derived from *Light Amplification by Stimulated Emission of Radiation*) is a spectacular manifestation of this process. It is a source which emits a kind of light of unrivalled purity and intensity not found in any of the previously known sources of electromagnetic radiation. This discovery made an enormous impact on the scientific world and showed that optics is very much alive. By being able to generate highly coherent signals, lasers made it possible to enrich optics. In one of the meetings, in 1956, Zernike [350] remarked "...the activity in optics proceeds in waves, and is emerging now from a trough and leading for a peak."

Physicists soon realized that they had at hand a new and beautiful tool which was simple in its basic ideas, requiring minimum of equipment and likely to have ingeneous applications. The first two successful lasers developed during

1960, were the pulsed ruby laser ($\lambda = 6943 \text{ \AA}$) and the helium-neon gas laser ($\lambda = 11,500 \text{ \AA}$). Since then enormous effort was devoted to the study of lasers. Laser action has been obtained with atoms, ions, and molecules in gases, liquids, solids, glasses, flames, plastics and semiconductors at wavelengths spanning from the ultraviolet to radio-frequency regions, with power ranging from a few milliwatts to megawatts. Some lasers emit only in pulses and others emit a continuous wave.

With lasers scientists have found possibilities and many new ways to probe the nature of matter and its interaction with light. The study in this direction has given rise to a number of novel and very unusual optical phenomena. One of the most interesting fields of research made possible by the development of powerful lasers is the field of nonlinear optics. A number of experiments of fundamental interest, which were hitherto completely out of range, have now become possible. The changes produced by lasers in spectroscopy are revolutionary achieving orders of magnitude improvement in resolution and accuracy. Laser spectroscopy has greatly extended our knowledge of atomic, molecular and solid state physics. Dramatic advances have been made in the understanding of complex processes occurring in the interactions of ultra-short light pulses produced by lasers with matter. Recently Bell Laboratory scientists [Fork, Greene and Shank, 124] have succeeded in producing a burst of laser light that lasts for a mere 30 femtoseconds — 30 millionths of a thousand millionth of a second ($30 \times 10^{-15} \text{ secs}$) — a time in which light would travel no further than one-third the thickness of a human hair. It should be now possible to measure electrons moving through solids and liquids.

The remarkable properties of lasers open ways for unprecedented scientific and technological applications. They have been used in telecommunications, meteorology, metrology, biology, cybernetics, computer circuitry, etc. New information has been obtained about primary photobiological interactions and excited state relaxation kinetics in molecules. Focussed intense laser beams are used to initiate nuclear reactions. In medicine, lasers have been particularly useful. More complex, fine operations in surgery today are conducted in affluent countries, not with the traditional scalpel and lancet, but with the laser beams, which make surgery quick, bloodless and less painful. The fact that laser treatment requires no anaesthetics has been a source of great relief to some people. Like the other scientific and technological fields, the laser is also linked to military warfare. This has resulted into exponential rise of military research budgets, which recently roared to astronomical figures in some countries.

The laser is proving a valuable tool for combustion studies as well. It can be used as an ignition source. Usually gas mixtures are very transparent to visible light and, hence, radiation does not cause any heating. It is, however, found experimentally that focussed laser pulses do cause ignition. The detailed mechanism of laser breakdown is still somewhat obscure; the initial process,

perhaps, involves multiphoton absorption followed by ionization and cascade build up of electron concentration [Brown 69].

The distance of the moon from the earth was measured with considerable accuracy with the help of what is known as a Laser Ranging Retro-reflector. This is a precise mirror which would reflect an intense beam of laser light shot up to the moon. By bouncing the laser beam off the reflector and back to earth, astronomers could measure the distance with an accuracy of 15 cm in 3,84,000 km. [127A].

Experimental proliferation is also accompanied by theoretical interpretations, which have prompted a considerable amount of theoretical work in the nature of coherence and other aspects. Theorists may have to sharpen their pencils now, since, the findings of such investigations have shown that some of the theories considered so far to be almost full-proof, may need reconsideration.

There, thus, definitely exists a need not only for research scientists but also for engineers and others, to have some sort of familiarity with this recent addition to science and technology.

What is so special about lasers? What are the characteristics which distinguish them from other light sources?

The significant feature of a laser is the enormous difference between the character of its light and the light from other sources such as the sun, a flame or an incandescent lamp. The most striking features of lasers are: (1) its directionality, (2) its high intensity, (3) its extraordinary monochromacy, and (4) its high degree of coherence.

But this list does not reveal any novel property. All these properties were also associated, to some extent, with the light sources used in pre-laser era and have been exploited by the scientists in their research programmes. It is, indeed, so and yet the laser differs from every other conventional light source in all these four characteristics. Let us examine these characteristics more closely.

1.1 DIRECTIONALITY

The conventional light sources emit in all directions. When we need a beam for a particular experiment, we get it with the help of an aperture in front of the source. Lasers, on the other hand, emit only in one direction. The directionality of laser beams is usually expressed in terms of the *full angle beam divergence*, which is twice the angle that the outer edge of the beam makes with the axis of the beam. How do we determine the outer edge of a beam? This is defined as a point at which the strength of the beam has dropped to $1/e$ times its value at the centre. When a beam with planar wavefront radiates from an aperture of diameter d , the beam propagates as a parallel beam for a distance of about d^2/λ —which is sometimes called Rayleigh range—and then begins to spread linearly with distance because of the unavoidable effects of diffraction (Fig. 1.1) (λ here is the wavelength of light).

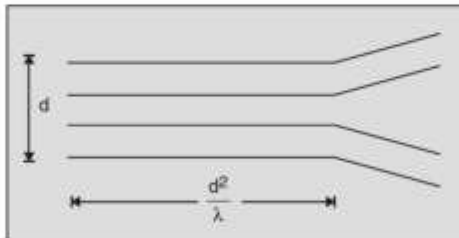


Fig. 1.1 Directionality of the laser beam

The angular spread $\Delta\theta$ of the far field beam is related to the aperture diameter d by

$$\Delta\theta = \frac{\lambda}{d} \quad \dots(1.1)$$

For a typical laser, the beam divergence is less than 0.01 milliradian. That is, the beam spreads less than 0.01 mm for every meter. Output in a laser beam is many millions of times more concentrated than the best search-light available. The beam from the latter spreads to about a kilometre in diameter for every kilometre that the light traverses. One can imagine its spread on the surface of the moon, which is at a distance of 384,400 km, if it ever reaches the moon. As against this, the spread of the laser beam on the surface of the moon would be just a few kilometres.

1.2 INTENSITY

The light from a lamp streams out more or less uniformly in all directions. If we look at a 100 watt lamp filament at a distance of 30 cm, the power entering the eye is less than a thousand of a watt. The laser gives out light into a narrow beam and its energy is concentrated in a small region. This concentration of energy, both spatially and spectrally, accounts for the great intensity of lasers. If we were to look directly along the beam from a laser (which one should never do), then all the radiated power would enter the eye. Thus even a 1 watt laser would appear many thousand times more intense than 100 watt ordinary lamp. Some lasers produce light which differs enormously in intensity from the other sources. Light beams with power densities many millions of times greater than those on the surface of the sun are produced by laser beams. A better idea of the intensity of a laser beam can be had by considering a specific example.

Let us compare the photon output of a laser with that of a very hot body. The power output from a small gas laser is $\sim 10^{-3}$ W, while that from a pulsed solid state laser may be as high as 10^9 W. Since one photon of visible light represents $\sim 10^{-19}$ joules of energy, the photon output of lasers ranges over

$$\text{Laser photons/sec} = \frac{P}{h\nu} \sim 10^{16} \text{ to } 10^{28} \quad \dots(1.2)$$

The amount of energy emitted by a black body per unit area per unit time in the range of frequency between ω and $\omega + d\omega$ — i.e., its emissivity—is given by [233]

$$\begin{aligned} e(\omega, T)d\omega &= \frac{1}{4} \rho(\omega, T)cd\omega \\ &= \frac{1}{4} \cdot \frac{\hbar\omega^3}{\pi^2 c^2} \cdot \frac{1}{e^{\hbar\omega/kT} - 1} d\omega \end{aligned} \quad \dots(1.3)$$

where $\rho(\omega, T)$ is the radiation density for the band width given by Planck's formula

$$\rho(\omega) d\omega = \frac{\hbar\omega^3}{\pi^2 c^3} \cdot \frac{1}{e^{\hbar\omega/kT} - 1} d\omega \quad \dots(1.4)$$

$$\begin{aligned} \therefore \text{Thermal photons/sec} &= \frac{1}{h\omega} \cdot \frac{\hbar\omega^3 c}{4\pi^2 c^3} \cdot \frac{1}{e^{\hbar\omega/kT} - 1} d\omega \\ &= \frac{\omega^2}{4\pi^2 c^2} \cdot \frac{1}{e^{\hbar\omega/kT} - 1} d\omega \end{aligned} \quad \dots(1.5)$$

Let us assume the band width of a line in the visible region, $\lambda = 6,000 \text{ \AA}$, to be $1,000 \text{ \AA}$ and the temperature to be $1,000 \text{ K}$.

$$\therefore \omega = 2\pi\nu = 2\pi \times 5 \times 10^{14}; d\omega = \frac{2\pi}{12} \times 10^{15}$$

Substituting these values in the formula obtained above, we find the emission from an area equal to 1 sq. cm. of the hot body to be

$$\text{Thermal photons/sq. cm/sec} \sim 10^{12} \quad \dots(1.6)$$

We thus see that it takes a fairly large and fairly hot body to generate as much visible light as is produced by even a fairly small laser.

A good lens with a focal length of one centimetre can focus a laser beam to a spot a thousandth of a centimetre in diameter. If the intensity of a laser beam is a billion watts per square centimetre, the intensity in the focal spot would be about 10^{15} watts per square centimetre. It is usually assumed that the radiation pressure of light is negligibly small; but in such a focussed beam it would be over a million kilogrammes per square centimetre [Schawlow, 333].

1.3 MONOCHROMACY

The light emitted by a laser is vastly more monochromatic than that of any conventional monochromatic source. An inspection of a line emitted by the latter shows that it is never perfectly sharp, but it spreads over a frequency range of the order of thousands of megacycles per second. A similar inspection of the light from a laser would reveal virtually very little spreading (Fig. 1.2).

It must be noted, however, that no light source, laser included, is capable of producing absolute monochromatic light; we can only seek better and better approximation to the ideal. To speak more qualitatively of the degree of monochromacy of light, we characterize the spread in frequency of a line by the line width $\Delta\nu$. The degree of non-monochromacy of a wave may be defined as its relative band width given by

$$\xi = \frac{\Delta\nu}{\nu_0} \quad \dots(1.7)$$

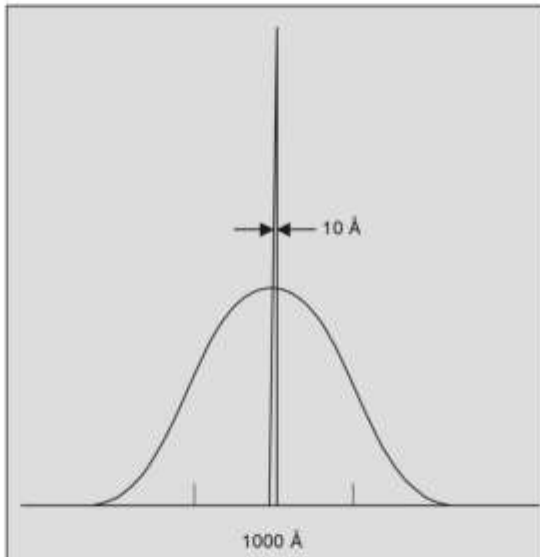


Fig. 1.2 Normal and laser band widths

where ν_0 is the central frequency of the light beam. Absolute monochromacy for which $\Delta\nu = 0$ is an unattainable goal. We can say that the laser light has a higher degree of monochromacy. The output from a laser is very nearly a perfectly monochromatic sine wave with a very small bandwidth about 1 kc/sec. The output from a high quality stable gas laser, locked to the centre of the absorption line has a bandwidth $\Delta\nu \sim 500$ Hz i.e., $\Delta\lambda = 10^{-8}$ Å at $\lambda = 6,000$ Å. Even a poor quality solid state laser can have a bandwidth of $\Delta\nu \sim 10^9$ Hz i.e., $\Delta\lambda \sim 10^{-2}$ Å. For example, the linewidth of a line emitted by ruby, ordinarily is 3 Å, while, the linewidth of the laser line with the same material is 5×10^{-4} Å.

1.4 COHERENCE

Laser radiation is characterized by a high degree of ordering of the light field than the other sources. In other words, it has a high degree of coherence. The

high coherence of laser emission makes it possible to realize a tremendous spatial concentration of light power, such as 10^{13} W in a space with linear dimensions of only 1 μm . Radiation of such intensity can cut metals, produce microwelding, drill microscopic holes through diamond crystals and so on. We will discuss coherence in some more detail in Chapter 5.

It is necessary to mention here that inspite of its remarkable properties lasers do not provide solutions to all our problems. The present situation is correctly summarized in the following comments by Schawlow [336].

"The monochromacy, directionality and intensity of laser light are making possible a wide range of scientific investigations that would have been unimaginable without them ... Even so, we are still sometimes limited by the properties of available lasers, and have to try to extend laser technology. Perhaps someday we will have tunable gamma-ray lasers that we can use to excite coherent superpositions of nuclear energy levels and to alter radioactive decay of nuclei. The existence of lasers has not provided solutions to all our problems. But it has given us a pretty good hint as to where some interesting solutions might be found."

Current research effort is, indeed, aimed at further broadening the "laser range", specially lowering the short-wavelength limit down to gamma-ray range of the spectrum.

We have attempted to provide in this book an account of the invention of lasers, its several forms and their properties. We will indicate, the most promising lines of progress and discuss their applications particularly in the field of nonlinear optics. We will also outline briefly some of the interesting and novel laser-induced phenomena, so far thought to be "unthinkable" and which need further scrutiny and study. Laser is yet another example in which the beauty and fascination of physics becomes more and more apparent as one follows its story through the various stages of development.

2

EINSTEIN'S QUANTUM THEORY OF RADIATION

The essential ingredients for the fabrication of a laser were provided by Einstein as early as in 1917 [23, 111], when he showed that for adequate description of the interaction of radiation with matter, the notion of *stimulated emission* is essential. Einstein's theory of absorption and emission of light by an atom depends upon simple phenomenological considerations, but leads to correct predictions. The theory is based on a few assumptions about the emission and absorption of radiation by matter which are closely related to quantum theory. He showed that the molecules distributed in temperature equilibrium over states in a way which is compatible with quantum theory, are in dynamic equilibrium with Planck radiation. "Einstein's investigation gives the clearest insight into the origin of Planck's radiation law." [Eddington 107]

2.1 EINSTEIN COEFFICIENTS

Consider an enclosure containing atoms capable of being raised by absorption of radiation from the level m to the excited level n . In the absence of any radiation of appropriate frequency, there is no way in which atoms can pass from state m to state n . Suppose now that the enclosure contains also the isotropic radiation of frequency between ω_{nm} and $\omega_{nm} + d\omega_{nm}$ corresponding to the transition of the atoms from state m to state n ($\hbar\omega_{nm} = E_n - E_m$), where E_i represents the energy of the state i . Radiation as it is streaming out of the walls of the enclosure and back into them, may interact with the atoms and a transition from state m to the n may occur by absorption of a photon $\hbar\omega_{nm}$. The rate of transition from state m to state n , R_{mn} , will, obviously, be proportional to the population of the lower level per unit volume N_m , to the probability of absorption per unit time B_{mn} and to the density of radiation $\rho(\omega_{nm})$. We, therefore, assume that

$$R_{mn} = \rho(\omega_{nm}) B_{mn} N_m \quad \dots(2.1)$$

The atoms which absorb the radiation, become excited and eventually return to the ground state emitting *spontaneously* their excess energy (Fig. 2.1). The process is independent of the radiation field energy. There is a finite probability A_{nm} per unit time that the atom will spontaneously fall to the ground state emitting a photon $\hbar\omega_{nm}$. The number of atoms spontaneously emitting radiation per unit time is

$$R_{nm(sp)} = A_{nm} N_n \quad \dots(2.2)$$

where N_n is the number of atoms per unit volume in the state n .

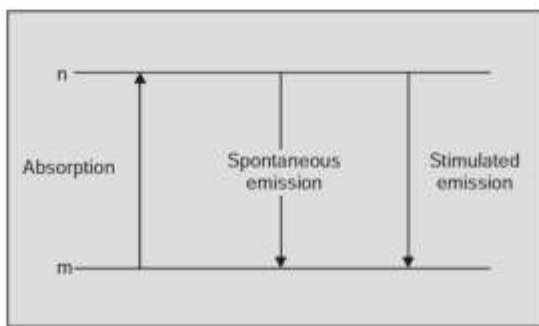


Fig. 2.1 Absorption and emission of radiation

When a steady state is reached, there must clearly be a balance achieved between the absorption and emission processes. When the light and the atoms have settled down in a steady equilibrium state, the mean number of the atoms N_m, N_n in the lower and the upper states remains constant, i.e., $\frac{dN}{dt} = 0$. Hence, under the condition of equilibrium

$$\text{The number of atoms absorbing radiation per unit time} = \text{The number of atoms emitting radiation per unit time} \quad \dots(2.3)$$

so that the number of atoms in any level does not change.

If absorption and spontaneous emission were the only processes operative, the principle of detailed balancing would give

$$\rho(\omega_{nm}) B_{nm} N_m = A_{nm} N_n \quad \dots(2.4)$$

$$\text{i.e.,} \quad \rho(\omega_{nm}) = \frac{A_{nm}}{B_{nm}} \cdot \frac{N_n}{N_m} \quad \dots(2.5)$$

In thermal equilibrium the total number of atoms N will be distributed over the available levels according to the Boltzmann distribution

$$N_i = \frac{N g_i \exp(-E_i/kT)}{\sum_i g_i \exp(-E_i/kT)} \quad \dots(2.6)$$

where g_i is the statistical weight of the level i , T the temperature, E_i the energy of the level i and k is the Boltzmann constant.

$$\therefore \frac{N_n}{N_m} = \frac{g_n \exp(-E_n/kT)}{g_m \exp(-E_m/kT)} \quad \dots(2.7)$$

We assume in the present case $g_n = g_m = 1$

$$\therefore \frac{N_n}{N_m} = \frac{\exp(-E_n/kT)}{\exp(-E_m/kT)} = \exp\left\{-\left(E_n - E_m\right)/kT\right\} = \exp(-\hbar\omega_{nm}/kT) \quad \dots(2.8)$$

Hence, Eqn. (2.5) changes to

$$\rho(\omega_{nm}) = \frac{A_{nm}}{B_{nm}} \exp(-\hbar\omega_{nm}/kT) \quad \dots(2.9)$$

The expression Eqn. (2.9) for the variation of radiation density $\rho(\omega_{nm})$ with temperature is not in accordance with experimental measurements which support Planck's law viz.

$$\rho(\omega_{nm}) d\omega_{nm} = \frac{\hbar\omega_{nm}^3}{\pi^2 c^3} \frac{1}{\exp(\hbar\omega_{nm}/kT) - 1} d\omega_{nm} \quad \dots(2.10)$$

Einstein's treatment of this problem uses an elegant thermodynamic argument. He pointed out that the two kinds of radiations indicated above are not sufficient for explaining the existence of the state of equilibrium between radiation and matter. The probability of spontaneous transition is determined only by the internal properties of atoms; whereas the probability of absorbing transition depends both on the properties of atoms and on the density of radiation. Therefore, while considering the detailed balance between two energy levels m and n , in the presence of radiation, we cannot ignore the possibility of the radiation influencing the atoms in the excited state and causing them to return to the lower state, the excess energy being given out as radiation. This radiative process is called *induced* or *stimulated emission* of radiation.

As in the case of absorption, the transition rate for stimulated emission is assumed to be

$$R_{nm(n)} = \rho(\omega_{nm}) B_{nm} N_n \quad \dots(2.11)$$

where B_{nm} is the probability per unit time that the atom will undergo transition from state n to state m by stimulated emission.

Thus, the transition from the lower to the upper energy state can occur in only one way, namely by the absorption of a photon of energy from the radiation field; whereas, the atoms in the excited state can make a radiative transition to the lower state by two alternative ways: (i) by stimulated emissions and (ii) by spontaneous emission. Absorption and stimulated emission are the processes induced by radiation.

The equation for the rate of change of N_n is

$$\frac{dN_n}{dt} = -N_n A_{nm} + N_m B_{mn} \rho(\omega_{nm}) - N_n B_{nm} \rho(\omega_{nm}) \quad \dots(2.12)$$

Under the condition of equilibrium $\frac{dN_n}{dt} = 0$

$$\therefore N_n A_{nm} = (N_m B_{mn} - N_n B_{nm}) \rho(\omega_{nm})$$

$$\text{i.e., } \rho(\omega_{nm}) = \frac{A_{nm}}{\frac{N_m}{N_n} B_{mn} - B_{nm}} \quad \dots(2.13)$$

The ratio of the number densities of particles in the two energy states in presence of degeneracy as obtained from Boltzmann law is

$$\begin{aligned} \frac{N_n}{N_m} &= \frac{g_n \exp(-E_n/kT)}{g_m \exp(-E_m/kT)} = \frac{g_n}{g_m} \exp[-(E_n - E_m)/kT] \\ &= \frac{g_n}{g_m} \exp(-\hbar\omega_{nm}/kT) \end{aligned} \quad \dots(2.14)$$

Substituting this in Eqn. (2.13), we get

$$\begin{aligned} \rho(\omega_{nm}) &= \frac{A_{nm}}{\frac{g_m}{g_n} \exp(\hbar\omega_{nm}/kT) B_{mn} - B_{nm}} \\ &= \frac{A_{nm}}{B_{nm} \cdot \frac{1}{\frac{g_m}{g_n} \exp(\hbar\omega_{nm}/kT) - 1}} \end{aligned} \quad \dots(2.15)$$

This expression, derived using Einstein coefficients A_{nm} , B_{nm} , B_{mn} and the Boltzmann distribution law, must be consistent with Planck's law (2.10).

To determine the coefficient A_{nm}/B_{nm} , Einstein took advantage of the fact that at high frequencies, Eqn. (2.10) must transform into Wien's radiation law. Thus, when $\hbar\omega_{nm} \gg kT$, Eqn. (2.10) takes the form

$$\rho(\omega_{nm}) = \frac{\hbar\omega_{nm}^3}{\pi^2 c^3} \exp(-\hbar\omega_{nm}/kT) \quad \dots(2.16)$$

Under the same conditions, Eqn. (2.15) changes to

$$\rho(\omega_{nm}) = \frac{A_{nm}}{B_{nm}} \cdot \frac{1}{\frac{g_m}{g_n} \frac{B_{mn}}{B_{nm}} \exp(\hbar\omega_{nm}/kT)} \quad \dots(2.17)$$

If we now assume

$$g_m B_{mn} = g_n B_{nm} \quad \dots(2.18)$$

Equation (2.17) reduces to

$$\rho(\omega_{nm}) = \frac{A_{nm}}{B_{nm}} \exp(-\hbar\omega_{nm}/kT) \quad \dots(2.19)$$

Comparison of Eqns. (2.16) and (2.19) gives

$$\frac{A_{nm}}{B_{nm}} = \frac{\hbar\omega_{nm}^3}{\pi^2 c^3} \quad \dots(2.20)$$

The relations Eqns. (2.18) and (2.20) make Eqn. (2.15) identical with Eqn.(2.10) and also show that three Einstein coefficients are interrelated.

For non-degenerate states $g_n = g_m = 1$

$$\therefore B_{nm} = B_{mn} \quad \dots(2.21)$$

That is, when an atom or a molecule with two energy levels is placed in an electromagnetic field, the probability of an upward transition —absorption, weighting factors apart, is equal to the probability of downward transition *i.e.*, stimulated emission.

2.2 MOMENTUM TRANSFER

The discussion so far is based on the hypothesis concerned only with the exchange of energy between the radiation and the atom. According to the law of conservation of momentum, this energy transfer corresponds also to a momentum transfer. From the point of view of classical electrodynamics, if a body emits energy ϵ , it receives a recoil (momentum) ϵ/c , if all the radiation is emitted in the same direction. On the other hand, if the emission takes place as an isotropic process, say, in the form of spherical waves, no recoil occurs. Einstein assumed that the transfer of quantized energies and momenta must leave the Maxwell-Boltzmann distribution undisturbed. This is possible if we assume that each elementary process is completely directional. Thus, if a beam of radiation causes an atom to absorb or emit (stimulated process) an amount of energy $\hbar\omega$ the momentum $\hbar\omega/c$ is always transferred to the atom in such a way that the momentum is directed along the *direction* of propagation of the beam if the energy is absorbed, and directed in the opposite direction, if the energy is emitted. Spontaneous emission is also a *directed* process. There is no emission in spherical waves. In the process of spontaneous emission, for a single event, the atom suffers a recoil of magnitude $\hbar\omega/c$ with sharp directionality; but its direction is different in different cases and is decided only by "chance". Averaged over a large number of events, spontaneous transition will behave according to classical picture and leave momentum unaltered.

Although no explicit quantum-mechanics was used by Einstein (it was not extant then) in the development of his theory, his postulates can be rigorously justified by quantum mechanical treatment as will be shown in the next chapter.

The weakness of the theory according to Einstein [23, 111] "...lies, on the one hand, in the fact that it does not bring any nearer the connection with the wave theory and, on the other hand, in the fact that it leaves the moment and direction of the elementary process to "chance". However, Einstein had complete confidence in the reliability of his theory.

One cannot ignore, however, some of the inadequacies of Einstein's theory. For instance, the theory gives no prescription for computing the values of the coefficients A and B . For this, one has to take recourse to quantum-mechanical theory. Similarly, it is an established fact that a transition of an atom from one state to another does not occur at a sharply defined frequency, but over a spread of frequencies. A measurement of the distribution of frequencies over a linewidth can yield useful information. Einstein's theory gives no account of the linewidth of atomic transitions.

2.3 LIFE-TIME

We may digress here for a while from our discussion of stimulated emission, to explain the concept of *life-time*, frequently used in describing transitions between different states.

The time τ during which the number of atoms in a given excited state diminishes to $(1/e)$ th of its initial value is called the *life-time* of the excited state. The life-time determined in this way coincides with the average time spent by atoms in the excited state. We shall now show how the concept of the life-time of a state is related to the probability of transition from that state.

Suppose the atom is in an excited state n . Let the probability that the atom will leave that state in time dt be pdt . Therefore, if N is the number of atoms in state n at any time t ,

$$-\frac{dN}{dt} = Np \quad \dots(2.22)$$

Integrating this equation, we have

$$\ln N = -pt + \text{a constant}$$

If $N = N_0$ at $t = 0$

$$N = N_0 e^{-pt} \quad \dots(2.23)$$

The average life-time of an atom in the state n is

$$\tau = \frac{1}{N_0} \int_0^{\infty} tp N_0 e^{-pt} dt = \frac{1}{p} = \frac{1}{A_{nn}} \quad \dots(2.24)$$

The Einstein coefficient A is normally determined by measuring the radiative life-time τ . This is not an easy measurement, in view of the shortness of the value of τ which is of the order of 10^{-8} sec.

2.4 POSSIBILITY OF AMPLIFICATION

We now revert to our discussion of stimulated emission. We have seen above that the spontaneous emission gives out radiation at random moments and in random directions. Stimulated emission, on the other hand, has very important properties. If a narrow beam of radiation passing through a region containing only excited atoms, persuades them to release their excess energy, the radiation thus induced has the same direction as that of the incoming radiation. The same relates to the frequency, phase and polarization of the stimulated emission and stimulating radiation. Consequently, the stimulating radiation and stimulated emission are strictly coherent and the resultant beam is amplified. The fact that this amplification is coherent is, perhaps, less obvious at this stage as Einstein's theory does not account for coherence. A detailed discussion on coherence is given in Chapter 5.

It is now clear that for the amplification of the beam, stimulated emission must predominate over spontaneous emission, which has been termed "quantum noise" in this context. The ratio of the magnitudes of the two emission rates is

$$\frac{A_{nm}}{B_{nm}\rho(\omega_{nm})} = \exp(\hbar\omega_{nm}/kT) - 1 \quad \dots(2.25)$$

where we have used Eqns. (2.15) and (2.18).

Let us put some figures into this formula to examine the possibility of an amplifying device.

In the microwave region, say at $\lambda = 10$ cm and for a cavity maintained at room temperature ($T = 300^\circ\text{K}$),

$$\frac{\hbar\omega}{kT} \sim 5 \times 10^{-4}$$

and, hence

$$\frac{A_{nm}}{B_{nm}\rho(\omega_{nm})} = \exp(5 \times 10^{-4}) - 1 \approx 0 \quad \dots(2.26)$$

That is, stimulated emission rate is much higher than the spontaneous emission rate. The populations of the two states also become comparable, $N_n \sim N_m$. Amplification in this region is, therefore, possible and has been obtained in MASERS as will be shown in Chapter 4.

On the other hand, in the optical region, say, at $\lambda = 5000$ Å ($v = 6 \times 10^{14}$) and $T = 300^\circ\text{K}$, $(\hbar\omega/kT) \sim 100$.

$$\therefore \frac{A_{nm}}{B_{nm}\rho(\omega_{nm})} = e^{100} - 1 \quad \dots(2.27)$$

which is pretty high indicating that spontaneous emission is more predominant in the optical region. This led some of the research workers in the field to conclude that there is no future in extending the device of amplification to frequencies higher than those of microwaves. Subsequent developments, as we now know, proved the contrary.

The discussion above shows that one of the consequences of Einstein's theory is that there is a possibility of radiation growing in intensity as it passes through matter; and, yet, the discovery of lasers had to wait for about forty years.

"Stimulated emission was proposed in 1917 by Einstein. Why did it take so long to produce lasers?" This question was asked by Professor Stoicheff to Nobel laureates Professors Bloembergen and Schawlow in a panel session organised by the Optical Society of America in 1982 [290]. The reactions of these eminent scientists whose scientific interests have centred on the properties of light, may interest the readers.

Bloembergen: "...people were very close (to light amplification) in 1930.... Kramers was well aware that the atoms in the excited state of a two-level system would make a contribution to the susceptibility of opposite sign from that in the ground state. Laudenberg, around 1930, actually observed in electric discharges that when excited state was more populated, the susceptibility decreased..., it could have been done in 1930, but it wasn't".

Schawlow: "...That (time lag) was necessary because people were taught to believe that the world is pretty close to being in equilibrium and that you can't really think about it except in terms of slight deviations from equilibrium...at equilibrium, at any temperature whatever, there are always more atoms in every lower state than in any higher state...So, I think, this was the conceptual stumbling block".

There was occasional reference in the published literature in thirties to the "negative absorption" which would occur if there were predominance of atoms in the upper state. Lamb and Rutherford [226] in 1950, in a footnote to a paper on the measurement of the "Lamb shift" in hydrogen, briefly discussed negative absorption. However, the main reason for the delay in this important discovery is, perhaps, that scientists did not have sufficient knowledge of energy levels and that techniques did not exist for exploiting the principle. Constructive thinking in this direction started when more data were available, technology advanced and there was better interplay between science and technology. Despite this, some people may still think that considering the simplicity of the device and the fact that the principle was suggested as early as in 1917, the laser could have been invented years ago. To these, we may quote Sanders [123]: "This is a case where a touch of brilliance was needed to realize what in the hindsight, seems so obvious".

3

INTERACTION OF RADIATION WITH MATTER

Everything we know about light comes from its interaction with matter. This interaction cannot be explained on the lines of classical physics. Quantum mechanics is inevitably necessary for the full comprehension of such phenomena. One can employ perturbation theory for the study of interaction, if it is sufficiently weak. The purpose of the perturbation theory is an attempt to describe what happens to a quantum system when its potential system changes slightly. The radiation may be regarded as a source of perturbation of the energy levels of the scattering system; a suitable interaction Hamiltonian may be introduced to determine the redistribution of charges in the material on a microscopic scale and quantum mechanical technique may be used to investigate the transitions between the energy levels of the perturbed system and the scattering that ensues. This technique has been extremely successful in quantum electrodynamics where the agreement between theory and experiment is found to exist to a very high degree of accuracy.

Let us first discuss the time-dependent perturbation theory which is the basis of understanding quantum optics. We shall develop the theory in two stages:

(i) In the first stage we shall present what is generally known as *Semiclassical Theory* in which the electromagnetic field is regarded as a classical field and atomic states are treated quantum-mechanically. This treatment, although simpler, is incomplete. The theory takes into account the influence that the radiation field has on the atomic systems; but does not consider how the field is modified by the interaction and does not account for the spontaneous emission. Nevertheless, the theory provides theoretical expressions for a wide range of quantities, which are identical to those obtained using the "complete" theory. In fact, almost all optical experiments made before the advent of lasers, can best be explained on the basis of appropriate semi-classical models and concepts.

(ii) In the second stage we develop the "complete" theory in which both the atoms and the field are treated quantum-mechanically.

It must be mentioned here that the theory in either form, is an approximate theory and is based on the assumption that the perturbation is small. The theory appears to describe the interaction of radiation with matter precisely, but exact calculations are still not possible for anything beyond the simplest atoms and molecules. For instance, the theory cannot yet tell us exactly at what wavelength and how strongly a given substance absorbs or emits light.

3.1 TIME DEPENDENT PERTURBATION THEORY

Frequently we have to deal with a perturbation that changes with time. Let us quickly skim over the elements of quantum-mechanical perturbation theory in its time dependent form.

The Schrödinger equation for an unperturbed atom is

$$\hat{H}_0 |\Psi, t\rangle = i\hbar \frac{\partial}{\partial t} |\Psi, t\rangle \quad \dots(3.1)^*$$

where the Hamiltonian \hat{H}_0 is independent of time and $|\Psi, t\rangle$ is the time dependent state.

The time dependence of an unperturbed state $|\psi_n, t\rangle$ has the form

$$|\psi_n, t\rangle = \exp(-iE_n t/\hbar) |u_n\rangle \quad \dots(3.2)$$

where $|u_n\rangle$ is independent of time and satisfies the equation

$$\hat{H}_0 |u_n\rangle = E_n |u_n\rangle \quad \dots(3.3)$$

and E_n is the energy eigenvalue of the n th state. The atomic states described by the Eqn. (3.3) are known as stationary states. The average value of any observable, when the atom is in one of these states, is independent of time, provided the corresponding operator does not involve time explicitly.

We assume that the basic solutions $|\psi_1, t\rangle, |\psi_2, t\rangle, \dots$ corresponding to the stationary states are known. The general solution of Eqn. (3.1) can be expressed as a linear combination of these basic states

$$|\Psi, t\rangle = \sum_n C_n |\psi_n, t\rangle = \sum_n C_n \exp(-iE_n t/\hbar) |u_n\rangle \quad \dots(3.4)$$

where C_n are time independent constants. If there are only two levels with energy eigenvalues E_a and E_b ,

$$|\Psi, t\rangle = C_a \exp(-iE_a t/\hbar) |u_a\rangle + C_b \exp(-iE_b t/\hbar) |u_b\rangle \quad \dots(3.5)$$

If the atom is isolated, the probability that the atom is in state a or in state b is given by

$$C_a^* C_a = |C_a|^2 \text{ and } C_b^* C_b = |C_b|^2 \text{ respectively.}$$

Following Dirac [101] we represent the state corresponding to the wave-function u_n by $|u_n\rangle$; its complex conjugate by $\langle u_n|$ and the scalar product $\int u_m^ u_n dt$ by $\langle u_m | u_n \rangle$.

If the external forces act upon the system, the situation is changed. The system may undergo a transition from one stationary state to another under the action of these external factors. Such external factors appear in quantum mechanics in the form of an interaction potential which must be added to the unperturbed Hamiltonian H_0 . Suppose an atom is in the n th stationary state defined by the eigenfunction $|u_n\rangle$ and eigenvalue E_n and at a time $t = 0$, we switch on any extra perturbing potential. The atom is no longer in a quantum state, since $|u_n\rangle$ and E_n are not an eigenfunction and an eigenvalue of the new potential. By applying Schrödinger equation to the atom in the new potential distribution, we can find how the wavefunction Ψ changes from its value at $t = 0$ to a new function at a later time. The Schrödinger equation is

$$\hat{H} |\Psi\rangle = i\hbar \frac{\partial}{\partial t} |\Psi\rangle \quad \dots(3.6)$$

where the Hamiltonian H is now

$$H = H_0 + H'(t) \quad \dots(3.7)$$

where $H'(t)$ is a small term arising from interaction with the external forces. Its functional form depends upon the nature of the forces.

Following the usual techniques of quantum mechanics, we assume the solution of this equation to be a linear superposition of the basic wavefunctions $|\psi_1, t\rangle$, $|\psi_2, t\rangle$ etc. as in Eqn. (3.4), the only difference being that the coefficients $C_n(t)$ are now time dependent, *i.e.*,

$$|\Psi\rangle = \sum_n C_n(t) \exp(-iE_n t/\hbar) |u_n\rangle \quad \dots(3.8)$$

The probability of finding the system in any particular state is given simply by the square of the modulus of the corresponding amplitude of the state. Substituting Eqn. (3.8) in Eqn. (3.6), we have

$$\begin{aligned} \text{L.H.S.} &= \hat{H} |\Psi\rangle = (\hat{H}_0 + \hat{H}'(t)) |\Psi\rangle \\ &= (\hat{H}_0 + \hat{H}'(t)) \sum_n C_n(t) \exp(-iE_n t/\hbar) |u_n\rangle \end{aligned} \quad \dots(3.9)$$

$$\text{R.H.S.} = i\hbar \frac{\partial}{\partial t} |\Psi\rangle = i\hbar \sum_n \left\{ \dot{C}_n(t) - \frac{iE_n}{\hbar} C_n(t) \right\} \exp(-iE_n t/\hbar) |u_n\rangle \quad \dots(3.10)$$

Multiplying both sides on the left by the complex conjugate of an eigen state $|u_m\rangle$, integrating over the whole range of coordinates and equating we have

$$\begin{aligned}
& \sum_n C_n(t) \exp(-iE_n t/\hbar) \langle u_m | \hat{H}_0 | u_n \rangle \\
& + \sum_n C_n(t) \exp(-iE_n t/\hbar) \langle u_m | \hat{H}' | u_n \rangle \\
= & i\hbar \sum_n \dot{C}_n(t) \exp(-iE_n t/\hbar) \langle u_m | u_n \rangle \\
& + \sum_n E_n C_n(t) \exp(-iE_n t/\hbar) \langle u_m | u_n \rangle \quad [\text{See (3.3)}] \\
\text{or} \\
& \sum_n C_n(t) E_n \exp(-iE_n t/\hbar) \langle u_m | u_n \rangle \\
& + \sum_n C_n(t) \exp(-iE_n t/\hbar) \langle u_m | \hat{H}' | u_n \rangle \\
= & i\hbar \sum_n \dot{C}_n(t) \exp(-iE_n t/\hbar) \langle u_m | u_n \rangle \\
& + \sum_n C_n(t) E_n \exp(-iE_n t/\hbar) \langle u_m | u_n \rangle \\
& i\hbar \dot{C}_m(t) \exp(-iE_m t/\hbar) \\
= & \sum_n \dot{C}_n(t) \exp(-iE_n t/\hbar) \langle u_m | \hat{H}' | u_n \rangle
\end{aligned}$$

or $\dot{C}_m(t) = -\frac{1}{i\hbar} \sum_n C_n(t) \exp[-(i/\hbar)(E_n - E_m)t] \langle u_m | \hat{H}' | u_n \rangle \quad \dots(3.11)$

where we have used the orthogonality condition

$$\langle u_m | u_n \rangle = \int u_m^* u_n d\tau = \delta_{mn} \quad \dots(3.12)$$

where δ_{mn} is the Kronecker delta symbol defined as

$$\begin{aligned}
\delta_{mn} &= 0 \text{ for } m \neq n \\
&= 1 \text{ for } m = n
\end{aligned} \quad \dots(3.13)$$

We can write Eqn. (3.11) in the form

$$\dot{C}_m(t) = -\frac{1}{i\hbar} \sum_n C_n(t) \exp(-i\omega_{nm}t) \hat{H}'_{mn} \quad \dots(3.14)$$

where

$$\omega_{nm} = \frac{E_n - E_m}{\hbar}$$

and

$$\hat{H}'_{mn} = \langle u_m | \hat{H}' | u_n \rangle = \int u_m^* \hat{H}' u_n d\tau \quad \dots(3.15)$$

where $d\tau$ is the volume element. This is called a matrix element of the Hamiltonian \hat{H}' .

We have assumed that the system is in a state n when the perturbation was switched on at $t = 0$. If the perturbation is off at $t = t'$, what is the probability that the system is in state m ? This probability is given by $|C_m(t)|^2$.

To obtain the expression for $|C_m(t)|^2$ we integrate, Eqn. (3.14)

$$C_m(t) = \frac{1}{i\hbar} \sum_n \int_0^{t'} C_n(t) \exp(-i\omega_{nm}t) \hat{H}'_{mn} dt \quad \dots(3.16)$$

From this the probability sought can be found.

To illustrate the method we assume that there are only two levels a and b . Then, by Eqn. (3.14)

$$\dot{C}_b(t) = \frac{1}{i\hbar} \left\{ C_a(t) \exp(-i\omega_{ab}t) \hat{H}'_{ba} + C_b(t) \exp(-i\omega_{bb}t) \hat{H}'_{bb} \right\} (\because \omega_{bb} = 0) \quad \dots(3.17)$$

and

$$\dot{C}_a(t) = \frac{1}{i\hbar} \left\{ C_a(t) \hat{H}'_{aa} + C_b(t) \exp(-i\omega_{ab}t) \hat{H}'_{ab} \right\} \quad \dots(3.18)$$

We have now to determine the form of the interaction Hamiltonian \hat{H}' . The physical nature of the external force which causes the quantum transition of the system is arbitrary. In optical experiment the perturbing potential is an electromagnetic field.

3.2 ELECTRIC DIPOLE INTERACTION

Maxwell's equations of electromagnetic field, viz.

$$(i) \nabla \cdot \mathbf{D} = \rho \quad (ii) \nabla \cdot \mathbf{B} = 0 \\ (iii) \nabla \times \mathbf{E} = -\frac{d\mathbf{B}}{dt} \quad (iv) \nabla \times \mathbf{H} = \mathbf{J} + \frac{d\mathbf{D}}{dt} \quad \dots(3.19)$$

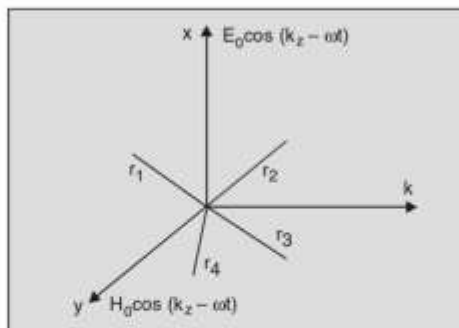


Fig. 3.1 Atom and the electromagnetic wave incident upon it

lead directly to the equations

$$\nabla^2 \mathbf{E} - \mu \epsilon \frac{\partial^2 \mathbf{E}}{\partial t^2} = 0 \quad \dots(3.20)$$

$$\text{and} \quad \nabla^2 \mathbf{H} = \mu \epsilon \frac{\partial^2 \mathbf{H}}{\partial t^2} = 0 \quad \dots(3.21)$$

We can show by direct substitution that Eqn. (3.20) has a solution of the form

$$\mathbf{E} = \mathbf{E}_0 \exp [i(\mathbf{k} \cdot \mathbf{r} - \omega t)] \quad \dots(3.22)$$

Suppose the atom is at the origin of the coordinate system and interacts with an electromagnetic wave polarized in the x -direction (Fig. 3.1). We represent the field, by real time dependent parts, *i.e.*,

$$\mathbf{E} = \mathbf{E}_0 \cos (kz - \omega t) \quad \dots(3.23)$$

The order of the magnitude of the atomic electronic radii can be judged from the size of the Bohr radius

$$a_0 = \frac{4\pi \epsilon_0 \hbar^2}{me^2} \approx 5 \times 10^{-11} \text{ m} \quad \dots(3.24)$$

where m is the electron mass and e its charge. This radius is much smaller than the wavelength of the electromagnetic radiation in the optical region ($\sim 6 \times 10^{-7}$ m). Hence, for this region

$$ka_0 \ll 1$$

which indicates that the spatial variation of the electric field across the dimensions of the atom is negligible. We may, therefore, ignore the term kz in Eqn. (3.23) and write

$$\mathbf{E} = \mathbf{E}_0 \cos \omega t \quad \dots(3.25)$$

The dipole moment of a point charge e at position \mathbf{r} is $e\mathbf{r}$. The electric dipole moment of the atom, therefore, is

$$-\sum_j e\mathbf{r}_j = -e\mathbf{D} \quad \dots(3.26)$$

where \mathbf{r}_j is the location vector of the j th electron and

$$\mathbf{D} = \sum_j \mathbf{r}_j \quad \dots(3.27)$$

The dipole moment interacts strongly with an electromagnetic wave whose wavelength is long compared to the dimensions of the atom. Its potential energy in the electric field \mathbf{E} is

$$\sum_j e\mathbf{r}_j \cdot \mathbf{E}_0 \cos \omega t = e\mathbf{D} \cdot \mathbf{E}_0 \cos \omega t \quad \dots(3.28)$$

Taking this to be the main contribution to the interaction Hamiltonian, we may write

$$\hat{H}' = e\mathbf{D} \cdot \mathbf{E}_0 \cos \omega t \quad \dots(3.29)$$

$$\text{Now } \hat{H}'_{bb} = \langle u_b | \hat{H}' | u_b \rangle = \int u_b^* (\sum_j e\mathbf{r}_j \cdot \mathbf{E}_0 \cos \omega t) u_b d\tau$$

Because \hat{H}' as given by Eqn. (3.28) has odd parity—that is, it changes sign when \mathbf{r}_j is replaced by $-\mathbf{r}_j$ —the integrand in \hat{H}'_{bb} is an odd function of position, and, hence, the integral must vanish.

$$\therefore \hat{H}'_{bb} = \langle u_b | \hat{H}' | u_b \rangle = \hat{H}'_{aa} \langle u_a | \hat{H}' | u_a \rangle = 0 \quad \dots(3.30)$$

The other matrix elements \hat{H}'_{ba} and \hat{H}'_{ab} will not vanish if u_a and u_b have opposite parity. We can, therefore, write Eqn. (3.17) as

$$\dot{C}_b(t) = \frac{1}{i\hbar} C_a(t) \exp(-i\omega_{ab}t) \hat{H}'_{ba} \quad \dots(3.31)$$

Assuming that t' , duration of perturbation, is very small and the perturbation is fairly weak so that the probability of transition is very small, we may put $C_a(t) = 1$ and $C_b(t) = 0$. With this approximation (3.31) reduces to

$$\dot{C}_b(t) = \frac{1}{i\hbar} \exp(-i\omega_{ab}t) \hat{H}'_{ba} \quad \dots(3.32)$$

leading to the approximate solution

$$i_b(t) = \frac{1}{i\hbar} \int_0^{t'} \exp(-i\omega_{ab}t) \hat{H}'_{ba} dt \quad \dots(3.33)$$

Similarly, starting from Eqn. (3.18), we can find $C_a(t)$. These are the first order solutions.

Substituting these on the right-hand side of Eqns. (3.17) and (3.18) and integrating, we get a second-order approximation of the solution, and so on to higher orders.

In order to find the probability of transition to the state b —which is given by $|C_b(t')|^2$ —let us integrate Eqn. (3.33)

$$\begin{aligned} C_b(t') &= \frac{1}{i\hbar} \int_0^{t'} \exp(-i\omega_{ab}t) \hat{H}'_{ba} dt \\ &= \frac{1}{i\hbar} \int_0^{t'} \exp(-i\omega_{ab}t) \langle u_b | \sum_j e \mathbf{r}_j \cdot \mathbf{E}_0 \cos \omega t | u_a \rangle dt \\ &= \frac{\langle u_b | e X E_0 | u_b \rangle}{i\hbar} \int_0^{t'} \exp(-i\omega_{ab}t) \cos \omega t dt \quad \dots(3.34) \end{aligned}$$

where X is the component of \mathbf{D} in the direction of \mathbf{E} , i.e., in the x -direction.

$$\begin{aligned} \therefore C_b(t') &= \frac{e E_0 \langle u_b | X | u_a \rangle}{i\hbar} \int_0^{t'} \exp(-i\omega_{ab}t) \frac{\exp(i\omega t) + \exp(-i\omega t)}{2} dt \\ &= \frac{e E_0 X_{ba}}{2i\hbar} \int_0^{t'} [\exp(-i(\omega_{ab} - \omega)t) + \exp(-i(\omega_{ab} + \omega)t)] dt \\ &= \frac{e E_0 X_{ba}}{2i\hbar} \left[\frac{1 - \exp(-i(\omega_{ab} - \omega)t')}{i(\omega_{ab} - \omega)} + \frac{1 - \exp(-i(\omega_{ab} + \omega)t')}{i(\omega_{ab} + \omega)} \right] \end{aligned}$$

$$= \frac{eE_0X_{ba}}{2\hbar} \left[\frac{1 - \exp(i(\omega_{ba} + \omega)t')}{\omega_{ba} + \omega} + \frac{1 - \exp(i(\omega_{ba} - \omega)t')}{\omega_{ba} - \omega} \right] \quad \dots(3.35)$$

(Note $\omega_{ab} = -\omega_{ba}$)

Because of the presence of the denominators the transition probability $|C_b(t)|^2$ from state $|u_a\rangle$ to state $|u_b\rangle$ can be large only if $\omega_{ba} = \omega$. In this case, the contribution of the second term in brackets will be much larger than that of the first which can be ignored. The probability of transition to the state $|u_b\rangle$ per unit time, in the limit of long time, therefore, is

$$\begin{aligned} \frac{1}{t'} |C_b(t')|^2 &= \frac{e^2 E_0^2 |X_{ba}|^2}{4\hbar^2} \lim_{t' \rightarrow \infty} \frac{1}{t'} \left| \frac{1 - \exp(i(\omega_{ba} - \omega)t')}{\omega_{ba} - \omega} \right|^2 \\ &= \frac{e^2 E_0^2 |X_{ba}|^2}{\hbar^2} \lim_{t' \rightarrow \infty} \frac{\sin^2(\omega_{ba} - \omega)t'/2}{(\omega_{ba} - \omega)^2 t'} \end{aligned} \quad \dots(3.36)$$

The transition probability per unit time can be expressed in a more convenient form using Dirac delta function, which is a generalization of the Kronecker delta function, when the discrete variables n, m , are replaced by continuous variables say, a, a' . The function is defined as

$$\delta(a - a') = 0 \text{ for } a \neq a' \quad \dots(3.37)$$

and $\int \delta(a - a') da = 1$ provided the range of integration includes the point $a = a'$

One of the important properties of delta function is

$$\int_{-\infty}^{\infty} f(\alpha) \delta(\alpha - \alpha') d\alpha = f(\alpha') \quad \dots(3.38)$$

The delta function can be represented in a variety of ways. One of its useful representation is

$$\delta(\alpha - \alpha') = \frac{2}{\pi} \lim_{l \rightarrow \infty} \frac{\sin^2 l(\alpha - \alpha')/2}{(\alpha - \alpha')^2 l} \quad \dots(3.39)$$

We can use this expression to cast the last factor in Eqn. (3.36) in terms of delta function. Thus,

$$\delta(\omega_{ba} - \omega) = \frac{2}{\pi} \lim_{t' \rightarrow \infty} \frac{\sin^2(\omega_{ba} - \omega)t'/2}{(\omega_{ba} - \omega)^2 t'} \quad \dots(3.40)$$

and, hence,

$$\frac{1}{t'} |C_b(t')|^2 = \frac{e^2 E_0^2 |X_{ba}|^2 \pi}{2\hbar^2} \delta(\omega_{ba} - \omega) \quad \dots(3.41)$$

We have assumed so far that the transition frequency ω_{ba} is a well-defined quantity. In practice, however, there is always some uncertainty in the value of ω_{ba} . Even in an idealized experiment with perfect frequency resolution, there is always an uncertainty in the intrinsic value of the spectral line width owing to the spontaneous emission. This uncertainty can be accounted for by integrating the expression Eqn. (3.41) over the range of uncertainty $\Delta\omega$.

The energy density $\rho(\omega)$ in an electromagnetic wave is related to E_0 by [233]

$$\frac{1}{2} \epsilon_0 E_0^2 = \int \rho(\omega) d\omega \quad \dots(3.42)$$

Using this relation, we can write Eqn. (3.41) as

$$\frac{1}{t} |C_b(t)|^2 = \frac{\pi e^2 |X_{ba}|^2}{\epsilon_0 h^2} \int_{\omega_{ba} - (1/2)\Delta\omega}^{\omega_{ba} + (1/2)\Delta\omega} \rho(\omega) \delta(\omega_{ba} - \omega) d\omega \quad \dots(3.43)$$

Or since the delta-function is zero everywhere except at $\omega = \omega_{ba}$, we can change the limits of integration and write

$$\begin{aligned} \frac{1}{t} |C_b(t)|^2 &= \frac{\pi e^2 |X_{ba}|^2}{\epsilon_0 h^2} \int_{-\infty}^{\infty} \rho(\omega) \delta(\omega_{ba} - \omega) d\omega \\ &= \frac{\pi e^2 |X_{ba}|^2}{\epsilon_0 h^2} \rho(\omega_{ba}) \end{aligned} \quad \dots(3.44)$$

where we have used Eqn. (3.38).

This expression for $|C_b(t)|^2$ has been derived for a single atom and needs be modified when generalizing it for a gas of similar atoms.

We can write the matrix element X_{ba} as

$$\begin{aligned} X_{ba} &= \langle u_b | X | u_a \rangle = \langle u_b | \hat{\mathbf{e}}_x \cdot \mathbf{D} | u_a \rangle \\ &= \hat{\mathbf{e}}_x \cdot \mathbf{D}_{ba} \end{aligned} \quad \dots(3.45)$$

where $\hat{\mathbf{e}}_x$ is a unit vector in the direction of the field, i.e., in the x -direction. Now even in a gas of identical atoms the spatial directions of \mathbf{D}_{ba} vary randomly owing to the random orientations of the atoms. It is, therefore, necessary to average $|X_{ba}|^2$ over the random orientation of \mathbf{D}_{ba} . If θ is the angle between \mathbf{D}_{ba} and $\hat{\mathbf{e}}_x$

$$|X_{ba}|^2 = |\mathbf{D}_{ba}|^2 \overline{\cos^2 \theta} = \frac{1}{3} |\mathbf{D}_{ba}|^2 \quad \dots(3.46)$$

Hence, the matrix element $|X_{ba}|^2$ in Eqn. (3.44) will have to be replaced by Eqn. (3.46).

We have seen in the last chapter, that in terms of Einstein coefficients, the transition probability per unit time for the transition from state $|u_a\rangle$ to state $|u_b\rangle$ is $B_{ab} \rho(\omega_{ba})$.

$$\therefore B_{ab} \rho(\omega_{ba}) = \frac{\pi e^2 |D_{ba}|^2}{3\epsilon_0 \hbar^2} \rho(\omega_{ba})$$

i.e., $B_{ab} = \frac{\pi e^2 |D_{ba}|^2}{3\epsilon_0 \hbar^2}$... (3.47)

We can similarly calculate the transition probability for a downward transition B_{ba} starting from Eqn. (3.18) and using the initial conditions $C_a(t) = 0$ and $C_b(t) = 1$. The calculations will show that for non-degenerate levels

$$B_{ab} = B_{ba} \quad \dots (3.48)$$

The theory does not permit a correct prediction of Einstein A coefficient. However, this can be found by using Eqns. (2.18) and (2.20).

$$A_{ba} = \frac{\hbar \omega_{ba}^3}{\pi^2 c^3} B_{ba} = \frac{\hbar \omega_{ba}^3}{\pi^2 c^3} \cdot \frac{g_a}{g_b} B_{ab}$$

$$= \frac{g_a}{g_b} \cdot \frac{e^2 \omega_{ba}^3 |D_{ba}|^2}{3\epsilon_0 \hbar \pi c^3} \quad \dots (3.49)$$

We, thus, have quantum-mechanical expressions for the three Einstein coefficients.

In order to illustrate the use of these formulae we shall calculate the A coefficient, for the transition $2P-1S$, in hydrogen atom.

There are three $2P$ states in hydrogen atom having equal rates of transition from the $1S$ state. Hence, the composite B_{12} coefficient has the value

$$B_{12} = \frac{\pi e^2 |D_{21}|^2}{\epsilon_0 \hbar^2} \quad \dots (3.50)$$

where D_{21} is the matrix element between anyone of the three $2P$ states and $1S$ state.

$$\therefore A_{21} = \frac{g_1}{g_2} \cdot \frac{e^2 \omega_{21}^3 |D_{21}|^2}{\epsilon_0 \hbar \pi c^3}$$

$$= \frac{e^2 \omega_{21}^3 |D_{21}|^2}{3\epsilon_0 \hbar \pi c^3} \quad (\because g_1 = 1, g_2 = 3) \quad \dots (3.51)$$

The wave functions for the two states are

$$\psi_{1s} = \pi^{-1/2} a_0^{-3/2} \exp(-r/a_0) \quad \dots (3.52)$$

$$\text{and } \phi_{2px} = 2^{-5/2} \pi^{-1/2} a_0^{-5/2} x \exp(-r/2a_0) \quad \dots(3.53)$$

where a_0 is the Bohr radius Eqn. (3.24).

$$\therefore |D_{21}| = \int 2^{-5/2} \pi^{-1/2} a_0^{-5/2} x \exp(-r/2a_0) x \pi^{-1/2} a_0^{-3/2} \exp(-r/a_0) d\tau$$

Using polar coordinates,

$$\begin{aligned} |D_{21}| &= 2^{-5/2} \pi^{-1} a_0^{-4} \int_0^{\infty} \int_0^{\pi} \int_0^{2\pi} \exp(-3\pi/2a_0) \pi^4 \sin^3 \theta \cos^2 \phi d\theta d\phi dr \\ &= 2^{-5/2} \pi^{-1} a_0^{-4} \frac{4\pi}{3} \int \exp(-3r/2a_0) r^4 dr = \frac{2^{15/2} a_0}{3^5} \end{aligned} \quad \dots(3.54)$$

The frequency of transition ω_{21} is given by

$$\omega_{21} = \frac{me^4}{32\pi^2 \epsilon_0^2 h^3} \cdot \frac{3}{4} \quad \dots(3.55)$$

Substituting these values in Eqn. (3.51), we have

$$\begin{aligned} A_{21} &= \frac{e^2}{3\epsilon_0 h \pi c^3} \cdot \frac{3^3}{4^3} \cdot \frac{m^3 e^{12}}{32^3 \pi^6 \epsilon_0^6 h^9} \cdot \frac{2^{15}}{3^{10}} \cdot \frac{16\pi^2 \epsilon_0^2 h^4}{m^2 e^4} \\ &= \frac{me^{10}}{3^8 \cdot 2^2 \pi^5 \epsilon_0^5 h^6 c^3} = 6.3 \times 10^8 \text{ s}^{-1} \end{aligned} \quad \dots(3.56)$$

The radiative life-time of the $2P$ state, therefore, is

$$\tau = 1/A_{21} = 1.6 \times 10^{-9} \text{ s.} \quad \dots(3.57)$$

3.3 QUANTUM ELECTRODYNAMICS

We will now take a stride forward and develop the second stage wherein the radiation field also will be treated quantum-mechanically. We first describe the procedure by which quantum-mechanics is applied to electromagnetic field. The transition to quantum-mechanics can be accomplished easily if the equations of classical electromagnetic theory are first put into a suitable suggestive form. To this end we will show how the electromagnetic field can be decomposed into modes each behaving like a harmonic oscillator. The quantization is then effected by the replacement of the classical harmonic oscillator equation by the corresponding quantum-mechanical equation.

3.3.1 Creation and Annihilation Operators

We will first treat the simple and familiar problem of quantum-mechanical harmonic oscillator in new terms using the operator technique.

The Hamiltonian of a one-dimensional quantum-mechanical harmonic oscillator of unit mass is

$$\hat{H} = \frac{1}{2} (\hat{p}^2 + \omega^2 \hat{q}^2) \quad \dots(3.58)$$

where the position and momentum operator \hat{q} and \hat{p} satisfy the commutation relation

$$[\hat{q}, \hat{p}] = \hat{q}\hat{p} - \hat{p}\hat{q} - i\hbar \quad \dots(3.59)$$

To find the eigenvalues of the operator \hat{H} , it is convenient to introduce two non-Hermitian operators \hat{a} and \hat{a}^\dagger such that

$$\hat{a} = (2\hbar\omega)^{-\frac{1}{2}}(\omega\hat{q} + i\hat{p}) \quad \dots(3.60)$$

$$\text{and } \hat{a}^\dagger = (2\hbar\omega)^{-\frac{1}{2}}(\omega\hat{q} - i\hat{p}) \quad \dots(3.61)$$

We find from these that

$$\begin{aligned} (i) \quad & \hat{a}^\dagger \hat{a} = (2\hbar\omega)^{-1}(\omega^2 \hat{q}^2 + \hat{p}^2 + i\omega\hat{q}\hat{p} - i\omega\hat{p}\hat{q}) \\ & = (2\hbar\omega)^{-1}(2\hat{H} - \hbar\omega) = (\hbar\omega)^{-1}(\hat{H} - (1/2)\hbar\omega) \end{aligned} \quad \dots(3.62)$$

$$\text{and } (ii) \quad \hat{a}\hat{a}^\dagger = (\hbar\omega)^{-1}(\hat{H} + (1/2)\hbar\omega) \quad \dots(3.63)$$

where we have used Eqns. (3.58) and (3.59).

$$\text{Hence, } [\hat{a}\hat{a}^\dagger] = \hat{a}\hat{a}^\dagger - \hat{a}^\dagger\hat{a} = 1 \quad \dots(3.64)$$

Equation (3.62) can be written as

$$\hat{H} = \hbar\omega(\hat{a}^\dagger\hat{a} + 1/2) \quad \dots(3.65)$$

This equation expresses the Hamiltonian operator in terms of the operators \hat{a} and \hat{a}^\dagger .

The operator $\hat{a}^\dagger\hat{a}$ plays an important role in the field theory. It is called the *number operator* and is denoted by

$$\hat{n} = \hat{a}^\dagger\hat{a} \quad \dots(3.66)$$

$$\therefore \hat{H} = \hbar\omega(\hat{a}^\dagger\hat{a} + 1/2) = \hbar\omega(\hat{n} + 1/2) \quad \dots(3.67)$$

In order to find the eigenvalues of \hat{H} , it suffices, therefore, to find the eigenvalues of \hat{n} . If $|n\rangle$ is a normalized eigenvector of the operator \hat{n} ,

$$\hat{n}|n\rangle = n|n\rangle \quad \dots(3.68)$$

where n is the eigenvalue of \hat{n} .

Hence,

$$\begin{aligned} \hat{H}|n\rangle &= \hbar\omega(\hat{n} + 1/2)|n\rangle = (n + 1/2)\hbar\omega|n\rangle \\ &= E_n|n\rangle \end{aligned} \quad \dots(3.69)$$

The eigenvalue of \hat{H} is

$$E_n = (n + 1/2)\hbar\omega \quad \dots(3.70)$$

We have yet to determine the possible values that n may have.
We can easily show that

$$[\hat{a}, \hat{n}] = \hat{a}\hat{n} - \hat{n}\hat{a} = \hat{a} \quad \dots(3.71)$$

and $[\hat{a}^\dagger, \hat{n}] = \hat{a}^\dagger\hat{n} - \hat{n}\hat{a}^\dagger = -\hat{a}^\dagger \quad \dots(3.72)$

$$\begin{aligned} \therefore \hat{n}\hat{a}^\dagger |n\rangle &= (\hat{a}\hat{n} - \hat{a}) |n\rangle \\ &= (n-1) \hat{a} |n\rangle \end{aligned} \quad \dots(3.73)$$

and $\begin{aligned} \hat{n}\hat{a}^\dagger |n\rangle &= (\hat{a}^\dagger\hat{n} + \hat{a}^\dagger) |n\rangle \\ &= (n+1) \hat{a}^\dagger |n\rangle \end{aligned} \quad \dots(3.74)$

We see that $\hat{a}|n\rangle$ and $\hat{a}^\dagger|n\rangle$ are also eigenvectors of \hat{n} with eigenvalues $n-1$ and $n+1$ respectively. The eigenvalues of the operator \hat{n} , thus, form an equally spaced ladder of unit steps ($n-1, n, n+1\dots$). The ladder can terminate only if further application of \hat{a} or \hat{a}^\dagger leads to a vector which vanishes. Now the square of $\hat{a}|n\rangle$ is

$$\langle n | \hat{a}^\dagger \hat{a} | n \rangle = \langle n | \hat{n} | n \rangle = n \langle n | n \rangle = n \quad \dots(3.75)$$

This is necessarily a non-negative quantity. Hence, none of the eigenvalues can be negative. Thus, the ladder must terminate at $n=0$. This means, the eigenvalues of \hat{n} are $n=0, 1, 2, \dots$ and correspondingly, the energy eigenvalues of \hat{H} are $(1/2)\hbar\omega, (3/2)\hbar\omega\dots$ an equally spaced ladder with spacing $\hbar\omega$.

The Eqn. (3.73) suggests that $\hat{a}|n\rangle$ is proportional to the eigenvector $|n-1\rangle$.

Let $\hat{a}|n\rangle = C_n |n-1\rangle \quad \dots(3.76)$

where C_n is the constant of proportionality.

Multiplying both sides by their Hermitian conjugates, we get

$$\langle n | \hat{a}^\dagger \hat{a} | n \rangle = \langle n-1 | C_n^* C_n | n-1 \rangle$$

i.e., $n = |C_n|^2$ or $C_n = n^{1/2} \quad \dots(3.77)$

multiplied by a phase factor which can be taken to be unity by suitable choice of the arbitrary phases in the eigenvectors. Thus

$$\hat{a}|n\rangle = n^{1/2} |n-1\rangle \quad \dots(3.78)$$

Similarly,

$$\hat{a}^\dagger |n\rangle = (n+1)^{1/2} |n+1\rangle \quad \dots(3.79)$$

Equation (3.78) implies that \hat{a} is an operator that annihilates a quantum of energy and is, therefore, called *annihilation* or *destruction* operator; while Eqn. (3.79) indicates that \hat{a}^\dagger creates a quantum of energy and is called the *creation* operator.

3.3.2 Fock States

We can write Eqn. (3.79) in the form

$$|n+1\rangle = (n+1)^{-1/2} \hat{a}^\dagger |n\rangle$$

Putting $n = 0, 1, 2, 3, \dots$, we get

$$|1\rangle = 1^{-1/2} \hat{a}^\dagger |0\rangle$$

$$|2\rangle = 2^{-1/2} \hat{a}^\dagger |1\rangle = 2^{-1/2} \cdot 1^{-1/2} \hat{a}^{\dagger^2} |0\rangle$$

$$|3\rangle = 3^{-1/2} \hat{a}^\dagger |2\rangle = 3^{-1/2} \cdot 2^{-1/2} \cdot 1^{-1/2} \hat{a}^{\dagger^3} |0\rangle$$

Hence,

$$|n\rangle = (n!)^{-1/2} \hat{a}^{\dagger^n} |0\rangle \quad \dots(3.80)$$

Thus, any excited state $|n\rangle$ can be expressed in terms of its ground state. The normalized states defined as above are called *Fock states* or occupation number states.

3.3.3 Quantization of the Field

We will first consider the electromagnetic field in free space and then take up its interaction with electrons.

The solution of Maxwell's equations (3.19) in terms of \mathbf{E} and \mathbf{H} illustrate in a simple way the properties of electromagnetic waves. They do not show, however, how the fields are generated by the time varying distribution of current and charge. The relation of radiation fields to their sources can be easily found if the fields are expressed in terms of electromagnetic potentials \mathbf{A} and ϕ .

$$\mathbf{E} = -\nabla\phi - \frac{\partial \mathbf{A}}{\partial t}; \quad \mathbf{B} = \nabla \times \mathbf{A} \quad \dots(3.81)$$

It can be shown [233] that the use of the above relations together with the Lorentz condition

$$\nabla \cdot \mathbf{A} = 0 \quad \dots(3.82)$$

in Maxwell's equations leads to the equation

$$\nabla^2 \mathbf{A} - \frac{1}{c^2} \cdot \frac{\partial^2 \mathbf{A}}{\partial t^2} = -\mu \mathbf{J} \quad \dots(3.83)$$

In free space this equation becomes

$$\nabla^2 \mathbf{A} - \frac{1}{c^2} \cdot \frac{\partial^2 \mathbf{A}}{\partial t^2} = 0 \quad \dots(3.84)$$

We assume that the field is enclosed in a cavity of volume $\mathbf{V} = \mathbf{L}^3$ satisfying certain boundary conditions on the walls. The vector potential in the cavity can be expanded in a Fourier series.

$$\mathbf{A} = \sum_k \left\{ \mathbf{A}_k(t) \exp(i\mathbf{k} \cdot \mathbf{r}) + \mathbf{A}_k^*(t) \exp(-i\mathbf{k} \cdot \mathbf{r}) \right\} \quad \dots(3.85)$$

In the Coulomb gauge the vector potential has to satisfy Eqn. (3.82). This is possible if

$$\mathbf{k} \cdot \mathbf{A}_k(t) = \mathbf{k} \cdot \mathbf{A}_k^*(t) = 0 \quad \dots(3.86)$$

For each \mathbf{k} there will be two independent directions of $\mathbf{A}_k(t)$.

Each component of \mathbf{A} must satisfy Eqn. (3.84).

$$\therefore k^2 \mathbf{A}_k(t) + \frac{1}{c^2} \cdot \frac{\partial^2 \mathbf{A}_k(t)}{\partial t^2} = 0 \quad \dots(3.87)$$

$$\text{i.e., } \frac{\partial^2 \mathbf{A}_k(t)}{\partial t^2} + \omega_k^2 \mathbf{A}_k(t) = 0 \quad (\because \omega_k = ck) \quad \dots(3.88)$$

which is a simple harmonic equation.

One can easily verify that

$$A_k(t) = A_k \exp(-i\omega_k t) \quad \dots(3.89)$$

is a solution of Eqn. (3.88).

Therefore, from Eqn. (3.85)

$$\mathbf{A} = \sum_k \left\{ \mathbf{A}_k \exp(-i\omega_k t + i\mathbf{k} \cdot \mathbf{r}) + \mathbf{A}_k^* \exp(i\omega_k t - i\mathbf{k} \cdot \mathbf{r}) \right\} \quad \dots(3.90)$$

Hence,

$$\begin{aligned} \mathbf{E}_k &= \nabla \phi - \frac{d\mathbf{A}_k}{dt} = -\frac{\partial \mathbf{A}_k}{\partial t} \quad (\because \phi = 0) \\ &= i\omega_k \left\{ \mathbf{A}_k \exp(-i\omega_k t + i\mathbf{k} \cdot \mathbf{r}) - \mathbf{A}_k^* \exp(i\omega_k t - i\mathbf{k} \cdot \mathbf{r}) \right\} \end{aligned} \quad \dots(3.91)$$

$$\begin{aligned} \text{and } \mathbf{H}_k &= \frac{\mathbf{B}}{\mu_0} = \frac{1}{\mu_0} \nabla \times \mathbf{A}_k \\ &= \frac{1}{\mu_0} \mathbf{k} \times \left\{ \mathbf{A}_k \exp(-i\omega_k t + i\mathbf{k} \cdot \mathbf{r}) - \mathbf{A}_k^* \exp(i\omega_k t - i\mathbf{k} \cdot \mathbf{r}) \right\} \end{aligned} \quad \dots(3.92)$$

The last two equations lead to the relation

$$H = \left(\frac{\epsilon_0}{\mu_0} \right)^{1/2} E \quad \dots(3.93)$$

The energy contained in an electromagnetic field is given by the integral $(1/2) \int (\epsilon_0 E^2 + \mu_0 H^2) dV$. Since the variation in energy occurring during a cycle is not susceptible to measurement, it is convenient to average the field energy over a cycle of oscillation. The cycle averaged energy content of a single mode k is

$$\bar{E}_k = (1/2) \int (\epsilon_0 \bar{E}_k^2 + \mu_0 \bar{H}_k^2) dV \quad \dots(3.94)$$

where the bars denote the cycle average.

Substituting Eqns. (3.91) and (3.92) in Eqn. (3.94) and evaluating the time average, we have

$$\bar{E}_k = 2\epsilon_0 V \omega_k^2 \mathbf{A}_k \cdot \mathbf{A}_k^* \quad \dots(3.95)$$

We introduce here two new variables Q_k and P_k such that

$$\mathbf{A}_k = (4\epsilon_0 V \omega_k^2)^{-1/2} (\omega_k Q_k + i P_k) \hat{\mathbf{e}}_k \quad \dots(3.96)$$

and

$$\mathbf{A}_k^* = (4\epsilon_0 V \omega_k^2)^{-1/2} (\omega_k Q_k - i P_k) \hat{\mathbf{e}}_k \quad \dots(3.97)$$

where Q_k , P_k are scalar quantities and $\hat{\mathbf{e}}_k$ is unit polarization vector for the mode. Substituting these in Eqn. (3.95), we get

$$\bar{E}_k = (1/2) (\omega_k^2 Q_k^2 + P_k^2) \quad \dots(3.98)$$

This is the usual form of the energy of a harmonic oscillator of unit mass. The electromagnetic field, thus, has been decomposed into modes each behaving like a harmonic oscillator. We can thus visualise the electromagnetic field as consisting of an infinite set of harmonic oscillators. The complete Hamiltonian for the cavity is found by summing over k and the two independent directions of $\hat{\mathbf{e}}_k$.

The two quantities Q_k and P_k may be called a generalized mode ‘position’ coordinate and a generalized mode ‘momentum’ coordinate respectively. The quantization of the field is now straightforward. We have only to replace Q_k and P_k by the operators \hat{q}_k and \hat{p}_k respectively.

The energy of each oscillator can increase or decrease by a quantum of energy $\hbar\omega_k$ which is the energy of a photon of wave vector k . This means the energy of an oscillator corresponding to the k th mode is determined by the number of photons n_k excited in the cavity. The state of the total field is represented by

$$|\{n_k\}\rangle = |n_{k_1}, n_{k_2}, \dots, n_{k_i}, \dots\rangle \quad \dots(3.99)$$

where on the left-hand side we have used a short-hand notation for the field.

Since the different cavity modes are independent, we can as well represent the field as

$$|\{n_k\}\rangle = |n_{k_1}\rangle |n_{k_2}\rangle \dots |n_{k_i}\rangle \dots \quad \dots(3.100)$$

Considering the radiation field as made up of a number of harmonic oscillators, its energy is

$$E = \sum_k E_k = \sum_k n_k \hbar \omega_k \quad \dots(3.101)$$

Note that the operators \hat{a}_k and \hat{a}_k^\dagger affect only the photons in mode k and, hence, the effect of any of these operators on $|\{n_k\}\rangle$ is to change the value of the label n_k by one unit, leaving all other labels unaltered. Thus,

$$\hat{a}_{k_1} |\{n_k\}\rangle = n_{k_1}^{1/2} |n_{k_1}, n_{k_2}, \dots, n_{k_l} - 1, \dots\rangle \quad \dots(3.102)$$

$$\text{and} \quad \hat{a}_k^\dagger |\{n_k\}\rangle = (n_{k_1} + 1)^{1/2} |n_{k_1}, n_{k_2}, \dots, n_{k_l} + 1, \dots\rangle \quad \dots(3.103)$$

The vector potentials \mathbf{A} and \mathbf{A}_k^* in the operator formalism are given by

$$\begin{aligned} \mathbf{A}_k &= \left(4\epsilon_0 V \omega_k^2\right)^{-1/2} (\omega_k Q_k + i P_k) \hat{\mathbf{e}}_k \\ &\rightarrow \left(4\epsilon_0 V \omega_k^2\right)^{-1/2} (\omega_k \hat{q}_k + i \hat{p}_k) \hat{\mathbf{e}}_k \\ &= \left(\frac{\hbar}{2\epsilon_0 V \omega_k}\right)^{1/2} \hat{a}_k \hat{\mathbf{e}}_k \end{aligned} \quad \dots(3.104)$$

$$\text{and} \quad \mathbf{A}_k^* = \left(\frac{\hbar}{2\epsilon_0 V \omega_k}\right)^{1/2} \hat{a}_k^\dagger \hat{\mathbf{e}}_k \quad \dots(3.105)$$

where we have used Eqns. (3.60) and (3.61).

The operator corresponding to the total vector potential \mathbf{A} can be found by substituting these in Eqn. (3.85). Thus

$$\hat{\mathbf{A}} = \sum \left(\frac{\hbar}{2\epsilon_0 V \omega_k}\right)^{1/2} \left\{ \hat{a}_k \exp(-i\omega_k t + i\mathbf{k} \cdot \mathbf{r}) - \hat{a}_k^\dagger \exp(i\omega_k t - i\mathbf{k} \cdot \mathbf{r}) \right\} \hat{\mathbf{e}}_k \quad \dots(3.106)$$

The electric and magnetic field operators are found by substituting Eqns. (3.104) and (3.105) in Eqns. (3.91) and (3.92).

$$\hat{\mathbf{E}}_k = i \left(\frac{\hbar \omega_k}{2\epsilon_0 V}\right)^{1/2} \left\{ \hat{a}_k \exp(-i\omega_k t + i\mathbf{k} \cdot \mathbf{r}) - \hat{a}_k^\dagger \exp(i\omega_k t - i\mathbf{k} \cdot \mathbf{r}) \right\} \hat{\mathbf{e}}_k \quad \dots(3.107)$$

$$\begin{aligned} \hat{\mathbf{H}}_k &= i \left(\frac{\hbar c^2}{2\mu_0 V \omega_k}\right)^{1/2} \mathbf{k} \times \left\{ \hat{a}_k \exp(-i\omega_k t + i\mathbf{k} \cdot \mathbf{r}) - \hat{a}_k^\dagger \exp(i\omega_k t - i\mathbf{k} \cdot \mathbf{r}) \right\} \hat{\mathbf{e}}_k \\ &\quad \dots(3.108) \end{aligned}$$

The field energy content in the new notation becomes

$$\bar{\epsilon}_k = \frac{1}{2} \overline{\langle n_k | \epsilon_0 \hat{\mathbf{E}}_k \cdot \hat{\mathbf{E}}_k + \mu_0 \hat{\mathbf{H}}_k \cdot \hat{\mathbf{H}}_k | n_k \rangle} dV \quad \dots(3.109)$$

where the bar denotes the cycle-average.

It is a simple matter to prove

$$\begin{aligned} \epsilon_0 \langle n_k | \hat{\mathbf{E}}_k \cdot \hat{\mathbf{E}}_k | n_k \rangle &= \mu_0 \langle n_k | \hat{\mathbf{H}}_k \cdot \hat{\mathbf{H}}_k | n_k \rangle \\ &= \frac{\hbar \omega_k}{V} \left(n_k + \frac{1}{2} \right) \end{aligned} \quad \dots(3.110)$$

$$\therefore \bar{\epsilon}_k = \left(n_k + \frac{1}{2} \right) \hbar \omega_k \quad \dots(3.111)$$

We see that the quantization procedure leads to the same mode energy expression as that of the usual harmonic oscillator.

You were, perhaps, puzzled at the choice of the numerical factors in the expressions Eqns. (3.96) and (3.97). It should now be clear that the choice was governed by the requirement that the mode energy should have the harmonic oscillator form both in classical and quantum mechanical theories.

The Hamiltonian for the total electromagnetic field, obviously, is

$$\hat{H} = \sum_k \hbar \omega_k \left(\hat{a}_k^\dagger \hat{a}_k + \frac{1}{2} \right) \text{ [see eqn.(3.65)]} \quad \dots(3.112)$$

and its energy eigenvalue is

$$\bar{\epsilon} = \sum_k \bar{\epsilon}_k = \sum_k \left(n_k + \frac{1}{2} \right) \hbar \omega_k \quad \dots(3.113)$$

3.3.4 Zero-point Energy

If no photons are excited in any of the field modes

$$n_{k_1} = n_{k_2} = \dots = 0 \quad \dots(3.114)$$

Such a state is known as the *vacuum state* of the field. An interesting feature of the vacuum state is that although no excitations are present, the energy of the state, as given by Eqn. (3.113), is

$$\bar{\epsilon}_0 = \sum_k \frac{1}{2} \hbar \omega_k \quad \dots(3.115)$$

This is called the *zero-point energy* of the field and is equal to the sum of the energies of the ground state of the harmonic oscillators associated with all the field modes. This interesting property leads, however, to an awkward feature of the quantized electromagnetic field.

The number of modes per unit volume of cavity having this wave vector in the range k to $k + dk$ is given by (see Chapter 6)

$$\rho_k dk = \frac{k^2 dk}{\pi^2} \quad \dots(3.116)$$

In terms of ω , this relation becomes

$$\rho_\omega d\omega = \frac{\omega^2 d\omega}{\pi^2 c^3} \quad \dots(3.117)$$

Using these results, we can convert summation over k or ω to integration

$$\sum_k \rightarrow \int \frac{V k^2}{\pi^2} dk \rightarrow \int \frac{V \omega^2}{\pi^2 c^3} d\omega \quad \dots(3.118)$$

Hence, the zero-point energy Eqn. (3.115) can be written as

$$\bar{\epsilon}_0 = \int \frac{1}{2} \hbar \omega_k \cdot \frac{V \omega_k^2}{\pi^2 c^3} d\omega_k = \int \frac{V \hbar \omega_k^3}{2 \pi^2 c^3} d\omega_k \quad \dots(3.119)$$

Since there is no upper bound to ω_k , the integral is highly divergent and the zero-point energy is infinite—a feature difficult to explain. Fortunately, however, we can by-pass this point since in the majority of experiments we are concerned only with the excitation energy of the field above the zero-point energy. That is with the energy given by

$$\bar{\epsilon}' = \bar{\epsilon} - \bar{\epsilon}_0 = \sum_k \bar{\epsilon}'_k = \sum_k n_k \hbar \omega_k \quad \dots(3.120)$$

It is, therefore, convenient to subtract the zero-point energy from the expression for the Hamiltonian and consider the system defined by the Hamiltonian

$$\hat{H} = \sum_k \hbar \omega_k \hat{a}_k^\dagger \hat{a}_k. \quad \dots(3.121)$$

3.3.5 Coherent-state Description of the Electromagnetic Field

In this section we show that in the quantum theory of the electromagnetic field there exist quantum coherent states in which the field satisfies the full coherence conditions. These states have properties similar to those of classical electromagnetic wave. The coherent states were first introduced by Schrödinger [338A] and were studied by Klauder [216] and others. Glauber [146 – 48] used them to study the quantum coherence of optical fields.

Consider the eigenvalue equation of the annihilation operator \hat{a}

$$\hat{a}|\alpha\rangle = \alpha|\alpha\rangle \quad \dots(3.122)$$

We can expand $|\alpha\rangle$ in terms of the kets $|n\rangle$

$$\text{i.e., } |\alpha\rangle = \sum_n C_n |n\rangle \quad \dots(3.123)$$

The left-hand side of Eqn. (3.122), therefore, is

$$\begin{aligned} \hat{a}|\alpha\rangle &= \sum_n C_n \hat{a}|n\rangle = \sum_n C_n n^{1/2} |n-1\rangle \\ &= (C_1 \cdot 1^{1/2} |0\rangle + C_2 \cdot 2^{1/2} |1\rangle + C_3 \cdot 3^{1/2} |2\rangle + \dots) \end{aligned}$$

where we have used Eqn. (3.78).

The right-hand side is

$$\begin{aligned} \alpha|\alpha\rangle &= \alpha \sum_n C_n |n\rangle \\ &= \alpha \{ C_0 |0\rangle + C_1 |1\rangle + C_2 |2\rangle + C_3 |3\rangle + \dots \} \\ \therefore &\quad \alpha \{ C_0 |0\rangle + C_1 |1\rangle + C_2 |2\rangle + \dots \} \\ &= C_1 \cdot 1^{1/2} |0\rangle + C_2 \cdot 2^{1/2} |1\rangle + C_3 \cdot 3^{1/2} |2\rangle + \dots \end{aligned}$$

Comparing the coefficients, we get

$$\begin{aligned} C_1 &= \alpha \cdot 1^{-1/2} C_0 \\ C_2 &= 2^{-1/2} \alpha C_1 = 2^{-1/2} \cdot 1^{1/2} \alpha^2 C_0 \\ C_3 &= 3^{-1/2} \alpha C_2 = 3^{-1/2} \cdot 2^{-1/2} \cdot 1^{-1/2} \alpha^3 C_0 \end{aligned}$$

Generalizing,

$$C_n = (n!)^{-1/2} \alpha^n C_0$$

Hence,

$$|\alpha\rangle = C_0 \sum_n \frac{\alpha^n}{(n!)^{1/2}} |n\rangle$$

Normalisation of $|\alpha\rangle$ gives

$$\begin{aligned} \langle \alpha | \alpha \rangle &= |C_0|^2 \sum_m \sum_n \frac{\alpha^m \alpha^n}{(n!)^{1/2} (m!)^{1/2}} \langle m | n \rangle \\ &= |C_0|^2 \sum_n \frac{(|\alpha|^2)^n}{n!} = |C_0|^2 \exp(|\alpha|^2) = 1 \end{aligned}$$

Hence,

$$C_0 = \exp\left(-\frac{1}{2} |\alpha|^2\right)$$

Using this value of C_0 , we can write

$$|\alpha\rangle = \exp\left(-\frac{1}{2}|\alpha|^2\right) \sum_n \frac{\alpha^n}{(n!)^{1/2}} |n\rangle \quad \dots(3.124)$$

These eigen states of the annihilation operator \hat{a} are known as *coherent states*. The eigenvalue α is in general a complex number since \hat{a} is not a Hermitian operator. Coherent states, thus, form a double continuum corresponding to the continuous range of values of the real and imaginary parts. The Eqn. (3.122) shows that since the annihilation operator \hat{a} does not change the state $|a\rangle$, it must contain uncertain number of photons.

Note that $|a\rangle$ is not an eigen state of the creation operator \hat{a}^\dagger .

We shall now discuss some of the properties of the coherent states:

(1) The expectation value of the number operator \hat{n} is given by

$$\begin{aligned} \langle \alpha | \hat{n} | \alpha \rangle &= \exp(-|\alpha|^2) \sum_m \sum_n \frac{\alpha^m}{(m!)^{1/2}} \cdot \frac{\alpha^n}{(n!)^{1/2}} n \langle m | n \rangle \\ &= \exp(-|\alpha|^2) \sum_{n=1,2,\dots} \frac{n |\alpha|^{2n}}{n!} \\ &= \exp(-|\alpha|^2) |\alpha|^2 \sum_{n=0,1,2} \frac{|\alpha|^{2n}}{n!} \\ &= |\alpha|^2 = \langle n \rangle \end{aligned} \quad \dots(3.125)$$

This shows that the mean number of photons in the mode is $|\alpha|^2$.

(2) From Eqn. (3.124) we see that

$$\langle n | \alpha \rangle = \exp\left(-\frac{1}{2}|\alpha|^2\right) \frac{\alpha^n}{(n!)^{1/2}}$$

This gives

$$|\langle n | \alpha \rangle|^2 = \frac{|\alpha|^{2n}}{n!} \exp(-|\alpha|^2)$$

Since

$$\langle n \rangle = |\alpha|^2$$

$$|\langle n | \alpha \rangle|^2 = \frac{\langle n \rangle^n}{n!} \exp(-\langle n \rangle) \quad \dots(3.126)$$

This is a Poisson distribution. Thus the probability that there are n photons in the coherent state is given by the Poisson distribution.

(3) The scalar product of two coherent states $|\alpha\rangle$ and $|\beta\rangle$ is

$$\langle \alpha | \beta \rangle = \exp\left(-\frac{1}{2}|\alpha|^2\right) \exp\left(-\frac{1}{2}|\beta|^2\right) \sum_n \sum_m \frac{\alpha^n \beta^m}{(n!m!)^{1/2}} \langle n | m \rangle$$

$$\begin{aligned}
 &= \exp\left(-\frac{1}{2}|\alpha|^2 - \frac{1}{2}|\beta|^2\right) \exp(\alpha^*\beta) \\
 &= \exp\left(-\frac{1}{2}|\alpha|^2 - \frac{1}{2}|\beta|^2 + \alpha^*\beta\right) \\
 \therefore |\langle\alpha|\beta\rangle|^2 &= \exp(-|\alpha - \beta|^2) \quad \dots(3.127)
 \end{aligned}$$

This means that the coherent states are not orthogonal. However, if $|\alpha - \beta| \gg 1$ the states $|\alpha\rangle$ and $|\beta\rangle$ become approximately orthogonal.

(4) We can transform Eqn. (3.60) and (3.61) to express the canonical variables \hat{q} and \hat{p} in the form

$$\hat{q} = \left(\frac{\hbar}{2\omega}\right)^{1/2} (\hat{a} + \hat{a}^\dagger) \quad \dots(3.128)$$

$$\hat{p} = -i\left(\frac{\hbar\omega}{2}\right)^{1/2} (\hat{a} - \hat{a}^\dagger) \quad \dots(3.129)$$

Using the relations

$$\begin{aligned}
 \hat{a}|\alpha\rangle &= a|\alpha\rangle \\
 \langle\alpha|\hat{a}^\dagger &= \langle\alpha|a^* \quad \dots(3.130)
 \end{aligned}$$

We obtain for the expectation values of \hat{q} and \hat{p} in the coherent states

$$\langle\hat{q}\rangle = \left(\frac{\hbar}{2\omega}\right)^{1/2} (\alpha + \alpha^*); \langle\hat{p}\rangle = -i\left(\frac{\hbar\omega}{2}\right)^{1/2} (\alpha - \alpha^*) \quad \dots(3.131)$$

Hence,

$$\langle(\Delta q)^2\rangle = \frac{\hbar}{2\omega}; \langle(\Delta p)^2\rangle = \frac{\hbar\omega}{2} \quad \dots(3.132)$$

where,

$$\begin{aligned}
 (\Delta q)^2 &= \langle\alpha|q^2|\alpha\rangle - \langle\alpha|q|\alpha\rangle^2 \\
 (\Delta p)^2 &= \langle\alpha|p^2|\alpha\rangle - \langle\alpha|p|\alpha\rangle^2 \\
 \therefore (\hat{q})^2 - (\hat{p})^2 &= \frac{\hbar^2}{4} \quad \dots(3.133)
 \end{aligned}$$

This shows that the coherent states are closest to the classical states.

(5) *Time Development of the Coherent States:* For simplicity, consider a single mode field with renormalized Hamiltonian $\hat{H} = \hbar\omega\hat{a}^\dagger\hat{a}$. The time dependence of the coherent states $|\alpha(t)\rangle$ is given by Schrödinger equation

$$i\hbar\frac{\partial|\alpha(t)\rangle}{\partial t} = \hat{H}|\alpha(t)\rangle \quad \dots(3.134)$$

If initially at $t = 0$, $|\alpha(0)\rangle = |\alpha\rangle$ the solution of Eqn. (3.134) can be written as

$$|\alpha(t)\rangle = \exp\left(-\frac{i\hat{H}t}{\hbar}\right)|\alpha\rangle \quad \dots(3.135)$$

and for \hat{H} given above

$$|\alpha(t)\rangle = |\alpha \exp(-i\omega t)\rangle \quad \dots(3.136)$$

Thus, for the Hamiltonian considered above the coherent states remain coherent at all times.

The basic property of coherence states is that they have a known phase but uncertain number of particles; while Fock states have a definite number of particles but uncertain phase. Hence, in quantum electrodynamics Fock states can approximately describe the interaction of several particles, whereas, coherent states can describe cooperative phenomena such as coherence.

3.3.6 Interaction of Radiation with Matter

The Hamiltonian for the atom radiation system can be written as

$$\hat{H} = \hat{H}_a + \hat{H}_R + \hat{H}_I \quad \dots(3.137)$$

where \hat{H}_a is the Hamiltonian of the isolated atom, \hat{H}_R is the Hamiltonian of the free radiation field and \hat{H}_I is the Hamiltonian for the interaction of the atom with the radiation field. We have seen that the radiation part of the Hamiltonian, viz., \hat{H}_R can be expressed in terms of the photon creation and destruction operators Eqn. (3.121). If the entire Hamiltonian could be expressed as products of algebraic magnitudes with creation and destruction operators, it would be easy to deal with the complicated radiation processes involving interaction of light and atoms. Let us, therefore, see how \hat{H}_a and \hat{H}_I can be cast into a form involving creation and destruction operators.

Let $|i\rangle$ be an eigen state of the Hamiltonian \hat{H}_a with eigen value $\hbar\omega_i$, i.e.,

$$\hat{H}_a|i\rangle = \hbar\omega_i|i\rangle \quad \dots(3.138)$$

The closure theorem of quantum-mechanics states [101] that

$$\sum_i |i\rangle\langle i| = 1 \quad \dots(3.139)$$

where the sum runs over all the eigen-states of \hat{H}_a . Using this theorem twice leads to the identity

$$\hat{H}_a = \sum_i |i\rangle\langle i| \hat{H}_a \sum_j |j\rangle\langle j| \quad \dots(3.140)$$

Now

$$\begin{aligned}\langle i | \hat{H}_a | j \rangle &= \langle i | \hbar \omega_j | j \rangle \\ &= \hbar \omega_j \delta_{ij} \quad \dots(3.141)\end{aligned}$$

where we have used Eqn. (3.138) and the orthonormality of the eigen-states.

Therefore,

$$\hat{H}_a = \sum_i \hbar \omega_i |i\rangle\langle i| \quad \dots(3.142)$$

Let us now digress a little to consider the effect of the general combination $|i\rangle\langle j|$ when applied to an eigen-state $|l\rangle$.

$$|j\rangle\langle j|l\rangle = |l\rangle\delta_{jl} \quad \dots(3.143)$$

This shows that the combination $|i\rangle\langle j|$ when applied to an eigen-state $|l\rangle$ different from $|j\rangle$ gives zero; but if $|l\rangle$ is the same as $|j\rangle$, it changes the state to $|i\rangle$. Thus $|i\rangle\langle j|$ is an operator whose application to an atom in state $|j\rangle$, removes it from that state and puts it in the state $|i\rangle$; or, in other words, it destroys atomic state $|j\rangle$ and creates atomic state $|i\rangle$. It must be noted, however, that since electrons cannot be created nor destroyed but only shifted from one state to another, the atomic operator must always occur in creation-destruction pair. The notation Eqn. (3.142) for the Hamiltonian \hat{H}_a is now self-explanatory.

'Quantization' as we know is strictly the restriction of the values of certain variables to discrete values. The transition from classical particle mechanics to the Schrödinger equation, which is the consequence of regarding the particle variables as operators, is called the 'first quantization'. The fields that appear in this process are now to be subjected to the same process and this is called 'second quantization'. The transformation of \hat{H}_a to the form Eqn. (3.142), in which the Hamiltonian is expressed in terms of the solutions of the energy eigen value problem assumed to have been determined is known as second quantization of the Hamiltonian.

We have now to express the interaction Hamiltonian \hat{H}_I in terms of creation and destruction operators.

The form of interaction Hamiltonian \hat{H}_I depends on the nature of the interaction. Besides the electric dipole interaction, it may have contribution from the electric-quadrupole interaction and the magnetic-dipole interaction. Normally, a quadrupole moment is a bad radiator, because the radiation waves from its two opposite dipoles interfere destructively. But, if the wavelength is of the same order as the atomic size, the quadrupole moment can interact strongly as well. Even so, the quadrupole and magnetic dipole moments generally interact very weakly compared to electric dipole moment and, hence, we should consider here only the contribution of the electric-dipole interaction.

Therefore

$$\hat{H}_I = \hat{H}_{ED} = e \sum_j \mathbf{r}_j \cdot \sum_k \mathbf{E}_k = e \mathbf{D} \cdot \sum_k \mathbf{E}_k \quad \dots(3.144)$$

Use of closure theorem twice establishes the identity

$$\begin{aligned} \mathbf{D} &\equiv \sum_i |i\rangle\langle i| \mathbf{D} \sum_j |j\rangle\langle j| \\ &= \sum_{i,j} \mathbf{D}_{ij} |i\rangle\langle j| \end{aligned} \quad \dots(3.145)$$

We will use this identity in the second quantization of \hat{H}_{ED} .

$$\hat{H}_{ED} = e \sum_k \sum_{i,j} \mathbf{E}_k \cdot \mathbf{D}_{ij} |i\rangle\langle j| \quad \dots(3.146)$$

Inserting the values of E_k from Eqn. (3.107) with r set equal to zero

$$\begin{aligned} \hat{H}_{ED} &= ie \sum_k \sum_{i,j} \left(\frac{\hbar \omega_k}{2\epsilon_0 V} \right)^{1/2} \hat{\mathbf{e}}_k \cdot \mathbf{D}_{ij} (\hat{a}_k \exp(-i\omega_k t) \\ &\quad - \hat{a}_k^\dagger \exp(i\omega_k t)) |i\rangle\langle j| \end{aligned} \quad \dots(3.147)$$

We, thus, have the complete Hamiltonian for the atom-radiation system in the second quantized notation.

Let us now consider some of the interaction processes allowed by \hat{H}_{ED} as given by Eqn. (3.147).

Suppose there are only two states $|a\rangle$ and $|b\rangle$, the latter being at a higher energy level than the former, i.e., $\hbar\omega_b > \hbar\omega_a$. Since i or j in Eqn. (3.147) can be either a or b

$$\begin{aligned} \hat{H}_{ED} &= ie \sum_k \left(\frac{\hbar \omega_k}{2\epsilon_0 V} \right)^{1/2} \hat{\mathbf{e}}_k \cdot \mathbf{D}_{ab} (\hat{a}_k \exp(-i\omega_k t) \\ &\quad - \hat{a}_k^\dagger \exp(i\omega_k t)) (|a\rangle\langle b| + |b\rangle\langle a|) \end{aligned} \quad \dots(3.148)$$

We have assumed here that the wave-functions corresponding to the states $|a\rangle$ and $|b\rangle$ are real so that

$$\mathbf{D}_{ab} = \mathbf{D}_{ba} \quad \dots(3.149)$$

When the brackets are multiplied out, we get four distinct terms representing four different interaction processes. The terms involve the creation and destruction operators in the order shown below:

$$\begin{array}{ll} (i) \quad \hat{a}_k |a\rangle\langle b|, & (ii) \quad \hat{a}_k |b\rangle\langle a|, \\ (iii) \quad \hat{a}_k^\dagger |a\rangle\langle b|, & (iv) \quad \hat{a}_k^\dagger |b\rangle\langle a|. \end{array} \quad \dots(3.150)$$

Consider process (ii). The order of operators in this process indicates the destruction of state $|a\rangle$ and creation of the state $|b\rangle$, i.e., excitation of the atom

from state $|a\rangle$ to the state $|b\rangle$ by absorption of a photon; while process (iii) represents the decaying of the atom from state $|b\rangle$ to state $|a\rangle$ by the emission of a photon. The processes (i) and (iv) do not correspond to allowed absorption and emission processes. We are not interested in these non-energy-conserving processes. They, however, play a role in some nonlinear processes which we will discuss in Chapter 14.

We shall now show how the rates of absorption and emission are calculated using the second quantized interaction Hamiltonian.

Suppose n_k photons are present in the mode k of the field when the atom is in the state $|a\rangle$. The state of the combined atom-radiation system is denoted by $|n_k, a\rangle$. The matrix element for the photon absorption corresponding to process (ii) above is

$$\begin{aligned} & \langle n_k - 1, b | \hat{H}_{ED} | n_k, a \rangle \\ &= ie \left(\frac{\hbar\omega_k}{2\varepsilon_0 V} \right)^{1/2} \hat{\mathbf{e}}_k \cdot \mathbf{D}_{ab} \exp(-i\omega_k t) \langle n_k - 1, b | \hat{a}_k | n_k, a \rangle \quad \dots (3.151) \end{aligned}$$

Here, $|n_k - 1, b\rangle$ represents the final state of the system, in which the atom goes to state $|b\rangle$ by absorption of a photon which accounts for the effect of the operator $|b\rangle\langle a|$.

Using Eqn. (3.78), the above relation changes to

$$\langle n_k - 1, b | \hat{H}_{ED} | n_k, a \rangle = ie \left(\frac{\hbar\omega_k}{2\varepsilon_0 V} \right)^{1/2} \hat{\mathbf{e}}_k \cdot \mathbf{D}_{ab} \exp(-i\omega_k t) n_k^{1/2} \quad \dots (3.152)$$

Similarly for emission we have process (iii)

$$\begin{aligned} \langle n_k + 1, a | \hat{H}_{ED} | n_k, b \rangle &= -ie \left(\frac{\hbar\omega_k}{2\varepsilon_0 V} \right)^{1/2} \hat{\mathbf{e}}_k \cdot \mathbf{D}_{ab} \exp(i\omega_k t) (n_k + 1)^{1/2} \\ &\quad \dots (3.153) \end{aligned}$$

Using the time-dependent perturbation theory with the matrix elements given above, transition rates for absorption and emission of photons can be calculated on the same lines as in the case of semiclassical theory.

You may recall that in the semiclassical theory, in order to find the probability of transition to the state b , $|C_b(t)|^2$, we had to integrate

$$C_b(t) = \frac{1}{i\hbar} \int_0^{t'} \exp(-i\omega_{ab}t) \hat{H}_{ba} dt \quad \dots (3.154)$$

The matrix element \hat{H}_{ba} used in the integration was

$$\hat{H}_{ba} = \langle u_b | \sum_h e_{r_j} \cdot \mathbf{E}_0 \cos \omega t | u_a \rangle$$

$$= eE_0 X_{ba} \cos \omega t = eE_0 X_{ba} \frac{e^{i\omega t} + e^{-i\omega t}}{2}$$

We had further shown that the contribution of the term involving $e^{i\omega t}$ was negligible and, hence, the effective matrix element was

$$\hat{H}_{ba} = \frac{eE_0 X_{ba}}{2} \exp(-i\omega t) \quad \dots(3.155)$$

The final result obtained for the transition probability per unit time was

$$\frac{1}{t} |C_b(t)|^2 = \frac{\pi e^2 E_0^2 |X_{ba}|^2}{2\hbar^2} \delta(\omega_{ba} - \omega) \quad \dots(3.156)$$

The matrix element in the present treatment is given by Eqn. (3.152).

Comparison of Eqns. (3.155) and (3.152) shows that the two matrix elements have the same form of time dependence, the only difference being that

instead of the factor $\frac{eE_0 X_{ba}}{2}$ which appears in the semi-classical expression,

we have $ie(\hbar\omega_k/2\epsilon_0 V)^{1/2} \hat{\mathbf{e}}_k \cdot \mathbf{D}_{ba} n_k^{1/2}$ in the new expression. The transition probability sought, therefore, can be found by replacing X_{ba} in Eqn. (3.156) by $(2ieE_0)(\hbar\omega_k/2\epsilon_0 V)^{1/2} \hat{\mathbf{e}}_k \cdot \mathbf{D}_{ba} n_k^{1/2}$ and ω by ω_k .

Thus,

$$\frac{1}{t} |C_b(t)|^2 = \frac{\pi e^2 |\hat{\mathbf{e}}_k \cdot \mathbf{D}_{ba}|^2 \hbar\omega_k n_k}{\hbar^2 \epsilon_0 V} \delta(\omega_{ba} - \omega_k) \quad \dots(3.157)$$

$$= \frac{\pi e^2 |\hat{\mathbf{e}}_k \cdot \mathbf{D}_{ba}|^2 \epsilon'_k}{\hbar^2 \epsilon_0 V} \delta(\omega_{ba} - \omega_k) \quad \dots(3.158)$$

where we have put $\epsilon'_k = n_k \hbar\omega_k$. The transition rate, thus is proportional to the number of photons n_k present in the beam.

Using the relation $\bar{\epsilon}'_k = V \int \rho(\omega_k) d\omega_k$ and averaging the random orientations of \mathbf{D}_{ba} as in Sec. 3.1, we have in terms of Einstein coefficients

$$\begin{aligned} B_{ab}\rho(\omega_{ba}) &= \frac{1}{t} |C_b(t)|^2 = \frac{\pi e^2 |\hat{\mathbf{e}}_k \cdot \mathbf{D}_{ba}|^2}{\hbar^2 \epsilon_0 V} \int V \rho(\omega_k) \delta(\omega_{ba} - \omega_k) d\omega_k \\ &= \frac{\pi e^2 |D_{ba}|^2}{3\epsilon_0 \hbar^2} \rho(\omega_{ba}) \end{aligned} \quad \dots(3.159)$$

$$\text{Therefore, } B_{ab} = \frac{\pi e^2 |D_{ba}|^2}{3\epsilon_0 \hbar^2} \quad [\text{see Eqn. (3.47)}] \quad \dots(3.160)$$

Assuming that the atom is initially in its excited state $|b\rangle$ at time $t = 0$, using Eqn.(3.153) and following the same line of calculations as for the absorption

process, we arrive at the expression for the probability that the atom has decayed into state $|a\rangle$ with emission of a photon, viz.

$$\begin{aligned} \frac{1}{t} |C_a(t)|^2 &= \frac{\pi e^2 \omega_k}{\hbar \epsilon_0 V} |\hat{\mathbf{e}}_k \cdot \mathbf{D}_{ba}|^2 (n_k + 1) \delta(\omega_{ba} - \omega_k) \\ &= \frac{\pi e^2 \omega_k}{\hbar \epsilon_0 V} |\hat{\mathbf{e}}_k \cdot \mathbf{D}_{ba}|^2 n_k \delta(\omega_{ba} - \omega_k) \\ &\quad + \frac{\pi e^2 \omega_k}{\hbar \epsilon_0 V} |\hat{\mathbf{e}}_k \cdot \mathbf{D}_{ba}|^2 \delta(\omega_{ba} - \omega_k) \quad \dots(3.161) \end{aligned}$$

The first term on the right-hand side gives a rate proportional to n_k the number of photons already present and, hence, corresponds to stimulated emission. This term is identical to (3.157), which shows that the rate of stimulated emission is equal to the rate of photon absorption. In other words, it leads to the equality of Einstein coefficients,

$$B_{ab} = B_{ba} \quad \dots(3.162)$$

expected for a pair of non-degenerate states. It should be evident from (3.153) that the photon emitted in the stimulated process has a wave vector \mathbf{k} and polarization direction the same as that of n_k photons already present. Thus, when stimulated emission takes place, the radiated light wave has a definite phase relation to the oscillation of the atomic wave-function, which itself is locked in phase to the initial wave. Hence, if there is an avalanche process taking place, the emitted light causes stimulated emission in a number of other atoms and the radiation produced will have a definite phase coherence and direction.

The second term does not depend on n_k and corresponds to spontaneous emission. The photon emitted spontaneously can have its wave vector oriented in any direction allowed by the cavity geometry. The total spontaneous emission rate is obtained by summing over all modes. Thus

$$A_{ba} = \frac{\pi e^2}{\hbar \epsilon_0 V} \sum_k \omega_k |\hat{\mathbf{e}}_k \cdot \mathbf{D}_{ba}|^2 \delta(\omega_{ba} - \omega_k) \quad \dots(3.163)$$

Changing the summation to integration and averaging over the orientation of \mathbf{D}_{ba} . We have

$$\begin{aligned} A_{ba} &= \frac{\pi e^2}{\hbar \epsilon_0 V} \int \frac{V \omega_k^3}{\pi^2 c^3} |\hat{\mathbf{e}}_k \cdot \mathbf{D}_{ba}|^2 \delta(\omega_{ba} - \omega_k) \delta \omega_k \\ &= \frac{e^2 \omega_b^3 |D_{ba}|^2}{3 \hbar \epsilon_0 \pi c^3} \frac{1}{\tau_{sp}} \quad \dots(3.164) \end{aligned}$$

which is the same as (3.49) with $g_a = g_b = 1$.

The treatment above shows that absorption and stimulated emission occurs in definite modes prescribed by incident photons; while spontaneous emission can occur in any direction.

We, thus, see that Einstein coefficients which were introduced phenomenologically, appear naturally as a result of calculation using quantized radiation field and also satisfy the relations between the coefficients predicted by him.

MASERS

4

It would be appropriate to start the account of lasers with a discussion of the theory and working of a maser, as it is the forerunner of laser and some of the concepts underlying its working also form a basis for the operation of lasers. Maser amplification is the key process in the field of the so called "quantum electronics". In Townes' words, "It was the mixture of electronics and molecular spectroscopy which set appropriate conditions for invention of maser" [340].

The important factor that has emerged from the discussion in the preceding chapter is that the energy transfer stimulated by an applied electromagnetic wave can be either positive or negative. If the atom is in the lower state when the field of correct frequency is applied, the energy is transferred to the atom which is then raised to a higher state. If the atom is initially in the state of higher energy, the application of the wave will stimulate a transfer to the lower state, and the radiation emitted will increase the energy of the wave. There are two ways in which the radiated energy (the number of photons) produced by the stimulated emission may be increased: (*i*) by increasing the radiation density $\rho(\omega)$ and (*ii*) by increasing the population N_2 in the upper level. But at any temperature T , the atoms obey the Boltzmann distribution by which $N_2 < N_1$. Hence, the number of photons absorbed is larger than the number produced by stimulated emission making absorption more predominant than emission. To make the stimulated emission more prominent, it is necessary to alter the normal population distribution.

In 1954, microwave engineering, statistical mechanics and the quantum theory of matter came together and the first man-made quantum-mechanical device ever to amplify electromagnetic radiation by stimulated emission with extraordinary fidelity was realized. This is the MASER acronym for Microwave Amplification by Stimulated Emission of Radiation—conceived by Townes and independently by Basov and Prokhorov. Briefly, the idea they conceived was: equilibrium could be disturbed in a beam of molecules so as to produce a

predominance of the molecules in the upper state. The molecules then could be passed into a cavity tuned to the frequency of transition between the energy levels. A signal of correct frequency then passed into the cavity, would stimulate the molecules to emit their energy, thus amplifying the signal. If the number of molecules is large enough, the radiation in the cavity may be maintained at such a level that the cavity losses are compensated by the energy from the molecules so that the device would oscillate continuously. Subsequently Gordon, Zeiger and Townes [150] reported the successful operation of a maser in 1954. In the same year Basov and Prokhorov [27] published a paper giving a theory of a beam type device very similar to that of Townes.

4.1 THE TWO-LEVEL MASER SYSTEM AMMONIA MASER

The basic element of the early maser was gaseous ammonia. The ammonia molecule is tetrahedral in structure, having a shape of a pyramid (Fig. 4.1). The three hydrogen atoms lie at the corner of a triangle and the nitrogen atom is at the apex of the pyramid. The nitrogen atom is flipping back and forth along a line perpendicular to the plane of the hydrogen atom. It has a certain probability of being on either side—in a sense it is partly on both sides. Since the molecules can point in any direction in space, we can say that the position of the nitrogen atom relative to the centroid of the molecule lies on a sphere. The potential function measured as a function of r of the nitrogen atom, is spherically symmetric but has a minimum lying on a sphere of radius, say r_0 . The plot of this function against r is of the type shown in Fig. 4.2.

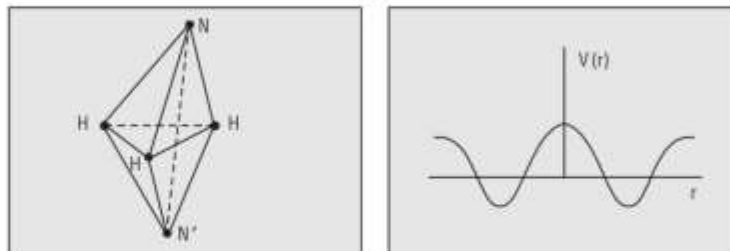


Fig. 4.1 Ammonia molecule

Fig. 4.2 Potential energy curve for ammonia molecule

The solution of Schrödinger equation, subject to this potential distribution, gives a spectrum of energy levels similar to that of a single oscillator but with each level split in a doublet. If ψ_1 and ψ_2 are the solutions corresponding to the two positions of the nitrogen atom, the general solution is

$$\Psi = a_1 \psi_1 + a_2 \psi_2 \quad \dots(4.1)$$

where a_1 and a_2 are constants. The probability that the molecule is in state i is given by $|a_i|^2$. Since the molecule is equally likely to be in either state

$$\begin{aligned} |a_1|^2 &= |a_2|^2 = \frac{1}{2} \\ \therefore \psi &= \frac{1}{\sqrt{2}} (\psi_1 \pm \psi_2) \end{aligned} \quad \dots(4.2)$$



Fig. 4.3 Vibrational energy levels of ammonia molecule

The anti-symmetric state $\frac{1}{\sqrt{2}} (\psi_1 - \psi_2)$ has slightly higher energy than the symmetric state $\frac{1}{\sqrt{2}} (\psi_1 + \psi_2)$. Hence, what would have been a single level in a single potential well is a double level in a double potential well. Thus the ammonia molecule has a level scheme consisting of pairs of energy levels with fairly small separation compared to the separation of one pair from another (Fig. 4.3).

The vibrational levels corresponding to the lowest pair were used in the ammonia maser. The energy difference between these levels corresponds to a microwave frequency of 23870 megacycles per second, i.e., the radiation of wave length 1.25 cm.

Two separate operations are involved in the design of a maser: (i) to obtain inverted population, and (ii) to allow maser action to occur.

To produce excited ammonia molecules is not a problem. Even at the normal temperature, there are excited molecules present in ordinary ammonia. But the number of molecules in the lower state is always higher than that in the upper state and, hence, the crucial problem is how to reduce the number of molecules in the lower state so that the condition $N_2 > N_1$, necessary for amplification is satisfied. Such a non-equilibrium distribution would be possible if some differing physical property of the molecules in the two levels is used to separate them. An electric field applied to molecules induces a dipole moment in the molecules by distorting its charge distribution. The induced dipole moment is given by

$$P = P_0 + \alpha E \quad \dots(4.3)$$

where α is the polarizability. For the lowest pair of energy levels $P_0 = 0$; but

the polarizability α is of opposite sign in the two states. If the mixture of molecules is made to pass through an inhomogeneous electric field, the forces acting on the molecules in the two states will be different. The molecules in the upper state are repelled by the field, whereas those in the lower state are attracted. This fact can be utilized to separate the molecules in the two states and the forces can be arranged to focus the beam of molecules in the upper energy levels in a cavity.

In the first ammonia maser built by Gordon, Zcigcr and Townes [150, 151], the oscillating state was achieved by literally separating in space, as indicated above, the molecules that were in the upper level and those in the lower one. A block diagram of the apparatus used by them is given in Fig. 4.4.

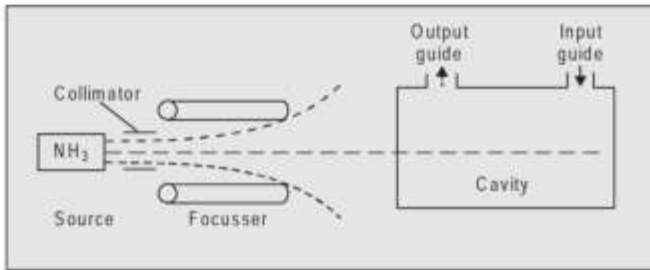


Fig. 4.4 Ammonia maser

A beam of ammonia molecules emerges from an aperture in an oven, heated to a certain temperature, which can be closely controlled. The beam containing the molecules both in the upper and the lower state traverses a region of highly non-uniform electrostatic field—an electrostatic focuser. In the first arrangement of Gordon *et al.*, four hollow metal rods each 55 cm long were placed round the beam [Fig. 4.5 (a)]. The inner faces of these rods were shaped as hyperbolas which facilitated the calculation of the field gradient. Figure 4.5(b) shows their potential contours. The spacing between the rods was 0.2 cm and a d.c. voltage of 15 kV was applied. This system formed the focuser.

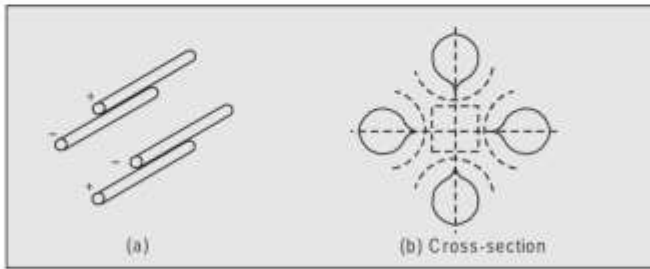


Fig. 4.5 Electrostatic focuser

In the vicinity of the rods the field is strong. When a mixture of upper and lower state molecules passes through the system, due to the interaction between the applied field and the induced dipole moment, the molecules in the lower state are pulled towards the electrodes, whereas the molecules in the upper state are drifted towards the axis. In this way, the molecules in the upper state are focussed into the cavity and those in the lower state are dispersed. The molecules arriving at the cavity are virtually all in the upper state. A feeble signal wave is fed at one end of the cavity and an amplified wave resulting from the amplification by stimulated emission from the ammonia molecules emerges at the other end. It must be noted, however, that the amplification achieved by a wave in a single passage is very small as many of the excited molecules present would not be de-excited in a single transit of the wave. Hence, the cavity is made with highly reflecting walls, so that the radiation inside it can make many to-and-fro reflections, thus increasing its chance of interacting with a molecule in the beam. Whenever there is a collision, a new photon is born which is also trapped in the chamber for a time and may collide with another molecule producing a second new photon. The radiation thus grows in intensity. If there are enough molecules in the cavity, this chain-reaction becomes self-sustaining. The amplifier now becomes an oscillator generating its own wave without any input signal.

It must be mentioned here that not all of the power emitted by the ammonia molecules in the cavity can be extracted as a useful power output, as some of it is lost in the cavity. In order that the oscillations are sustained, the power supplied as stimulated radiation from the beam should be equal or greater than the power absorbed in the cavity. The power supplied by the beam is

$$P = N_n B_{nm} \rho(\omega_{nm}) \hbar \omega_{nm} \quad \dots(4.4)$$

where N_n is the number of upper state molecules entering the cavity per second, ω_{nm} is the frequency of transition and B_{nm} is the probability per unit time for the upper state molecule to revert to the lower state.

For efficient maser action it is imperative that the cavity losses are as small as possible. These losses depend upon the quality of the cavity. The quality factor Q of a cavity is defined by

$$Q = \frac{\omega_{nm} \times \text{energy stored}}{\text{energy lost per second}} \quad \dots(4.5)$$

The power lost by absorption in the cavity walls P_L is

$$P_L = \frac{\omega_{nm} W}{Q} \quad \dots(4.6)$$

where W is the energy stored in the cavity

$$W = \rho(\omega_{nm}) V \quad \dots(4.7)$$

V being the volume of the cavity.

The threshold condition for oscillations, therefore, is

$$N_n B_{nm} \rho(\omega_{nm}) \hbar \omega_{nm} = \omega_{nm} \rho(\omega_{nm}) V/Q \quad \dots(4.8)$$

From Eqn. (3.47) of the preceding chapter

$$B_{nm} = \frac{\pi e^2 |D_{nm}|^2}{3\epsilon_0 \hbar^2} \quad \dots(4.9)$$

Therefore, Eqn. (4.8) changes to

$$\frac{N_n \rho(\omega_{nm}) \hbar \omega_{nm} \pi e^2 |D_{nm}|^2}{3\epsilon_0 \hbar^2} = \frac{\omega_{nm} \rho(\omega_{nm}) V}{Q}$$

i.e., $N_n = \frac{3\epsilon_0 \hbar V}{\pi e^2 |D_{nm}|^2 Q} \quad \dots(4.10)$

This is the minimum number of molecules per second required to maintain oscillation.

In the second maser, Gordon *et al.* used six rods instead of four, each 20 cm long with inter-rod separation of 0.4 cm the voltage applied being 30 kV. This increased the efficiency from 10% to 40%. Subsequently, other modifications were introduced to increase the efficiency still further.

The device acts as a very high resolution microwave spectrometer, a microwave amplifier or a stable oscillator. It can detect much weaker signals than other amplifiers can. As an amplifier the ammonia maser has a remarkably narrow band-width. It will not amplify waves which depart from its central frequency by more than 3,000 to 5,000 cycles.

The great virtue of the maser is that it generates practically no 'noise'. It would be interesting to consider what makes the maser so 'quiet'. In the discussion above we have not considered the spontaneous emission which is likely to occur causing random variations in the output which constitutes what is called the 'noise'. Fortunately, as shown in Chapter 2, the noise is very small in the microwave region in which the ammonia maser works.

Ammonia masers have very low power output—around 10^{-9} watts. However, their frequency of oscillation is very stable varying in time by a few parts in 10^{10} . Ammonia masers, thus, are useful as very precise frequency sources of 'clocks'.

4.2 HYDROGEN MASER

Once the feasibility of the working maser had been demonstrated other beam masers came into existence.

Kleppner *et al.* [219] developed a maser operating on the hyperfine structure transition in the ground state ${}^2S_{1/2}$ of hydrogen.

It is known that a magnetic moment, represented by a quantum number I , is associated with the nuclear spin of the atom. The angular momentum J of the extra-nuclear electrons combines with I to give the total angular momentum of

the whole atom. This is represented by the quantum number F and takes values $F = |J + 1|, J, \dots, |J - 1|$... (4.11)

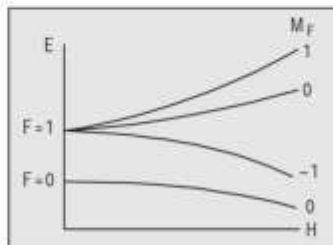


Fig. 4.6 Zeeman splitting for the ground state of hydrogen atom

In the case of the ground state $^2S_{\frac{1}{2}}$ of hydrogen atom the possible values of F are 1 and 0.

When the atom is placed in a magnetic field, a space quantization of F takes place precisely as in the case of J . The levels are split into components specified by quantum number M_F which takes values

$$M_F = -F, F-1, \dots, -F \quad \dots (4.12)$$

Figure 4.6 gives the Zeeman splitting for the ground state of hydrogen atom. At low fields, the $F = 1$ state will split into three components $M_F = 1, 0, -1$ and $F = 0$ state will remain unaffected. The splitting increases with increasing field. If some means could be devised to get $F = 1$ level more highly populated than $F = 0$ level, the radiation corresponding to the transition $F = 1 \rightarrow F = 0$ could be amplified. Experiments to this end were carried out by Ramsay and his co-workers. A schematic diagram of a typical hydrogen maser is given in Fig. 4.7 (a).

Molecular hydrogen at pressure ~ 0.2 Torr is dissociated in the source by a r.f. discharge. The emerging beam of atomic hydrogen then passes through a six pole state selecting magnet. The cross-section of such a magnet is shown in Fig. 4.7(b). The magnetic field on the axis of the selector is zero, but increases rapidly off-axis. It can be shown that $M_F = 1$ and 0 levels of the $F = 1$ state gain in potential energy, as the magnetic field is increased, whereas

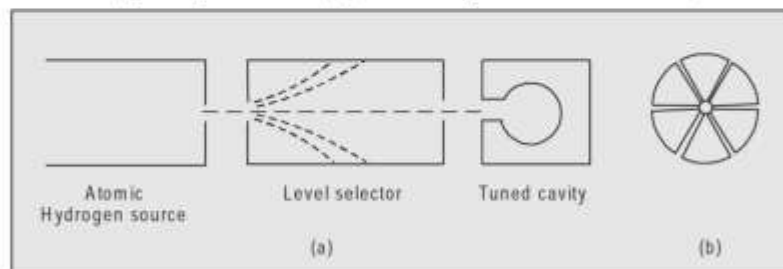


Fig. 4.7 Schematic diagram of a typical hydrogen maser

$M_F = -1$ of $F = 1$ and $F = 0$ state lose energy as the field is increased. The atoms in the $F = 0$ state, therefore, are defocussed. On the other hand, atoms in the $M_F = 1$ and 0 of $F = 1$ state are focussed on to a small hole in the cavity tuned to the frequency of transition. Since the cavity contains predominantly atoms in the $F = 1$ level, a radiation corresponding to the transition $F = 1 \rightarrow F = 0$ will be amplified.

The coherence of maser radiation produces an extremely narrow linewidth. The transition on which the hydrogen maser operates has been measured as $1420, 405,751, 786 \pm 0.010$ Hz [365]. This high accuracy was possible because hydrogen atom has a lifetime of few seconds in the cavity (Note: $\Delta E \Delta t \sim \hbar$). This system has provided the best available time standard.

4.3 THE THREE-LEVEL MASER SYSTEM

However, two-level maser does not have wide application. Its chief disadvantage is that it can operate only in bursts. For stimulated emission to occur, inverted population will have to be first established. The generation of photons by stimulated emission reduces the number of atoms in the upper state and amplification stops. The inversion process must then be repeated for amplification to occur. The two-level maser is, thus, a pulsed maser. In certain cases such as in a communication system, a major requirement is that the amplifier should operate continuously. For this, it is necessary that the atoms or molecules in the maser medium are excited—or pumped—to a non-thermal equilibrium distribution continuously, through the application of some external sources of energy.

One may think, at first sight, that it would be possible to achieve population inversion in a two-level system by pumping molecules to the higher state by stimulated absorption using a strong electromagnetic field. The absorption transition will continue as long as the gas remains absorptive, i.e., $N_1 > N_2$. When the molecules are pumped by intense pumping radiation, the populations in the two energy states are driven to equality until at the limit no more energy is absorbed, i.e., a state of saturation is reached.

A continuous maser operation is possible in a three-level maser, conceived independently by Basov and Prokhorov [25] in USSR and Bloembergen [40] in USA. In these masers, atoms or molecules are not separated in space as in the ammonia maser. Instead, what is known as frequency separation is used.

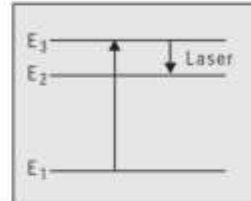


Fig. 4.8 Three-level system

Consider a system with three unequally spaced energy levels $E_3 > E_2 > E_1$ (Fig. 4.8). In thermal equilibrium the populations of the three levels are N_1 ,

$$N_2 = N_1 \exp\left(-\frac{E_2 - E_1}{kT}\right) = N_1 \exp(-\hbar\omega_{21}/kT) \quad \dots(4.13)$$

$$N_3 = N_1 \exp\left(-\frac{E_3 - E_1}{kT}\right) = N_1 \exp(-\hbar\omega_{31}/kT)$$

If $(\hbar\omega/kT) \ll 1$, the last two relations lead to

$$N_2 = N_1 \left(1 - \frac{\hbar\omega_{21}}{kT}\right) \quad \dots(4.14)$$

$$\text{and} \quad N_3 = N_1 \left(1 - \frac{\hbar\omega_{31}}{kT}\right) \quad \dots(4.15)$$

The difference in population between levels 1 and 3 is

$$|N_3 - N_1| = N_1 \frac{\hbar\omega_{31}}{kT} \quad \dots(4.16)$$

When a radiation of frequency ω_{31} is applied to the medium, absorption will take place and if the pumping power is sufficiently high, levels 3 and 1 will be saturated and their population will be equalized. That is, the populations of level 3 will be increased by $(1/2) N_1 \hbar\omega_{31}/kT$ while that of level 1 will be decreased by the same amount. When this takes place the population of level 3 is

$$N_3 + \frac{1}{2} N_1 \frac{\hbar\omega_{31}}{kT} = N_1 \left(1 - \frac{\hbar\omega_{31}}{2kT}\right) \quad \dots(4.17)$$

where we have used Eqn. (4.15). The population of the level 2 is not disturbed during the transition. If the transition between levels 3 and 2 is the signal transition, the condition for obtaining an inverted population across the signal level is that

$$N_1 \left(1 - \frac{\hbar\omega_{31}}{2kT}\right) > N_1 \left(1 - \frac{\hbar\omega_{21}}{kT}\right)$$

$$\text{i.e.,} \quad 2\omega_{21} > \omega_{31} \quad \dots(4.18)$$

Materials in which this condition is satisfied are suitable as maser media. Unpaired electrons in paramagnetic substances provide such levels and make solid state masers possible. In paramagnetic single crystals, energy levels with difference appropriate for microwave region are found and were used as maser media. A paramagnetic atom of spin 1/2 has two energy levels. If such an atom is placed in a magnetic field of strength H , the separation of levels becomes approximately equal to $0.28H$ Mc. Such masers, therefore, are tunable and most of the microwave frequency range can be covered by varying the magnetic field H . Apart from ammonia these were the first materials in which maser action was observed. Bloembergen's first microwave maser used Cr^{3+} in

potassium chromicyanide. Numerous other solid state three-level masers of this kind utilizing a variety of paramagnetic ions embedded in host crystals have since gone into operation.

The solid state masers have a 'noise' level even lower than that of ammonia maser.

One version of the solid state maser uses chromium ions in a ruby crystal as the active element. Zeeman levels in the ground state of chromium ions provide amplification around 9300 MHz and since these are affected by the external magnetic field it is possible to tune the amplifiers by varying the field. One such solid state maser was used by Arno Penzias and Robert W. Wilson in 1965 to discover the blackbody radiation from Big-Bang.

Maser action is now even believed to exist in nature. A surprising observation of radio emission at about 1670 MHz coming from OH molecules located near some stars was reported by Wever in 1965. The emission actually consists of four known OH transitions at 1612, 1665, 1667 and 1720 MHz. The intensity ratio of these lines was quite different from that expected for spontaneous emission. The line-widths were such that the temperature of the source would have to be lower than 50K to have such a small Doppler broadening. As against this, emission intensity was so strong as to correspond to a source temperature of $10^{12} - 10^{13}$ K [43].

The tentative explanation that has been offered is that the radiation was emitted spontaneously in some part of an OH cloud and was then selectively amplified by a maser amplifier as it was passing through the other region of the cloud. The pumping mechanism for the population inversion is not yet clear; but is suggested to be due to ultraviolet radiation from nearby stars [Wever, 396, 397].

We do not propose to discuss masers any further and end this chapter here. In fact we have not discussed the technological details involved in the fabrication of masers. Our purpose was only to explain the basic principles on which a maser build and which would be useful in understanding how the theory was extended to lasers.

THEORY OF SOME SIMPLE OPTICAL PROCESSES

5

To gain a better understanding of laser, a working familiarity with the properties of light and the theory of some optical processes is necessary. We will discuss in this chapter some such background material connected with coherence, absorption and emission processes and line-width.

5.1 WAVES AND INTERFERENCE

Let us first consider some very general properties of waves and their interference. We know that an atom consists of positively charged nucleus with electrons revolving around it in their respective orbits. A collision with an incoming electron or atom results into the transfer of energy to the atom which causes an electron in the atom to be shifted to a higher level. In this state, the atom possesses more energy than in the ground state and is unstable. After about 10^{-8} seconds, the atom spontaneously returns to its ground state emitting the excess energy in the form of radiation. When an assembly of excited atoms lose their excitation energy by emitting at random moments randomly phased wave-packets, interference of these waves results and what is observed is some mean amplitude of resultant emission.

Let us consider the disturbance produced by the simultaneous action of a number of oscillators. Let ψ_1, ψ_2, \dots be the disturbances produced by individual oscillators. The resultant disturbance can be found using the *principle of superposition*—a physical hypothesis which states that for light waves, the disturbance at a point due to the passage of a number of waves is equal to the algebraic sum of the disturbances produced by individual waves. Since the calculations based on this principle can give satisfactory explanation of the observed effects, the principle can be considered as having been confirmed. Therefore,

$$\Psi = \Psi_1 + \Psi_2 + \dots \quad \dots(5.1)$$

Consider an extended source of light (Fig. 5.1) consisting of idealized two-level atoms capable of emitting at frequency ω of the total light received at a point Q , some will come from an atom A_1 , some from A_2 , and so on, each acting independently. The waves are randomly phased and we may write for a typical wave

$$\Psi_k = a_k \exp(i(\omega_t + \delta_k)) \quad \dots(5.2)$$

where a_k is the amplitude of the wave and δ_k is the phase angle.

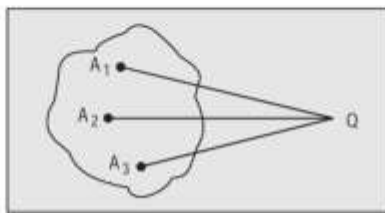


Fig. 5.1 Light received at a point Q from an extended source

Classically the energy of the wave is proportional to a_k^2 . Writing $X = \omega t - kx$, Eqn. (5.2) can be expressed as

$$\Psi_k = a_k \exp(i(X + \delta_k)) = a_k \{\cos(X + \delta_k) + i \sin(X + \delta_k)\} \quad \dots(5.3)$$

By the principle of superposition, the resultant disturbance is given by

$$\begin{aligned} \Psi &= \sum_i \Psi_i = \sum_i a_i \cos(X + \delta_i) + i \sum_i a_i \sin(X + \delta_i) \\ &= A \cos \Delta + i A \sin \Delta = A \exp(i\Delta) \end{aligned} \quad \dots(5.4)$$

where we have put

$$A \cos \Delta = \sum_i a_i \cos(X + \delta_i)$$

$$\text{and} \quad A \sin \Delta = \sum_i a_i \sin(X + \delta_i)$$

Hence, the energy of the resultant wave is proportional to A^2 given by

$$\begin{aligned} A^2 &= \left[\sum_i a_i \cos(X + \delta_i) \right]^2 + \left[\sum_i a_i \sin(X + \delta_i) \right]^2 \\ &= \sum_i a_i^2 \{ \cos^2(X + \delta_i) + \sin^2(X + \delta_i) \} \\ &\quad + \sum_i \sum_{j \neq i} a_i a_j \{ \cos(X + \delta_i) \cos(X + \delta_j) \} \\ &\quad + \sin(X + \delta_i) \sin(X + \delta_j) \\ &= \sum_i a_i^2 + \sum_{i \neq j} a_i a_j \cos(\delta_i - \delta_j) \end{aligned} \quad \dots(5.5)$$

Since the phase differences vary in a random way, the average value of the summation of the cross-products in the second term will be zero, because for every possible positive value of any term there will be equally probable negative value.

Therefore,

$$\Psi = \sum_k \psi_k = \sum_k a_k^2 = n\bar{a}^2 \quad \dots(5.6)$$

where n is the number of excited atoms and \bar{a}^2 is the mean square amplitude of disturbances. We, thus, see that the intensity of illumination—which is proportional to the energy of the waves—is proportional to the number of excited atoms.

Suppose now that by introducing some sort of device we can make the atoms to emit waves which have the same phase, say δ , in which case Eqn. (5.4) takes the form

$$\begin{aligned} \Psi &= a_1 \{\cos(X + \delta) + i \sin(X + \delta)\} \\ &\quad + a_2 \{\cos(X + \delta) + i \sin(X + \delta)\} + \dots \\ &= \cos(X + \delta) \sum_k a_k + i \sin(X + \delta) \sum_k a_k \\ &= A' (\cos \Delta + i \sin \Delta) \end{aligned} \quad \dots(5.7)$$

where we have put

$$A' \cos \Delta = \cos(X + \delta) \sum_k a_k$$

and

$$A' \sin \Delta = \sin(X + \delta) \sum_k a_k$$

Therefore, the energy of the resultant wave E is

$$E \propto A'^2 = \left(\sum_k a_k \right)^2 = (n\bar{a})^2 = (n^2 \bar{a}^2) \quad \dots(5.8)$$

That is, the intensity is proportional to the square of the number of excited atoms and, hence, is much higher than the intensity of the resultant wave produced by randomly phased waves. It is thus obvious that in order to increase the intensity, the atoms must be made to emit waves that are in phase. This leads us to the question of *coherence*—a property closely linked with the functioning of a laser.

5.2 COHERENCE

The light that emerges from a conventional light source is a jumble of tiny, separate waves that reinforce or cancel each other in random fashion; the wave-front thus produced varies from point to point and changes from instant to instant. There are, thus, two independent concepts of coherence namely, *temporal coherence* and *spatial coherence*.

- (a) *Temporal Coherence:* This type of coherence refers to the correlation between the field at a point and the field at the same point at a later time; that is to the relation between $E(x, y, z, t_1)$ and $E(x, y, z, t_2)$. If the phase difference between the two fields is constant during the period normally covered by observations, which is of the order of a few microseconds, the wave is said to have *temporal coherence*. If the phase difference changes many times and in an irregular way during the shortest period of observation, the wave is said to be *noncoherent*.
- (b) *Spatial Coherence:* Two fields at two different points on a wavefront of a given electro-magnetic wave are said to be space coherent if they preserve a constant phase difference over any time t . This is possible even when the two beams are individually time incoherent, as long as any phase change in one of the beams is accompanied by a simultaneous equal phase change in the other beam. With the ordinary light sources, this is only possible if the two beams have been produced in the same part of the source. For example, when a point source is placed at the focus of a convex lens, the radiation transmitted by the lens consists of nearly plane waves. The disturbances at different points on the wavefront, at a given time are highly correlated and produce interference fringes as can be observed in the case of the Fizeau Stellar interferometer.

Time incoherence is a characteristic of a single beam of light, whereas, space incoherence concerns the relationship between two separate beams of light. Two beams of light originating in different parts of a source will have been emitted by different groups of atoms. Each beam will be time-incoherent and will suffer random phase changes, as a result of which the phase difference between the two beams will also suffer rapid and random changes. Two such beams are said to be space incoherent.

Interference is a manifestation of coherence. For the production of interference fringes, it is a necessary condition that the sets of interfering waves remain coherent over a period of time. If one of the waves changes in phase, the fringes will change with time. With the natural sources of light these changes are rapid and no interference fringes are seen.

The simplest way of producing interference fringes is the one adopted by Young in his double slit experiment (Fig. 5.2). In this experiment Young used one source as the originator of two separate sources. The light from a source S passes through a slit A and then through two small holes made in the screen B . The phase relationship between successive pulses remains constant and interference fringes are produced on the screen C . One has to be careful to see that the slit A is fairly small compared with the size of the fringes. Otherwise, the fringes produced by the different parts of the slit are likely to overlap.

giving uniform illumination. This will not happen if the disturbances at different points across the beam are highly correlated *i.e.*, if there is space coherence. In practice, for a point P on the wave front there is some finite area around it, any point within which will have a good phase correlation with P . By holding one pin-hole fixed and moving the other pin-hole about, one can look for any reduction in the fringe visibility. The area of the wave-front over which pin-hole can be moved and the fringes still be seen is known as the *coherent area* of the light wave and is a measure of the *spatial or transverse* coherence of the wave. It characterizes the spatial variation in coherence across the wave-front in the direction transverse to the direction of propagation. From this point of view *temporal* coherence is known as *longitudinal* coherence.

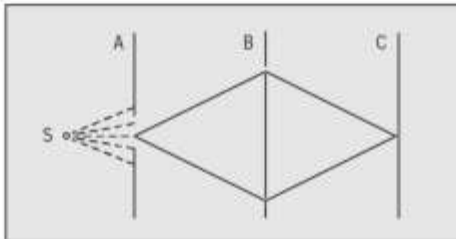


Fig. 5.2 Young's experiment

The measure of fringe contrast called the *fringe visibility* serves also as a useful measure of coherence.

Michelson defined the visibility of fringes as

$$V = \frac{E_{\max} - E_{\min}}{E_{\max} + E_{\min}} \quad \dots(5.9)$$

where E_{\max} is the relative energy of a bright fringe and E_{\min} , the energy of a neighbouring dark fringe. If the fringes are produced by coherent beams of equal amplitude, the visibility of fringes is unity, ($E_{\min} = 0$); while that of the fringes produced by non-coherent beams is zero; ($E_{\max} = E_{\min}$), *i.e.*, no fringes. The visibility of the fringes actually observed in the laboratory, however, is less than unity, even with the waves of equal amplitude. Rigorously speaking, therefore, only partially coherent waves is a physical reality and both ideally coherent and ideally incoherent waves are abstractions.

The ability of light waves to produce interference is measured by the "degree of coherence of light waves". Higher the degree of coherence higher is the probability that the waves produce a contrast interference pattern. Zermike defined the *degree of coherence*, V_2 , to be equal to the visibility of fringes when the path difference between the beams is small and the amplitudes are equal, these being the conditions most favourable for the production of fringes. In Young's experiment the fringe visibility can be taken as a direct measure of the degree of coherence the light exhibits at the two pin-holes. By convention, if

$V_2 > 0.85$, the two secondary sources are said to be highly coherent. It can be shown that only light that is perfectly monochromatic can be completely coherent in both time and space.

The discussion so far is idealized since we have assumed that the sets of waves produced by the source remain perfect sine waves over a period of time. However, a text-book is the only place where light could 'exist' as sine waves. Actually, the frequency varies slowly and randomly with time about the central frequency to the extent of the width of the line. A monochromatic radiation is characterized by a centre of frequency ω_0 and a band width $\Delta\omega_0$ so defined that the frequency interval from $\omega_0 - \Delta\omega_0/2$ to $\omega_0 + \Delta\omega_0/2$ contains a large part of the energy of radiation. The various causes of this frequency spread are discussed in a later section.

Over an interval of time shorter than the duration of one wavepacket, the waves will appear to be pure sine waves (Fig. 5.3). The average time during which the ideal sinusoidal emission exists is called the *coherence time* τ_c . The corresponding length, $L_c = C\tau_c$ where C is the velocity of light, is called the *coherence length*. After time τ_c , there is no correlation between the phase of the waves.

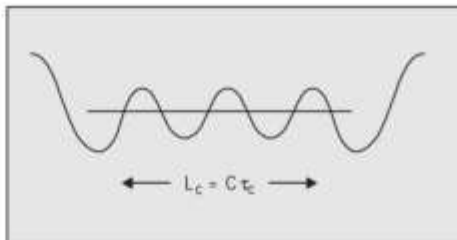


Fig. 5.3 Coherence time

5.3 COHERENCE OF THE FIELD AND THE SIZE OF THE SOURCE

Let us obtain a mathematical relation between the coherence of the field and the size of the source. Consider an extended source of light S (Fig. 5.4). Each point on the source radiates incoherently. Let S_1 and S_2 be the two extreme points on the source and $X = S_1S_2$. The disturbances at S_1 and S_2 may be represented by

$$f(S_1) = \exp(i\omega t + \phi(S_1)) \quad \dots(5.10)$$

$$\text{and} \quad f(S_2) = \exp(i\omega t + \phi(S_2)) \quad \dots(5.11)$$

where $\phi(S_1)$ and $\phi(S_2)$ fluctuate irregularly with time. The disturbance E_p at a point P on one of the slits in a double slit experiment is

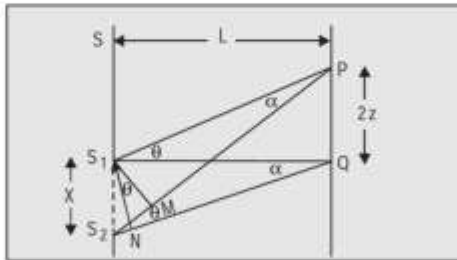


Fig. 5.4 Dependence of coherence on the size of the source

$$\begin{aligned} E_P &= f(S_1) \exp(-ik(S_1P)) + f(S_2) \exp(-ik(S_2P)) \\ &= \exp(i\omega t) [\exp(\phi(S_1) - ik(S_1P)) + \exp(\phi(S_2) - ik(S_2P))] \end{aligned} \quad \dots(5.12)$$

The corresponding expression for another point Q on the other slit is

$$E_Q = \exp(i\omega t) [\exp(\phi(S_1) - ik(S_1Q)) + \exp(\phi(S_2) - ik(S_2Q))] \quad \dots(5.13)$$

If P and Q coincide $ik(S_1P) = ik(S_1Q)$ and $ik(S_2P) = ik(S_2Q)$ and, hence, the two disturbances E_P, E_Q are identical and coherent. This leads to the question: how far can P and Q be separated before the coherence disappears? Let this distance be represented by $PQ = 2z$. Since the distance of the screen from the source, L , is very large compared to the distance PQ and X , we can use the following approximate relations which would be clear from the geometry of the figure. Note that M and N are the feet of the perpendiculars from S_1 to S_2P and S_2Q respectively.

$$\begin{aligned} S_1P - S_2P &\sim S_2M; & S_1Q - S_2Q &\sim S_2N \\ S_2M - S_2N &\sim \lambda\theta; & X - L\alpha; \frac{2z}{L} &\sim \theta \end{aligned}$$

The angles θ and α are shown in the figure.

Therefore,

$$S_2M - S_2N \sim L\alpha \cdot \frac{2z}{L} = 2z\alpha \quad \dots(5.14)$$

For fairly clear fringes to appear, the path difference must be less than λ , the wavelength of the light. Therefore, coherence disappears when

$$2z\alpha = \lambda \text{ or } PQ = \frac{\lambda}{\alpha} \quad \dots(5.15)$$

This means, in order to obtain a distinct interference pattern, the distance between the two slits must be less than $\frac{\lambda}{\alpha}$.

This relation, although derived by using approximate relations, is close to the one that can be derived by rigorous mathematical treatment and is a good measure of spatial coherence.

5.4 VISIBILITY AND THE SIZE OF THE SOURCE

We will calculate in this section the visibility as a function of the size of the source. The treatment given below is on the lines of that given by Ditchburn [102]. Let S (Fig. 5.5) be the primary source of light and P_1 and P_2 the two slits receiving light from S and producing interference at a point Q on the observation plane. Suppose a_1 and a_2 are the amplitudes of the disturbance at P_1 and P_2 due to an element dS of the source. The relative energies at the two points, therefore, are:

$$E_{P_1} = \int a_1 a_1^* dS; E_{P_2} = \int a_2 a_2^* dS \quad \dots(5.16)$$

Suppose, further, that the disturbance of unit amplitude and zero phase at P_1 gives rise to a disturbance at a point Q on the screen of complex amplitude

$$f_1 = g_1 \exp(ikd_1) \quad \dots(5.17)$$

where d_1 is the optical path from P_1 to Q and g_1 is the transmission factor. The corresponding quantity due to a similar disturbance at P_2 is

$$f_2 = g_2 \exp(ikd_2) \quad \dots(5.18)$$

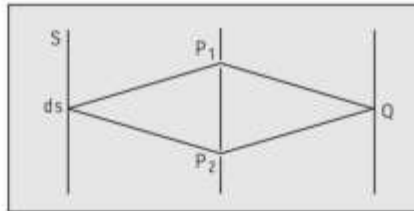


Fig. 5.5 Visibility as a function of the size of the source

Therefore, the amplitude at Q is $f_1 a_1 + f_2 a_2$. The corresponding energy is

$$\begin{aligned} dE_Q &= (f_1 a_1 + f_2 a_2) (\bar{f}_1^* a_1^* + \bar{f}_2^* a_2^*) \\ &= f_1 \bar{f}_1^* a_1 a_1^* + f_2 \bar{f}_2^* a_2 a_2^* + f_1 \bar{f}_2^* a_1 a_2^* + f_2 \bar{f}_1^* a_2 a_1^* \\ &= f_1 \bar{f}_1^* a_1 a_1^* + f_2 \bar{f}_2^* a_2 a_2^* + 2\text{Re}(f_1 \bar{f}_2^* a_1 a_2^*) \end{aligned} \quad \dots(5.19)$$

where we have used the relation

$$\phi_1 \phi_2^* + \phi_1^* \phi_2 = 2\text{Re}(\phi_1 \phi_2^*) \quad \dots(5.20)$$

which can be easily proved for any complex function.

Integrating Eqn. (5.19) we get the expression for the energy E_Q at Q

$$\begin{aligned} E_Q &= \int f_1 \bar{f}_1^* a_1 a_1^* dS + \int f_2 \bar{f}_2^* a_2 a_2^* dS + 2 \int \text{Re}(f_1 \bar{f}_2^* a_1 a_2^*) dS \\ &= g_1^2 \int a_1 a_1^* dS + g_2^2 \int a_2 a_2^* dS + 2 \int \text{Re}(f_1 \bar{f}_2^* a_1 a_2^*) dS \end{aligned}$$

$$\begin{aligned}
 &= g_1^2 E_{R_1} + g_2^2 E_{R_2} + 2(E_{R_1} E_{R_2})^{1/2} \operatorname{Re} \frac{f_1 f_2^*}{(E_{R_1} E_{R_2})^{1/2}} \int a_1 a_2^* dS \\
 &= g_1^2 E_{R_1} + g_2^2 E_{R_2} + 2(E_{R_1} E_{R_2})^{1/2} \operatorname{Re}(f_1 f_2^* \gamma_{12})
 \end{aligned} \quad \dots(5.21)$$

where we have used Eqns. (5.16), (5.17) and (5.18) and have further put

$$\gamma_{12} = \frac{1}{(E_{R_1} E_{R_2})^{1/2}} \int a_1 a_2^* dS \quad \dots(5.22)$$

This quantity γ_{12} is called the phase coherence function for light from P_1 and P_2 and provides a measure of the coherence between two different points of the wave.

Let us express this phase coherence function as a complex quantity

$$\begin{aligned}
 \gamma_{12} &= V_{12} \exp(\beta_{12}) \\
 \text{so that} \quad |\gamma_{12}| &= V_{12}
 \end{aligned} \quad \dots(5.23)$$

Using this expression and writing

$$E'_1 \text{ for } g_1^2 E_{R_1} \text{ and } E'_2 \text{ for } g_2^2 E_{R_2}$$

We can express Eqn. (5.21) as

$$\begin{aligned}
 E_Q &= E'_1 + E'_2 + 2(E_{R_1} E_{R_2})^{1/2} \operatorname{Re}\{g_1 g_2 \exp(i k(d_1 - d_2)) V_{12} \exp(\beta_{12})\} \\
 &= E'_1 + E'_2 + (E'_1 E'_2)^{1/2} V_{12} \cos(\beta_{12} + k(d_1 - d_2))
 \end{aligned} \quad \dots(5.24)$$

Therefore, maximum and minimum values of E_Q are

$$E_{Q_{\max}} = E'_1 + E'_2 + 2V_{12}(E'_1 E'_2)^{1/2} \quad \dots(5.25)$$

$$\text{and} \quad E_{Q_{\min}} = E'_1 + E'_2 - 2V_{12}(E'_1 E'_2)^{1/2} \quad \dots(5.26)$$

Hence, the visibility is given by

$$V = \frac{E_{Q_{\max}} - E_{Q_{\min}}}{E_{Q_{\max}} + E_{Q_{\min}}} = \frac{2(E'_1 E'_2)^{1/2}}{E'_1 + E'_2} V_{12} \quad \dots(5.27)$$

Clearly, if $E'_1 = E'_2$

$$V = V_{12} = |\gamma_{12}| \quad \dots(5.28)$$

That is, the modulus of the phase coherence factor is equal to the visibility under the most favourable conditions which is the same as the degree of coherence as defined by Zermike.

It may be noted, however, that if the intensities of the two sources are unequal, the visibility of the fringes will never be unity, even if the two sources are perfectly coherent. Hence, the measurement of the visibility is convenient for the determination of the correlation only between sources of equal intensity.

5.5 COHERENCE AND MONOCHROMACY

The degree of non-monochromacy is related to the coherence time τ_c and the central frequency v_0 by the relation

$$\xi = \frac{1}{\tau_c v_0} = \frac{c}{L_c v_0} = \frac{\Delta\nu}{v_0} \quad \dots(5.29)$$

That is, higher the coherence time smaller is the value of ξ i.e., higher is the monochromacy.

The concept of temporal coherence, therefore, is intimately connected with monochromacy. For example, the bandwidth of a He:Ne laser line is ~ 500 Hz corresponding to $L_c \sim 600$ km. ($\tau_c \sim 2 \times 10^{-3}$ sec). Compare this with the coherence length of a conventional light source, e.g., a sodium lamp which is $L_c \approx 3$ cm ($\tau_c \approx 10^{-10}$ sec). No wonder that in the case of Michelson interferometer fringes can be observed for a difference between its arms of up to a few centimeters only.

In terms of a photon picture, the degree of coherence of light waves is determined by the distribution of photons in various states. A light beam would be ideally coherent if all its photons have the same energy, same direction of momentum and identical polarization. This is not observed in actual light beams and, hence, we talk of 'degree of coherence', which is higher if the degree of monochromacy is higher, the degree of divergence of the beam is lower, and the degree of polarization is higher.

We, thus, see that the principle characteristics of laser light, viz. its intensity, its directionality, its monochromacy are, in one way or the other, intimately related to the high degree of coherence exhibited by it. The main aspect which distinguishes lasers from other sources, therefore, is coherence.

5.6 KINETICS OF OPTICAL ABSORPTION

We will examine in this and the following section some of the physical and mathematical tools which allow a quantitative interpretation of some optical processes connected with the formation of absorption and emission lines.

Consider an ensemble of atoms. For simplicity we assume that the atoms are characterized by two energy state $|a\rangle$ and $|b\rangle$. If a beam of light from a source emitting a continuous spectrum is sent through a cell containing these atoms, the spectrum shows a dark line in the continuous spectrum, its frequency being

$$\omega_{ba} = \frac{E_b - E_a}{h} \quad (E_b > E_a) \quad \dots(5.30)$$

The appearance of the dark line is evidently a consequence of the atoms having absorbed energy at a frequency ω_{ba} from the light beam and have undergone a transition from states $|a\rangle$ and $|b\rangle$. There, thus, will be a reduction

in the light level on the output screen at the frequency ω_{ba} . Because, this absorption process is stimulated by the incident light beam, it is referred to as *stimulated absorption*.

What happens to the excited atoms? Natural tendency of any system is to seek out the lowest energy configuration. The atom excited to the higher level by absorption may eventually return to the ground state by spontaneous emission, which occurs without any external stimulation, emitting a quantum of energy at ω_{ba} . This may also be accompanied by stimulated emission at the same frequency. There, thus, will be both absorption and emission as the beam passes through the ensemble. However, since the number of atoms N_1 in the lower state is much greater than the number N_2 in the upper state, the beam will suffer a net loss of intensity and the material will have a positive absorption coefficient.

The discussion so far is based on the mathematical idealization concerning the sharpness of the levels and, hence, of the corresponding spectral lines. No such line, in fact, can exist. As a consequence of the uncertainty principle the energy levels cannot be perfectly sharp and, as a result the frequency of transition cannot be perfectly monochromatic. The atomic transition is associated with a finite spread of energy and, hence, of frequency as shown in Fig. (5.6). In such cases it is said that the gas possesses an absorption line at the frequency ω_0 corresponding to the centre of the line.

Intensity of a light beam is defined as the energy incident on unit area per unit time. If ρ is the energy density of the light field, then the intensity is given by

$$I = \rho v \quad \dots(5.31)$$

where v is the velocity of light in the given medium. In terms of photons

$$I = \hbar \omega n v \quad \dots(5.32)$$

where n is the number of photon per unit volume.

When light passes through an absorbing medium, the energy absorbed in a distance dz is proportional both to dz and the incident flux. This change in

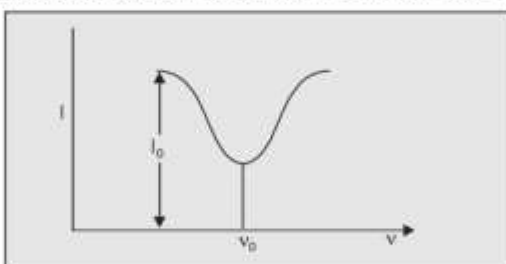


Fig. 5.6 Transmitted light as a function of frequency

intensity is given by

$$-dI_v(z) = k_v I_v(z) dz \quad \dots(5.33)$$

where the constant of proportionality k_v , called the *absorption coefficient*, is, generally a function of frequency and is measured in m^{-1} . I_v is the intensity per unit frequency interval. The minus sign corresponds to the normal attenuation of the incident beam.

Integrating Eqn. (5.33), we have

$$I_v(z) = I_v(o) \exp(-\int_0^z k_v dz) \quad \dots(5.34)$$

If the medium is homogeneous

$$I_v(z) = I_v(o) \exp(-k_v z) \quad \dots(5.35)$$

Transforming this relation suitably, one can express k_v as a function of v . A plot of k_v against v , gives a curve similar to the one shown in Fig. 5.7.

It must be emphasized that Fig. 5.7 is not just Fig. 5.6 upside down. It would be so only if $k_v z < < 1$ in which case Eqn. (5.35) can be written as

$$I_v(z) = I_v(o) (1 - k_v z)$$

and hence,

$$I_v(o) - I_v(z) = k_v z I_v(o) \quad \dots(5.36)$$

In this case the profile of k_v is the mirror image of Fig. 5.6

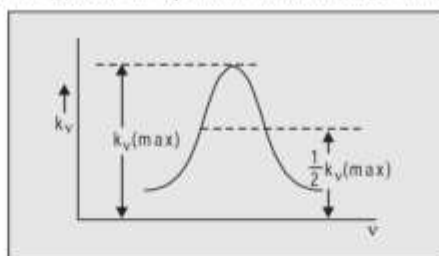


Fig. 5.7 Absorption coefficient

But if the terms of the order of $k_v^2 z^2$ are to be retained in the expansion of the exponential, the two curves will differ in shape.

Since the width of spectral line is somewhat indeterminate, it is customary to use 'half-width'.

The width of the curve at the place where k_v has fallen to one half of its maximum value is called the 'half-width' of the line and is denoted by Δv . Note that 'half-width' does not mean one-half of the width of the curve; it is the full width of the line at half its peak value.

Consider a beam of light of frequency between v and $v + dv$ and intensity I_v per unit frequency interval travelling in the z -direction through a layer of atoms bounded by the planes z and $z + dz$ (Fig. 5.8). The energy incident per unit area per unit time on the slab in the frequency band dv is $I_v d_v$.

The energy absorbed per unit time is by Eqn. (5.33)

$$-\delta I_v = I_v d_v k_v dz \quad \dots(5.37)$$

Neglecting the slight variation in v throughout the line and assuming that I_v does not vary appreciably over the line profile, the total energy absorbed per second is

$$-dI = I_v dz \int k_v d_v = v\rho(v)dz \int k_v dv \quad \dots(5.38)$$

(as $I_v = v\rho(v)$)

where v is the velocity of light in the medium and $\rho(v)$ is the density of radiation at frequency v . The integral is taken over the width of the line.

If N_1 is the number of atoms per c.c. in the lower level 1 and N_2 in the upper level, the energy absorbed in terms of Einstein coefficients is

$$-dI = h\rho(v) (B_{12}N_1 - B_{21}N_2)dz \quad \dots(5.39)$$

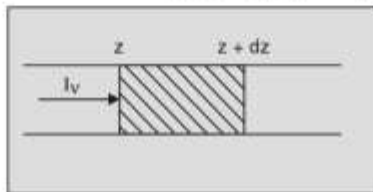


Fig. 5.8 Absorption through a slab

We have ignored the effect of spontaneous emission in view of the fact that it emits in all directions and, hence, its contribution to the beam energy in the direction z is very little. Equating Eqn. (5.38) and Eqn. (5.39)

$$v\rho(v) dz \int k_v dv = h\rho(v) (B_{12}N_1 - B_{21}N_2)dz$$

$$\begin{aligned} \text{i.e., } \int k_v dv &= \frac{hv}{v} N_1 B_{12} \left(1 - \frac{B_{21}N_2}{B_{12}N_1} \right) \\ &= \frac{\eta h\omega}{c} N_1 B_{12} \left(1 - \frac{g_1 N_2}{g_2 N_1} \right) \end{aligned} \quad \dots(5.40)$$

$$= \eta \frac{c^2 \pi^2 g_2 A_{21} N_1}{g_1 \omega^2} \left(1 - \frac{g_1 N_2}{g_2 N_1} \right) \quad \dots(5.41)$$

where we have put $v = \frac{c}{\eta}$ (η : refractive index of the medium) and have used

Eqns. (2.18) and (2.20). This relation is known as *Füchbauer Ladendurag formula*. It provides a link between the population difference between the two levels and the absorption coefficient.

When $g_2 N_1$ approaches $g_1 N_2$ asymptotically the rate of absorption approaches zero. This phenomenon is called *saturation*.

Absorption is often expressed in terms of the *atomic absorption coefficient*, usually denoted by σ_v and given by

$$\sigma_v = \frac{k_v}{N} \quad \dots(5.42)$$

where N is the number of atoms per unit volume. It is also called *atomic cross-section* since it has the dimensions of area. Sometimes it is convenient to analyze the problem of interaction in terms of the absorption cross-section σ_{12} and the corresponding emission cross-section σ_{21} of a single atom, both being functions of frequency. Thus

$$\int k_v dv = \sigma_{12} N_1 - \sigma_{21} N_2 \quad \dots(5.43)$$

Comparing this with Eqn. (5.40), we have

$$\sigma_{12} = \frac{\eta h\omega}{c} B_{12}; \sigma_{21} = \frac{\eta h\omega}{c} \frac{g_1}{g_2} B_{12} = \frac{\eta h\omega}{c} B_{21} \quad \dots(5.44)$$

In the case of non-degenerate systems

$$\sigma_{12} = \sigma_{21} = \frac{\int k_v dv}{N_1 - N_2} \quad \dots(5.45)$$

5.7 SHAPE AND WIDTH OF SPECTRAL LINES

As stated above, absorption and emission do not take place at a single frequency, but over a range of frequencies spanning the atomic line width. The mean absorption of a beam of resonance radiation in traversing a gas depends upon the frequency distribution of the line. An understanding of the mechanism responsible for the broadening of the linewidth is necessary for the development of laser sources with sufficient spectral purity. Further, for detailed calculation of the interaction of radiation with atom it is necessary to have accurate knowledge of the line profile. The width and shape of spectral lines also provide information about temperature and density in the source. In order to account for the frequency dependence of absorption, we modify the relation Eqn. (5.41) and write

$$k_\omega = \frac{\eta c^2 \pi^2 g_2 A_{21}}{g_1 \omega_0^2} \left(N_1 - \frac{g_1}{g_2} N_2 \right) g(\omega) \quad \dots(5.46)$$

Hence, the atomic cross-section is

$$\sigma_\omega = \frac{\eta c^2 \pi^2 g_2 A_{21}}{g_1 \omega_0^2} g(\omega) \quad \dots(5.47)$$

where $g(\omega)$ is called the *line shape function* and represents the frequency behaviour of k_ω ; ω_0 is the central frequency or the *resonance frequency*. The function $g(\omega)$ is such that, it is different from zero in the neighbourhood of ω_0 and is a normalized function, that is, it satisfies the relation

$$\int_{-\infty}^{\infty} g(\omega) d\omega = 1 \quad \dots(5.48)$$

One can see that with this condition k_m as defined in Eqn. (5.46) satisfies Eqn. (5.48).

The peak value of absorption in the unexcited material ($N_1 = N_0$, $N_2 = 0$) is given by

$$k_{m_0} = \frac{\eta c^2 \pi^2 g_2 A_{21} N_0}{g_1 \omega_0^2} g(\omega_0) = N_0 \sigma_0 \quad \dots(5.49)$$

5.8 LINE BROADENING MECHANISMS

The particular shape of the function $g(\omega)$ depends on the phenomenon responsible for the line broadening. There are several physical mechanisms that can broaden the resonant response of a transition. These can broadly be classified into two groups: (i) homogeneous and (ii) non-homogeneous. Some broadening mechanisms broaden the response of each individual atom equally and hence, have the same effect on all the atoms in the ensemble. Every atom, therefore, has the same centre frequency and the same atomic line-shape. This is *homogeneous* broadening, e.g., natural broadening, collision broadening. The other type of broadening mechanism operates by shifting or spreading out the centre frequencies of individual atoms. The essential feature of this mechanism is that different atoms, or groups of atoms, within the ensemble have slightly different resonance frequencies on the same transition. These broaden the overall response of the ensemble without broadening the response of the individual atoms, e.g., Doppler broadening, broadening due to crystalline strains and defects. This is *non-homogeneous* broadening.

5.8.1 Natural or Intrinsic Broadening

1. Classical Treatment

The simplest model of an emitter is the classical electron oscillator. The equation of an electron performing simple harmonic motion is of the form

$$\ddot{x} + \gamma \dot{x} + \omega_0^2 x = 0 \quad \dots(5.50)$$

where ω_0 is the characteristic angular frequency ($\omega_0 = 2\pi v_0$) and γ is the damping factor resulting from radiation [233]. The oscillator has a lifetime

$$\tau_{\text{class}} = 1/\gamma \quad \dots(5.51)$$

The electric field associated with such an oscillator is

$$\begin{aligned} E(t) &= E_0 \exp\left(-\frac{\gamma}{2}t\right) \exp(-i\omega_0 t) && \text{for } t \geq 0 \\ &= 0 && \text{for } t < 0 \end{aligned} \quad \dots(5.52)$$

The frequency spectrum corresponding to Eqn. (5.52) is given by its Fourier transform

$$\begin{aligned}
 E(\omega) &= \frac{1}{2\pi} \int_0^\infty E_0 \exp \left\{ \left(-\frac{\gamma}{2} - i\omega_0 + i\omega \right) t \right\} dt \\
 &= \frac{E_0}{2\pi} \frac{1}{i(\omega - \omega_0) + \gamma^2/2}
 \end{aligned} \quad \dots(5.53)$$

The intensity distribution is given by

$$I(\omega) \propto |E(\omega)|^2 = \left(\frac{E_0}{2\pi} \right)^2 \frac{1}{(\omega - \omega_0)^2 + \gamma^2/4}$$

Hence, the frequency distribution is

$$g(\omega) = \frac{K}{(\omega - \omega_0)^2 + \gamma^2/4}$$

where K is a constant to be found from the normalization condition Eqn. (5.48).

Now,

$$\begin{aligned}
 \int_{-\infty}^{\infty} g(\omega) d\omega &= \frac{4K}{\gamma^2} \int_{-\infty}^{\infty} \frac{d\omega}{\frac{4}{\gamma^2} (\omega - \omega_0)^2 + 1} \\
 &= \frac{2K}{\gamma} \left[\tan^{-1} \frac{2(\omega - \omega_0)}{\gamma} \right]_{-\infty}^{\infty} = 1
 \end{aligned}$$

For small values of γ

$$\begin{aligned}
 \left[\tan^{-1} \frac{2(\omega - \omega_0)}{\gamma} \right]_{-\infty}^{\infty} &= \pi \\
 \frac{2K}{\gamma} \pi &= 1 \text{ or } K = \frac{\gamma}{2\pi}
 \end{aligned}$$

Hence,

$$g_L(\omega) = \frac{\gamma}{2\pi} \frac{1}{(\omega - \omega_0)^2 + \gamma^2/4} \quad \dots(5.54)$$

The line shape of such a distribution is known as the *Lorentz line shape*. The shape is shown in Fig. 5.9.

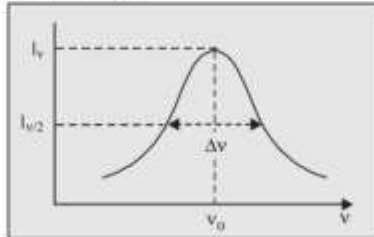


Fig. 5.9 Lorentzian line shape

The maximum value $g_L(\omega)$ at $\omega = \omega_0$ is $\frac{2}{\pi\gamma}$

\therefore The frequency corresponding to the half-intensity is given by

$$\frac{\gamma}{2\pi} \frac{1}{(\omega_{1/2} - \omega_0)^2 + \gamma^2/4} = \frac{1}{\pi\gamma}$$

This gives

$$(\omega_{1/2} - \omega_0)^2 = \gamma^2/4 \text{ i.e., } \omega_{1/2} = \omega_0 \pm \gamma/2 \quad \dots(5.55)$$

Therefore, the half width

$$\Delta\omega_0 = \gamma = 1/\tau_{\text{class}} \quad \dots(5.56)$$

We can write Eqn. (5.54) in terms of Eqn. (5.56) as

$$g_L(\omega) = \frac{2}{\pi\Delta\omega_0} \frac{1}{1 + (\omega - \omega_0)^2/(\Delta\omega_0/2)^2} \quad \dots(5.57)$$

We have derived the expression for the line shape considering only a single oscillator. It can be shown, however, that the spectrum of an ensemble of randomly phased oscillators is identical with Eqn. (5.54).

2. Quantum Mechanical Treatment

The discrete energy levels of atoms between which transition takes place cannot be infinitely narrow. The uncertainty principle $\Delta E \Delta t \sim \hbar$ requires an energy spread $\Delta E \sim \hbar/\Delta t = \hbar/\tau_c$, where τ_c is the life-time of the state concerned.

The frequency spread of a state i , therefore, is

$$\Delta\nu_i = \frac{1}{2\pi\tau_c} \quad (\text{Fig. 5.10}) \quad \dots(5.58)$$

This shows that greater the mean life of an atom in a given state, smaller will be the half-width of the state. It follows that the ground state or the metastable state, for which τ is very large, will be sharp; whereas, other states will be relatively broad. These upper states usually have a life-time of the order 10^{-8} s. Hence, a spectrum line resulting from a transition from the ground state to such an upper state will have a frequency spread of the order of

$$\Delta\nu = 16 \text{ MHz} \quad \dots(5.59)$$

Since in general, both the upper and lower levels have finite lifetimes, the uncertainty in the frequency of emitted radiation must include the uncertainty in the energy of both the levels. This frequency distribution has been derived by Weisskopf and Wigner [393]. This treatment is beyond the scope of this book and, hence, we will only mention here that the expression derived is identical with Eqn. (5.54).

The width of the line is given by

$$\Delta\nu = \delta_1 + \delta_2 \quad \dots(5.60)$$

where δ_1 , δ_2 are the widths of the two levels (Fig. 5.10).

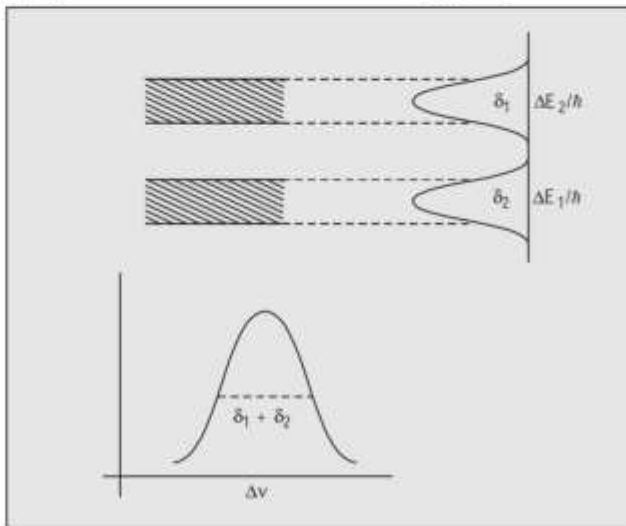


Fig. 5.10 Natural width of a spectral line

The natural broadening, though is quite fundamental, is relatively small in magnitude and is often overshadowed by other phenomena affecting the width.

5.8.2 Collision Broadening

We will now discuss another example of homogeneous broadening, namely, the broadening of a spectrum line produced by the sudden change of atomic radiation by collision. In a gas at high temperatures, collisions of atoms occur with other atoms, ions or walls of the container. If an atom is emitting a photon when such a collision occurs, the phase of the radiated wave-train is altered in the short collision time (Fig. 5.11). We can approximately describe the emitted wave by the function

$$E(t) = E_0 \exp \{-i(\omega_0 t - \phi)\} \quad \dots(5.61)$$

where ϕ changes discontinuously at each collision. Each atom in an ensemble containing a large number of atoms, experiences such a random dephasing collisions and then random changes in phase cause the broadening of the line.

The Fourier transform of Eqn. (5.61) is

$$E(\omega) = \frac{1}{2\pi} \int_{t_0}^{t_0 + \tau} E_0 \exp(-i\omega_0 t + i\phi) \exp(i\omega t) dt$$

where τ is the time between collisions.

$$\therefore E(\omega) = \frac{E_0}{2\pi} \exp \{i(\omega - \omega_0)t + i\phi\} \\ \times \left[\frac{\exp \{i(\omega - \omega_0)\tau\} - 1}{i(\omega - \omega_0)} \right] \quad \dots(5.62)$$

The intensity distribution is given by

$$I(\omega) \propto |E(\omega)|^2 = \left(\frac{E_0}{\pi} \right)^2 \frac{\sin^2 \{(\omega - \omega_0)\tau/2\}}{(\omega - \omega_0)^2} \quad \dots(5.63)$$

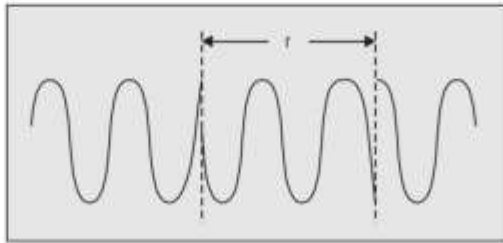


Fig. 5.11 Time behaviour of the electric field of an e.m.-wave as seen from an atom undergoing collision

Since the atoms have different values of τ , we have to average the distribution over all possible values of τ . It has been shown in books on Statistical mechanics [232] that if τ_c is the mean collision time, the probability of a collision between t' and $t' + dt'$ is

$$P(t') dt' = \frac{1}{\tau_c} \exp(-t'/\tau_c) dt' \quad \dots(5.64)$$

$$\therefore I(\omega) \propto \left(\frac{E_0}{\pi} \right)^2 \int_0^\infty \frac{\sin^2 (\omega - \omega_0)\tau/2}{(\omega - \omega_0)^2} \exp(-\tau/\tau_c) \frac{1}{\tau_c} d\tau \\ = \frac{1}{2} \left(\frac{E_0}{\pi} \right)^2 \frac{1}{(\omega - \omega_0)^2 + (1/\tau_c)^2}$$

Hence,

$$g_L(\omega) = \frac{K}{(\omega - \omega_0)^2 + (1/\tau_c)^2} \\ = \frac{1}{\pi} \frac{\tau_c}{(\omega - \omega_0)^2 \tau_c^2 + 1} \quad \dots(5.65)$$

where the constant K has been found from the normalization condition. The contour is again Lorentzian.

To find the half-width we put

$$\frac{\tau_c}{\pi \{(\omega_{1/2} - \omega_0)^2 \tau_c^2 + 1\}} = \frac{\tau_c}{2\pi}$$

$$\text{Hence } 1 + (\omega_{1/2} - \omega_0)^2 \tau_c^2 = 2 \text{ i.e., } \omega_{1/2} - \omega_0 = \pm 1/\tau_c \quad \dots(5.66)$$

Therefore

$$\Delta\omega_c = \frac{2}{\tau_c} \quad \text{or} \quad \Delta\nu_c = \frac{1}{\pi\tau_c} \quad \dots(5.67)$$

An order of magnitude estimate for the time interval τ_c between the collisions is given by

$$\tau_c = \frac{\text{Mean free path}}{\text{Mean velocity}}$$

$$\text{Mean free path} = \frac{kT}{4\sqrt{2}\pi Pa^2}$$

$$\text{Mean velocity} = \sqrt{\frac{8kT}{\pi m}}$$

where p is the pressure of the gas, a is the radius of the molecule and m its mass. [232].

$$\therefore \tau_c = \frac{kT}{4\sqrt{2}\pi pa^2} \cdot \frac{\sqrt{\pi m}}{\sqrt{8kT}} = \frac{(mkT)^{1/2}}{16\pi^{1/2} pa^2} \quad \dots(5.68)$$

For example, in the case of neon gas,

$$\text{atomic weight} = 20.18$$

$$\text{radius} \sim 1.12 \text{ Å}$$

Assuming the temperature to be 300 K and pressure 0.5 Torr we have

$$\tau_c \sim 0.5 \times 10^{-6} \text{ sec} \quad \dots(5.69)$$

$$\text{giving} \quad \Delta\nu_c = 0.64 \text{ MHz} \quad \dots(5.70)$$

This type of broadening mechanism is dominant in high temperature arcs and plasmas. It also occurs in solids. One cannot, of course, visualize collisions in solids as impacting of two particles since the atoms or ions of the active medium are locked in place in crystalline or amorphous solids. However, each atom in a solid is under the influence of the a.c. field resulting from the internal oscillations of the other atoms. These fields, though weak, are close to the resonances of the atom. Each atom is, thus, randomly coupled with the neighbouring atoms through these dipole interactions and the net result is essentially the same as that of the collisions that occur in a gas.

5.8.3 Doppler Broadening

In the discussion of the lineshape, up to this point, we have consistently assumed that all atoms are liable to make the same contribution to the line

broadening. The corresponding relaxation processes being the same throughout. We shall now discuss a different type of process that affects the line width.

It is well known that the atoms or molecules in a gas, though otherwise free and undisturbed, are almost inevitably moving with high thermal velocities. Because of the Doppler effect there is an apparent shift in the frequency of the signal emitted by such atoms. The atoms moving towards the observer appear to emit or absorb light of a higher frequency than those at rest; whereas, the receding atoms emit or absorb at lower frequencies.

In a gas with atoms moving in all directions, therefore, spectral line is spread out over a range of frequencies. This is clearly an example of inhomogeneous broadening.

If v is the velocity of the atom and θ is the angle between v and the direction of observation, the change in frequency due to Doppler effect is given by

$$\frac{\Delta v}{v_0} = \frac{v - v_0}{v_0} = \frac{v \cos \theta}{c} = \frac{u}{c} \quad \dots(5.71)$$

where v_0 is the centre frequency of the line when $v = 0$, v is the observed frequency and

$$u = v \cos \theta$$

Assuming a Maxwellian distribution of velocities, the probability that an atom of mass M has a velocity component between u and $u + du$ at a temperature T is [232].

$$P(u)du = \left(\frac{M}{2\pi kT}\right)^{1/2} \exp(-Mu^2/2kT)du \quad \dots(5.72)$$

Substituting from Eqn. (5.71), the probability that the atom emits in the frequency range v and $v + dv$ is

$$P(v)dv = \frac{c}{v_0} \left(\frac{M}{2\pi kT}\right)^{1/2} \exp\left(-\frac{Mc^2}{2kT} \left(\frac{v - v_0}{v_0}\right)^2\right)dv \quad \dots(5.73)$$

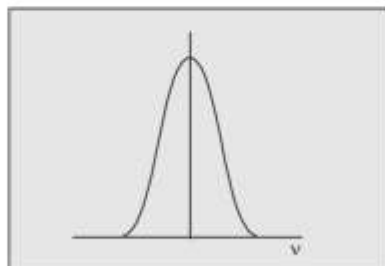


Fig. 5.12 Gaussian lineshape

Since the intensity I_ν at the frequency ν is proportional to this probability we can write for lineshape

$$g_D(\omega) = \frac{c}{\omega_0} \left(\frac{M}{2\pi kT} \right)^{1/2} \exp \left(-\frac{Mc^2}{2kT} \left(\frac{\omega - \omega_0}{\omega_0} \right)^2 \right) \quad \dots(5.74)$$

Note that the relation Eqn. (5.74) satisfies Eqn. (5.48).

The plot of this relation shows a Gaussian lineshape (Fig. 5.12).

To find the frequency at which the intensity drops to half its maximum value, we set

$$\begin{aligned} \exp \left(-\frac{Mc^2}{2kT} \left(\frac{\nu - \nu_0}{\nu_0} \right)^2 \right) &= 1/2 \\ \text{i.e.,} \quad \frac{Mc^2}{2kT} \left(\frac{\nu - \nu_0}{\nu_0} \right)^2 &= \ln 2 \\ \text{or} \quad (\nu - \nu_0) &= \left(\frac{2kT}{Mc^2} \right)^{1/2} \nu_0 \sqrt{\ln 2} \end{aligned}$$

Therefore,

$$\Delta\omega_D = 2\omega_0 \left(\frac{2kT \ln 2}{Mc^2} \right)^{1/2} \quad \dots(5.75)$$

For example, for the Ne line at $\lambda = 6328 \text{ Å}$ at the room temperature $\Delta\nu_n = 1.13 \text{ GHz}$ $\dots(5.76)$

It is sometimes convenient to express the lineshape function Eqn. (5.74) in terms of $\Delta\omega_D$ given by Eqn. (5.75). Thus

$$g_D(\omega) = \frac{2}{\Delta\omega_D} \left(\frac{\ln 2}{\pi} \right)^{1/2} \exp \left(-\left(\frac{\omega - \omega_0}{\Delta\omega_D/2} \right)^2 \ln 2 \right) \quad \dots(5.77)$$

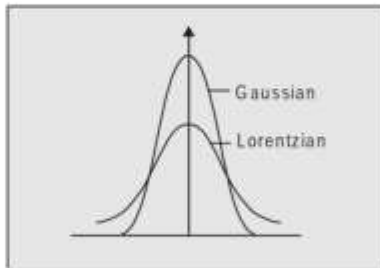


Fig. 5.13 Comparison of Lorentzian and Gaussian lineshapes

In order to give an idea of the order of the magnitude of the broadening produced by the three effects discussed above, we have estimated approximately

the line width in Eqns. (5.59), (5.70) and (5.76). A comparison of these shows that the Doppler broadening is much greater than natural broadening and the latter is much greater than the collision broadening. It must be emphasized here, however, that this is not always true. At high pressures collision broadening becomes predominant and heavily outweighs the broadening due to natural damping.

We present in Fig. 5.13 Gaussian and Lorentzian types of curves of the same line-width drawn with the same width at half-power points.

Note that the Gaussian curve is much sharper than the Lorentzian.

$$g_L(\omega) = \frac{2}{\pi \Delta \omega_0} = \frac{0.637}{\Delta \omega_0} \quad \dots(5.78)$$

$$G_D(\omega) = \frac{2}{\Delta \omega_0} \left(\frac{\ln 2}{\pi} \right)^{1/2} = \frac{0.939}{\Delta \omega_0} \quad \dots(5.79)$$

6

BASIC PRINCIPLES OF LASERS

We have now enough background information to take up the discussion of the operation of laser oscillators. We will discuss in this chapter the fundamentals of laser amplification.

6.1 POPULATION INVERSION

The quantity dI in Eqns. (5.38) and (5.39) is usually negative and is responsible for the normal attenuation of the incident beam. Is it possible to make dI positive? In other words, can there be what may be called a *negative absorption process* causing the amplification of the beam as it passes through a medium? In the pre-laser era it was not observed and was even considered to be unthinkable. The discussion in the preceding chapters indicates how such amplification may occur. Suppose, for example, that all the atoms in a cell are in the upper level with energy E_2 . As a beam of frequency $\omega_{21} = (E_2 - E_1)/\hbar$ where E_1 is the lower energy level, passes through the medium, there can be no absorption, but there will be stimulated emission. The additional quantum of energy liberated due to the atom undergoing stimulated transition will be in the same state as the primary photon and, thus, adds to the incident wave on a constructive basis, reinforcing the light beam. The process is illustrated in Fig. 6.1. The physical nature of the process is clear. Two photons in their turn will induce two other atoms to emit photons of the same frequency and, thus, will cause an avalanche of secondary photons in the same state as the primary photon. This is the direct consequence of the "bosonic nature" of photons; *i.e.*, their tendency to populate predominantly just those states that already have a sufficiently high population density. [232]

In fact, it is not necessary to have such a stringent condition as envisaged above for amplification to occur. We can see from relation (5.41) that if

$$N_2 \gg N_1 \quad \dots(6.1)$$

the absorption coefficient k_v is negative. Thus, if the majority of the atoms are in the upper state, the absorption coefficient will be negative causing amplification of the incident beam by stimulated emission. To achieve laser action it is necessary, therefore, to devise a means of achieving condition (6.1). This is known as *population inversion* and is one of the basic requirements of laser action.

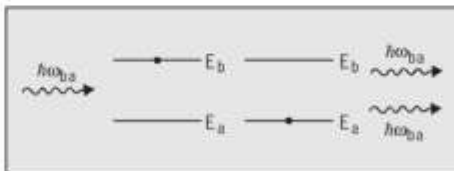


Fig. 6.1 Stimulated emission

6.2 LASER PUMPING

We have seen in Chapter 4, how the condition (6.1) was achieved by Gordon, Zeiger and Townes in the case of ammonia maser. The question that confronts us is "how the necessary population inversion can be obtained in a laser device?" The process by which atoms are raised from the lower level to the upper one, is called the pumping process. The pumping process in lasers typically involves a large number of energy levels with complex excitation processes. Diverse techniques of excitation are used in laser devices such as: excitation by a strong source of light, say flash lamp or arc lamp (optical pumping), excitation by electron impact (electrical pumping), excitation by chemical reaction (chemical pumping) excitation by means of supersonic gas expansion (gas-dynamic pumping) and so on. These processes will be dealt with in detail later when we describe the various types of lasers. In this section we propose to consider the possibility of creating stationary inversion under optical pumping.

6.2.1 A Two-Level System

Let us first consider the time evolution of the population of a two level system in the presence of a monochromatic electromagnetic wave.

If the frequency of the electromagnetic wave is equal to the transition frequency ω_{21} some of the atoms will absorb energy and arrive at the upper level. Let N_1, N_2 be the populations of the two levels per unit volume and N_0 the total population which we assume to be constant.

$$\therefore \quad N_1 + N_2 = N_0 \quad \dots(6.2)$$

$$\text{Let} \quad \Delta N = N_1 - N_2 \quad \dots(6.3)$$

Combining this with Eqn. (6.2), we get

$$N_1 = \frac{N_0 + \Delta N}{2}; N_2 = \frac{N_0 - \Delta N}{2} \quad \dots(6.4)$$

Excited atoms undergo transition to the lower level by spontaneous and stimulated emissions. Besides radiative transition, atoms can also undergo non-radiative transitions by imparting their excess energy to the surrounding atoms as in the case of a gas or to the lattice as in the case of a solid. We represent the probability of spontaneous transition by $1/\tau_{sp}$ ($= A_{sp}$) where τ_{sp} is the spontaneous emission decay time. Similarly the probability of non-radiative transition is represented by $1/\tau_{nr}$ where τ_{nr} is the lifetime of the non-radiative process.

The overall time decay, therefore, is τ given by

$$\frac{1}{\tau} = \frac{1}{\tau_{sp}} + \frac{1}{\tau_{nr}} \quad \dots(6.5)$$

The rate of change of the population of the upper level is given by

$$\begin{aligned} \frac{dN_2}{dt} &= B_{12}\rho(\omega_{21})N_1 - B_{21}\rho(\omega_{21})N_2 - \frac{N_2}{\tau} \\ &= B_{12}\Delta N\rho(\omega_{21}) - \frac{N_2}{\tau} \end{aligned} \quad \dots(6.6)$$

where B_{12} , B_{21} are Einstein's coefficients. The last term accounts for the spontaneous and non-radiative transitions.

In the steady state $\frac{dN_2}{dt} = 0$

$$\therefore B_1\Delta N\rho(\omega_{21}) = \frac{N_2}{\tau} = \frac{N_0 - \Delta N}{2\tau}$$

$$\text{Hence, } \Delta N = \frac{N_0}{1 + 2 B_{21} \rho(\omega_{21})\tau} \quad \dots(6.7)$$

This relation shows that the population difference between the two levels in a steady state depends on the decay time of the upper level and on the density of the incident radiation $\rho(\omega_{21})$. $B_{12} \rho(\omega_{21})$ is the probability per unit time that the atoms are excited to the upper level and may be called the *pumping rate*. We represent it by Ω

$$\therefore \Delta N = \frac{N_0}{1 + 2 \Omega \tau} \quad \dots(6.8)$$

We see that whatever the value of Ω , ΔN is always positive and, hence, inversion is not possible.

$$\text{If } \Omega \rightarrow \infty, \Delta N \rightarrow 0 \text{ i.e., } N_1 = N_2 = \frac{N_0}{2}$$

A two level system, therefore, is not suitable for optical pumping.

The pump power absorbed by the material per unit volume, to maintain a given population difference ΔN is

$$\frac{d\hbar}{dV} = \hbar \omega_{21} B_{12} \rho(\omega_{21}) \Delta N = \frac{\hbar \omega_{21} B_{12} \rho(\omega_{21}) N_0}{1 + 2 B_{12} \rho(\omega_{21}) \tau}$$

If $B_{12} \rho(\omega_{21}) \gg 1$

$$\frac{dP}{dV} = \frac{\hbar \omega_{21} N_0}{2\tau} \quad \dots(6.9)$$

We see that the pump power also depends upon the decay time τ .

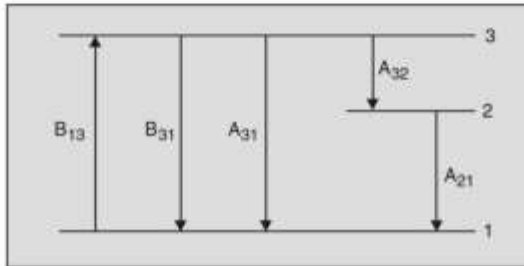


Fig. 6.2 Three-level system

6.2.2 A Three-Level System

Let us now consider a three-level system, shown in Fig. 6.2.

Of the total number of atoms that the pump lifts from level 1 to level 3, some go back to level 1 by spontaneous and stimulated emissions and some to level 2 by radiative and non-radiative processes. The rate equations in the steady state are:

$$(i) \frac{dN_3}{dt} = N_1 B_{13} \rho(\omega_{31}) - N_3 B_{13} \rho(\omega_{31}) - N_3 A_{31} - N_3 S_{32} = 0$$

where,

- (a) the first term represents the number of atoms arriving at the level 3, per unit time per unit volume, due to induced absorption,
- (b) the second term represents the number of stimulated emissions,
- (c) the third term represents the number of spontaneous emissions, and
- (d) the fourth term represents the transitions to the level 2 due to radiative and non-radiative processes. (S_{32} represents the probability of transition due to radiative and non-radiative processes).

$$(ii) \frac{dN_2}{dt} = N_3 S_{32} - N_2 A_{21} + B_{12} \rho(\omega_{21}) N_1 - B_{12} \rho(\omega_{21}) N_2 = 0$$

Here, the last two terms represent the induced transitions between levels 1 and 2 due to the presence of laser radiation.

$$(iii) \frac{dN_1}{dt} = N_3 B_{13}\rho(\omega_{31}) + N_3 A_{31} + N_2 B_{12}\rho(\omega_{21}) + N_2 A_{21} - N_1 B_{13}\rho(\omega_{31}) - N_1 B_{12}\rho(\omega_{21}) = 0$$

$$(iv) N_0 = N_1 + N_2 + N_3 \quad \dots(6.10)$$

We see from (i) to (iii) that

$$\frac{dN_1}{dt} + \frac{dN_2}{dt} + \frac{dN_3}{dt} = 0$$

which is consistent with (iv)

Solving these equations we get,

$$N_2 = \frac{N_0 \left\{ B_{12}\rho(\omega_{21}) + \frac{B_{13}\rho(\omega_{31})S_{32}}{B_{13}\rho(\omega_{31}) + A_{31} + S_{32}} \right\}}{2B_{12}\rho(\omega_{21}) + A_{21} + \frac{B_{13}\rho(\omega_{31})S_{32} + B_{13}\rho(\omega_{31}) \{B_{12}\rho(\omega_{21}) + A_{21}\}}{B_{13}\rho(\omega_{31}) + A_{31} + S_{32}}}$$

$$N_1 = \frac{N_0 \{B_{12}\rho(\omega_{21}) + A_{21}\}}{2B_{12}\rho(\omega_{21}) + A_{21} + \frac{B_{13}\rho(\omega_{31})S_{32} + B_{13}\rho(\omega_{31}) \{B_{12}\rho(\omega_{21}) + A_{21}\}}{B_{13}\rho(\omega_{31}) + A_{31} + S_{32}}}$$

$$\therefore N_2 - N_1 = \frac{N_0 \left\{ \frac{B_{13}\rho(\omega_{31})S_{32}}{B_{13}\rho(\omega_{31}) + A_{31} + S_{32}} - A_{21} \right\}}{2B_{12}\rho(\omega_{21}) + A_{21} + \frac{B_{13}\rho(\omega_{31})S_{32} + B_{13}\rho(\omega_{31}) \{B_{12}\rho(\omega_{21}) + A_{21}\}}{B_{13}\rho(\omega_{31}) + A_{31} + S_{32}}} \quad \dots(6.11)$$

The number of atoms arriving per unit time at the level 2 is

$$N_3 S_{32} = \frac{N_1 B_{13}\rho(\omega_{31})S_{32}}{B_{13}\rho(\omega_{31}) + A_{31} + S_{32}}$$

where we have used (i) of Eqn. (6.10)

Hence, the probability Ω that an atom arrives at the level 2 is

$$\Omega = \frac{B_{13}\rho(\omega_{31})S_{32}}{B_{13}\rho(\omega_{31}) + A_{31} + S_{32}} \quad \dots(6.12)$$

Using this in Eqn. (6.11)

$$N_2 - N_1 = \frac{N_0 (\Omega - A_{21})}{2B_{12}\rho(\omega_{21}) + A_{21} + \frac{B_{13}\rho(\omega_{31})S_{32} + B_{13}\rho(\omega_{31}) \{B_{12}\rho(\omega_{21}) + A_{21}\}}{B_{13}\rho(\omega_{31}) + A_{31} + S_{32}}} \quad \dots(6.13)$$

For population inversion *i.e.*, for $N_2 - N_1$ to be positive, it is necessary that

$$\Omega > A_{21}$$

$$\text{I.e., } \frac{B_{13}P(\omega_{31})S_{32}}{B_{13}P(\omega_{31}) + A_{31} + S_{32}} > A_{21} \quad \dots(6.14)$$

We, thus, see that using a beam of suitable intensity it is possible to produce the required population inversion.

The quantity $\Omega_{inv} = A_{21}$ is called the *inversion threshold pumping rate*.

It will be shown in the next chapter how the circumstances in the four level system are more advantageous for obtaining population inversion.

6.3 RESONATORS

The condition (6.1) in itself is not enough for laser oscillations to occur. A large number of excited atoms decay spontaneously and each spontaneous photon can initiate in the active medium many other stimulated transitions. Photon states are characterized by a definite energy, momentum and polarization of photons. The photons occupying the same state are indiscernible. They are discernible only when they are in different states. Since the spontaneous photons initiating the transitions are generally in different photon states, they are useless from the point of view of coherent amplification. In order to obtain coherent radiation, it is necessary to restrict the number of photon states. The selectivity of photon states and the positive feedback that is necessary to offset the various types of losses, can be obtained by enclosing the radiation in a resonator tuned to the frequency concerned.

6.4 VIBRATIONAL MODES OF A RESONATOR

The electric field of an electromagnetic wave satisfies the equation

$$\nabla^2\mathbf{E} = \frac{1}{c^2} \frac{\partial^2\mathbf{E}}{\partial t^2} \quad \dots(6.15)$$

where c is the velocity of light.

Suppose the waves are confined to a region inside a rectangular cavity, the walls of which are assumed to be perfectly conducting. This is the simplest cavity whose resonance frequencies can be easily calculated. The waves in the cavity are obviously standing waves. Note that we are considering here a cavity which does not contain any amplifying active medium. Such a resonator is called a *passive resonator* as distinguished from an *active resonator* which contains an active medium.

The simplest plane wave solution of (6.15) is

$$E(\mathbf{r}, t) = E_0 \exp\{i(\mathbf{k} \cdot \mathbf{r} - \omega t)\} \quad \dots(6.16)$$

where E_0 is the amplitude and \mathbf{k} the wave vector. The complete solution with real spatial parts is

$$E_x(t) = E_{0x}(t) \cos k_x x \sin k_y y \sin k_z z$$

$$E_y(t) = E_{0y}(t) \sin k_x x \cos k_y y \sin k_z z \quad \dots(6.17)$$

$$E_z(t) = E_{0z}(t) \sin k_x x \sin k_y y \cos k_z z$$

with

$$k^2 = k_x^2 + k_y^2 + k_z^2 \quad \dots(6.18)$$

The Eqn. (6.17) have to satisfy Maxwell's equation $\nabla \cdot \mathbf{E} = 0$

$$\therefore k_x E_{0x}(t) + k_y E_{0y}(t) + k_z E_{0z}(t) = 0$$

i.e., $\mathbf{k} \cdot \mathbf{E}(t) = 0$

Hence, $\mathbf{k} \perp \mathbf{E}$.

The waves have to satisfy a boundary condition at the walls viz. the tangential

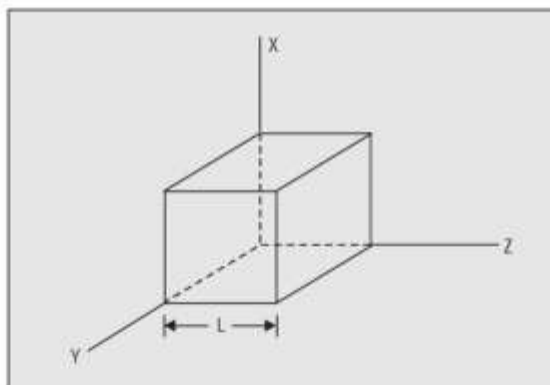


Fig. 6.3 Cubic cavity

component of the field must vanish at the walls. For simplicity let us assume the cavity to be a cube of length L (Fig. 6.3). Since $E_x(t)$ must vanish on the

planes $y = 0$; $y = L$ and $z = 0$; $z = L$; $k_y = \frac{m\pi}{L}$; $k_z = \frac{q\pi}{L}$. Similarly, $E_y(t)$ must vanish on the planes $x = 0$, $x = L$ and $z = 0$, $z = L$

$$k_x = \frac{m\pi}{L} \quad \dots(6.19)$$

where $m, n, q = 0, 1, 2$.

Thus, the boundary conditions force the wave vector components to take discrete values specified by m, n, q . Each set of integers (m, n, q) defines a mode of vibration. These modes are known as Transverse Electromagnetic Modes and are designated by TEM_{mnq} where m, n are the transverse indices and q the longitudinal index. Each mode has a characteristic distribution of amplitude and phase. This distribution in a plane perpendicular to the resonator

axis is described by transverse indices m, n . A given combination of m, n characterizes a *transverse mode* regardless of the value of q . This is designated as a TEM_{mn} mode. For each combination of m, n , there correspond a number of modes with different values of q . These are called *longitudinal* or *axial modes*. There is, thus, an infinite number of resonant frequencies of the cavity corresponding to the different values of m, n, q . Any excitation of the electromagnetic field observed in the resonator can be expressed as a linear combination of these modes.

6.5 NUMBER OF MODES PER UNIT VOLUME

We can plot the wave vectors k in a three-dimensional space with the components k_x, k_y, k_z as shown in Fig. 6.4.

We are now dealing with what is called a *k -space*. In this space the allowed values of k given by Eqn. (6.19) form a cubic point lattice, the spacing between consecutive points being $\frac{\pi}{L}$. Each point in k -space is surrounded by

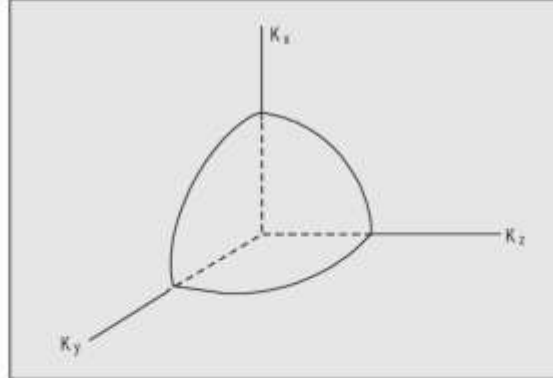


Fig. 6.4 k -space

an empty volume $\left(\frac{\pi}{L}\right)^3$.

Suppose, we want to find the number of such normal modes of standing waves with wave vectors whose magnitude lies between k and $k + dk$.

Since $k_x, k_y, k_z > 0$, we are interested only in the positive octant. The volume between the consecutive shells in the positive octant is $\frac{1}{8} 4\pi k^2 dk$ and, hence, the required number of modes is

$$f(k) dk = \frac{1}{\left(\frac{\pi}{L}\right)^3} \frac{4\pi k^2 dk}{2\pi^2} = \frac{L^3 k^2 dk}{\pi^2} \quad \dots(6.20)$$

Since there are two directions of polarization the number of modes is

$$\frac{L^3 k^2 dk}{\pi^2} \quad \dots(6.21)$$

Thus, the number of modes per unit volume of the cavity *i.e.*, the density of the field modes $\rho_k dk$ is given by

$$\rho_k dk = \frac{k^2 dk}{\pi^2} \quad \dots(6.22)$$

Since $k = \frac{\omega}{c}$, the number of modes per unit volume of the cavity having their frequency between ω and $\omega + d\omega$ is

$$\rho_\omega d\omega = \frac{\omega^2 d\omega}{c^3 \pi^2} \quad \dots(6.23)$$

As an example let us calculate the number of modes per unit volume that fall within a linewidth $dv = 2.5 \times 10^{14}$ Hz of a line at

$$\lambda = 6000 \text{ \AA} \text{ i.e., } v = 5 \times 10^{14} \text{ Hz}$$

$$\rho_\omega d\omega = \frac{\omega^2 d\omega}{c^3 \pi^2} = \frac{8\pi v^2 dv}{c^3} = 5 \times 10^{12} / \text{cm}^3$$

Under actual conditions this large number of modes will all be existing and the intensity pattern resulting from their superposition will be far from monochromatic. It can be seen from (6.23) that with increasing frequency there will be further condensation of resonance spectra.

The question that confronts us is, how to ensure the excitation of only a small number of modes? One of the ways of doing this is to use a cavity resonator of the dimensions of the order of radiation wavelength. In the example above *i.e.*, at $\lambda = 6000 \text{ \AA}$, if we have a cavity with volume $\lambda^3 = 6^3 \times 10^{-15} \text{ cm}^3$, the number of modes in the cavity will be $6^3 \times 10^{-15} \times 5 \times 10^{12} \sim 1$. In fact, if we have a cavity with its linear dimension λ *i.e.*, with its volume

$$V = \lambda^3 = \frac{8\pi^3 c^3}{\omega^3}, \text{ the number of modes in this volume will be}$$

$$V \frac{\omega^2 d\omega}{c^3 \pi^2} = \frac{8\pi^3 c^3}{\omega^3} \cdot \frac{\omega^2 d\omega}{c^3 \pi^2} = \frac{8\pi d\omega}{\omega} \quad \dots(6.24)$$

That is, the number of modes will go on decreasing with increasing frequency. However, the construction of such a resonator is impractical. Besides,

such a small volume of active medium is useless from the point of view of the output power. A way out of this problem was found by Schawlow and Townes [331] and also by Prokhorov [318] who suggested the use of *open resonators*.

6.6 OPEN RESONATORS

An open resonator consists of a pair of reflecting mirrors set on an optical axis. The resonator does not have any conducting side walls. The active medium is placed between the mirrors. In such resonators the photons that travel in the direction of resonator axis and those that deviate very slightly from it, go through a longer path which is further elongated by multiple reflections from the end mirrors. These photons first initiate a stimulated emission and subsequently produce a powerful avalanche of stimulated photons in the same direction.

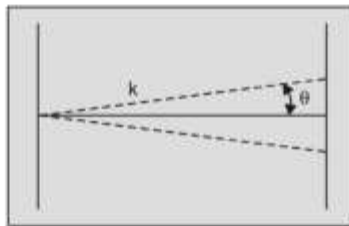


Fig. 6.5 A Photon beam making a small angle with the resonator axis

Suppose the photon beam with the wave vector \mathbf{k} travels in the direction making a very small angle θ with the resonator axis (Fig. 6.5). The direction cosines of the wave vector are

$$\begin{aligned} \frac{k_x}{k} &= \frac{m}{\sqrt{m^2 + n^2 + q^2}} = \frac{m\lambda}{2L} \\ \left(\because k = \frac{2\pi}{\lambda} = \sqrt{k_x^2 + k_y^2 + k_z^2} = \frac{\pi}{L} \sqrt{m^2 + n^2 + q^2} \right) \\ \frac{k_y}{k} &= \frac{n\lambda}{2L} \quad \frac{k_z}{k} = \frac{q\lambda}{2L} \end{aligned} \quad \dots(6.25)$$

Since the beam travels close to the resonator axis, x - and y - direction cosines must be very small; that is m, n must be very small compared to q . Hence, the resonant frequencies are given by ($\because k = \omega/v$)

$$\begin{aligned} \omega &= \frac{v\pi q}{L} \text{ or } v = \frac{vq}{2L} \\ L &= \frac{\lambda q}{2} \end{aligned} \quad \dots(6.26)$$

where v is the velocity of photons in the medium and L is the length of the resonator, i.e., the separation of the two mirrors. Thus, the resonance occurs when integral number of half-wavelengths cover the length between the mirrors. The relation (6.26) can be written as

$$\omega = \frac{c\pi q}{L\eta}$$

where η is the refractive index of the medium. The difference between the adjacent frequencies is

$$\Delta\omega' = \frac{c\pi}{L\eta} = \text{a constant} \quad \dots(6.27)$$

If $\Delta\omega$ is the linewidth of the radiation the number of resonant frequencies within it is

$$N = \frac{\Delta\omega}{\Delta\omega'} = \frac{L\eta\Delta\omega}{c\pi} \quad \dots(6.28)$$

The resonator, therefore, transforms a gain line into a set of narrow lines. (Fig. 6.6)

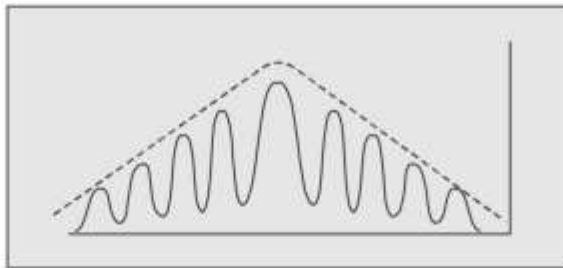


Fig. 6.6 Transformation of a gain line into a set of narrow lines

6.7 THE CONFOCAL RESONATOR

The difficulty of aligning a Fabry Perot interferometer with a spacing of 100 cm is not small. Hence, an alternative system is adopted in which spherical mirrors are employed in a confocal or near confocal configuration (Fig. 6.7). In a confocal resonator the radius of curvature of each mirror is equal to the cavity length. The region marked by the dotted lines is covered by the bouncing light beams. The surface that includes this volume is a hyperboloid of revolution. The diffraction losses of such a configuration are low and the alignment is much less critical. The divergence, however, is large, but can be reduced by placing a circular aperture in front of the exit mirror. A rigorous treatment of various types of resonators has been given by Fox and Li [125] and by Boyd and Gordon [61].



Fig. 6.7 Confocal resonator

6.8 THE QUALITY FACTOR Q

We have seen above that for a definite field configuration, the cavities have some discrete resonant frequencies. This means, if we try to excite a particular mode of oscillation in the cavity, the right sort of field will not be built up unless the exciting frequency is equal to the resonant frequency.

The resonant frequency in a resonator, however, is not quite sharp. Appreciable excitation occurs over a narrow band of frequencies around the resonant frequency. This smearing out of the frequency is due to the various losses associated with the modes in the cavity (scattering, absorption, diffraction etc.). The measure of these losses is often expressed in terms of the *quality factor*-Q of the cavity which is defined as

$$Q = \frac{\omega \times \text{Energy stored in the mode}}{\text{Energy dissipated per second in the mode}} \quad \dots(6.29)$$

That is, smaller the amount of energy dissipated, higher is the Q of the cavity.

Let $W(t)$ be the energy stored in a mode in a passive cavity at time t . The energy will gradually decay with time due to the various losses. The reduction in energy will obviously be proportional to $W(t)$ and the time interval dt .

$$\therefore -dW(t) = AW(t)dt \quad \dots(6.30)$$

where A is a constant. Integrating we get

$$W(t) = W_0 \exp(-At) \quad \dots(6.31)$$

where W_0 is the energy at $t = 0$

The decay time τ_c is defined as the time after which the energy reduces to $1/e$ times its initial value

$$\therefore A\tau_c = 1 \text{ i.e., } \tau_c = 1/A \quad \dots(6.32)$$

$$\text{and } W(t) = W_0 \exp(-t/\tau_c) \quad \dots(6.33)$$

From the definition of the quality factor

$$-\frac{dW(t)}{dt} = \frac{\omega \times W(t)}{Q}$$

$$\text{i.e., } W(t) = W_0 \exp(-\omega t/Q) \quad \dots(6.34)$$

Comparing Eqns. (6.33) and (6.34), we have

$$\tau_c = Q/\omega \text{ or } Q = 2\pi\nu\tau_c \quad \dots(6.35)$$

which is a dimensionless quantity.

We can also relate the Q of a cavity to the linewidth of a radiation. We have seen in Chapter 5 that $\tau_c = 1/\Delta\omega$

$$\therefore Q = \frac{\omega}{\Delta\omega} \quad \dots(6.36)$$

that is, smaller the linewidth, higher is the Q factor of the cavity

6.9 LOSSES INSIDE THE CAVITY

Intensity of a light beam in a cavity, gradually diminishes owing to various losses such as absorption, radiation through the side surface, etc. The intensity diminishes by an exponential law

$$I(z) = I_0 \exp(-\alpha z) \quad \dots(6.37)$$

where α is the loss factor.

We have seen above that the energy in the beam diminishes exponentially according to the equation

$$W(t) = W_0 \exp(-t/\tau_c)$$

which shows that the energy falls to its $1/e$ value in time τ_c . Naturally, the intensity will also be reduced by a factor $1/e$ in the same time. The distance covered by the light flux in time τ_c is $z = c\tau_c$.

$$\therefore I(z) = I_0/e$$

where $\alpha z = \alpha c\tau_c = 1$
i.e. $\alpha = 1/c\tau_c$
Hence

$$Q = 2\pi\nu\tau_c = \frac{2\pi\nu}{\alpha c} = \frac{2\pi}{\alpha\lambda} \quad \dots(6.38)$$

If the losses are of different types we may associate a loss factor α_i with each of them, and, further, if they are independent of one another we may write $\alpha = \sum \alpha_i$

$$\text{Hence, } \frac{1}{Q} = \sum \frac{1}{Q_i} \quad \dots(6.39)$$

6.10 THE THRESHOLD CONDITION

It was primarily the work of Schawlow and Townes [331] and Prokhorov [318] which initiated the dynamic field which we now associate with the concept of "laser". These workers independently discussed the conditions

necessary for achieving laser action. Since it is not possible to construct an optical resonator of the dimensions of the wavelength concerned, as can be done in the microwave region, they suggested two plane parallel reflecting surfaces as a suitable resonator. It has been shown in Sec. 6.6 that if the atoms are placed between two such mirrors, the emitted light can build up into a standing wave. The mirrors reflect the emitted light back into the atomic assembly, thus serving as a means of achieving feedback. (Fig. 6.8)

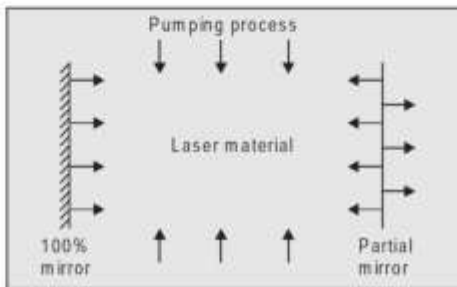


Fig. 6.8 Optical resonator

If L is the length of the cavity and η is the refractive index of the medium, the optical length is $L' = L\eta$. The condition for reinforcement is

$$L' = L\eta = \frac{q\lambda}{2} \text{ i.e., } \frac{v}{c} = \frac{q}{2L\eta} \quad \dots(6.40)$$

where q is an integer. Optical standing waves can be set up in such a cavity if the frequency fulfills condition (6.40). In the case of solid state laser the mirrors are deposited on the end faces of the material and, hence, $L' = \eta L$; whereas in the case of gas lasers, they are outside the active material.

Not all of the intensity of light, I , falling on the mirror is reflected. If I_r is the intensity of the reflected light

$$I_r = rI \quad \dots(6.41)$$

where r , the fraction of the light intensity reflected, is called the *reflection coefficient*. If one of the mirrors is made partially transparent a useful output beam can be extracted. The reflection coefficient of such a mirror must, obviously, be less than 1.

In the normal course, when a beam of light passes through a material, its intensity diminishes as it emerges out of the material of length z as given by

$$I_v(z) = I_v(0) \exp(-k_v z) \quad (\text{see Eqn. 5.35}) \quad \dots(6.42)$$

However, if k_v is negative, there will be amplification and the intensity will increase by a factor $e^{\alpha z}$, i.e.,

$$I_v(z) = I_v(0) e^{\alpha z} \quad \dots(6.43)$$

where $\alpha = -k_v$ is called the *unsaturated gain coefficient*. It determines the gain that exists before amplification.

Let r_1, r_2 be the reflection coefficients of the two mirrors. Then the energy of the wave in one complete passage, back and forth, will diminish by a factor $r_1 r_2$. We write for convenience,

$$r_1 r_2 = e^{-2\gamma} \quad \text{or} \quad \gamma = -\frac{1}{2} \ln r_1 r_2 \quad \dots(6.44)$$

where γ is positive and may be regarded as a measure of loss of light in a single passage. That is, the intensity after each passage will be diminished by a factor $e^{-\gamma}$ i.e., I reduces to $Ie^{-\gamma}$. Assuming that the reflection losses are the only losses present in the cavity, the intensity in each passage changes from I to $I \exp(\alpha L - \gamma)$. For oscillations to be sustained in a laser, the amplification must be sufficient to compensate for the energy lost. For oscillations to build up, therefore,

$$\exp(\alpha L - \gamma) > 1 \quad \text{or} \quad \alpha L > \gamma \quad \dots(6.45)$$

Hence, the threshold will be reached when

$$\alpha L = \gamma \quad \dots(6.46)$$

A laser with a length L and given mirror reflectivity will operate only if

$$\alpha \geq \frac{\gamma}{L} \quad \dots(6.47)$$

Now, by (5.46)

$$\alpha = -k_v = \frac{\eta c^2 \pi^2 g_2 A_{21}}{g_1 \omega_0^2} \left(\frac{g_1 N_2 - N_1}{g_2} \right) g(\omega) \quad \dots(6.48)$$

where $g(\omega)$ accounts for the frequency distribution in the line. Thus, in the case of a line profile dominated by Lorentz broadening, the gain coefficient is given by

$$\alpha_L(\omega) = \frac{\eta c^2 \pi^2 g_2 A_{21} N_1}{g_1 \omega_0^2} \left(\frac{g_1 N_2 - 1}{g_2 N_1} \right) \frac{\gamma}{2\pi (\omega - \omega_0)^2 + \gamma^2/4} \quad \dots(6.49)$$

where we have used (5.54).

The maximum value of the gain coefficient is obtained at $\omega = \omega_0$

$$\alpha_L^0(\omega_0) = \frac{2\eta c^2 g_2 N_1}{g_1 \omega_0^2} \left(\frac{g_1 N_2 - 1}{g_2 N_1} \right) \quad \dots(6.50)$$

$$\left(\because \gamma = \frac{1}{\tau_{21}} = A_{21} \right).$$

Incidentally we see that the maximum gain decreases as the square of the transition frequency increases. This explains why laser oscillations are easier to achieve in the infrared region than in the visible and ultraviolet regions. For lasers to operate, we must have

$$\frac{\eta c^2 \pi^2 g_2 A_{21}}{g_1 \omega_0^2} \left(\frac{g_1}{g_2} N_2 - N_1 \right) g(\omega) \geq \frac{\gamma}{L} \quad \dots(6.51)$$

The laser will operate in the frequency interval in which the above condition is satisfied.

At the threshold the condition becomes

$$\frac{g_1}{g_2} N_2 - N_1 = \frac{\gamma g_1 \omega_0^2}{\eta L c^2 \pi^2 g_2 A_{21} g(\omega)} \quad \dots(6.52)$$

For non-degenerate states

$$N_2 - N_1 = \frac{\gamma \omega_0^2}{\eta L c^2 \pi^2 A_{21} g(\omega)} \quad \dots(6.53)$$

This value of population inversion is known as the *critical inversion*. The formula suggests that for the onset of oscillations γ and L must be properly adjusted.

We can express the condition (6.53) in a different form.

Let P_0 be the number of photons travelling back and forth in a laser. The number of photons after m passages will be

$$P = P_0 e^{-\gamma m} \quad \dots(6.54)$$

If τ_L is the time taken by a photon for a single passage, the time taken for m passages will be $t = m\tau_L$

$$\therefore P = P_0 \exp(-\gamma t / \tau_L) \quad \dots(6.55)$$

The average life-time τ_p of a photon is, by convention, the time by which P_0 is reduced to P_0/e .

\therefore From (6.55)

$$\tau_p = \frac{\tau_L}{\gamma} = \frac{L'}{c\gamma} \quad \left(\because \tau_L = \frac{L'}{c} \right) \quad \dots(6.56)$$

Using this, we can express (6.53) in the form

$$N_2 - N_1 = \frac{L' \omega_0^2 \tau_{21}}{\eta c^3 \tau_p L \pi^2 g(\omega)} \quad \left(\because A_{21} = \frac{1}{\tau_{21}} \right) \quad \dots(6.57)$$

Since $L' = \eta L$

$$N_2 - N_1 = \frac{\omega_0^2 \tau_{21}}{c^3 \pi^2 \tau_p g(\omega)} \quad \dots(6.58)$$

Or using (5.78)

$$N_2 - N_1 = \frac{\omega_0^2 \tau_{21}}{2c^3 \pi^2 \tau_p} \Delta \omega_0 \quad \dots(6.59)$$

This is known as *Schawlow-Townes condition* for laser oscillations. The population difference required to set off laser oscillations, thus, depends on the

two life-times: the spontaneous life-time of the upper energy level and the effective decay time of the cavity.

To gain some feeling for the size of the population inversion required, let us consider the case of a ruby laser in which the appropriate parameters have the following values:

$$\nu_0 = 4.3 \times 10^{14} \text{ Hz}; \quad \Delta\nu_0 = 1.5 \times 10^{11} \text{ Hz}; \\ \tau_{21} = 4.3 \times 10^{-3} \text{ sec}; \quad \tau_p = 6 \times 10^{-9} \text{ sec}$$

Putting these values in (6.57), we get

$$N_2 - N_1 = 3 \times 10^{16}/\text{cm}^3$$

It is necessary to mention here that Schawlow and Townes, in their original paper, expressed this condition in c.g.s units and in terms of different parameters. In their formula $\Delta\nu$ represents the half-width of the resonance line at half maximum; the decay time τ_p was expressed in terms of the reflection coefficient r of the cavity walls, i.e.,

$$\tau_p = \frac{6V}{(1-r)Ac} \quad \dots(6.60)$$

The formula can be derived on the basis of following arguments:

A plane wave which is set off at $t = 0$ from one mirror, will be reflected back and forth losing intensity on successive reflections. If the medium is non-absorbing, losses will be due to the mirrors alone and the intensities of successive reflected beams will be

$$Ir, Ir^2, Ir^3, \dots, Ir^n, \dots$$

where r is the reflection coefficient. If the intensity falls to $1/e$ of its initial value after N reflections

$$Ir^N = 1/e \quad \therefore r^N = 1/e$$

$$\text{i.e., } N \ln r = -1$$

If, further, r is nearly unity

$$\ln r \sim r - 1 \quad \therefore N = \frac{1}{1-r}$$

$$\text{The decay time } \tau_p = \frac{NL}{c}$$

It can easily be shown in the case of a closed cavity, say a spherical one, with reflecting inner walls that

$$L = (\text{diameter}) = \frac{6V}{A}$$

where V is the volume and A the area of the walls

$$\therefore \tau_p = \frac{NL}{c} = \frac{1}{1-r} \frac{6V}{Ac}$$

For a cube

$$\tau_p = \frac{L}{(1-r)c}$$

If we now make the following substitutions in our formula

$$\Delta\omega_0 = 4\pi\Delta\nu, \tau_p = \frac{6V}{(1-r)Ac}$$

and

$$\begin{aligned} \tau_{21} &= \frac{1}{A_{21}} = \frac{3\hbar\epsilon_0\pi c^3}{4\pi\epsilon_0\omega_0^3\mu^2} \quad (\because \mu = e\mathbf{D}) \\ &= \frac{3hc^3}{64\pi^4 v^3 \mu^2} \end{aligned}$$

we arrive at the formula in the form given by Schawlow and Townes, viz.

$$n = (N_2 - N_1)V = \frac{\Delta\nu}{v} \frac{h(1-r)Ac}{16\pi^2 \mu^2}. \quad \dots(6.61)$$

6.11 QUANTUM YIELD

The rate of variation of the population of the upper state in a two level system when the stimulating radiation is cut off, is

$$\frac{dN_2}{dt} = -\frac{N_2}{\tau} = -N_2 \left(\frac{1}{\tau_{sp}} + \frac{1}{\tau_{nr}} \right) \quad \dots(6.62)$$

Integrating this equation, we find that

$$N_2(t) = N_2(o) \exp(-t/\tau) \quad \dots(6.63)$$

where $N_2(o)$ is the population at time $t = 0$.

If V is the volume of the material, the power emitted by spontaneous emission at time t is

$$P(t) = \frac{N_2(t)\hbar\omega_{21}V}{\tau_{sp}} = \frac{N_2(o)\hbar\omega_{21}V}{\tau_{sp}} \exp(-t/\tau) \quad \dots(6.64)$$

Thus, the light emitted as a result of spontaneous emission decays exponentially with a time constant τ and not τ_{sp} .

The fluorescence quantum yield ϕ is usually defined as

$$\phi = \frac{\text{Number of emitted photons}}{\text{Number of atoms initially present in the upper state}} \quad \dots(6.65)$$

The number of emitted photons = $\int_0^\infty \frac{P(t)}{\hbar\omega_{21}} dt$ and the number initially present = $N_2(o)V$

$$\therefore \phi = \frac{\int_0^\infty \frac{P(t)}{\hbar\omega_{21}} dt}{N_2(o)V} = \frac{1}{\tau_{sp}} \int_0^\infty \exp(-t/\tau) dt = \frac{\tau}{\tau_{sp}} \quad \dots(6.66)$$

The measurement of the quantum yield ϕ and life-time τ gives τ_{sp} and, hence, τ_{nr} .

If there are three levels 1, 2, 3, there may be spontaneous transitions $3 \rightarrow 1$ and $3 \rightarrow 2$, besides a non-radiative transition. In this case

$$\frac{1}{\tau} = \left(\frac{1}{\tau_{31}} \right)_{sp} + \left(\frac{1}{\tau_{32}} \right)_{sp} + \frac{1}{\tau_{nr}} \quad \dots(6.67)$$

and

$$\phi_{31} = \tau (\tau_{31})_{sp} \quad \dots(6.68)$$

The other quantity that characterizes a transition is the absorption cross-section σ . We now show how this can be found from the measurement of the quantum yield ϕ and the decay time τ .

From (5.47), for non-degenerate states

$$\begin{aligned} \sigma &= \frac{\eta c^2 \pi^2 A_{21}}{\omega_{21}^2} g(\omega) \\ &= \frac{\eta c^2 \pi^2}{\omega_{21}^2 \tau_{sp}} g(\omega) \end{aligned} \quad \dots(6.69)$$

Using (6.68)

$$\begin{aligned} \sigma &= \frac{\eta c^2 \pi^2}{\omega_{21}^2} g(\omega) \left(\frac{\phi_{21}}{\tau} \right) \\ &= \left(\frac{\lambda}{2} \right)^3 \eta^3 g(\omega) \left(\frac{\phi_{21}}{\tau} \right) \end{aligned} \quad \dots(6.70)$$

where

$$\lambda = \frac{2\pi c}{\eta \omega_{21}} \quad \dots(6.71)$$

is the wavelength, in the medium, of an electromagnetic wave whose frequency corresponds to the centre of the line. Thus, the measurements of ϕ_{21} and τ yield the value of the cross-section σ .

SOLID STATE LASERS

7

In this and the following few chapters (Chapters 7–10), we will describe some specific laser systems whose characteristics can be considered as representative of the entire category of lasers.

7.1 THE RUBY LASER—A THREE-LEVEL SYSTEM

Generally, in the solid substances used in laser devices, the active material is present in concentration less than one percent. The bulk of the material does not participate in the laser action. It only acts as the host. For laser action to be possible, the ions of the active material will have to be excited to the proper upper level which is usually accomplished by optical pumping. The first successful laser action was achieved in 1960 by Maiman [263] using a crystal of ruby as a laser material. The successful use of ruby was particularly interesting because theoretically it is a poor laser material and was not considered a promising candidate for this purpose. Maiman, however, had earlier carefully analysed ruby, to determine whether or not the required criteria for laser oscillations could be satisfied. In one of his papers [262] he had reported his observations on the fluorescence relaxation processes in this crystal. The predominant processes which ensue in this material when it is irradiated by the light of appropriate wavelength are shown in Fig. 7.1.

Ruby is crystalline Al_2O_3 doped with chromium. The triply ionized Cr ions, which replace some of the Al^{3+} ions, give the otherwise transparent crystal, a pink or red colour depending upon its concentration. The energy levels shown in Fig. 7.1 are those of Cr^{3+} ions in the Al_2O_3 lattice. There are two main pump bands, 4F_1 and 4F_2 centred around $0.42\ \mu\text{m}$ and $0.55\ \mu\text{m}$ respectively. $^4A_2-$ is the ground level. The absorption spectrum of chromium ion is given in Fig. 7.2 (a).

Maiman used a one centimetre cube of pink ruby with a concentration of about 0.05% of Cr corresponding to the chromium ion density $n_0 = 1.62 \times 10^{19}/\text{cm}^3$, and irradiated it with 5500\AA radiation causing absorption into the lower band 4F_1 . Two components of radiation reemitted were observed in a direction at right angles to the exciting beam. The luminescence spectrum of

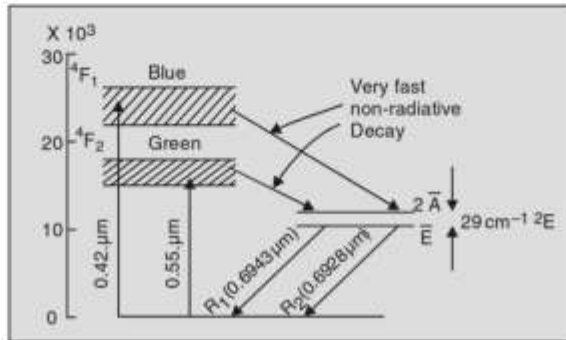


Fig. 7.1 Energy level diagram of Cr⁺³ ions in ruby
chromium ions in ruby is given in Fig. 7.2 (b). One of these was due to the re-emission of the incoming radiation, *i.e.*, spontaneous decay from 4F_2 level to the ground state. The second component was due to the fluorescence, *i.e.*, spontaneous decay from level 2E to the ground state. Note that the pair of closely spaced levels $2\bar{A}$ and \bar{E} in Fig. 7.1 is counted here as a single level. The ratio of the intensities of these two lines is

$$\frac{I_3}{I_2} = \frac{\hbar\omega_{31}N_3A_{31}}{\hbar\omega_{21}N_2A_{21}} \quad \dots(7.1)$$

where N_3 and N_2 are the populations of levels 3 and 2 respectively.

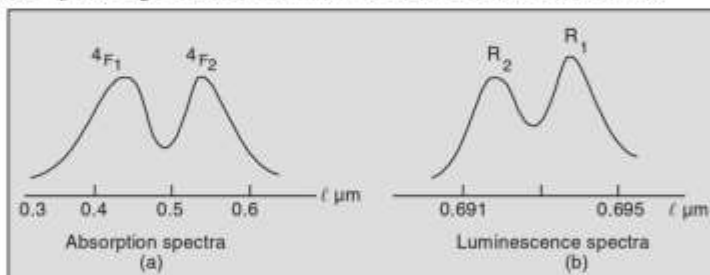


Fig 7.2

Let S_{nm} represent the decay rate from level n to level m which includes both radiative and non-radiative processes. Thus, S_{21} is the decay rate of

fluorescence level 2E . The life-time for this process was entirely due to spontaneous emission as was shown earlier by Varsanyi *et al.* [384].

$$\therefore S_{21} = A_{21} \quad \dots(7.2)$$

This life-time was determined by measuring S_{21} after the exciting source was turned off and was found to be over 4 m sec. This high value of life-time indicates that 2E is a metastable state as is expected from the doublet-quartet nature of its only allowed decay route. Further, in a steady state, the number of transitions from $3 \rightarrow 2$ must be equal to the number of transitions from $2 \rightarrow 1$, i.e.,

$$N_3 S_{32} = N_2 A_{21} \quad \dots(7.3)$$

$$\therefore \frac{I_3}{I_2} = \frac{\omega_{31} A_{31}}{\omega_{21} S_{32}} \quad \dots(7.4)$$

The Einstein coefficient A_{31} was calculated from the measurements of absorption coefficient and linewidth (see Chapter 5), and was found to be $\sim 3 \times 10^5/\text{sec}$. Using this value and the measured ratio of the intensities of the two components in Eqn. (7.4), S_{32} comes out to be $\sim 2 \times 10^7/\text{sec}$, which shows that the decay from the pump band to the upper laser level is sufficiently fast.

The fluorescent quantum efficiency ϕ , i.e., the ratio of the number of fluorescent quanta emitted to the number of quanta absorbed by the crystal from the exciting beam, was found to be near unity, which confirmed that the life-time of level 2 is entirely radiative and also showed that $S_{32} > > S_{31}$, i.e., the atoms drop down to level 2E much faster than to level 1. The conditions, therefore, are quite suitable for achieving population inversion and, hence, laser action.

We have described this Maiman's earlier experiment in detail, not only to indicate the preliminary observations that led to the discovery of lasers, but more so, to acquaint the readers with the various measurements that may be usually necessary to ascertain the suitability of a substance as a laser material.

Maiman's first laser was in the form shown in Fig. 7.3.

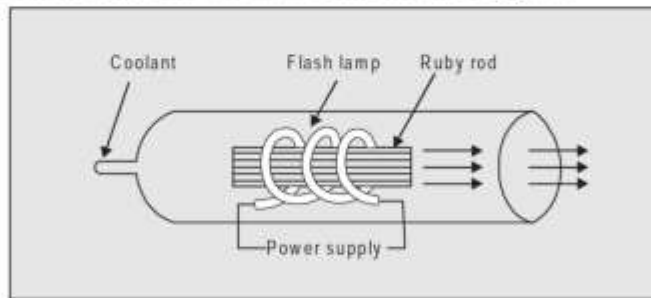


Fig. 7.3 Ruby laser

The ruby was in the form of a cylinder 4 cm in length and 0.5 cm in diameter. Its ends were ground and polished plane and parallel. One end was silvered to give a completely reflecting surface with about 10% transmission. A helical photographic flash lamp filled with xenon, provided white light in the form of a pulse which lasted for about one thousandth of a second. Above a certain critical light intensity, an inversion of population was achieved and the laser oscillations started. An intense beam of red light emerged from the end of the rod. The beam divergence was about half a degree and the emerging beam was spatially coherent, as was demonstrated by producing interference fringes with two slits placed in the beam. The power during the output pulse was nearly 10 kilowatts. In other words, the light flux in the beam was nearly million times that of the sunlight at the earth's surface.

Let us now examine the various intermediate steps occurring between the irradiation and the final laser output.

When the material is irradiated with green light at $\lambda \sim 5500 \text{ \AA}$, chromium ions are excited to the 4F_2 state. In order that the expanded power of the source be very useful, it is necessary that the bandwidth of the absorption bands be sufficiently wide. One of the advantageous features of the solid state systems is that they, generally, have a broad absorption band for the pump transition. In the case of ruby crystals, each of the bands 4F_1 , 4F_2 is about $0.1 \mu\text{m}$ wide which makes optical pumping effective. Since most high power optical sources have a broad spectral distribution in their radiant energy, a relatively high efficiency can be realized. The excited chromium ions quickly lose some of their energy via phonon-assisted non-radiative transition and fall to the pair of levels associated with 2E state. This state slowly decays by emitting a sharp doublet with components R_1 (6943 \AA) and R_2 (6928 \AA). Under very intense excitation, the population of this metastable state can become greater than that of the ground state. This metastable state plays the part of the upper laser level. The ruby laser, thus, fits in the three-level scheme. In this situation the initial spontaneously emitted fluorescent photons would travel in all directions, but those travelling parallel to the axis of the system would be reflected to-and-fro between the reflectors and so would pass many times through the amplifying medium and would stimulate the upper state atoms to radiate, thus causing amplification via stimulated emission. The laser action is, thus, actually initiated by spontaneous emission. The photons travelling in any other direction would be lost after a few reflections.

Actually, the laser action can be obtained on both $2\bar{A} \rightarrow ^4A_2$ and $\bar{E} \rightarrow ^4A_2$ transitions. However, usually it occurs on the $\bar{E} \rightarrow ^4A_2$ transition (R_1 line). This is not difficult to understand. The frequency separation of the levels of the 2E state is 870 GHz (i.e., 29 cm^{-1}) and the population of the level \bar{E} , at room temperature, is greater than that of the level $2\bar{A}$ as shown by the Boltzmann relation

$$\frac{N_2(2\text{A})}{N_2(E)} = 0.877. \quad \dots(7.5)$$

7.2 PUMPING POWER

Since the terminal level of the $2 \rightarrow 1$ transition is the ground state, in order to produce a stimulated emission component, it is necessary to have an incident pump radiation intensity large enough to excite, at least, one half of the total number of ground state atoms into level 2. This is an extremely difficult condition to achieve and requires very high power. We will now show how this power can be estimated for a three-level system.

We will use the following symbols:

$N_i \rightarrow$ Population density of the level i ,

$N_0 \rightarrow$ the total active ion density in the crystal,

$W_{mn} (= B_{mn}P(\omega_{mn})) \rightarrow$ the induced transition probability per unit time for the transition $m \rightarrow n$ caused by the exciting radiation of frequency ω_{mn}

$A_{mn} \rightarrow$ Einstein coefficient for spontaneous emission,

and $S_{mn} \rightarrow$ the transition probability for the non-radiative' transition*

In terms of these symbols, the steady-state rate equations are:

$$\frac{dN_3}{dt} = W_{13}N_1 - (W_{31} + A_{31} + S_{32})N_3 = 0 \quad \dots(7.6)$$

$$\frac{dN_2}{dt} = W_{12}N_1 - (A_{21} + W_{21})N_2 + S_{32}N_3 = 0 \quad \dots(7.7)$$

and $N_1 + N_2 + N_3 = N_0. \quad \dots(7.8)$

Eqns. (7.6) and (7.8), on eliminating N_3 , give

$$\frac{N_2}{N_1} = \left[\frac{W_{13}S_{32}}{W_{31} + A_{31} + S_{32}} + W_{12} \right] \frac{1}{A_{21} + W_{21}} \quad \dots(7.9)$$

Since, ruby has a high fluorescent quantum efficiency (as was observed by Maiman in his preliminary experiments), A_{31} and W_{31} are much smaller than S_{32} , and, hence, can be neglected.

$$\therefore \frac{N_2}{N_1} = \frac{W_{13} + W_{12}}{A_{21} + W_{21}}. \quad \dots(7.10)$$

Therefore,

$$\frac{N_2 - N_1}{N_2 + N_1} \approx \frac{N_2 - N_1}{N_0} = \frac{W_{13} - A_{21}}{W_{13} + A_{21} + 2W_{12}}. \quad \dots(7.11)$$

*Note that earlier we had used this symbol to represent both radiative and non-radiative transitions.

The condition necessary for laser oscillations to occur is that $N_2 - N_1$ must be positive, i.e., W_{13} must be greater than A_{21} . But this is not a sufficient condition because the excess population $N_2 - N_1$ must be large enough to overcome the cavity losses. Although the condition desirable for laser to oscillate effectively is $W_{13} \gg A_{21}$, in practice, it is difficult even to achieve the condition for threshold, viz. $W_{13} = A_{21}$.

Let us estimate the pumping power required to achieve gain.

Suppose a parallel beam of light at the central frequency ω_p of the pumping light is incident on the surface of an optically thin sample of the material. The power of the pumping light is

$$P_0 = n\hbar\omega_p \quad \dots(7.12)$$

where n is the number of incident photons per second. The flux density F_p is

$$F_p = \frac{P_0}{A} = \frac{n\hbar\omega_p}{A} \quad \dots(7.13)$$

where A is the area of the crystal perpendicular to the incident beam. The pumping rate $W_p = W_{13}$ is, by definition,

$$W_p = \frac{n}{A}\sigma_p \quad \dots(7.14)$$

where σ_p is the absorption cross-section for the absorption of pump light.

$$F_p = \frac{W_p\hbar\omega_p}{\sigma_p} \quad \dots(7.15)$$

For the threshold condition, $W_p = W_{13} = A_{21}$. Therefore, the power density required to be incident on the material for inversion just to commence is

$$F_p = \frac{A_{21}\hbar\omega_p}{\sigma_p} \quad \dots(7.16)$$

For example, consider the case of ruby for which $\tau = 1/A_{21} = 4.3$ msec, $\hbar\omega_p \sim 3 \times 10^{-19}$ joule and $\sigma_p \sim 10^{-19}$ cm⁻². The required power density is

$$F_p = \frac{3 \times 10^{-19}}{4.3 \times 10^{-3} \times 10^{-19}} \sim 700 \text{ W cm}^{-2}. \quad \dots(7.17)$$

The energy density in the crystal in the case of a parallel beam, is given by,

$$\rho_p c' = F_p \quad \dots(7.18)$$

where c' is the velocity of light in the crystal.

$$\therefore \rho_p = \frac{F_p}{c'} = \frac{F_p\eta}{c} = \frac{W_p\hbar\omega_p\eta}{c\sigma_p}, \quad \dots(7.19)$$

or $W_p = \frac{\rho_p c \sigma_p}{\hbar\omega_p \eta}, \quad \dots(7.20)$

In the case of broad-band radiation, this relation takes the form

$$W_p = \int \frac{c\rho(\omega)\sigma(\omega)}{\hbar\omega_p\eta} d\omega \quad \dots(7.21)$$

where $\sigma(\omega)$ is the frequency dependent absorption cross-section and $\rho(\omega)$ is the energy density per unit volume per unit frequency. Now

$$\rho(\omega) = \frac{\hbar\omega^2\eta^3}{\pi^2 c^3} \cdot \frac{1}{\exp(\hbar\omega/kT) - 1} \quad \dots(7.22)$$

and from Eqns. (5.47) and (5.49)

$$\frac{\sigma(\omega)}{\sigma_p} = \frac{g(\omega)}{g(\omega_p)} \quad \dots(7.23)$$

(Note: $\omega_0 = \omega_p$ and $\sigma_0 = \sigma_p$)

Assuming that the line has Lorentzian lineshape for which $g(\omega_p) = \frac{2}{\pi\Delta\omega_p}$

$$\sigma(\omega) = \frac{\pi g(\omega)\Delta\omega_p}{2} \sigma_p \quad \dots(7.24)$$

where we have used (5.78). Substituting these values in (7.21),

$$\begin{aligned} W_p &= \frac{\eta^2 \Delta\omega_p \sigma_p}{2\pi c^2 \omega_p} \int \frac{\omega^3}{\exp(\hbar\omega/kT) - 1} g(\omega) d\omega \\ &= \frac{\eta^2 \Delta\omega_p \sigma_p \omega_p^2}{2\pi c^2 \exp(\hbar\omega_p/kT) - 1} \end{aligned} \quad \dots(7.25)$$

(You may recall that the function $g(\omega)$ behaves like a delta-function.)

This relation gives the pumping rate in terms of frequency, band-width, atomic absorption cross-section and temperature. Since the rate is proportional to ω_p^2 , operation at shorter wavelengths requires a very high power.

The analysis, as outlined above has, no doubt, certain limitations; but is very useful because one can get from it, in a simple way, a fairly good idea about the sort of values required for ion density, pump power, etc.

Maiman's laser, though exceedingly useful and powerful, has the disadvantage that it requires a high pulsed light threshold energy. We have seen in the preceding chapter that the population inversion required for laser oscillations in ruby is $\sim 5 \times 10^{16}/\text{cm}^3$. The Cr^{3+} ion density in ruby is $\sim 10^{19}/\text{cm}^3$. Hence, the fractional degree of inversion required is very small, about 0.5 in 100. However, since it is a three level system, half the number of 10^{19} ions in the ground state must be lifted to the upper state which is a difficult task. It is not difficult to produce the required energy from a flash-tube. But a good deal of its energy is wasted, as part of it is released at other frequencies and the spurious light tends to warm up the crystal. The performance of ruby laser has since been considerably improved by introducing various modifications.

The most suitable configuration for a laser device is one in which the material is uniformly illuminated over most of its surface. It is for this reason that Maiman used a flash lamp in the form of a helix and threaded the ruby through it. Several other techniques have been suggested in the literature for coupling the pump light into the material. For example, the active material may be placed in close proximity of the pump light by packing it closely around by a number of flash tubes. Such a structure, although compact, has a disadvantage that the unused radiation from the source aggravates heat dissipation problem. A more elegant form of coupling is that of the elliptical cylinder. A cylinder with elliptical cross-section is made with a highly reflecting inner wall. The ruby rod with its axis parallel to that of the cylinder is placed in such a way that it occupies one of the foci of the elliptical cross-section. A long straight flash tube is then placed in the position of the other focus (Fig. 7.4). With such an arrangement all the light from the flash tube is focussed on the ruby rod. Air circulating around the rod can, to some extent, control its temperature.

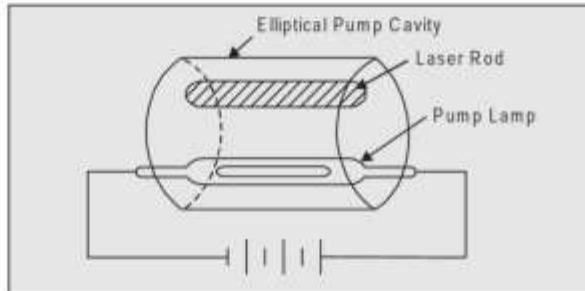


Fig. 7.4 Elliptic cylinder

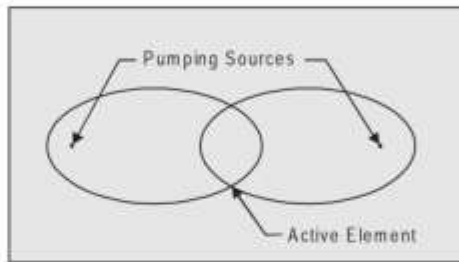


Fig. 7.5 Elliptical reflector

Sometimes reflectors of different forms and construction are employed. For example, a two lamp reflector whose cross-section is shown in Fig. 7.5 is often used. The active element is placed at the common focus and the sources of pumping radiation are placed at the foci of the two ellipses. This type of construction increases the output power of radiation.

More sophisticated techniques are now employed in making the required optical cavity. Maiman had, for this purpose, cut the ends of the ruby rod accurately plane and parallel and silvered them. Subsequently, depositing multilayer dielectric coating was found to give better result. A pair of external mirrors also could be used. This has the advantage that it allows other components to be placed in the cavity.

The xenon flash-lamp has also been replaced by a variety of other light sources. For example, cyanogen gas burning in oxygen generates an extremely energetic flame which has been used to pump ruby. A shock wave generated by the detonation of an explosive charge when passed through certain gases such as argon, the extreme compression of the gas in the shock-front rapidly heats and excites the gas, causing intense light emission. Light emitted by such "argon bomb" has been used as a rapid and intense pump source for pulsed ruby lasers.

7.3 SPIKING

The output of a pulsed ruby laser, if examined with a photocell and an oscilloscope, is found to consist of a series of pulses of duration of a microsecond or less. Duration of an individual spike is of the order of $0.1 - 1 \mu\text{s}$; the time interval between two adjacent spikes is about $1 - 10 \mu\text{s}$; the power of each spike is of the order of $10^4 - 10^5 \text{ W}$. Such spikes were first observed in experiments with ruby by Collins *et al* [81] (Fig. 7.6). This characteristic spiking can be explained as follows:

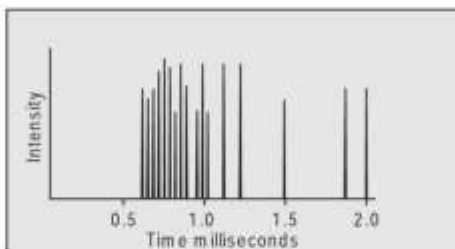


Fig. 7.6 Light output of a ruby laser

The duration of the exciting flash light is of the order of a millisecond and may be sufficiently intense to build up an inverted population very rapidly. As soon as a sufficiently larger population has been produced in the upper level, the laser action starts producing a pulse. This has the effect of depleting the upper level population more rapidly than it can be restored by the flash light. The laser oscillation then ceases for a few microseconds. Because the flash lamp is still active, it again builds up population inversion causing another spike and the sequence is repeated. A series of pulses is thus produced until the

intensity of the flash light has fallen to such a level that it can no longer rebuild the necessary inverted population.

The peak power radiated by a typical ruby laser is about 10^{12} times as high as the power radiated by the sun in the same narrow solid angle and frequency band; but the pulse lasts only for about 10^{-7} sec. It must be emphasized here that the energy in the pulse can be no greater than the energy which ruby emits in a normal fluorescence process. The only difference is that the energy is concentrated in a single pulse of very short duration, instead of being emitted randomly over a much longer period. The intensity of the beam consequently is very much greater.

7.4 U^{3+} IN CaF_2 LASER: A FOUR-LEVEL SYSTEM

Laser action in a four-level system was first reported by Sorokin and Stevenson [360]. They observed stimulated emission from trivalent uranium ions substituted for divalent calcium ions in calcium fluoride. The energy level system is represented in Fig. 7.7. In contrast to ruby laser, the oscillations take place in a transition from the metastable state 3 to the level 2, approximately 515 cm^{-1} above the ground state.

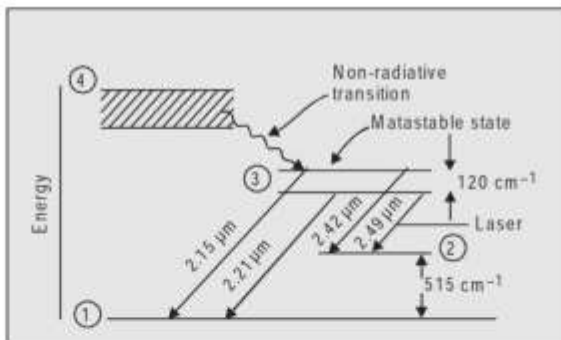


Fig. 7.7 Energy levels of $\text{CaF}_2: \text{U}^{3+}$

At low temperature the level 2 is relatively unpopulated and, hence, for oscillations to occur, the population of the metastable state 3 does not need to be very large as in the case of ruby laser. It was observed that the pumping power required to achieve stimulated emission was lower by a factor of 500 compared to ruby.

The uranium ion has very strong absorption band in the green and blue region. The room temperature fluorescence spectra consists of four peaks: $2.15 \mu\text{m}$, $2.21 \mu\text{m}$, $2.42 \mu\text{m}$ and $2.49 \mu\text{m}$. Laser oscillations were observed in the transition from the lower metastable state to the level 2, corresponding to the longest $\lambda = 2.49 \mu\text{m}$.

A single crystal of calcium fluoride doped with 0.05 mole per cent uranium was cut into a cylindrical shape of length 3.75 cm and diameter 0.93 cm. Its ends were cut in the same way as in ruby to obtain an optical cavity. The technique employed to inject pump power was also similar. However, the experimental set up was somewhat more complicated since the sample was placed in a specially constructed liquid helium Dewar. The linewidth of the pulse was very narrow and the beam was confined to an angle approximately 0.01 radian.

7.5 NEODYMIUM LASERS

There are, in fact, many four-level laser systems using rare-earth ions: neodymium, erbium, dysprosium, etc., in various crystals. The pump thresholds of these systems for either pulsed or cw operation are typically much lower than that for ruby. Unfortunately, all these systems oscillate at longer infrared wavelengths—between 1 and 3 μ —beyond the visible region, where the conventional types of photo-detectors are ineffective.

(a) Nd: YAG Laser

The neodymium ion is a particularly useful example of an optically pumped rare-earth laser system. The trivalent neodymium ion Nd^{3+} has now been incorporated into a great many lattices. The more widely used system is one in which Nd^{3+} ion is incorporated in the $\text{Y}_3\text{Al}_5\text{O}_{12}$ lattice. This crystal is represented by the symbol YAG—acronym for *Yttrium Aluminium Garnet*. A simplified energy level scheme for Nd: YAG, is presented in Fig. 7.8. The energy levels of this ion in almost any crystalline lattice are essentially the same.

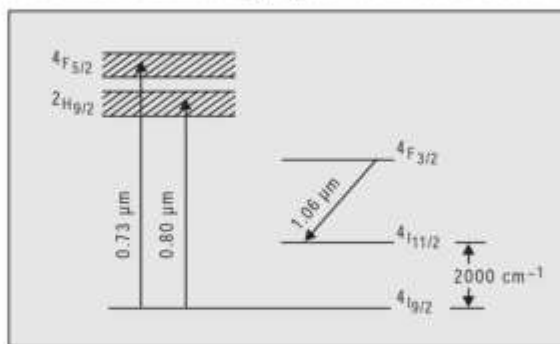


Fig. 7.8 Energy levels of Nd^{3+} : YAG

The levels shown in the figure are all associated with the inner $4f$ shell, which is screened from external fields by the $5d$ and $6s$ outer shells, as a result of which the lower levels are very narrow. The Nd^{3+} ion surrounds itself with

8

GAS LASERS

The incorporation of an ion into a lattice field results into relatively broad pump bands, so that broad-band or quasi-continuous radiation sources may be used for their excitation in solids. In gases, since there are no surroundings to perturb the atom, the energy levels of the atom are extremely narrow, of the order of 0.01 Å and, hence, wideband optical pumping is ineffective. Only an insignificant fraction of the optical power will be utilized for the excitation of the active centres and the major part of it will be wasted in heating the gas. A sharp emission line coinciding with the absorption line of the active centres, therefore, is necessary to excite the atoms. This creates a problem in finding an optical source for pumping. For this reason optical pumping is not generally used in gases. Instead, atoms are lifted to the higher level by electrical pumping. The only case in which laser action has been observed in a gas by means of optical pumping is that of Cs [Jacobs *et al.* 199], pumped by a discharge lamp containing He. The wavelength 3889.69 Å, corresponding to the $3^3 P - 2^3 S$ transition of He, is almost equal to the wavelength 3889.67 Å, corresponding to $8p^2 P_{1/2} - 6s^2 S_{1/2}$ transition of Cs. The helium line was used to irradiate Cs vapour, which gave a very efficient pumping and continuous laser amplification and oscillation was observed at 7.18 μ. This, perhaps, is the only example of this kind in which a suitable coincidence in wavelengths exists. The Cs-He system, however, did not find much favour with the workers because, Cs, which vapourizes at 175°C, is a highly reactive substance.

8.1 NEUTRAL ATOM GAS LASERS : HELIUM-NEON LASER

The main problem in a gas laser is, how the atoms can be selectively excited to proper levels in quantities sufficient to achieve the required population inversion. The primary mechanism for excitation used in gas lasers is by

electron impact. Suppose atoms of a kind *A* are excited in a discharge tube, by this method, to a metastable state. Such a state can be populated appreciably at moderate electron densities. If the discharge tube also contains atoms of other kind *B*, whose excited state lies very close to that of the metastable state of *A*, a resonant energy transfer may take place and the atoms *B* be lifted from their ground state to the excited state. If the rate of transfer of excitation is larger than the rate of radiative decay of the excited state, the population of the excited state of the atom *B* will steadily increase and the state will be so populated that inversion may exist between it and another level.

This process was used by Javan *et al.* [202] in He-Ne laser, the first continuously operated gas laser. This is a typical example of a laser in which atomic transitions have been used. The energy level schemes of He and Ne are shown in Fig. 8.1.

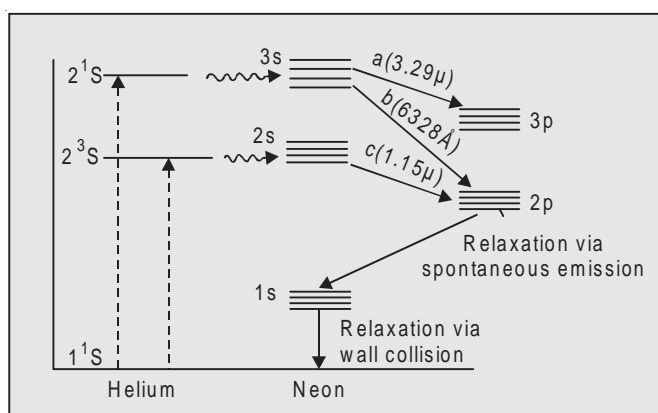


Fig. 8.1 Energy levels of He-Ne system

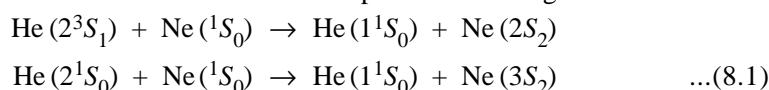
He atoms are found to be much more readily excited by electron impact than Ne atoms. The atoms can be excited either by d.c. or a.c. power supply. The 2^1S and 2^3S levels of He have relatively long life time *i.e.*, they are metastable levels. Laser action, however, occurs between energy levels of Ne. The role of He atoms is to assist in the pumping process.

There is a close coincidence between the 2^3S_1 metastable level of helium at ~ 19.81 eV and the $2S_2$ level of neon ($\Delta E = 0.04$ eV). A similar coincidence exists between the 2^1S_0 state of helium at ~ 20.5 eV and the $3S_2$ level of neon ($\Delta E = 0.05$ eV). The notation used here to represent Ne levels is Paschen's notation.

Thus,	1s	band corresponds to	$2p^5\ 3s$	configuration
	2s	band corresponds to	$2p^5\ 4s$	configuration
	3s	band corresponds to	$2p^5\ 5s$	configuration
	2p	band corresponds to	$2p^5\ 3p$	configuration
	3p	band corresponds to	$2p^5\ 4p$	configuration

Each *s*-band consists of four levels and each *p*-band of ten levels. They may also be represented using Russell-Saunders terminology. For example, the four components of *2s*-band can be represented as 1P_1 , 3P_0 , 3P_1 , 3P_2 . However, *L-S* coupling is not suitable for the description of the Ne system, as many transitions which are forbidden by the selection rules for *L-S* coupling, are actually observed.

When a helium atom in the metastable state collides with a neon atom in the ground state, an exchange of energy takes place, and a neon atom is lifted to *2s* or *3s* level and the helium atom drops back to the ground state.



This provides a selective population mechanism which supplies continuously Ne atoms to *2s* and *3s* levels increasing their population. Laser oscillations occur between *s*(*2s*, *3s*) and *p*(*2p*, *3p*) states.

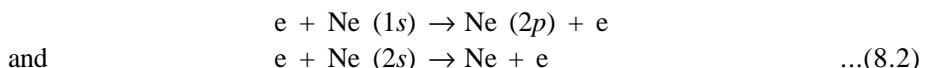
In neon the *2S₂* and *3S₂* levels are connected to the ground level by strong allowed transitions. As shown by Lawrence and Liszt [235], they have at low pressures, radiative lifetime ~ 10.20 ns.

One may ask: Since *2s* states are also radiatively connected to the ground state, they would decay quickly to the ground state. Is this not a disadvantage as far as the population inversion between *s* and *p* levels is concerned? It is, indeed, so, at very low pressures, when the probability of decay to the ground state vastly exceeds that to the *2p* levels. However, at a high pressure, of the order of a mm Hg, transitions to the ground state undergo complete resonance trapping; that is, every time a photon is emitted, it, instead of escaping from the gas, is absorbed by another atom in the ground state which thereby ends up in the excited state *2s*, and since the population of the ground state is large, the process is continuous. This increases the lifetime of *s*-levels to ~ 100 ns. In contrast the lifetime of *p*-levels is of the order of 20 ns [Bennett and Kindlmann 39]. There exists, therefore, a favourable lifetime ratio for producing the required population inversion, thus satisfying the condition for the operation as a four-level laser system.

Figure 8.1 shows the transitions on which laser oscillations can be expected. Of the various transitions from the component level of the *3s* and *2s* groups to the levels of *3p* and *2p* groups, the following are more prominent:

- (a) $3s_2 \longrightarrow 3p_4 \quad \lambda = 3.39 \text{ } \mu\text{m}$
- (b) $3s_2 \longrightarrow 2p_4 \quad \lambda = 0.633 \text{ } \mu\text{m}$
- (c) $2s_2 \longrightarrow 2p_4 \quad \lambda = 1.15 \text{ } \mu\text{m}$

For effective working of the laser, certain conditions will have to be satisfied which put severe restrictions on the values of some operational parameters. For instance, one has to ensure that (i) *2p* levels are not excited by inelastic collisions between electrons and the atoms in the metastable level *1s*; and (ii) the atoms in the levels *2s* are not de-excited to the ground state. Both these processes *viz.*



become prominent at high current densities and upset the population inversion between $2s$ and $2p$ levels. One cannot ignore the possibility of these processes occurring, because $1s$ levels have not allowed downward transition and may also be radiation trapped on the transition $2p \rightarrow 1s$. Consequently, they tend to build up sizeable population on the $2p$ level. The current density, therefore, must be adjusted to its optimum value. The population of the $1s$ level also must be kept at minimum value and this necessitates the adjustment of the total and partial pressures of the gas mixture and also the size of the tube. The Ne pressure is usually kept much below that of He ($P_{Ne} \sim 0.1$ Torr, $P_{He} \sim 1$ Torr) which decreases the probability of energy transfer in the reverse direction *i.e.*, from neon to helium, and the diameter of the tube is small (~ 2 mm) so that $1s$ atoms may collide with the wall and depopulate the level. There was enough evidence to show that the measures, as above, maximize the performance of lasers. Thus, when the discharge was switched off, the $2s$ levels were found to decay with time variation identical to that of 2^3S states and the amplification was found to be higher during the after-glow than during the current pulse. This is, obviously, because during the after-glow no electrons are available for the excitation of $1s$ atoms to $2p$ levels.

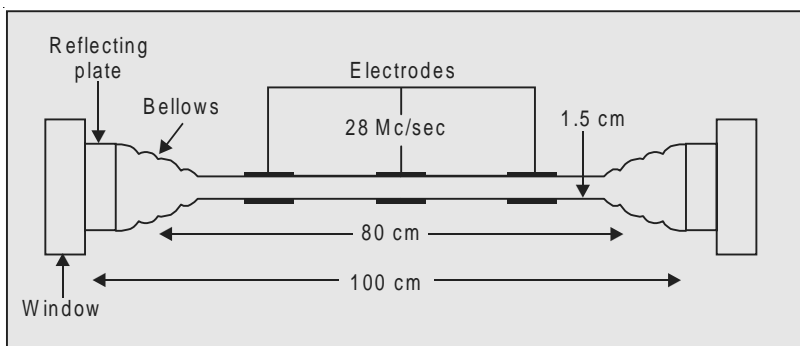


Fig. 8.2 Schematic diagram of the first He-Ne laser

Javan *et al.* [202] observed the continuous wave laser oscillations in a discharge tube containing Ne and He at pressures 0.1 Torr and 1 Torr respectively. The chamber consisted of a long quartz tube of length 80 cm and inside diameter 1.5 cm (Fig. 8.2). At each end of the tube, there was a metal chamber containing high reflection plates. Flexible bellows were used in the end chambers to allow external mechanical tuning of the Fabry-Perot plates. This enabled them to align the reflectors for parallelism to within 6 seconds of arc. Two optically flat windows were provided at the ends of the system which allowed the laser beam to be transmitted without any distortion. The end plates were separated by a distance of 100 cm. The discharge was excited by means of external electrodes using a 28 Mc/sec generator. The input power was around

50 watts. The flat plates were of fused silica and were flat to a hundredth of a wavelength. The high reflectance was achieved by means of 13-layer evaporated dielectric films. The reflectance was 98.9% in the wavelength range 11000 Å–12000 Å.

Javan *et al.* found that five different infrared wavelengths, *viz.* 1.118, 1.153, 1.160, 1.199 and 1.207 μm, corresponding to the different 2s–2p transitions, could be made to oscillate. The strongest oscillation was found to occur at 1.153 μm corresponding to $2s_2 \rightarrow 2p_4$ transition, with an output power of 15 mW. The beam divergence was about one minute of arc which is close to the theoretical diffraction limited value. A screen containing nine slits with spacing of 0.125 cm and each with slit width 0.005 cm was placed across the full 1.125 cm aperture of the beam. The resulting diffraction pattern indicated that there is a very small phase variation over the aperture which means that the beam consisted of perfectly spatially coherent light.

Since the alignment of concave mirrors is much less critical than that of plane mirrors, spherical mirrors are now employed in confocal configuration. The mirrors are placed external to the discharge tube. With such an arrangement, it is necessary to minimize unwanted reflections from the windows at the end of the discharge tube. Thus was found to be possible by the use of Brewster angle windows (Fig. 8.3). Brewster angle is an angle of incidence of a light ray such that it satisfies the condition

$$\tan \theta_B = \eta \quad \dots(8.3)$$

where θ_B is the angle between the normal to the Brewster window and the resonator axis and η is the refractive index. An unpolarized wave incident on a plate can be considered as a resultant of two superposed plane polarized

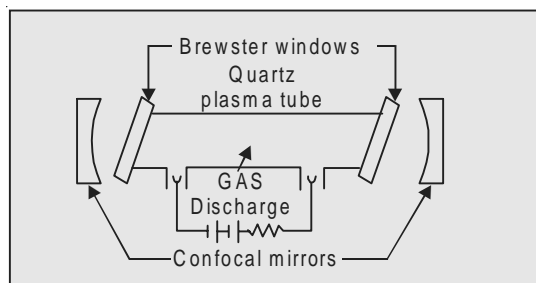


Fig. 8.3 Confocal mirror system with Brewster angle window

waves, one of which is polarized in the plane drawn through the normal to the window and the tube axis (plane of oscillation) and the other normal to this plane. The wave polarized normal to the ‘plane of oscillations’ is completely reflected by the window plate and, hence, is shut out of the picture; whereas, that polarized in the plane of oscillation is transmitted in the same direction and is repeatedly reflected by the mirrors without causing any losses. An additional advantage of this arrangement is that one obtains a plane polarized laser emission.

The spectral purity of the output of such a laser is remarkably high. For brief periods, the oscillation frequency which is around 3×10^{14} c/sec does not vary by more than 1 c/sec.

It can be seen from Fig. 8.1 that depending on certain factors, laser oscillation can also be achieved on the transitions of the type 'a' and 'b', and with the rapid development in the field, laser action was discovered at $3.39\text{ }\mu\text{m}$ (a) and $6328\text{ }\text{\AA}$ (b). The $6328\text{ }\text{\AA}$ He-Ne laser is one of the most popular and most widely used lasers. The commercial model of this type of laser requires 5 to 10 W of excitation power and produces 0.5 to 50 mW of cw laser output.

The He-Ne laser is made to oscillate on a particular transition by making the multilayer dielectric mirrors in such a way that they have a maximum reflectivity at the desired wavelength. Another interesting way of obtaining laser oscillations at a particular wavelength is to use a dispersion prism (Fig. 8.4). A prism placed inside the resonator provides wavelength selectivity. The light waves of different frequencies emitted by the active medium are spatially separated by the prism. If the right-hand mirror of the resonator is perpendicular to the propagation direction of, say λ_1 wave, then λ_2 , is incident on the mirror obliquely and is not returned into the active medium after reflection. One can change the wavelength by rotating the mirror about an axis perpendicular to the plane.

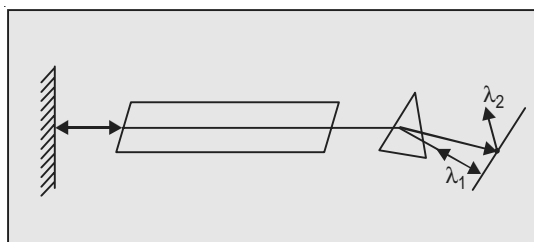


Fig. 8.4 Wavelength selection

The width of a laser line is much narrower than the normal linewidth. In Chapter 5, we have calculated the contributions to the linewidth from three different effects, *viz.*

- (i) Natural broadening: 16 MHz and ... (5.59)
- (ii) Collision broadening: 0.64 MHz and ... (5.70)
- (iii) Doppler broadening: 1300 MHz ... (5.76)
at room temperature for $\lambda = 6328\text{ }\text{\AA}$

We see that Doppler broadening is by far the most important broadening. In Chapter 6, we have shown that axial modes occur when $2L = q\lambda$ where L is the spacing between the reflectors and q is an integer

$$\therefore \frac{1}{\lambda} = \frac{q}{2L} \text{ i.e., } v = \frac{qc}{2L} \quad \dots(8.4)$$

Hence, the separation between the adjacent modes is

$$\Delta v = \frac{c}{2L} \quad \dots(8.5)$$

$$\therefore \text{For } L = 100 \text{ cm, } \Delta v = 150 \text{ MHz} \quad \dots(8.6)$$

One can see from the relative magnitudes of the Doppler width, the linewidth and the spacing between the modes, that several axial modes will attempt to resonate in the cavity as shown in Fig. 8.5.

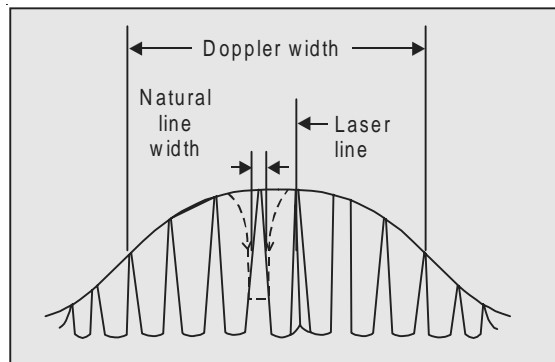


Fig. 8.5 Oscillating modes

The critical population inversion can be calculated from (6.57) using the following data:

$$v_0 = 4.74 \times 10^{14} \text{ Hz}, \quad \Delta v_0 = 1300 \text{ MHz} \\ \tau_{\text{rad}} = 7 \times 10^{-7} \text{ sec}, \quad \tau_p = 10^{-7} \text{ sec}$$

This gives

$$N_2 - N_1 \sim 3 \times 10^9 / \text{cm}^2 \quad \dots(8.7)$$

which is much smaller than the inversion density required for ruby laser.

Owing, in large part, to crystalline imperfections, scattering and thermal distortion, pulsed solid state lasers, although they possess a high degree of coherence, do not display perfect characteristics of monochromacy and directionality. In contrast, gas laser beams, are more monochromatic and more directional.

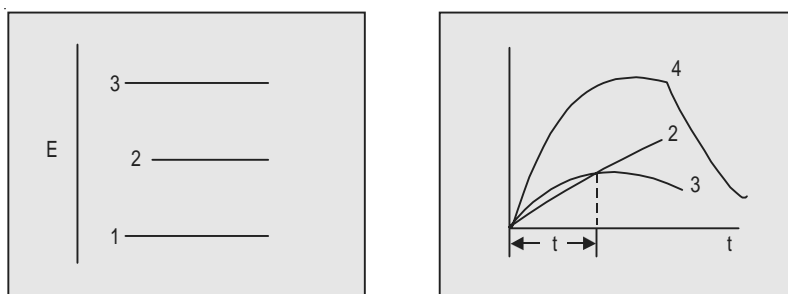
Besides, the He-Ne laser described above, there are other neutral atom gas lasers, covering most of the inert gases, the energy level schemes and the underlying principles for which are similar to those for He-Ne laser.

8.2 COPPER VAPOUR LASER

We will discuss in this section another atomic gas laser *viz. copper vapour laser*, which differs from He : Ne laser in its pumping mechanism and its working.

Consider a three-level system (Fig. 8.6) in which level 1 is the ground level; level 2 is a metastable level and level 3 is the upper level such that transitions $3 \rightarrow 1$ and $3 \rightarrow 2$ are allowed. Suppose the excitation is obtained in

a pulse mode of operation using rapid discharges. On switching on the exciting pulse, since the probability of excitation to level 3 is considerably higher, it is populated at a faster rate than the level 2, thus creating population inversion between levels 3 and 2. However, the two levels are only transiently inverted because the inversion is rapidly destroyed by accumulation of atoms in level 2. Figure. 8.7 shows the time variation of population in the two levels. Curve 4 shows the excitation pulse. Owing to the inversion created at the beginning of the excitation pulse, the laser operation is possible only during the short time t of the order of 5–10 ns.



Thereafter the inversion is destroyed. Such a laser pulse is said to be a *self-terminating laser pulse*.

Copper vapour laser belongs to this type of lasers. A pulsed discharge is employed in this case which has a two-fold function: evaporating copper and exciting atoms to create inversion. The energy level diagram of copper is given in Fig. 8.8. Here the levels $^2D_{3/2}$, and $^2D_{5/2}$ corresponding to the configuration $3d^9 4s^2$ are metastable states. The states $^2P_{3/2}$ and $^2P_{1/2}$ corresponding to the $3d^{10}4p$ configuration are the upper laser levels. Pulsed pumping lifts the atoms to the P levels from which they fall to the D levels giving rise to the laser lines at 5106 Å and 5782 Å. The output consists of amplified spontaneous emission.

Because of the high gain and short inversion time, these lasers are frequently operated without feedback mirrors. These lasers are referred to in the literature as ‘*superradiant lasers*’.

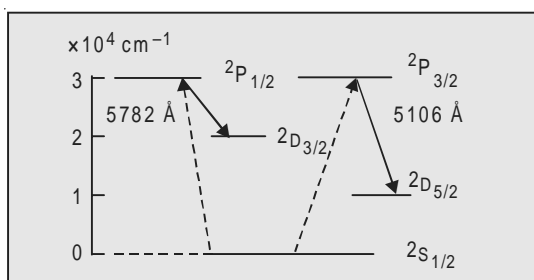


Fig. 8.8 Energy level diagram of copper

8.3 ION LASERS

Both pulsed and continuous laser action has been observed in singly ionized rare gases. The pump process in an ion gas laser is a two-step process. In the first step, ions are produced from neutral atoms by collisions with electrons in the discharge; in the second, the ions thus formed are excited to a higher level. The higher levels, thus, become populated by two successive collisions with the electrons in the discharge. The pump rate is proportional to J^2 , where J is the discharge current density. Such lasers require high pump power—several kilowatts—since the laser transitions are associated with excited states.

8.3.1 Argon Ion Laser [Bridges et al. 66]

A notable example of ion gas lasers is the ionized Argon laser. An energy level scheme showing the principal energy levels of Ar^+ is given in Fig. 8.9. In the figure $4p$ band corresponds to $3p^44p$ configuration and $4s$ to $3p^44s$ configuration. Each of these configuration consists of several levels. Laser oscillations occur in the $4p-4s$ transition. The argon ion ground state is ~ 15.6 eV above the ground state of the neutral atom. The levels involved in the laser transition lie ~ 20 eV above the argon ion ground state *i.e.*, in the neighbourhood of 35 eV. There are three possible ways by which the $4p$ level can be populated: (a) electron collisions with Ar^+ ions in their ground state,

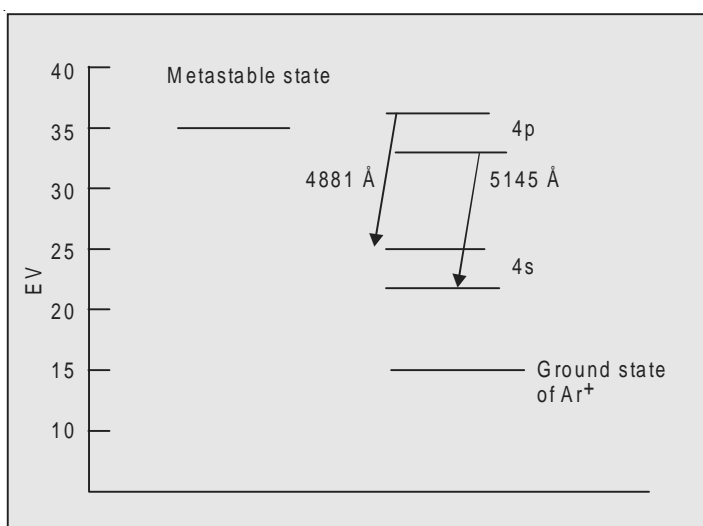


Fig. 8.9 Energy level scheme of Ar^+

(b) collision with ions in metastable states, and (c) radiative cascade from higher states. An interesting feature of this system is that the rate of excitation of the upper level is less than that of the lower level. In fact, the former is

about one-half of the latter. This condition is not at all satisfactory for creating population inversion. However, the lower laser level $4s$ is radiatively connected with the ground state and its lifetime is very short $\sim 10^{-9}$ sec; while that of the $4p$ level is 10^{-8} sec. The inversion is achieved because the lower level is depopulated considerably faster than the upper level.

The Ar^+ laser tube, in its principal aspects, is similar to the one used in He-Ne laser with two windows at the end, inclined at Brewster angle, but has some special additional features (Fig. 8.10). Because of the high current density there is a continuous migration of ions towards the cathode and electrons towards the anode. Because of the low mobility, the ions tend to pile up at the cathode where they are neutralized and diffuse slowly back into the discharge. To equalize their distribution, the discharge tube, is provided with a return tube. The ions are accelerated by the electric field in the discharge. The Doppler width is ~ 3500 MHz which implies a temperature $\sim 3000^\circ\text{K}$. Water cooling system, therefore, is necessary. These 'hot' ions collide with the tube causing it considerable damage. There are very few materials which are able to withstand the intense ion

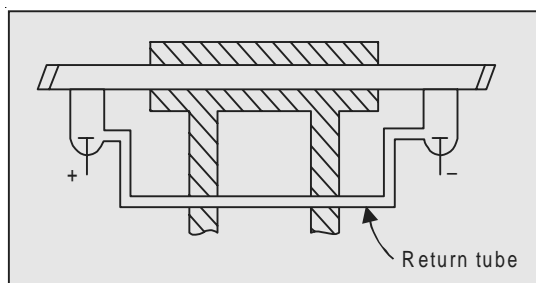


Fig. 8.10 Argon ion laser

bombardment and high wall temperature. The material must also have high thermal conductivity so that efficient heat transfer to water flowing in the cooling jacket is ensured. At present graphite or beryllia (BeO) is used for the purpose. The wall damage can also be reduced by using tubes of greater diameters; but in that case the total current required will be high. A static magnetic field is applied in the discharge region parallel to the axis. The advantage of this field is two-fold: firstly, by confining the discharge to the centre of the tube, it alleviates the problem of wall damage; and, secondly, it increases the number of electrons near the axis, thus increasing the pump rate which in turn, increases the output power by a factor of two or three.

The Ar^+ laser oscillates simultaneously on various transitions. The most important and the most intense lines are 4881 \AA (blue) and 5145 \AA (green). These two wavelengths are very useful since the human eye, photoemissive cathode and the photographic films have peak response at these wavelengths. Oscillations on a single line can be selected by introducing a prism inside the cavity as in Fig. 8.4. It has been possible to obtain very high output powers from Ar^+ lasers up to 100 W from a 1 cm diameter tube.

8.3.2 Krypton and Mercury Ion Lasers

Krypton ion laser is a close relative of argon laser, which oscillates at a number of wavelengths, the most powerful of which is the red line at 6471 Å.

Another useful ion laser is mercury ion laser oscillating at 6150 Å in the red region. This system operates in very short pulses (a few microseconds), but the pulses recur at a very high rate so that the output appears continuous to the human eye.

8.4 METAL VAPOUR LASER

The two other most widely used ion lasers are He : Cd and He : Se lasers. These are generally included in the category of *metal vapour lasers*. We briefly discuss the pump mechanism of these lasers.

8.4.1 He-Cd Laser

The energy levels of the system are shown in Fig. 8.11. The energies of the 2^1S and 2^3S states of He are greater than the ionization energy plus excitation energy of Cd^+ ions. He atoms, in 2^3S state on colliding with Cd atoms, therefore, can excite the D or P states of Cd^+ by the following process:

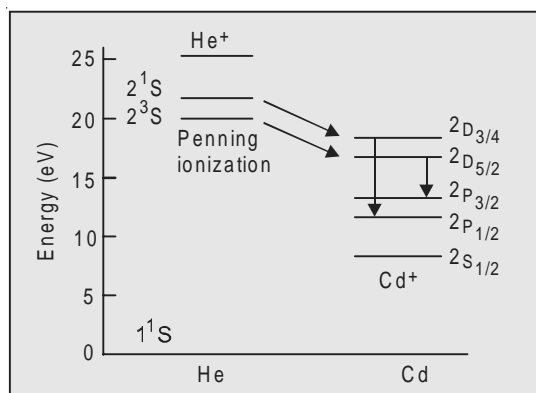
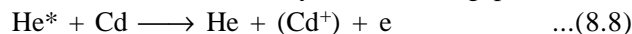


Fig. 8.11 Energy level scheme of He : Cd

The excess energy of He is transformed to the kinetic energy of the ejected electron. The process, obviously is not a resonant process. Such an ionization is known as *Penning ionization*. It is more effective in this case because 2^3S and 2^1S states of He are metastable states. Although excitation of both D and P states of Cd^+ is possible, it has been found that the cross-section for excitation of D states is about three times greater than that of the P states. Besides, the lifetime of D states is of the order of 10^{-7} sec, which is much longer than that of P states ($\sim 10^{-9}$ sec). The population inversion and, hence,

the laser action, therefore, can be readily achieved on the transition $^2D_{5/2} \rightarrow ^2P_{3/2}$ corresponding to 4416 Å and $^2D_{3/2} \rightarrow ^2P_{1/2}$ transition corresponding to 3250 Å. The laser may oscillate continuously at these wavelengths.

cw oscillations at these two wavelengths have been obtained by Silfvast [349] in a helium discharge tube containing a trace of cadmium. Helium pressure was ~ 1 Torr; while cadmium pressure was $\sim 5 \times 10^{-3}$ Torr. A maximum output of 300 mW on 4416 Å line and of 50 mW on 3250 Å line has been obtained. The transition at 3250 Å line is, perhaps, the shortest wavelength cw transition available and is widely used in photochemistry. [Corney, 88]

8.4.2 He-Se Laser

The energy level diagram is given in Fig. 8.12. As the diagram shows, the ionization energy plus the excitation energy of the Se atoms is of the order of 25 eV, which is much higher than the energy of the metastable states of He. However, as the current in a helium discharge tube is increased say from 100 mA, used in He : Cd system, to about 10 A and higher, helium is ionized and the density of the He^+ increases with the current. The ground state of

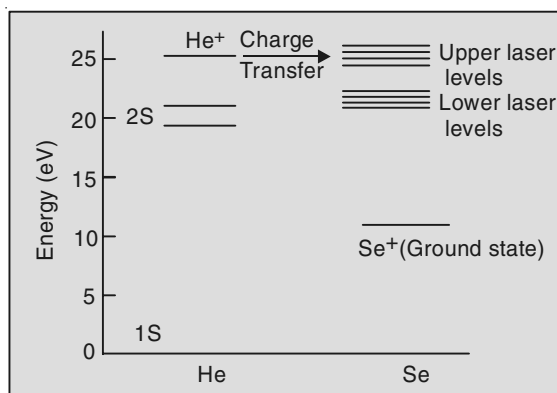
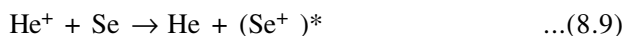


Fig. 8.12 Energy level scheme of He : Se

$\text{He}^+ \left(1^2S_{1/2}\right)$ lies 24.6 eV above the ground state of neutral atom and, hence, Se^+ atoms can be pumped to the upper laser levels on collision with He^+ ions by the process



This is known as *charge transfer ionization* and the process is resonant. The ionization energy of He is equal to the ionization plus excitation energy of Se. The process is very effective because He^+ ions have long life time.

Silfvast and Klein [348] have obtained cw laser oscillations on 24 visible transitions of Se^+ , ranging in wavelength from 4604 to 6535 Å.

The output power of both He : Cd and He : Se lasers is of the order of 50-100 mW, intermediate between He : Ne and Ar^+ ion lasers.

Laser oscillations on other metal vapours have been obtained by Piper and Webb [313] using hollow cathode discharge.

8.5 MOLECULAR GAS LASERS

There is yet another class of gas lasers which have proved to be very useful and are relatively easy to construct. These are molecular gas lasers. As in the case of atoms, electrons in molecules can be excited to higher energy levels, and the distribution of electrons in the levels define the electronic state of the molecule. Besides, these electronic levels, the molecules have other energy levels. The constituent atoms of the molecule can vibrate in relation to each other and the molecule as a whole can rotate. Both these motions are quantized giving rise to various vibrational and rotational levels. Some idea about the relative positions of these levels on the energy scale can be had from Fig. 8.13. The levels marked E_1 , E_2 , ... etc. are the electronic levels; those represented by quantum number v are vibrational levels and the closely spaced levels are the rotational levels represented by quantum number j . In molecular lasers oscillations are achieved on the transitions between vibration-rotation levels of the molecules. There are two types of molecular lasers. One uses the transition between vibrational states of the same electronic state—ground state, while in the other, oscillations are achieved on the vibrational levels of different electronic states *i.e.*, on what is known as ‘vibronic’ (vibrational-electronic) states. In the first the oscillation line falls in the infrared region; while in the second, it falls in the ultraviolet region.

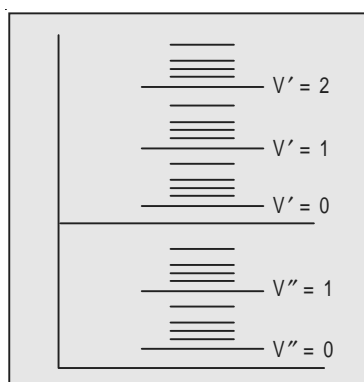


Fig. 8.13 Molecular energy levels

8.5.1 CO₂ Laser

The first laser of type 1 that we will discuss in this section is the CO₂ : N₂ laser. The first laser of this type was discovered by Patel [296, 298].

The fundamental modes of vibration of the CO₂ molecule are shown in Fig. 8.14. The three distinct modes of vibration are: (i) symmetric stretching

mode (frequency v_1) (ii) bending mode (v_2) and (iii) asymmetric stretching mode (v_3).

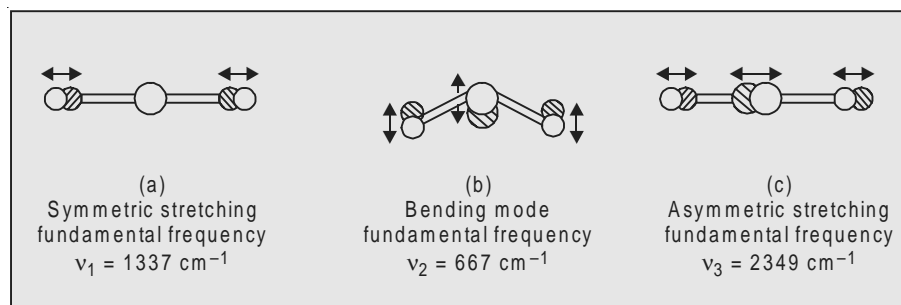


Fig. 8.14 Fundamental modes of vibration of CO_2

In the symmetric stretching mode, the oxygen atoms oscillate along the axis of the molecule simultaneously departing or approaching the carbon atom which is stationary. In asymmetric stretching, all the three atoms oscillate; but while both oxygen atoms move in one direction, carbon atom moves in the opposite direction. In the bending mode, the molecule ceases to be exactly linear as the atoms move perpendicular to the molecular axis.

The internal vibrations of carbon dioxide molecule can be represented approximately by the linear combination of three normal modes discussed above. The state of a vibrating molecule is specified by a set of three vibrational quantum numbers corresponding to the degree of excitation of each mode.

The labels used to classify the various vibrational levels are those used in spectroscopy. The label $nm^l p$ means, n quanta of frequency v_1 , m of frequency v_2 and p of frequency v_3 . The bending vibration is doubly degenerate; it can occur both in the plane of the figure and the plane perpendicular to it. The actual bending vibration of the molecule is a suitable combination of these two vibrations. The superscript l gives the angular momentum of this vibration about the axis of the molecule in units of \hbar . Thus, $02^{\circ}0$ indicates that the two vibrations combine to give an angular momentum $l = 0$.

The laser uses a mixture of CO_2 , N_2 and helium or water vapour. The active centres are the CO_2 molecules lasing on the transition between the rotational levels of vibrational bands of the electronic ground state. Figure 8.15 gives the vibrational energy level scheme for the electronic ground state of CO_2 and N_2 molecules.

When a discharge is passed in a tube containing CO_2 , electron impacts excite the molecules to higher electronic and vibrational-rotational levels. The electronic collision cross-section for the excitation to the level $00^{\circ}1$ is very large. This level is also populated by radiationless transition from upper excited levels. The resonant transfer of energy from other molecules, such as N_2 , added to the gas, increases the pumping efficiency. Nitrogen here plays the role that He plays in He : Ne laser. Nitrogen being a homonuclear diatomic molecule does not

possess a permanent electric dipole moment and, hence, radiation decay from $v'' = 1$ to $v'' = 0$ is forbidden. The lifetime of the level $v'' = 1$, therefore, is quite long ~ 0.1 s at 1 Torr. The vibrational level $00^{\circ}1$ of carbon dioxide is in near coincidence ($\Delta E = 18 \text{ cm}^{-1}$) with the highly populated $v'' = 1$ level of nitrogen.

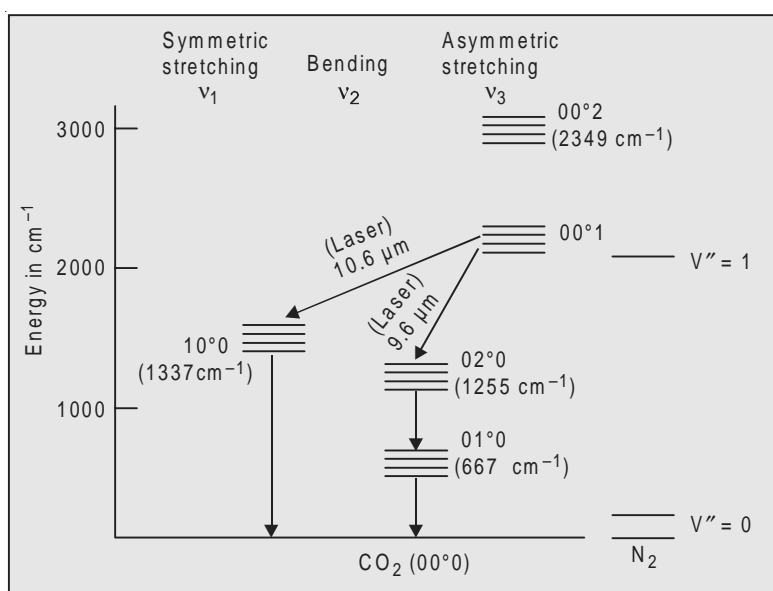


Fig. 8.15 Energy level scheme for the electronic ground states of CO_2 and N_2

Patel [296, 299] showed that the population inversion between the $00^{\circ}1$ level and the lower $02^{\circ}0$ and $10^{\circ}0$ levels, achieved by the above processes, leads to the laser oscillations near $9.6 \mu\text{m}$ and $10.6 \mu\text{m}$. Of these, the latter transition was found to give cw power output of 10 kilowatts, its efficiency being 30% which is quite extraordinary.

For a transition to lase, the decay times of the upper and lower levels have to satisfy the condition

$$\tau_{\text{upper}} \gg \tau_{\text{lower}} \quad \dots(8.10)$$

The decay times depend essentially on collision rates and can be determined from the knowledge of partial pressures. For a CO_2 laser with partial pressures

CO_2 (1.5 Torr), N_2 (1.5 Torr) and He (12 Torr)

the lifetime of the upper level was found to be $\tau_{\text{upper}} \sim 0.4 \text{ m sec}$ [94].

We have not yet explained the function of He, which we will presently do. The lower levels $10^{\circ}0$, $02^{\circ}0$ and $01^{\circ}0$ being very close, reach thermal equilibrium in a very short time. It is necessary that the decay from the lowest level $01^{\circ}0$ to the ground states is very fast; otherwise, there would be accumulation of molecules in this level and also in the other two levels since they are in equilibrium; and this would spoil population inversion. It has been found that the presence of He has a considerable influence on the lifetime of these levels.

For the partial pressures given above, the lifetime of the lower levels was found to be $20 \mu\text{ sec}$. The condition (8.10), therefore, is satisfied. This is not the only function of He though. To avoid population of the lower laser levels by thermal excitation, it is necessary that the temperature of CO_2 is low. Helium has high thermal conductivity, and, hence, helps to conduct heat away to the walls keeping CO_2 cold. Thus, while N_2 helps to increase the population of the upper level, He helps to depopulate the lower level.

Figure 8.16 shows the experimental arrangement for a typical CO_2 laser. In one such laser, discharge was produced in a tube 2.5 cm in diameter and 5 m long, by d.c. excitation. Alkali halide Brewster windows were used at the end. Near confocal silicon mirrors coated with aluminium, formed the resonant cavity. Pressures maintained were around $P_{\text{He}} \sim 7 \text{ Torr}$, $P_{\text{N}_2} \sim 1.2 \text{ Torr}$ and $P_{\text{CO}_2} \sim 0.33 \text{ Torr}$. It must be noted that for a given diameter there is an optimum set of values for the partial pressures in a mixture of gases. To remove the dissociation products, such as CO_2 , which would contaminate the laser, the continuous flow of the gas mixture is maintained in the tube. Since $00^{\circ}1 \rightarrow 10^{\circ}0$ transition has a higher gain, than the $00^{\circ}1 \rightarrow 02^{\circ}0$ transition, the laser usually oscillates at $10.6 \mu\text{m}$.

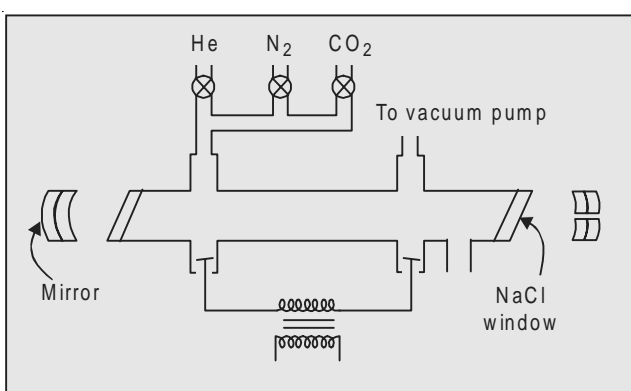


Fig. 8.16 Schematic of a CO_2 laser

We have said above that laser oscillates at a wavelength corresponding to a transition from the upper vibrational level $00^{\circ}1$ to the lower vibrational levels $10^{\circ}0$. Actually, a number of rotational levels are associated with each vibrational levels. Which of these rotational levels contribute to the laser oscillation? Obviously, the line resulting from the rotational level with largest population of the upper vibrational level will actually oscillate. The number of molecules N_j in the rotational level j at a temperature T is given by

$$N_j = N h c B (2j + 1) \exp(-B j (j + 1) hc/kT) \quad \dots(8.11)$$

where N is the total number of molecules and B the rotational constant [186 A]. In the case of CO_2 , the rotational level represented by the quantum number $J' = 21$ ($00^{\circ}1$ level) has the maximum population and the laser line corresponds to the transition $J' = 21 \rightarrow J'' = 22$. In spectroscopic notation this

is known as $P(22)$ line. Oscillation thus takes place in a single mode of a single rotational line of the $00^{\circ}1 \rightarrow 10^{\circ}0$ transition. To obtain oscillation on the $9.6 \mu\text{m}$ line, some selective device such as a diffraction grating is placed in the cavity. The maximum power that can be extracted from such longitudinal flow lasers is of the order of 50–60 W/m. Powers, higher than this, cannot be obtained from such lasers because 80% of the electric power is dissipated in the form of heat, which is removed from the centre to the walls by diffusion. The output power can be raised to about 1 kW/m, if the gas is flown perpendicular to the discharge (Fig. 8.17). If the rate of flow is maintained high, the heat is carried away by convection.

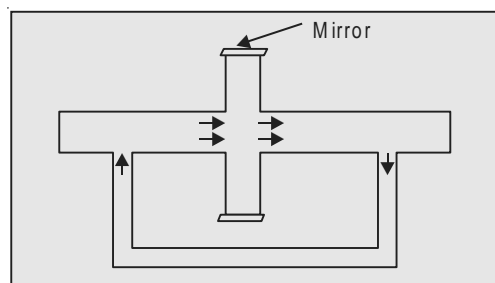


Fig. 8.17 Experimental arrangement for gas flow perpendicular to the discharge

The other class of CO_2 lasers is what is known as *Transversely Excited Atmospheric* pressure laser or TEA laser for short. In this, the current in the arc flows at right angles to the axis of the laser (Fig. 8.18). As the name implies it can be made to work at atmospheric pressures. These lasers are easy to construct and are inexpensive.

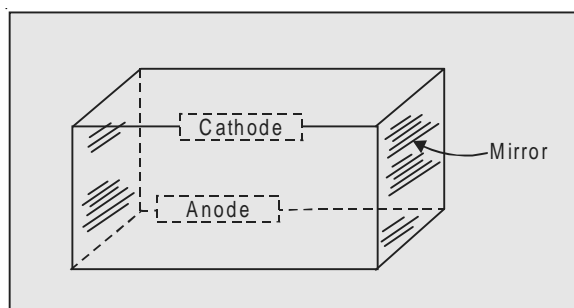


Fig. 8.18 TEA laser

The CO_2 lasers have very wide application in industry. However, considering the hazards to eyes and the other damages likely to be caused by these lasers, stringent precautions are necessary in working even with a low power CO_2 laser.

Besides CO_2 there are other gas lasers using vibrational-rotational transition. The HCN laser which oscillates at $\lambda = 773 \mu\text{m}$ is a laser of this type.

8.5.2 Electroionization Lasers

The discussion so far was restricted to the gas lasers operating at low pressures usually less than 10 Torr. The concentration of active centres in such media is much lower than that in solid state materials. If gas lasers are made to operate at high pressures, one can expect an enhanced output power from them. An increase in pressure, however, is not possible in a gas discharge because on increasing pressure the discharge loses its stability. Further, increase in pressure necessitates higher electric field intensity which, in turn, enhances the number of quenching collisions causing depopulation of the upper level.

An alternative method, therefore, is necessary for producing fast electrons capable of exciting the active atoms in the gas. A new technique now in use is what is known as *electroionization technique*, in which an ionization radiation is used in conjunction with an electric field for the excitation of the material. The technique was used successfully in high pressure CO₂ lasers.

A simplified version of such a laser is given in Fig. 8.19. The lasing volume contains a mixture of CO₂ + N₂ + He. The ionizing radiation enters the lasing volume through a foil which separates the evacuated accelerator space from the lasing volume under high pressure and is transparent to fast moving electrons. An electric field is applied to accelerate electrons. The ionizing radiation

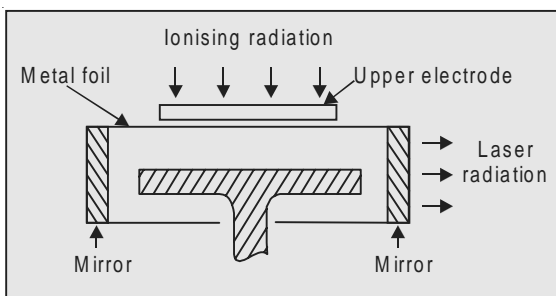


Fig. 8.19 Electroionization laser

knocks out free electrons from the active centres which are accelerated by the field applied. Thus the gas is ionized by the radiation and the active centres are excited by accelerated electrons. It may be noted that in gas discharges both these functions are performed by the same electrons. The rest of the technique and conditions of working are the same as in gas discharge lasers.

Pressures as high as 100 atmospheres have been realized in such compressed gas lasers. Increase of pressure leads to increase in output power of laser radiation and this dependence is found to be quadratic, i.e., output power $W \propto p^2$. The power generated by electroionization laser is about 10⁶ times that in a gas discharge laser.

For the ionization of the gas an electron beam from an electron gun is frequently used. Heavy particles produced in a nuclear reactor also can be used for this purpose.

The electroionization technique is also used in other lasers *e.g.*, (i) CO laser which operates at $5 \mu\text{m}$, (ii) Ar + N₂ laser which operates on transitions between electronic states of N₂ molecule at $0.358 \mu\text{m}$, argon playing the role of a buffer gas [372].

8.5.3 Gas-dynamic Laser

There is yet another class of CO₂ lasers known as gas-dynamic CO₂ laser [Gerry, 142].

The population distribution between the various vibrational and rotational levels of a molecule is governed by the Boltzmann law

$$N_n \propto \exp(-E_n/kT) \quad \dots(8.12)$$

according to which the population in the various levels decreases with increasing energy. With increasing temperature the population in each level increases but always in keeping with the above law. Hence, population inversion is not possible.

Let E₁, E₂ be the lower and upper levels of a molecule and τ₁, τ₂ their lifetimes such that τ₂ >> τ₁ that is, the relaxation rate of the lower level is much higher than that of the upper. Suppose now that the gas is heated to a very high temperature T₂ and then suddenly cooled by rapid expansion at supersonic velocities to a temperature T₁. Let τ be the time over which this temperature change takes place and is such that

$$\tau_2 \gg \tau \gg \tau_1$$

When the gas is suddenly cooled, the population of the lower level, because of the higher relaxation rate, will follow the drop in temperature and quickly decrease to the value corresponding to the temperature T₁; while the population

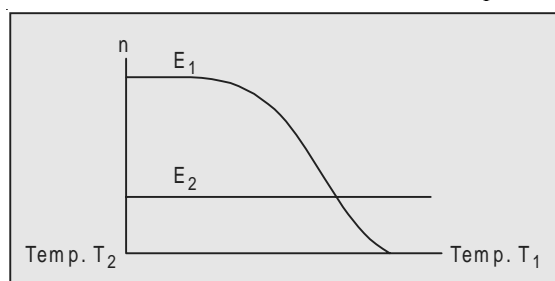


Fig. 8.20 Population of the levels E₁, E₂

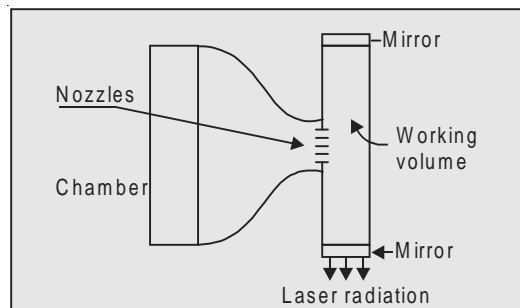


Fig. 8.21 Gas-dynamic laser

of the upper level virtually remains the same as at temperature T_2 thus producing the required population inversion between the levels of E_2 and E_1 (Fig. 8.20). This fact forms the basis of gas-dynamic lasers. The gas dynamic laser design is illustrated in Fig. 8.21.

The chamber contains the mixture $\text{CO}_2 + \text{N}_2 + \text{H}_2\text{O}$. The gas mixture is initially heated to a temperature ~ 1500 K, its pressure being over 20 atmospheres. For rapid cooling adiabatic expansion through nozzles is found to be very convenient. The gas is suddenly made to expand through an array of nozzles—a set of slits each 1 mm wide—into the working chamber where its temperature falls to 250–300 K and pressure ~ 0.1 atmos. The speed of the gas coming out of the nozzle is about 1500 m/s.

As in the gas discharge CO_2 laser, transitions on $00^1\text{1} \rightarrow 10^0\text{0}$ and $00^1\text{1} \rightarrow 02^0\text{0}$ are obtained. The CO_2 and N_2 molecules are excited thermally to 00^11 and $v'' = 1$ level respectively. On expansion 10^00 and 02^00 levels undergo rapid decay because of the shorter lifetimes; while 00^11 level of CO_2 and $v'' = 1$ level of N_2 are ‘frozen’. That is, because of the longer lifetime and low pressure, they do not deactivate in the short time available. The population of the 00^11 level, therefore, suffers insignificant loss, thus giving rise to population inversion.

It may be noted that nitrogen constitutes the main component of the mixture and the high population density of 00^11 level is mainly due to the resonant transfer of energy from N_2 . H_2O plays the same role that He plays in gas discharge CO_2 laser.

Output powers up to 100 kW have been obtained with such lasers.

8.5.4 Vibronic Lasers

There are a number of molecular lasers using transitions between vibronic states. These lasers show extremely high gain even in the absence of a resonant optical cavity. Stimulated emission and laser action occurs in these lasers in a single pass through the active medium. The radiation of this sort is known as *superradiance* (See Sec. 8.2). The term ‘superradiant’ was coined by Dicke [100]. The ordinary spontaneous emission is linearly proportional to the population of excited states. Dicke discussed the quantum theory of spontaneous emission from an assembly of N atoms and showed that the power radiated could be proportional to N_2 instead of N ; or more correctly

$$P \propto (N_2 - N_1)^2 \quad \dots(8.13)$$

This implies a kind of quantum coherence in emission.

We will discuss in this section a couple of such lasers which have some special importance.

(a) N_2 Laser [244]

The energy level scheme for N_2 molecule is given in Fig. 8.22. The laser oscillation is obtained on the transition from the lowest vibrational level

$v = 0$ of the excited states $C^3\Pi_u$ to the lowest level of the electronic state $B^3\Pi_g$ corresponding to $\lambda = 337$ nm. This transition is more favoured because: (i) the minima of the potential energy curves of the two states are at about the same internuclear distance, a requisite for satisfying Franck-Condon principle, and (ii) the level $v = 0$ in an electronic state is most populated, and, hence, the transition is very intense. It must be noted, however, that the lifetime of $C^3\Pi_u$ state is ~ 40 μ sec, which is much smaller than that of $B^3\Pi_g$ state, viz. 10 μ sec, and, hence, the population of two levels can only be transiently inverted. The inversion is rapidly destroyed by the accumulation of molecules in the lower level. It can be made to operate on pulse basis, provided the duration of electric pulse is shorter than 40 μ sec. The laser pulse lasts only 7–10 s and is self-terminating.

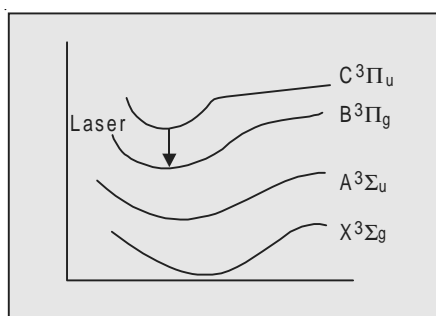


Fig. 8.22 Energy level scheme for N_2

A schematic diagram of a N_2 laser is given in Fig. 8.23. The excitation of N_2 molecule comes through its collision with free electrons. The probability of

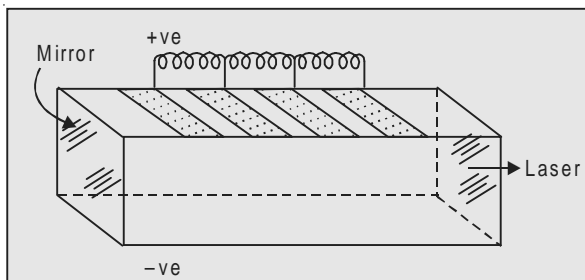


Fig. 8.23 N_2 laser

excitation of N_2 molecule from its ground state to the state $C^3\Pi_u$ by electron impact is much greater than that to the $B^3\Pi_g$ state. The electric field is applied perpendicular to the direction of stimulated emission. This arrangement allows a large gas volume to be excited at about 20 kV. If, instead, the electrodes were placed at the end, a voltage at least 25 times larger, would have been required. If the electronic pulse is made to travel in synchronism with laser pulse, it is possible to achieve a high gain even without a mirror. To this end inductances shown in the figure are introduced. They ensure that the voltage pulse applied to the plates travels along the axis at the same velocity as the light pulse.

Pulsed superradiant molecular nitrogen lasers operating at 3371\AA have been studied by a number of workers [8,114,244,295]. Current of several thousand amperes per sq cm in N_2 with suitable pressure (~ 20 Torr) excites several rotational lines of the $C^3\Pi_u \rightarrow B^3\Pi_g (0,0)$ band to superradiance, providing a peak power of about 20000 W. Designs using several dozen cables to supply the transverse currents have reached powers up to 1 MW in pulses ~ 10 nsec with repetition rate up to 100 Hz.

In contrast to these large transverse current lasers, Ericsson and Lidholt [114] have described small longitudinal discharge N_2 laser with peak power 10^3 W.

Various modifications of this laser have recently been developed. The nitrogen laser consisting of a rectangular channel 1 m long through which a rapid discharge is passed from a triggered high voltage capacitor system, is frequently used.

The attractive properties of the N_2 laser that make it suitable for various types of investigation, concern its short wavelength, high peak power, short pulse duration, high repetition rate and good amplitude stability.

(b) H_2 Laser

The other ‘vibronic’ laser that we will discuss briefly in this section is the H_2 Laser [188, 325].

The energy level scheme for the H_2 molecule is given in Fig. 8.24. The molecules are excited to the state $B'\Sigma_u^+$ by passing electrical discharge in the gas. Stimulated emission takes place on the $B'\Sigma_u^+(v') \rightarrow X'\Sigma_g^+(v'')$ transition and its rate is so fast that the molecules in the upper state do not have time to relax to the lowest vibrational level $v' = 0$. The laser action is obtained in the *P*-branch of the (5,12) and (6,13) bands at $\lambda \sim 160$ nm. Laser action has also been achieved on the $C'\Pi_u \rightarrow X'\Sigma_g^+$ transition at $\lambda \sim 116$ nm. Both these wavelengths fall in the vacuum ultraviolet region (vuv) and are, perhaps, the shortest wavelengths that have ever been produced from laser action. Output powers are around 100 kW with pulse duration of about 1 μsec .

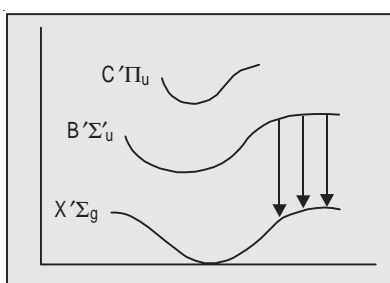


Fig. 8.24 The energy level scheme for H_2 molecule

8.6 EXCIMER LASERS

There are some diatomic molecules which are unstable in their ground state, *i.e.*, the potential energy curve of their ground state does not have a minimum and, hence, they do not exist as molecules in this state. They can only exist as ‘monomers’ in this state. However, the potential energy curves for the excited states of these molecules may have a minimum and the molecules can exist as excited dimers, *e.g.*, Xe_2^* , Kr_2^* , Ar_2^* . Such molecules are called ‘excimers’—a contraction of the words ‘*excited dimers*’, first suggested by Stevens and Hutton [366], to distinguish them from the normal type dimers which exist in the ground state. The broad bandwidth emission continue from noble gas excimers are well known. These characteristics of excimers can be exploited for producing laser action. When the molecules undergo a transition from the upper bound state to the repulsive ground state, they dissociate into a pair of unexcited ground state atoms and, hence, the lower state of the molecule is always empty. This facilitates achieving population inversion required for laser action. The potential of such systems as laser media was first pointed out by Houtermans [194] in 1960, although the first demonstration of laser action in an excimer system was not made until 1970 [30].

The energy level scheme for the Xe_2^* excimer is given in Fig. 8.25. Xe atoms in a gas at pressures greater than 10 atmospheres are excited by electron beams to the upper state where they combine to form Xe_2^* excimers in bound states. Laser action is obtained in their transition to the ground state at $\lambda \sim 172$ nm with $\Delta\lambda = 15$ nm. Since no welldefined vibrational-rotational transitions exist, the actual transition is broad-based, and, hence, the laser can be made tunable over the broad band region.

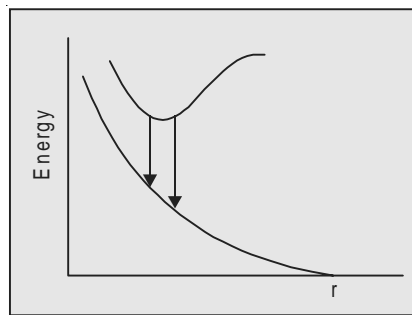


Fig. 8.25 Potential energy curves for Xe_2 excimer

For Xe_2^* excimer lasers, power densities of order of 15 MW cm^{-3} are required to produce a gain coefficient of 0.1 cm^{-1} . It is now possible to construct small generators with output power exceeding 10^9 W which enables

short wavelength, compact, frequency tunable lasers with megawatts powers to be developed in vuv region.

Argon excimer lasers oscillate on a transition corresponding to $\lambda \sim 126$ nm [198].

Excimer lasers have very wide applications. For example, Xe_2^* excimer can be used to produce excited Se atoms by vuv photodissociation of the triatomic molecule OCS.



Laser action has been observed in atomic Se using such an excitation scheme [316]. Another advantage of these lasers is that the third harmonic generation enables the wavelength of uv laser to be shifted to vuv region of the spectrum.

More details about excimers can be found in the review article on excimers by Birks [47].

SEMICONDUCTOR LASERS

9

We discuss in this chapter an important class of broadly tunable lasers which have proved to be very useful particularly in optical communication and optical-computer design, namely, the *semiconductor lasers*. This is the third historical development in lasers. The original concept dates from 1961, when Bernard and Duraffourg [41] and Bosov *et al.* [29] independently suggested that stimulated emission of photons may be obtained in semiconductor materials from transmission between conduction and valence bands. Since then, during the last twenty years or so, the semiconductor laser has grown and developed into a whole range of sophisticated opto-electronic devices.

9.1 CENTRAL FEATURES OF SEMICONDUCTOR LASERS

Let us look first into the basic physics of semiconductors.

We know from experience that materials exist with different electric properties. In order to pass a current in a material, we have to supply some energy to electrons accelerating them. In some solids the current flows easily. These are good conductors of electricity. In contrast, some others are non-conductors or poor conductors of electricity which are known as insulators. Let us look into this contrasting behaviour of materials.

The energy spectrum of an isolated atom consists of a number of discrete energy levels. In crystals the nature of these levels is different. Although, in general, the inner shells of electrons are bound to the nuclei of the atoms arranged in a specific order to form crystals, their outer electrons—the so called valence electrons—are donated into the crystal structure. We cannot talk, therefore, about the wavefunctions and energy levels of atoms; instead, we have to deal with the wave-functions and energy levels of the crystal as a whole. The valence electrons are in a free field created by ions. Due to the

perturbations caused by these ions, the levels of the electrons broaden and change to bands (Fig. 9.1). Each of these bands consists of a large number (of the order of 10^{24}) of electron states closely packed. Electrons are fermions and, hence, obey Pauli exclusion principle, which states that only one electron is allowed in each quantum state. The general tendency of electrons is to occupy the lowest energy states. Two kinds of electron distribution are of special interest in the context of the topic we are discussing:

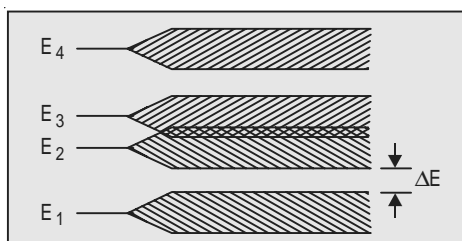


Fig. 9.1 Energy bands in a crystal

- (i) The distribution in which the lowest energy band E_1 (Fig. 9.2) is completely filled with electrons and no higher energy band contains any electrons. This lowest energy band is called the *valence band*. Since all available places in the valence band are already filled, the electrons have no place to go and, hence, they cannot serve as conductors of current. These materials are known as *insulators*. Quartz, mica are examples of this kind. The resistivity of quartz, for example, is 10^{16} ohm-metres. The next higher band is separated from the valence band by an energy gap ΔE which is known as ‘band gap’ or ‘forbidden gap’. Electrons in the solid may not take on the values of energy within the forbidden gap.

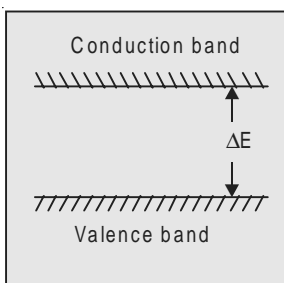


Fig. 9.2 Conduction and valence bands

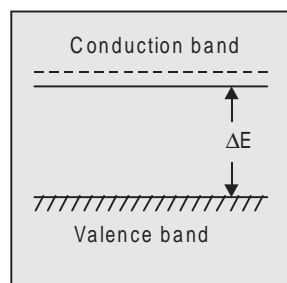


Fig. 9.3 Conduction band partially filled

- (ii) In the second case of distribution the lowest energy band is filled in such a way that the next higher band is also partially filled by electrons (Fig. 9.3). The electrons are now free to move because there are nearby empty states available. However, they cannot go beyond the crystal, as the space within which the electrons are permitted to travel is bounded by potential barriers. Such materials are called *good*

conductors and the higher band is called the *conduction band*. Metals such as copper, silver, etc., are good conductors. In fact, in metals, either the conduction and valence band overlap or the width of the forbidden zone is zero.

There is yet another class of materials which at $T = 0\text{ K}$ behave like insulators, but their band gap is so small (2 eV or less) that when the temperature is raised, the increasing thermal agitation raises some electrons to the empty conduction band making the material conductive. Their conductivity, however, lies between that of a good conductor and an insulator. These materials are known as *semiconductors*. Thus, it is the size of the band gap that decides whether a material is an insulator, a conductor or a semiconductor.

When an electron in a semiconductor is excited thermally to the conduction band, it leaves behind a vacant site in the valence band which is called a ‘hole’ and has the same properties as that of an electron except that a positive charge is assigned to it. Thermal excitation, thus, generates free electron–hole pairs in semiconductors.

When a semiconductor does not contain any impurity, it is called *intrinsic semiconductor* and in it the number of conduction electrons is equal to the number of holes.

9.2 INTRINSIC SEMICONDUCTOR LASERS

When a light beam with photons whose energy is slightly higher than the band gap energy, is passed through a semiconductor, there is a probability that an electron at the top of the valence band absorbs a photon and move to the conduction band. There is an equal probability that an electron already present at the bottom of the conduction band is persuaded by the incident photon to move to the valence band, where it recombines with a hole and in the process releases a photon in the same state as that of the incident photon, thus amplifying the radiation. In order that the process of stimulated emission dominates over that of absorption, it is necessary to create a population inversion in the semiconductor. That is, the concentration of electrons at the bottom of the conduction band must be higher than that of holes at the top of valence band. Such a population inversion can be obtained by optical pumping or by pumping with an electron beam with fast moving electrons ($\sim 100\text{ kV}$). This latter technique is used in cadmium sulphide lasers. The major impediment in this method is that a substantial part of the electron beam energy is lost in heating the semiconductor chip. This spoils the degree of inversion as the electrons in the conduction band are lifted to the higher level, reducing their number at the bottom of the band and also moving electrons at the top of the valence band. Cooling, therefore, is essential for such intrinsic semiconductor lasers. Cadmium sulphide laser is found to operate successfully at liquid helium temperature 4.2 K at $\lambda = 0.49\text{ }\mu\text{m}$.

9.3 DOPED SEMICONDUCTORS

When the crystal contains impurities, its conducting properties change drastically. The impurity atoms may be found in one of the two places: they may replace the original atoms in the lattice or may occur interstitially. In most cases they substitute for normal atoms.

This leads us to the consideration of the role of impurities in promoting conduction of a current in a semiconductor. The dopants are of two types: *donors* and *acceptors*. For example, suppose a semiconductor is prepared by adding a small amount of an element of group V of the periodic table, say, phosphorus to silicon, an element of group IV. Since each phosphorus atom carries five valence electrons, while the silicon atom, which it replaces, carries four, there will be excess electrons available for conduction. The impurity that has more valence electrons than host atoms is called a ‘donor’ impurity. Phosphorus is a donor. A donor can donate excess electrons to the conduction band. Their lowest states lie in the forbidden gap but fairly close to the conduction band (Fig. 9.4) their separation being of the order of 0.01 eV. The small value of ΔE suggests a weak bond of one of the electrons with the atom and, hence, even a small thermal excitation (~30K) is enough to raise the electron from the donor level to the conduction band. This process transforms the semiconductor into a degenerate *n*-type material.

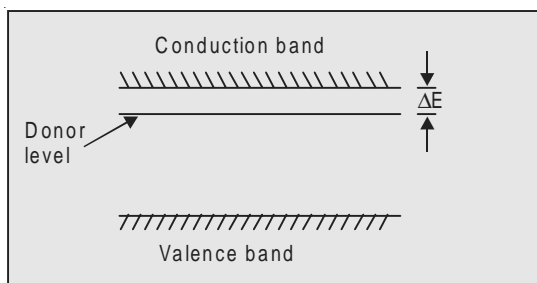


Fig. 9.4 Donor levels

Suppose now, instead of phosphorus, we add an element of group III, say, indium, which carries three valence electrons. There will, thus, be a shortage of valence electrons. Under these circumstances, the trivalent impurity atom will pick up an electron from the normal lattice atom and thus, will become negatively charged, thereby producing a ‘hole’ elsewhere, which acts as if it was positively charged. The semiconductor is transformed into a degenerate *p*-type material. The impurity which has fewer valence electrons than the host atoms (*e.g.*, indium) is called an ‘acceptor’. They take electrons from the valence band and leave holes behind. The states to which valence electrons are promoted also lie in the forbidden gap, but close to the valence band (Fig. 9.5).

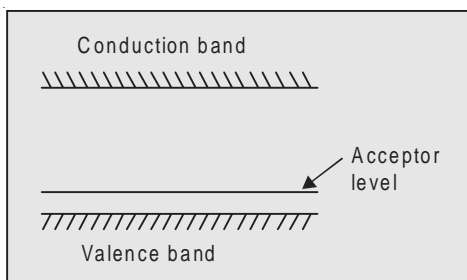


Fig. 9.5 Acceptor levels

A number of semiconductors of either form can thus be prepared by adding suitable impurity to the material. Thus, tellurium added to gallium arsenide makes it a *n*-type semiconductor; while zinc makes it *p*-type.

Crystals can also be prepared with one part *p*-type and the other *n*-type. The transition region is called a '*p-n* junction'. When *p*-region of a crystal is biased positively, holes are injected from *p*-region into the *n*-region and electrons from *n*-region into the *p*-region. The foreign carriers cannot live long when they have been injected. They soon recombine with carriers of opposite charges and in the process release the excess energy in the form of heat or light. If the recombination energy released is in the form of heat, as it is in the case of silicon and germanium, the materials are of no use for laser action. In gallium arsenide, most of the energy emitted appears as light and it is for this reason that this compound is extensively used in semiconductor lasers. The wavelength of light emitted depends on the 'activation energy' that is required to free a valence electron. The activation energy of gallium arsenide is ~1.4 eV and the photons emitted have a wavelength ~9000 Å.

Thus, when a current is passed through the *p-n* junction of a crystal prepared to certain specifications, the junction emits radiation. The population inversion that is necessary for amplification of the radiation is found in the narrow region near forward bias *p-n* junction, if the current density is sufficiently high. If the original photon is travelling exactly in the plane of the junction, which should be extremely flat, there may be amplification, and if the photons continue to travel near the junction, the amplification will grow. The photon which initiates the action may just be some recombination radiation emitted by the junction itself.

In order to make the amplified radiation travel to and fro so as to increase the gain, it is necessary to have an optical resonator containing *p-n* junction. This is done by cutting the crystal so that two end faces are exactly perpendicular to the junction and parallel to one another. Since most of the semiconductors have a high refractive index, reflection at an air-semiconductor interface is high and no special coating is necessary. The other two sides of the sample are usually rough sawn to inhibit undesired reflections.

9.4 CONDITION FOR LASER ACTION

The probability of occupation $f(E)$ of any energy state E is given by Fermi-Dirac statistics [232], *i.e.*,

$$f(E) = \frac{1}{1 + \exp[(E - F_0)/kT]} \quad \dots(9.1)$$

where F_0 is known as Fermi level for the system. The physical significance of this level can be found from the above formula: If $E < F_0$, the exponential in the denominator vanishes as $T \rightarrow 0$, and $f(E) = 1$. On the other hand, if $E > F_0$, $f(E) \rightarrow 0$ as $T \rightarrow 0$. That is, when $T \rightarrow 0\text{K}$

$$\begin{aligned} f(E) &= 1 \text{ if } E < F_0 \\ &= 0 \text{ if } E > F_0 \end{aligned} \quad \dots(9.2)$$

The Fermi level, thus, represents the boundary between fully occupied and completely empty levels at $T = 0\text{K}$. At absolute zero temperature, the electrons will necessarily occupy the lowest available energy states. An immediate consequence of the Pauli Exclusion principle is that each quantum state can contain only one fermion. Therefore, all the lowest states will be occupied with one fermion in each until all fermions are accommodated. Under these conditions, the gas is said to be *degenerate* and the topmost occupied level is the Fermi level. For non-degenerate semiconductors the Fermi level is situated inside the forbidden gap (Fig. 9.6).

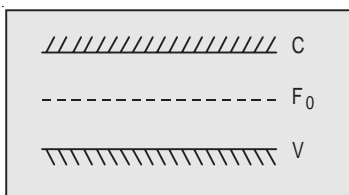


Fig. 9.6 Fermi level

Consider now a semiconductor at $T = 0\text{K}$ as shown in Fig. 9.7 (a). The hatched area in this figure represents completely full energy states. When there is a perfect thermal equilibrium between the conduction and valence bands, a single Fermi level can be defined as in (9.1), that uniquely determines the distribution of electrons in the conduction band f_c and that in the valence band f_v , over the whole range of energies of both bands. Suppose now that some electrons are raised from the valence band to the conduction band [Fig. 9.7(b)]. The semiconductor in this condition is not in thermal equilibrium. Nevertheless, the equilibrium will be reached in each band in a very short time $\sim 10^{-13}$ sec in which the electrons in the conduction band will have dropped to the lowest level in that band, and any electrons near the top of the valence band will also have dropped to the lowest unoccupied level, leaving the top of valence band full of ‘holes’. Under these conditions we have to assign two different levels—

so called quasi-Fermi levels—for the two separate bands, in such a way as to give a very good approximation to the distribution of electrons within the bands. It can easily be seen from (9.1) that the increase in the population of the conduction band leads to an increase in $f_c(E)$ i.e., decrease in $\exp\{(E_c - F_0)/kT\}$. This is possible if the quasi-Fermi level F_c is higher than F_0 ($F_c > F_0$). Similarly, increase in hole concentration depresses f_v below F_0 (Fig. 9.7). There is, thus, a population inversion between the conduction and valence bands which may give rise to laser action.

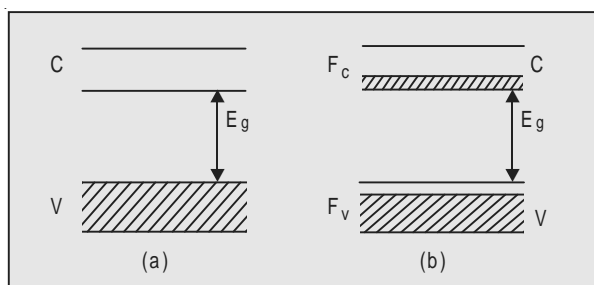


Fig. 9.7 Energy levels of a semiconductor: (a) $T = 0\text{K}$; (b) electrons excited to the conduction band

We now proceed to find the condition that must be satisfied in order to achieve laser action.

For a crystal not in equilibrium, the occupation probability $f_c(E_c)$, of any state of the conduction band can be expressed in terms of a different Fermi level F_c , as

$$f_c(E_c) = \frac{1}{1 + \exp[(E_c - F_c)/kT]} \quad \dots(9.3)$$

where E_c is the energy of the state concerned. The level separates the zones of fully occupied and completely empty levels of the conduction band. Similarly, we can express the occupation probability of the valence band as

$$f_v(E_v) = \frac{1}{1 + \exp[(E_v - F_v)/kT]} \quad \dots(9.4)$$

$$\text{At equilibrium, } F_c = F_v = F_0. \quad \dots(9.5)$$

When a light beam is incident on such a semiconductor, the number N_a of quanta absorbed per unit time will be proportional to, (i) probability per unit time of direct transition from the valence band to the conduction band, B_{vc} (ii) density of the incident radiation $\rho(\omega)$, (iii) the probability of the concerned state in the valence band being occupied $f_v(E_2)$, and (iv) the probability that the upper state in the conduction band is empty, $[1 - f_c(E_c)]$. That is,

$$N_a = AB_{vc} f_v(E_c) [1 - f_c(E_c)]\rho(\omega) \quad \dots(9.6)$$

The number of quanta N_e , emitted per unit time by stimulated emission is

$$N_e = AB_{cv} f_c(E_c) [1 - f_v(E_v)] \rho(\omega) \quad \dots(9.7)$$

The constant of proportionality A in the above formulae includes the density of states of the two bands. For amplification to occur

$$N_e > N_a \quad \dots(9.8)$$

$$\text{Assuming } B_{vc} = B_{cv} \quad \dots(9.9)$$

this condition can be written as

$$f_c(E_c)[1 - f_v(E_v)] > f_v(E_v)[1 - f_c(E_c)] \quad \dots(9.10)$$

Substituting for $f_c(E_c)$ and $f_v(E_v)$ from (9.3) and (9.4) and simplifying, we arrive at

$$F_c - F_v > E_c - E_v = \hbar\omega \quad \dots(9.11)$$

Thus, provided a ‘quasi-fermi level’ can be defined for each of the two bands of a semiconductor, the condition (9.11) must be satisfied to get stimulated emission.

Two requirements that must be fulfilled, if a semiconductor is to be used as a laser material, are: (i) the semiconductor must be such that the transition probability for a radiative transition across the gap must be high, and must exceed the probability for non-radiative transfer of energy to the lattice, etc., and (ii) excess population can be maintained across the laser transition. The latter requirement is met by carrier injection, the pumping source being a current passing through the semiconductor.

A simple way of achieving population inversion is to use a semiconductor in the form of a *p-n* junction diode heavily doped with donors and acceptors. Fig. 9.8(a) depicts the energy diagram of a *p-n* junction.

In the *n*-type semiconductor, there are enough electrons donated by impurities to fill the conduction band up to Fermi level F_c , which falls within the conduction band. In the *p*-type, holes are added by the acceptors down to energy F_v , which falls within the valence band. The energy difference between *p*- and *n*-regions is the built-in voltage or the *contact potential* of the *p-n* diode.

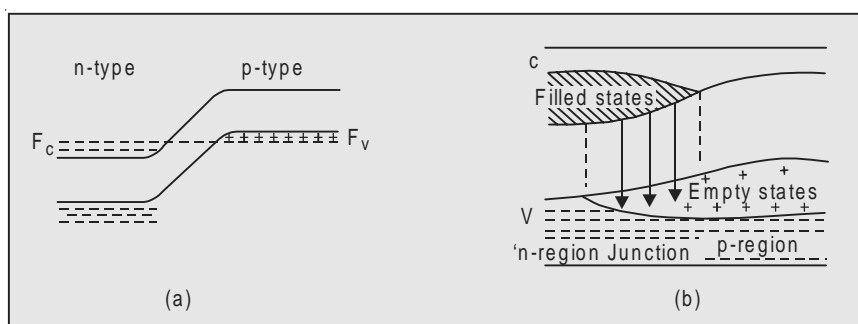


Fig. 9.8 Energy levels of a *p-n* junction

When no voltage is applied, electrons from the *n*-side, flow to the *p*-side until an electrical potential barrier is built up, which prevents further flow of current. The Fermi levels, under this condition, lie in the same horizontal line. When the junction is forward-biased, *i.e.*, when voltage is applied raising *n* (relative to *p*) side [Fig. 9.8 (*b*)], electrons flow to *p*-side and holes to the *n*-side and overlap, at least in part of the junction regions—the so called *depletion region*—where the injected electrons and holes, both appear in high concentrations. A high hole concentration means a large number of empty sites into which electron can fall. A population inversion, therefore, exists in this region and, hence, laser action will occur in the region when the current flow through the diode exceeds a certain threshold value. Thus when the electrons and holes are injected into the junction region from opposite sides at a sufficient high rate, a population inversion is created between the filled levels near the bottom of the conduction band and the empty levels near the top of the valence band, and the recombination of electrons and holes in this region can be used to generate coherent radiation. The *p*- and *n*-regions surrounding the junction layer are, however, lossy to the laser wavelength and, hence, the recombination energy is likely to be dissipated in a number of ways which are non-radiative such as, for example, by direct interaction with lattice phonons. The laser action, therefore, is confined to the very thin, planar junction region.

9.5 INJECTION LASERS

The first example of a laser involving transition between energy bands was reported by Hall *et al.* [158]. It was the first time that direct conversion of electrical energy to coherent infrared radiation was achieved. They observed coherent light emission from GaAs *p-n* junction. Diodes used were cubes with each edge 0.4 mm long, the junction lying in a horizontal plane through the centre. Current was passed through the junction by means of ohmic contacts attached to the top and bottom faces. The front and back faces were polished parallel to each other and perpendicular to the plane of the junction, thus forming an optical cavity. The other two faces were rough sawn. The diode was immersed in liquid nitrogen and the current was applied in the form of pulses of 5 to 20 μ sec duration. Interference fringes were obtained due to interaction between different parts of the wavefront. Their appearance indicated that a definite phase relationship exists between the light at different points along the junction, *i.e.*, the light is coherent.

Intensity measurements were made as a function of junction current. Below 5000 A/cm², the light intensity varied linearly with current density. Near 8500 A/cm², the intensity increased rapidly with current. At 20000 A/cm², it reached a value about ten times the value anticipated by extrapolating the low current plot, indicating the onset of stimulated emission. It was at this threshold

current that the interference fringes appeared. Below the threshold the spectral width was 125 Å. It decreased suddenly to 15 Å above the threshold, which is again a characteristic of stimulated emission. The emission was confined to a fairly narrow region of wavelengths, between 8380 to 8392 Å. Similar observations were made by Nathan *et al.* [285].

These lasers are called *injection lasers*, since the laser action is created by charge carriers injected into a semiconductor diode.

A schematic diagram of a *p-n* junction laser is given in Fig. 9.9.

The diode has small dimensions of the order of 1 mm × 1 mm. Because of the high rate of stimulated emission possible in semiconductors, the length of the F.P. resonator may be made much smaller, a length between 0.2 to 1 mm being suitable. The active region consists of a layer of thickness ~1 μm. The emitted beam, however, is much wider ~40 μm and extends well into the *p*- and *n*-regions and has divergence of the order of 5 to 15° [Fig. 9.9 (b)].

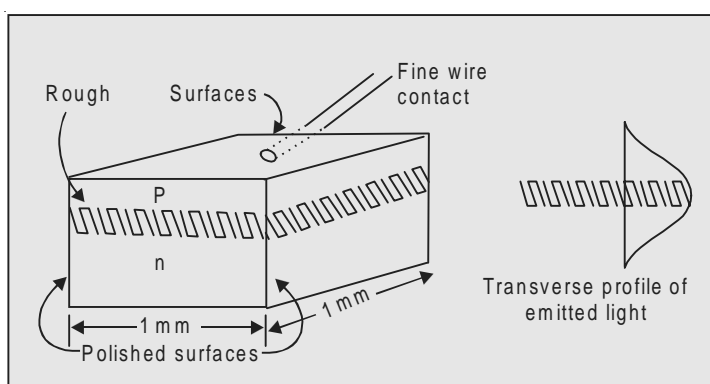


Fig. 9.9 Injection laser

9.6 INJECTION LASER THRESHOLD CURRENT

We will now show how the order of the magnitude of the threshold d.c. current required to obtain laser action in a diode injection laser can be calculated.

Let the area of the active region (Fig. 9.9) be A and its thickness ' d '. As stated above, the upper and lower level populations in this case consist of electrons in the lowest level of the conduction band and the highest level of the valence band respectively, in the junction region of the *p-n* diode. The ideal condition for the population inversion is when the number density of conduction band electrons in the junction region is, say N_2 and that in the valence band is $N_1 = 0$. The total number of electrons that must be maintained in the conduction band in this region is, thus, N_2Ad . Suppose these electrons decay down to the valence band with lifetime t_1 , and each such decay requires the transfer of one new electron charge ' e ' into the junction to maintain the upper state population. Therefore, current I is

$$I = \frac{N_2 Ade}{t_1} \quad \dots(9.12)$$

∴ The required threshold current density is

$$\begin{aligned} J &= \frac{I}{A} = \frac{N_2 de}{\tau_1} \\ &= \frac{\omega_0^2 \tau_{\text{rad}}}{2c^3 \pi \tau_p} \cdot \frac{de}{\tau_1} \Delta\omega_0 \end{aligned} \quad \dots(9.13)$$

where we have used (6.59).

Experimental results for GaAs are in good agreement with those calculated at liquid helium temperature. At temperatures > 77 K, the threshold current density J for a semiconductor laser increases rapidly as T^3 , lying in the range $35 - 100$ kA/cm 2 . This is because, as the temperature increases, the probability product $f_c(E_c)[1 - f_v(E_v)]$ decreases, while $f_v(E_v)[1 - f_c(E_c)]$ increases. The gain, therefore, decreases rapidly as can be seen from (9.10). To obtain the same gain, the current density must be increased which, in turn, raises the temperature. Hence, it is not possible to operate semiconductor lasers continuously above a certain temperature T_c which depends upon the diode construction. Continuous output powers up to a few watts have been obtained with GaAs laser at 77 K.

9.7 ADVANCES IN SEMICONDUCTOR LASERS

Semiconductor laser has undergone a very considerable metamorphosis since it was first made in 1962. In the original devices the junction was formed by gaseous diffusion of the p -type impurity into a crystal of n -type. At room temperature, the threshold current density required for such lasers was between 10000 and a million amperes per square centimetre and, hence, the device had to be cooled to 77 K or below. In the new method, p -type material from a liquid solution is grown on top of the n -type crystal. This has two advantages: (i) the new part of the crystal grows along the original crystal plane and, hence, the junction is extremely flat, which reduces the threshold current and increases the efficiency, and (ii) the concentration of the impurities in the junction region can be kept very high for solution growth. Threshold current densities of 10000 amperes per sq cm are now within reach. Special drive circuits have been developed for this purpose.

Laser action can now be obtained in the way described above in a number of semiconductor materials, at numerous wavelengths ranging from uv to about 10 μm . The lead selenide diode laser (PbSe) reported by Butler *et al.* [71] is of particular interest because its emission at 8.5 μm falls within the width of the atmospheric ‘window’ extending from 8 μm to 14 μm , in which the attenuation due to scattering by haze is low and the atmosphere transparency

is high. Further, since the magnitude of the energy gap in this semiconductor is strongly affected by temperature, magnetic field and pressure, the variation of these parameters enables the laser wavelength to be tuned over a significant range. The PbSe laser, therefore, is very suitable for application in terrestrial communications.

Laser action has also been obtained in indium arsenide and indium antimonide.

In pure gallium arsenide at room temperature, the laser light has a wavelength $\sim 9000 \text{ \AA}$ in the near infrared. At lower temperatures, the output wavelength decreases to $\sim 8400 \text{ \AA}$ as was shown by Hall *et al.* [158]. The output can, therefore, be tuned over a considerable range by varying the temperature. This transition wavelength can be further shifted down to as short as $\sim 6500 \text{ \AA}$ in the visible red spectrum by employing a mixed semiconducting alloy of GaAs and GaP [6].

The carrier recombination laser can be tuned in several ways [189-91], for example, by varying the composition of the semiconductor which determines where it will emit. Thus, by varying the ratio x in composition such as $\text{Pb}_{1-x}\text{Sn}_x\text{T}_c$, output anywhere between 5 and 25 μm can be obtained. The output can also be varied by varying the current in the diode. As the current is varied, the temperature of the diode changes which, in turn, causes the index of refraction of the material, and, hence, the wavelength satisfying the F.P. condition, to change. As the current is changed through a small range, the output wavelength is smoothly varied. The power output of lasers, however, is very small $\sim 1 \text{ mW}$.

There is yet another type of an important semiconductor laser known as 'spin-flip laser' which we will discuss in Chapter 15.

The main advantages of a semiconductor laser are: Its compactness, simplicity and efficiency. They require very little auxiliary equipment. Because large numbers of excited electrons are produced in a junction diode when a current flows, only a small diode is needed to produce laser action. Typically the area of the junction is $\sim 1 \text{ sq mm}$. The junction diode is very efficient because nearly every electron injected across the junction contributes a useful photon output.

These lasers have some disadvantages too. It is rather difficult to control the mode pattern and mode structure of the laser action because of the extreme thinness and small size of the laser region. The laser output is usually in the form of a wide beam, 5 to 15° , because the laser action originates not between two sharp and well-defined energy levels, but between the edges of two broad bands.

As a consequence, the spectral purity and monochromacy of the injection laser output is much poorer than in other types of lasers.

The semiconductor laser has provided spectroscopists with a very useful tunable light source and is making possible new advances in spectroscopy. Since it can be readily linked to optical fibres and can also be modulated, it is likely to play a vital part in optical communication.

9.8 C³ LASER

Won-Tien Tsang and his colleagues at Bell Laboratories, have recently developed a new kind of semiconductor laser [382], which has minimized the disadvantages to a large extent and has demonstrated a number of capabilities that promise to be of considerable importance for fibre-optic communication. The laser has been nicknamed as *C³ laser*. The spectral width of a conventional cavity diode laser is due to half a dozen or so Fabry-Perot modes that oscillate in it. This spectral width severely limits the rate of data transmission and the distance over which one can transmit information. The new laser uses a coupled-cavity resonance technique to get rid of all but one of these modes which results into a pulsed output with a spectral width of less than an angstrom at gigahertz rates of amplitude modulation. This extraordinary monochromacy of the pulse output makes it possible to transmit data at a wavelength of 1.55 microns where the optical fibres are at their clearest. Tsang points out that it is possible to transmit the entire text of Encyclopaedia Britannica in less than half a second.

10

LIQUID-, DYE- AND CHEMICAL LASERS

10.1 LIQUID LASERS

In general, good laser crystals are difficult to grow and are very expensive. Besides, optical strain, defects, imperfections and internal damage, which result at high power levels in crystals and which are mainly responsible for mode distortion, are difficult to eliminate. By contrast, the homogeneous liquids can have a very high optical cavity and would not crack or shatter if the output power becomes high. Of course, we cannot ignore the large thermal expansion coefficients and the change in the refractive index that will result as the temperature rises. These could be controlled by cooling and recirculating the laser solution through the active region. One can, therefore, use tubes filled with liquid (Fig. 10.1) instead of laser rods.

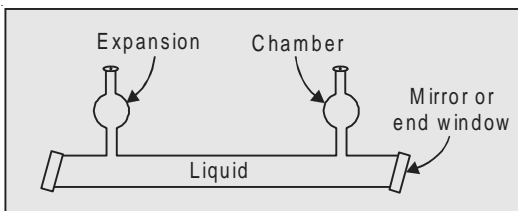


Fig. 10.1 Schematic of a typical liquid laser rod

When rare-earth ions commonly used in solid state lasers are dissolved in a solution, the energy levels of the ions associated with unfilled inner $4f$ shell remain almost unchanged. This makes it possible to obtain optically pumped laser action in liquids and has been observed on transitions of Eu^{3+} and Nd^{3+} ions at 6131 Å and 1.06 μm respectively.

The suitability of europium as a laser material was recognised in the original paper of 1958 by Shawlow and Townes [331]. Europium ions fluoresce in sharp, strong spectral lines, some of which end on a terminal level well

above the ground level. This terminal level is almost empty at moderate temperatures and any atoms put into it fall quickly to the ground state. Thus, if even a few atoms are raised to the upper state, it is possible to stimulate the emission without competitive absorption by atoms in the terminal level. Unfortunately, it is hard to excite even a few atoms to the upper state as europium has no broad absorption band in most crystals. One way around this difficulty is to dissolve europium in a liquid which has a strong absorption band. However, with the liquid lasers incorporating rare-earth ions, one has to face a difficult problem. Liquids usually offer an excited ion a great variety of ways to relax back to its ground level via fast non-radiative processes such as transmitting their vibrational energy to surrounding atoms in the liquid. To avoid this, some complicated organic liquids called *chelate* are used, in which the rare-earth ion becomes locked in the centre of a complex organic molecule; the surrounding ‘cage’ encloses it into a small pseudo-crystalline shield. The chelate has strong, broad absorption band and absorbs energy supplied by the pumping radiation at 3900 \AA and quickly transfers it through the processes shown in the diagram to the trapped europium ions lifting them to level 3 which is the upper level. The transition from level 3 to the level 2 is the laser transition.

The first successful liquid laser using europium was reported by Lempicki *et al.* [240] who used EuB_4P , an europium chelate prepared with benzoylacetonate and dissolved in alcohol to give an europium concentration $\sim 1.2 \times 10^{19}$ centres/cm³. The achievement was particularly surprising because one would expect in liquids, a spectral emission line to be broadened too much, due to thermal agitation, to sustain laser action. However, the immediate neighbourhood of the active ion being shielded from the effects of the motion of the surrounding solute molecules, the ions are not sensitive to such buffeting.

The energy level diagram is given in Fig. 10.2.

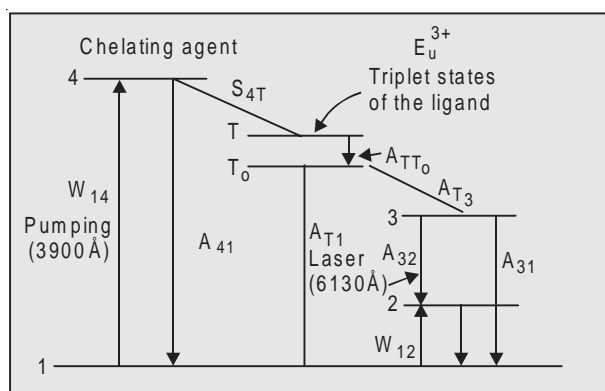


Fig. 10.2 Energy level diagram for chelate and E_u^{3+}

Confocal mirror arrangement was used to form an optical resonator and pumping energy was supplied by a conventional spiral flash tube surrounding

the resonator. Since very little pumping excitation penetrates any great depth into the liquid, in order to achieve high pumping rate, a tube of a very small diameter ~1 mm was used. With such a resonator, the threshold input power required was about 500 joules, which is almost half of the threshold energy for a standard ruby laser placed in the same flash tube and with similar mirror arrangement. At high input energies the output was ~30 millijoules per c.c.

Laser action has also been observed in a number of other chelates. There are some difficulties, however, which severely limit the performance of such lasers. The absorption coefficient of chelates being very high, gives rise to pumping problems and their viscosity is so high that circulating motion is not feasible.

The loss of atomic excitation to the solvent can also be considerably reduced if a liquid solvent consisting entirely of heavier atoms, eliminating the usual hydrogen content, is used. The best solution to date is the liquid selenium oxychloride (SeOCl_2), which has some good characteristics such as a low refractive index, good optical transmission and a density comparable to glass. The solution, however, is highly toxic.

10.2 DYE LASERS

The other important and useful type of liquid laser is the *organic dye laser* which has played a very prominent role in atoms and molecular spectroscopy and has led to a rapid growth in the nonlinear spectroscopy. In this laser an organic dye dissolved in a suitable liquid such as ethyl alcohol, methyl alcohol, toluene, benzene, acetone, water, etc., is used as the active medium. These lasers were first discovered by Sorokin and his colleagues [361, 362]. Laser generation has been observed in several hundred dyes. The dyes that are most effective are classified into eight groups: xanthenes, polymethines, oxaines, coumarins, anthracenes, acridines, azines and phthaloziamins. The lasing range covered by various dyes runs from 0.3 to 1.3 μm . By optical harmonic and laser difference frequency generation the accessible spectral region can be extended into the far infrared and vacuum ultraviolet. The most widely used dye is rhodamine 6 G (Xanthene dye) which emits in yellow-red region. For emission in the blue-green region coumarin dyes are used.

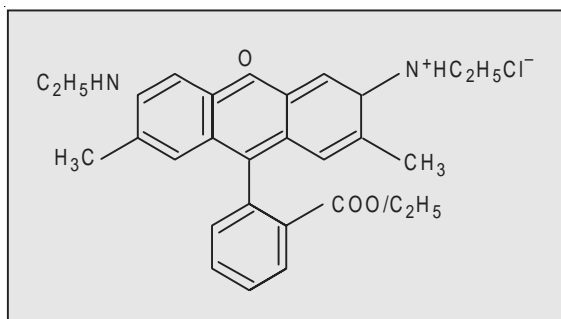


Fig. 10.3 Rhodamine 6 G

The dyes have a very complicated structure. The structure of rhodamine 6 G is given in Fig. 10.3 and absorption and luminescence spectra are shown in Fig. 10.4. The line width of the luminescence line is of the order of $0.1\text{ }\mu\text{m}$, while the width of the laser generated line is of the order of $10^{-4}\text{ }\mu\text{m}$ or less. It is, therefore, possible to tune continuously the wavelength of the laser line over a range of $0.1\text{ }\mu\text{m}$ by following the technique described below:

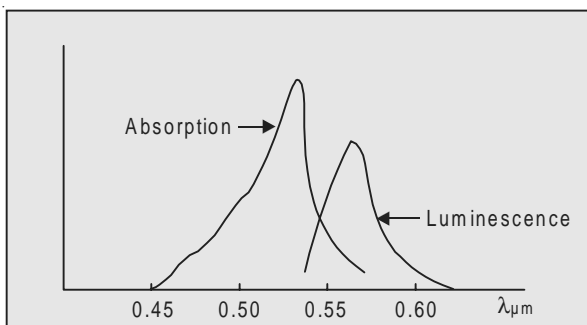


Fig. 10.4 Absorption and luminescence spectra of rhodamine 6 G

A typical energy level diagram for a dye in solution is given in Fig. 10.5. The molecules have singlet as well as triplet electronic states. Each electronic state comprises of several vibrational states and each of these, in turn, contains several rotational levels. The separation of the vibrational levels is about $1400\text{--}1700\text{ cm}^{-1}$; whereas that of the rotational levels is of the order of 150 cm^{-1} . The broadening mechanism in liquids being very effective, rotational

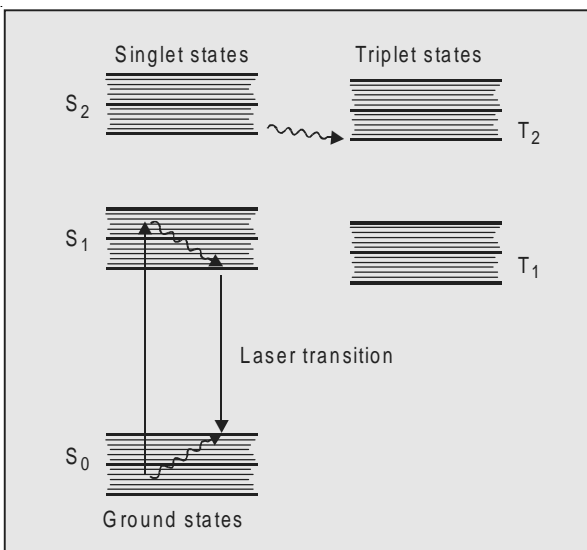


Fig. 10.5 Energy level diagram for a dye molecule

levels which are very close are not resolved and give rise to a continuum of levels between the vibrational levels. In the singlet states the spin of the active electron and that of the remainder of the molecule are anti-parallel; while in the

triplet state the spins are parallel. The selection rules allow transitions between the states of same multiplicity, *i.e.*, $\Delta S = 0$. The singlet \rightarrow triplet transition in which a spin flip is involved are forbidden.

The optical pumping raises the molecules from the lowest vibronic level of the ground state S_0 to one of the upper vibronic levels of the excited state S_1 , as this transition is allowed by the selection rule $\Delta S = 0$. A rapid relaxation, by a non-radiative process with a decay time of about $\tau_{nr} \sim 10^{-12}$ sec, to the lower vibronic level of S_1 state then follows. The laser action occurs between this level and one of the upper vibronic levels of S_0 , from which it returns to the lowest level by another non-radiative decay. The presence of the triplet levels, however, poses a problem which severely limits the laser action. It is true that the ground state molecules are not excited to the triplet levels by absorption of pump light, since singlet-triplet transitions are forbidden. However, when a molecule is in the state S_1 , it can decay to the triplet state T_1 . This is known as *intersystem crossing* and is caused by collisions. If the lifetime τ_{T_1} of the state T_1 is long compared to the time for intersystem crossing, the molecules will accumulate in the state T_1 . Further, since the transition $T_1 \rightarrow T_2$ is allowed, and the wavelength corresponding to this absorption is almost equal to that corresponding to the fluorescence transition $S_1 - S_0$, the intersystem crossing will reduce the number of molecules available in the upper state for laser action, thus reducing the gain. It has been found, however, that oxygen, when added to the solution, acts as a triplet state quenching additive. The lifetime τ_{T_1} is about 10^{-7} sec in an oxygen-saturated solution and about 10^{-3} sec or more in a solution that has been deoxygenated [362]. The lifetime τ_{T_1} therefore, can be reduced by adding oxygen to the solution. The radiative lifetime corresponding to the transition $S_1 \rightarrow S_0$ is much shorter (\sim a few nanoseconds), while τ_{s_1} is much longer ~ 100 nsec; most of the molecules decay from level S_1 by fluorescence, thus contributing to the laser action at the fluorescence wavelength. The solution is transparent to this wavelength since the emission frequency is lower than the absorption frequency. Since the levels that are actually being pumped are different from those involved in the stimulated emission process, the dye system is essentially a four-level system.

The dipole moment is given by $\mu = ex$ where x is the distance through which electrons in the molecules move, and it is usually an appreciable fraction of the molecular dimension ' a '. Since ' a ' for dye molecule is large, μ and, hence, the dipole matrix element for the S_0-S_1 transition is large. The absorption cross-section for this transition, therefore, is very large. This means, a small amount of the compound dissolved in the solvent is sufficient to give a strong absorption. The dye lasers have a very high gain, comparable to that of solid state lasers. This may seem to be surprising because the density of dye molecules in solution is generally three orders of magnitude less than that in the solid

state. It should be noted, however, that their emission cross-section is three orders of magnitude greater.

The dyes have fast relaxation time and, hence, they require very intense and rapid pumping to maintain population inversion. With the pumping radiation of very high intensity, over 100 kW cm^{-2} , a population inversion between S_1 and S_0 may be attained. Light amplification by stimulated emission is then possible over the entire luminescence band except the part overlapped by the absorption band (Fig. 10.4). Dye lasers yield high peak powers in pulses. Pulsed laser action can be obtained by pumping the laser by very fast flash lamps or by short pulses from other pulsed lasers, such as N_2 laser, which is very frequently used for this purpose, since its ultraviolet output is suitable for pumping many dyes that oscillate in the visible region. Fundamental frequencies or the second harmonic $\lambda = 0.53 \mu\text{m}$ or the third harmonic $\lambda = 0.35 \mu\text{m}$ of Nd:YAG laser are also frequently used. Some dye lasers are continuously pumped with an argonion laser. The problem of triplet is usually surmounted by flowing the dye solution through the laser cavity. If the rate of flow is sufficiently high, molecules are physically removed from the cavity before they are lost to the triplet level. Output powers of the order of 10^3 W/cm^2 can be obtained from these lasers.

For the tuning of laser radiation wavelength, it is necessary to employ a spectral selective element such as a grating or a dispersive prism. A schematic diagram of a pumped dye laser system is given in Fig. 10.6. The dye is pumped using a flashlamp or a laser. The large amount of thermal energy transferred to the dye solution causes a variation in the refractive index throughout the cell resulting into considerable losses in the cavity. In order to overcome these effects, the solution is rapidly circulated through the dye cuvette. One mirror of the usual laser cavity is replaced by a diffraction grating. In order that the radiation be reflected back along the cavity axis, the angle θ that the normal to the grating makes with the cavity axis must satisfy the condition

$$2d \sin \theta = n\lambda \quad n = 1, 2, \dots \quad \dots(10.1)$$

where d is the grating spacing and λ the radiation wavelength. Only for this wavelength, the radiation reflected back will be propagated along the axis of the cavity. Wavelength tuning is accomplished by rotating the grating which changes the angle θ and, hence, the output radiation wavelength.

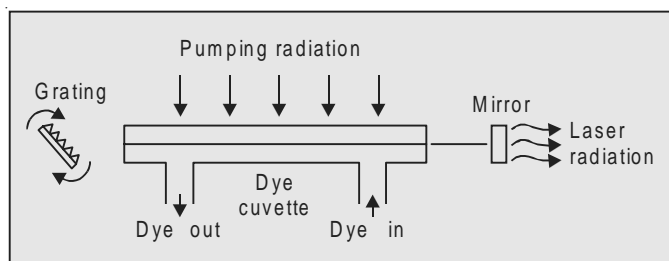


Fig. 10.6 Dye laser (with grating)

Tuning can also be accomplished using a prism in place of a grating. One such arrangement is shown in Fig. 10.7. In this arrangement the cuvette is tilted in such a way that the perpendicular to its wall makes Brewster angle φ with the direction of the dye radiation. The radiation generated, therefore, is linearly polarized. The prism plays the role of the selective element. The wavelength generated depends upon the orientation of the mirror M_1 to the prism.

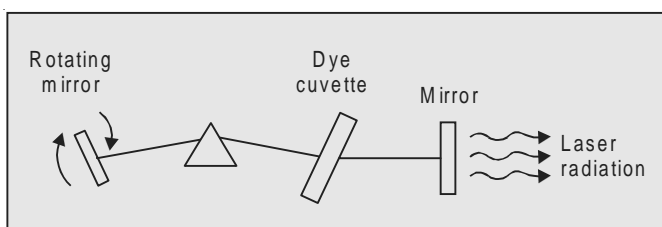


Fig. 10.7 Dye laser (with prism)

In order to achieve a narrow bandwidth, various modifications have since been suggested. See, for example, Hansch [162], Kogelnik [221].

The dye lasers can also be pumped longitudinally. A typical arrangement of longitudinal pumping is shown in Fig. 10.8. At one end of the cavity containing the dye cell there is a totally reflecting prism; while at the other end there is a mirror opaque to the pumping radiation which enters the cavity through the prism. The output radiation leaves the cavity through the mirror.

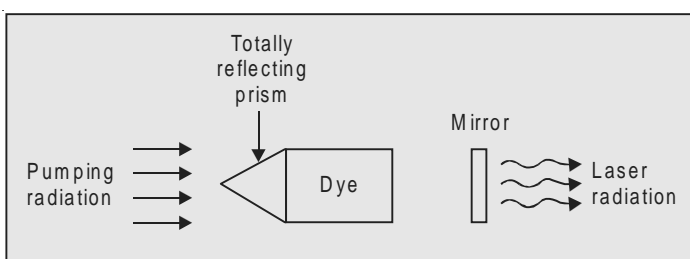


Fig. 10.8 Dye laser (with prism)

A noteworthy feature of dye lasers is that they operate between two fully allowed transitions with no intervening metastable state. This was thought to be impossible to realize until the accidental discovery of dye lasers.

The details concerning dye lasers are found in the monograph 'Dye lasers' edited by Schafer [330].

10.3 CHEMICAL LASERS

The excitation of atoms in the laser systems described so far was accomplished by optical pumping or by an electric discharge. The idea that intrigued a number of investigators for some years was whether the energy released in chemical reactions could be used for pumping. We know that the chemical

reactions occurring in flames or in explosions, produce a large number of excited atoms and a large amount of light. Chemical energy is, generally, the least expensive form of energy and is available in amounts per unit volume or per unit weight larger than that of the purely electrical energy that can be stored in comparable volumes and weights. The release of chemical energy is associated with the making and breaking of chemical bonds. In principle, the chemical reaction, once initiated, could proceed without any external source of power. In other words, a chemical laser could be self-pumping. It could also be highly efficient. There is, therefore, much interest in exploring ways by which inverted population might be created during a chemical reaction.

The chemical reactions that are most promising for laser action are those which are exothermic and are of the type



This shows that the chemical reaction yields products that are born excited in an energy level system, which is suitable for laser action. The energy level system, thus, intrinsically supplies its own pumping. The other advantage, which is much more important, is that a chemical reaction can achieve a very high population inversion in an energy level system. The distribution of energy in an energy level system which follows a chemical reaction might result exclusively in excited states leaving lower states completely depopulated. Hence, a chemical reaction could be extremely efficient.

10.3.1 HCl Laser

A number of systems of this type have been made to operate. One of the members of this class of lasers is the hydrogen chloride laser. When atomic hydrogen and chlorine combine, a substantial amount of energy is released and hydrogen chloride is formed in the excited state



In low pressure flames the vibrational anomaly could well show up. Anlauf *et al.* [12], in their work to develop the HCl laser have shown that the reaction of atomic hydrogen with chlorine at low pressure ~ 0.02 Torr, leads to high population in the upper vibrational levels, especially $v = 3$ and produces a population inversion. This gives laser emission on an HCl transition at $\lambda = 3.77 \mu\text{m}$. Thus, a general feature of the halogen-hydrogen reaction seems to be that a large part of the energy released by the chemical reaction is left as vibrational energy in the newly formed halogen-hydride molecules and in the low-pressure condition leads to laser action. This is, no doubt, a true chemical reaction; but, unfortunately, cannot yet be operated with purely chemical energy input. The only way to create the necessary free H atoms for this reaction is to dissociate the molecules in an H_2-Cl_2 mixture with a flash from a flash lamp (photodissociation) or dissociation by electron impingement. The latter technique

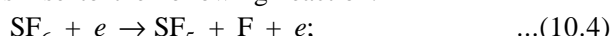
is more frequently used as it starts the reaction in a very short time of the order of 10^{-8} to 10^{-7} s. The electrical input in this case considerably exceeds the laser output.

High vibrational excitation leading to population inversion in certain rotational levels of the vibrational states $v = 1$ and $v = 2$, was also obtained by Kasper and Pementel [209] in the flash initiated reaction between hydrogen and chlorine at pressures between 3 and 10 Torr.

Anlauf *et al.* [12] have also shown that low pressure reaction of atomic hydrogen with bromine leads to high vibrational excitation of HBr.

10.3.2 HF Laser

One of the important members of this class is the hydrogen-fluoride chemical laser. In a mixture of H_2 and F_2 , the reaction is initiated by producing F atoms either by the conventional method of dissociation by electrical means, *e.g.*, by introducing sulphur hexafluoride in the discharge tube along with the mixture of H_2 and F_2 , which gives rise to the following reaction:



or by flash photodissociation of species such as ClF_3 ; or by chemical reaction, *e.g.*,



The first reaction that produces hydrogen-fluoride in the excited state is



This reaction is exothermic by 31.56 kcal/mole. It is followed by the reaction which restores the fluorine atom, *e.g.*,



with heat of reaction 98 kcal/mole.

The vibrational levels which are excited in the two cases are shown in Figs. 10.9 and 10.10. The relative populations are shown against each level. In the first reaction (cold reaction) twice as much HF is produced in the $v = 1$ level as in the $v = 0$ level and five times as much in the $v = 2$ level as in $v = 1$ level. Laser action is obtained on the $2 \rightarrow 1$ and $1 \rightarrow 0$ vibrational bands at 2.5 to 3 μm .

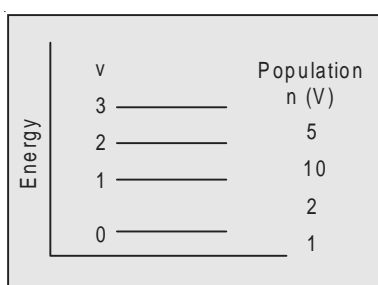


Fig. 10.9 Vibrational levels of excited molecules (cold reaction)

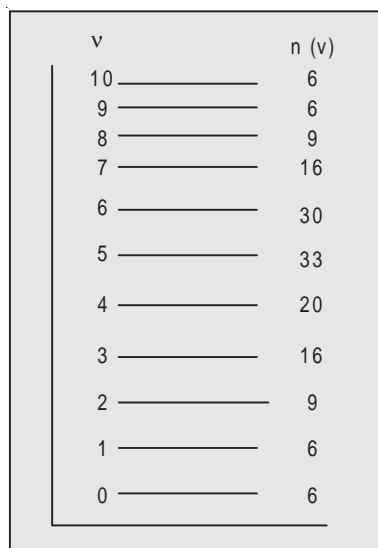


Fig. 10.10 Vibrational levels of excited molecules (hot reaction)

Jonathan *et al.* [205] have shown that reaction (hot) of atomic hydrogen with F_2 , leads to the formation of HF particularly in the vibrational states $v = 5$ and $v = 6$, the former showing the greatest population inversion. It must be noted that when oscillations occur on a number of transitions, then the oscillations on one transition will help oscillations on the other. Thus, when oscillations occur in $2 \rightarrow 1$ transition, the population of level 1 increases, while level 2 is depopulated and, hence, any oscillation on $3 \rightarrow 2$ and $1 \rightarrow 0$ transitions become prominent.

Laser type emission has also been observed by Deutsch [99], who used pulsed electric discharge to start reaction in flowing gas mixture $CF_4 + H_2$ and obtained stimulated emission lines of $1 \rightarrow 0$, $2 \rightarrow 1$ and $3 \rightarrow 2$ bands.

10.3.3 DF-CO₂ Laser

In the lasers we discussed above, the emitting molecule was a direct result of a chemical reaction. The population inversion, therefore, is direct. In this case, the rate at which the upper level is populated is proportional to the rate of chemical reaction. In some lasers population inversion is created by indirect processes. In such systems, the excited diatomic molecules produced by the chemical reaction resonantly transfer their excitation energy to the unexcited polyatomic molecules, which then radiate in the cavity resonator.

One such important system is the DF-CO₂ system. In this case, F atoms are produced by the chemical reaction (10.5). The DF* molecules in the excited state are produced by the reactions.



These excited DF molecules then transfer their energy to CO_2 .



The molecule that actually lases is CO_2 . The population inversion of these molecules, however, is not produced directly by chemical reaction and for this reason, this laser is known as a *hybrid laser*. The working of such a laser is illustrated in Fig: 10.11. A mixture of fluorine and helium is first introduced into the chamber. You may recall the role helium plays in a CO_2 laser. Carbon dioxide and nitric oxide are then injected into the flow. Atomic fluorine produced by the reaction (10.5) then reacts with deuterium injected into the chamber. The excited DF molecules produced by the reactions (10.8) and (10.9) transfer their excitation energy to CO_2 molecules which are then carried to the resonator where they radiate.

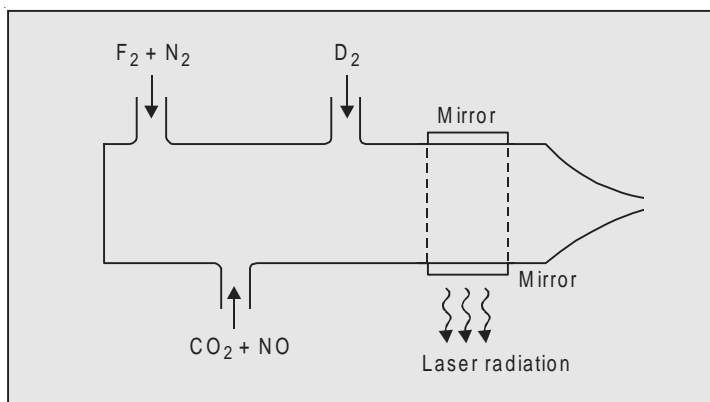


Fig. 10.11 DF- CO_2 laser

The lasers described above can operate both continuously or in a pulsed fashion.

One must be careful in handling these lasers as F_2 is the most corrosive and reactive element known.

10.3.4 CO Chemical Laser

Recently, some interest has been shown in developing chemical lasers using chemiluminescent reactions in the non-equilibrium reaction zones of flames. The $O + CS_2$ flame gives strong infrared chemiluminescence [Hancock *et al.* 159, Pollack 314], in which CO is strongly excited to $v'' = 14$, giving emission around 1.8 and 2.6 μm , which may have laser application.

10.3.5 Brommi Laser

A laser in which the pumping reaction is of the form



in which C^* is an electronically excited atom, was first reported by Spencer and Witting [364]. Laser oscillations were achieved on the atomic bromine transitions $4^2P_{1/2} \rightarrow 4^2P_{3/2}$ at 3685 cm^{-1} . The laser action was obtained via the reactions



The possibility of such electronic transition lasers was first suggested by Houston [193].

11

DYNAMICS OF THE LASER PROCESSES AND ADVANCES IN LASER PHYSICS

We have given in the preceding chapters an account of the essential features of various types of lasers and also outlined a simple theoretical basis for the laser action. We propose to describe in this chapter some of the advances made in laser physics in order to improve their performance.

11.1 PRODUCTION OF A GIANT PULSE— Q-SWITCHING

We recall that in Chapter 7 we had pointed out that the output of a typical pulsed solid state laser consists of 1 msec long burst of spikes, each lasting for ~ 550 nsec with the average spacing between spikes \sim a few microseconds. We had also offered an explanation for their occurrence. If a method is found of preventing these pulses *i.e.*, preventing the laser from oscillating until the exciting flash is over, a population inversion, greatly exceeding the usual threshold value, can be established. If the laser action is allowed to commence when this condition is reached, all the available energy will be concentrated into one giant pulse of extremely short duration. A judiciously arranged time-dependent loss in the cavity can be used to produce such intense pulses of laser light. If the Q of the resonator is reduced until a substantial inversion is achieved, it is possible to release a much larger amount of energy. The technique was first proposed by Hellwarth [180]. Since the technique involves switching the cavity Q factor from a low to a high value, it is known as *Q-Switching*. The method consists of closing the optical cavity by any of a number of means, until the population inversion is built up far above the threshold, and then suddenly opening it to permit a large fraction of stored energy to be dumped in a single short pulse.

The switching systems widely used are:

11.1.1 Mechanical Shutter

In this case one of the end mirrors of the laser resonator, the total reflector, is kept rotating rapidly about an axis perpendicular to the axis of the resonator (Fig. 11.1), so that it is only instantaneously aligned parallel to the output reflector. If the mirror is driven with a synchronous motor, the flash lamp can be timed to fire, so that the mirror is aligned only when population inversion is maximum. To avoid multiple pulsing, it is necessary to use a high speed of rotation. The speed required for a resonator of length 50 cm is of the order of 30,000 revolutions per minute. The time in which the Q of the resonant cavity switches from its maximum value to minimum is ~ 100 ns.

A totally reflecting prism which spins rapidly about its axis at right angles to the resonator axis is found to be more effective than the rotating mirror.

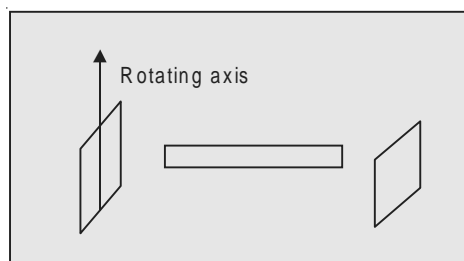


Fig. 11.1 Mechanical shutter

11.1.2 Electro-optical Shutters

These shutters exploit an electro-optical effect such as *Kerr effect* or *Pockels effect*.

(a) Kerr Effect

Consider an isotropic liquid comprising asymmetric molecules placed in an electric field. Its molecules tend to align themselves parallel to the direction of the field. Because the molecules are not symmetrical, the alignment causes the liquid to become an isotropic and birefringent. That is, a light wave which enters the liquid, splits into two waves travelling at different velocities, which results into the material offering different refractive indices for differently polarized light. This electric field induced birefringence in isotropic liquids is called the Kerr effect. If a constant electric field is applied, the liquid behaves as a birefringent crystal with indices n_0 and n_e . The optic axis is parallel to the direction of the field. The birefringence is proportional to the square of the applied voltage. In other words, the change in refractive index is proportional to the square of the electric intensity of the external field. A cell containing one

such liquid between two flat, parallel plates, spaced by several millimetres is called a *Kerr cell*. Such a cell can be used in conjunction with a polarizer as an *electro-optic shutter*. The arrangement is shown in Fig. 11.2. The Kerr cell is biased and oriented in such a way that it converts the linearly polarized light passed by the polarizer into circularly polarized light. After reflection at the

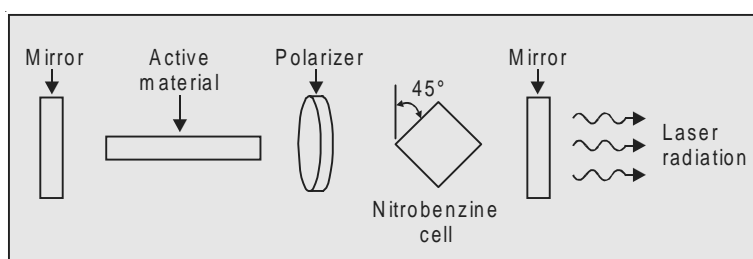


Fig. 11.2 Electro-optic shutter (Kerr cell)

mirror it passes again through the Kerr cell which reconverts it into linearly polarized light but with its polarization orthogonal to its original direction and is, therefore, blocked by the polarizer. The switch in this condition is closed; the gain is low and the overall regeneration is insufficient for oscillations. To produce a single giant pulse the operational sequence of events is as follows: The Kerr cell is activated by applying the electric field, flash lamp fired, and after about 0.5 msec, the Kerr cell is turned off as suddenly as possible. The Kerr cell birefringence is thereby removed, the shutter is opened and the light is transmitted without change of polarization.

The output of a ruby laser 3 cm in length and 0.9 cm in diameter with a shutter of this kind was found to have increased from 6 kW to 600 kW. It must be emphasized that this is not the increase in total energy of the pulse but an increase in the peak intensity. Within two years from the first experiment, giant pulses with output powers of 100 MW were obtained.

A Kerr cell usually requires a high bias voltage of 10–20 kV. If this voltage is applied as a fast pulse, the cell acts as a fast shutter. Shutter speeds in the 10 nsec range can be obtained in this fashion.

(b) Pockels Effect

When an electric field is applied to certain crystals such as potassium dihydrogen phosphate ($\text{KDP} \rightarrow \text{KH}_2\text{PO}_4$), it behaves like a birefringent crystal. This electro-optic effect is known as *Pockels effect*. It differs from the Kerr effect, described above, in that the Pockels effect is linear in applied electric field, whereas the Kerr effect is quadratic in applied electric field. A Pockels cell, usually requires a small voltage *e.g.*, 1–5 kV and it is for this reason these cells have nearly replaced Kerr cells in shutters.

The arrangement for *Q-Switching* with a Pockels cell is shown in Fig. 11.3. In this arrangement there are two polarizers P_1 , P_2 between the active material and output mirror. The polarizers are oriented in the same sense, transmitting light polarized in the same plane. The Pockels cell consisting of a crystal (KDP) and confined in an electric capacitor, is placed between the polarizers.

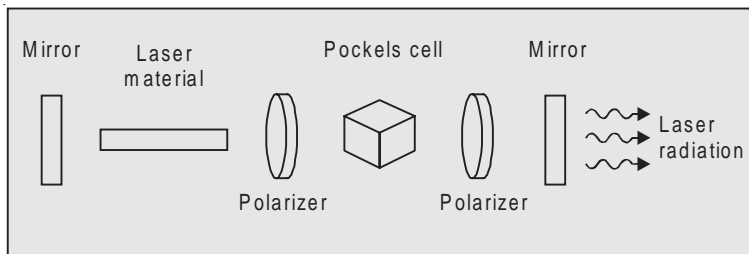


Fig. 11.3 Electro-optic shutter (Pockels cell)

The light from the active material passes through the polarizer P_1 and becomes polarized in a plane. We may consider this polarized radiation as made up of two component waves, one polarized in the x -direction and the other in the y -direction. The polarizer P_1 and the cell are so oriented that x -axis makes an angle of 45° with the plane of polarization.

When the field is switched on, the two waves travel within the cell with different speeds $\frac{c}{\eta_1}$ and $\frac{c}{\eta_2}$ respectively, where

$$\eta_1 = \eta_0 + j\eta_0^3 E/2$$

$$\eta_2 = \eta_0 - j\eta_0^3 E/2 \quad \dots(11.1)$$

E being the field applied, η_0 the refractive index in the absence of the field, and j is an electro-optic constant.

If the length of the cell is l , the two waves emerge out of the cell with a phase difference $\Delta\phi$ given by

$$\begin{aligned} \Delta\phi &= \frac{2\pi l}{\lambda_0}(\eta_1 - \eta_2) \\ &= \frac{2\pi j \eta_0^3 E l}{\lambda_0} = \frac{2\pi j \eta_0^3 V}{\lambda_0} \end{aligned} \quad \dots(11.2)$$

where λ_0 is the wavelength of light in vacuum and $V = E l$ is the voltage applied to the cell. The light which was plane polarized before entering the cell, is now elliptically polarized. If we now adjust the voltage V so as to make $\Delta\phi = \pi$, the cell functions as a half-wave plate. The emerging beam is again plane polarized, but the plane of polarization now, is orthogonal to the initial plane of polarization.

and hence, the beam will not pass through the polarizer P_2 . Thus, when the field is off ($\eta_1 = \eta_2, \Delta\phi = 0$) the beam passes through the polarizers and the cell almost without any losses *i.e.*, the Q is maximum, and when the field is on, it is minimum. The system, therefore, can be used as a shutter. The switching time in this case is about a nanosecond which is much smaller than that for mechanical shutters.

11.1.3 Shutters Using Saturable Dyes

This kind of a shutter is known as a *passive shutter*. It consists of a cell containing some suitable dye solution. A dye chosen for this purpose is such that, considering it to be a two-level system, its energy difference must correspond to that of the laser transition. For example, in the case of ruby laser, vanadium phthalocyanine in nitrobenzene is used; while polymetine dye solutions are employed in the case of neodymium lasers. The concentration is adjusted in such a way that oscillations can just take place with the dye cell in the cavity. The laser pumps the dye molecules into the upper level, and the population in the upper level builds up until it is saturated. The cell is completely bleached and absorption ceases. The cell now being in the highest Q condition, a giant pulse develops, after which the molecules in the upper level of the dye gradually decay to the lower level and the cell returns to its original unbleached state. This Q -switching technique can also help to force the laser to oscillate in a single axial mode.

11.1.4 Peak Power Emitted During the Pulse

The rough estimate of the total energy emitted during the pulse of a Q -switched laser and its peak power can be obtained as follows:

If N_1, N_2 are the populations of the two levels, the total number N_0 per unit volume being given by

$$N_0 = N_1 + N_2 \quad \dots(11.3)$$

then

$$n_2 = \frac{N_2}{N_0} \text{ and } n_1 = \frac{N_1}{N_0} \quad \dots(11.4)$$

are called the normalized populations of the levels, *i.e.*,

$$n_1 + n_2 = 1 \quad \dots(11.5)$$

The single-pass gain of the rod is given by

$$G = \exp[\sigma_0(n_2 - n_1)L] \quad \dots(11.6)$$

where σ_0 is the absorption cross-section. The quantity $n_2 - n_1$ is the normalized population inversion.

Suppose, the normalized population inversion before the shutter is switched on, is n_i and at the end of the pulse it is n_f . Then the total energy emitted during the pulse is

$$E = \frac{1}{2}(n_i - n_f)N_0V\hbar\omega \quad \dots(11.7)$$

where V is the volume of the active material. The factor $\frac{1}{2}$ appears because the population difference changes by two units every time a quantum is emitted.

The duration of the Q -switched pulse can be estimated from the decay of the pulse in an isolated cavity. If L is the length of the cavity the time taken by the pulse to make a round trip is

$$t_1 = \frac{2L}{c} \quad \dots(11.8)$$

Further, if r is the reflection coefficient of the output mirror, each time the pulse strikes the mirror it loses $(1 - r)$ of its energy. The fraction of the energy lost in unit time, therefore, is $(1 - r)/t_1$. Hence, the cavity life time t_c is given by

$$t_c = \frac{t_1}{1 - r} \quad (\text{see Chapter 6}). \quad \dots(11.9)$$

We can assume this to be the decay time of the Q -switched pulse in which case the symmetrical pulse will have a full width of about $2t_c$.

Assuming a nearly triangular shape for the pulse an estimate of the peak power can be made using the relation

$$P_m = \frac{E}{2t_c}. \quad \dots(11.10)$$

11.2 GIANT PULSE DYNAMICS

We will now consider the evolution of a giant pulse in time and deduce an expression for the peak power generated by the laser. The treatment below is mostly on the basis of the one given by Lengyl [243].

Let

N_0 be the number of active ions per unit volume,

k_{ω_0} be the absorption coefficient of the unexcited laser material, measured at the central frequency,

l be the length of the laser rod,

V be the volume of the laser material,

Φ be the photon density in the laser material and

$N = (g_1/g_2) N_2 - N_1$ be the population inversion per unit volume.

The intensity of a photon packet travelling through a distance x along the x -axis is given by

$$I = I_0 e^{\alpha x} \quad \dots(11.11)$$

where α is the coefficient of amplification given by

$$\begin{aligned}\alpha = -k_{\omega} &= \frac{\eta c^2 \pi^2 g_2 A_{21}}{g_1 \omega_0^2} \left(\frac{g_1}{g_2} N_2 - N_1 \right) g(\omega) \\ &= \frac{\eta c^2 \pi^2 g_2 A_{21}}{g_1 \omega_0^2} N g(\omega) = \alpha_0 \frac{N}{N_0} = \alpha_0 n \quad \dots(11.12) \\ (\alpha_0 &= -k_{\omega_0} \text{ Sec. (5.49)})\end{aligned}$$

We have used here the normalized population inversion

$$n = \frac{N}{N_0}. \quad \dots(11.13)$$

The initial number of photons in the laser material is ΦV . The increase in this number due to amplification in the laser rod of length l is

$$\Phi V \exp(\alpha l) - \Phi V \approx \Phi V \alpha l \text{ assuming } \alpha l \ll 1. \quad \dots(11.14)$$

The time taken for this amplification is

$$t_1 = \frac{l}{c}. \quad \dots(11.15)$$

The rate of loss of photons is $\frac{\Phi V}{\tau_p}$,

where τ_p is the lifetime of a photon.

Therefore, the rate of change of the photon density with time is given by

$$\begin{aligned}\frac{d\Phi}{dt} &= \left(\frac{\alpha l}{t_1} - \frac{1}{\tau_p} \right) \Phi \\ &= \left(\frac{\alpha_0 n l}{\tau_p \gamma} - \frac{1}{\tau_p} \right) \Phi \quad \dots(11.16)\end{aligned}$$

where we have used (11.12) and (6.56).

For convenience we use the normalized variable

$$\varphi = \frac{\Phi}{N_0} \quad \text{instead of } \Phi.$$

Equation (11.16) now changes to

$$\frac{d\varphi}{dt} = \left(\frac{\alpha_0 n l}{\gamma} - 1 \right) \frac{\varphi}{\tau_p}. \quad \dots(11.17)$$

The threshold condition (6.48) gives

$$\alpha l = \alpha_0 n_p l = \gamma \quad \dots(11.18)$$

where n_p is the inversion at the peak photon density.

Now if one photon is emitted, N_2 changes to $N_2 - 1$ and N_1 to $N_1 + 1$. The resulting change in N is

$$\frac{g_1}{g_2}(N_2 - 1) - (N_1 + 1) - \frac{g_1}{g_2}N_2 + N_1 = - \left(1 + \frac{g_1}{g_2}\right) \quad \dots(11.19)$$

Therefore, the rate of change of the population inversion n is this change in N multiplied by the number of photons emitted per unit time, *viz.* $\frac{\Phi\alpha l}{t_1}$

$$\begin{aligned} \text{i.e., } \frac{dn}{dt} &= \frac{1}{N_0} \frac{dN}{dt} = - \left(1 + \frac{g_1}{g_2}\right) \frac{\alpha l \Phi}{N_0 t_1} \\ &= - \left(1 + \frac{g_1}{g_2}\right) \frac{\alpha_0 n l \phi}{\tau_p \gamma}. \end{aligned} \quad \dots(11.20)$$

Equations (11.17), (11.18) and (11.19) give

$$\frac{d\phi}{dt} = \left(\frac{n}{n_p} - 1\right) \frac{\phi}{\tau_p} \quad \dots(11.21)$$

and
$$\frac{dn}{dt} = - \left(1 + \frac{g_1}{g_2}\right) \frac{n \phi}{n_p \tau_p} \quad \dots(11.22)$$

Figure (11.4) illustrates the behaviour of ϕ and n with time. At the start the inversion is high and photon density low. As time advances, photon density rises at first very slowly and then more and more rapidly because rate of photon production is proportional to the photon density present. After reaching a peak value ϕ_p , it declines to zero. Population inversion n is a monoatomic decreasing function.

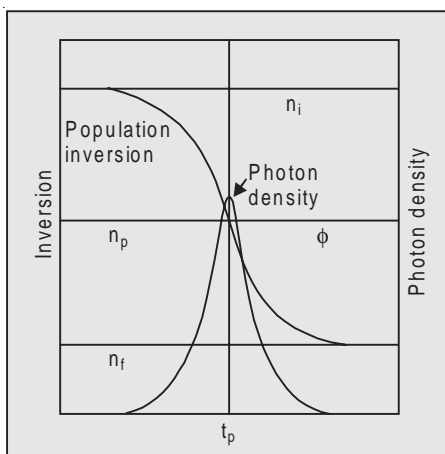


Fig. 11.4 Variation of n and ϕ with time

Equations (11.21) and (11.22) give

$$\frac{d\varphi}{dn} = \frac{g_2}{g_1 + g_2} \left(\frac{n_p}{n} - 1 \right). \quad \dots(11.23)$$

Integrating

$$\varphi = \frac{g_2}{g_1 + g_2} [n_p \ln n - n] + C. \quad \dots(11.24)$$

Using initial conditions $n = n_i$ when $\varphi = \varphi_i$

$$C = -\frac{g_2}{g_1 + g_2} [n_p \ln n_i - n_i] + \varphi_i \quad \dots(11.25)$$

$$\therefore \varphi = \varphi_i + \frac{g_2}{g_1 + g_2} \left[n_p \ln \frac{n}{n_i} - (n - n_i) \right] \quad \dots(11.26)$$

The final population inversion can be found from this relation by putting $\varphi_i = \varphi_f = 0$ and $n = n_f$, which gives

$$n_p \ln \frac{n_f}{n_i} = n_f - n_i \quad \dots(11.27)$$

The total energy generated by the laser is given by

$$E = \frac{g_2}{g_1 + g_2} (n_i - n_f) V N_0 \hbar \omega \quad \dots(11.28)$$

When the levels are non-degenerate $g_1 = g_2 = 1$ and

$$E = \frac{1}{2} (n_i - n_f) V N_0 \hbar \omega$$

as shown in (11.7).

Part of this energy is contained in the energy beam, the remaining is lost in the cavity due to scattering, absorption at the mirrors etc. Let γ_c represent the radiation loss due to coupling and γ_i the other losses. We can then write

$$\gamma = \gamma_c + \gamma_i \quad \dots(11.29)$$

The output energy of the pulse is the fraction γ_c/γ of the total generated energy, viz.,

$$E_0 = \frac{E \gamma_c}{\gamma} \quad \dots(11.30)$$

The peak power is calculated from the peak number of photons in the laser which is $\varphi_p N_0 V$. The value of φ_p can be found from (11.26) by putting $\varphi_i = 0$ and $n = n_p$. Thus

$$\varphi_p = \frac{g_2}{g_1 + g_2} \left[n_p \ln \frac{n_p}{n_i} - (n_p - n_i) \right] \quad \dots(11.31)$$

The peak power radiated is the fraction γ_c/γ of the total peak power dissipated

$$\therefore P = \frac{\varphi_p N_0 V \hbar \omega \gamma_c}{\tau_p \gamma} = \frac{\varphi_p N_0 V \hbar \omega \gamma_c}{t_1} \quad \dots(11.32)$$

11.3 LASER AMPLIFIERS

Laser beams of still higher intensity can be obtained by amplifying the output of the giant pulse laser. This is done by directing the pulse through another similar rod devoid of external reflectors. In fact to keep the amplifier from oscillating spontaneously, its ends must be treated to prevent reflection. The amplifier is pumped with its own flash lamp, so that it is ready to amplify the instant the giant pulse is delivered.

When several laser amplifiers are cascaded in series, high power and monochromacy can be achieved by the use of certain types of elements called *bleachable absorbers* discussed above. At low power levels these absorbers strongly absorb light at the characteristic wavelength of the active ions in the laser rods. As the power is increased, they tend to the state of *saturation* and at high power levels become highly transparent to the same light. For example, a cell 1 cm long containing a solution of metal phthalocyanine, transmits less

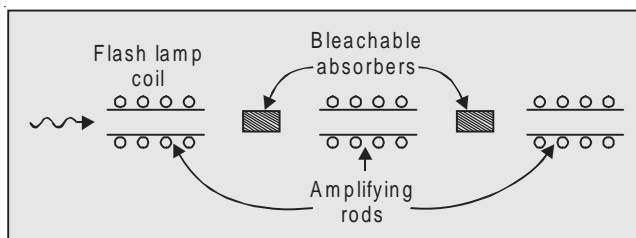


Fig. 11.5 Laser amplifier

than one per cent at $\lambda = 6943 \text{ \AA}$ at low levels; but when placed in front of a ruby laser of 20 kW peak power, transmits light almost unattenuated. The bleachable absorbers are usually used with amplifier rods in arrangement shown in Fig. 11.5. The amplifying rods used have uncoated ends or have antireflecting coatings.

When a laser light pulse is incident on the left-hand end of the chain, it is amplified by the first rod. If the intensity of the amplified beam is sufficiently high, it will pass unattenuated through the first bleachable absorber cell. It will then be further amplified by the second rod and will pass through the second bleachable absorber and so on, and finally a greatly intensified beam emerges on the right-hand side.

The other stabilizing technique for cascade amplifiers, uses what is known as *non-reciprocal isolators*. Instead of bleachable absorbers, the successive amplifiers are now separated by these isolators (Fig. 11.6).

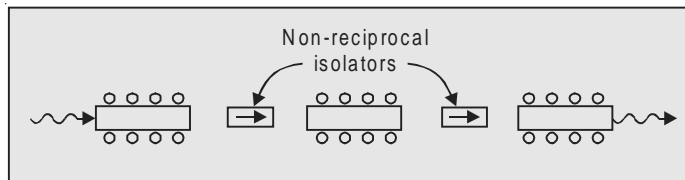


Fig. 11.6 Laser amplifier with non-reciprocal isolators

The isolators which allow light to move only in the direction of the arrow, are simply constructed using the Faraday effect (Fig. 11.7). A wave enters from the left with its plane of polarization defined by the dichroic polarizer. As the beam

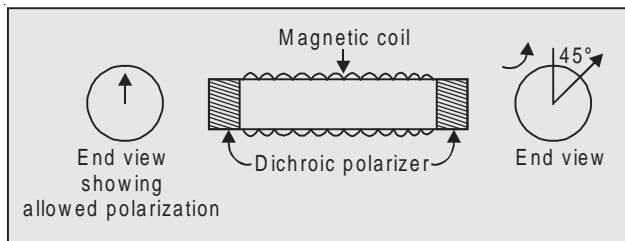


Fig. 11.7 Isolators

passes through the Faraday rotator, the plane of polarization is rotated clockwise by 45°. It then passes through the right-hand polarizer which is suitably oriented. The wave-entering from the right-hand is also rotated by 45°, but its plane of polarization is such that it is not transmitted by the left-hand-polarizer. The materials suitable for Faraday rotation are PbO glass, CaF₂ : Cu⁺⁺ crystals etc.

11.4 MODE LOCKING

A laser usually oscillates in a large number of spectral modes and, hence, the output is in the form of irregular spikes, because the modes do not oscillate at the same time and their phases have random values. It would be interesting to see what would happen if the modes are forced to oscillate together with comparable amplitudes and with their phases locked. This operation is known as *mode locking operation*.

For simplicity let us assume that the modes have the same amplitude A . The field inside the cavity is

$$E(t) = A \sum_{N=0}^{N-1} \exp(i(\omega_n t + \delta_n)) \quad \dots(11.33)$$

where N is the total number of modes, ω_n is the angular frequency of the n th mode and δ_n its relative phase. The total intensity is found by adding the intensities of the modes. Therefore, with the modes uncoupled, the intensity is

$$I = NA^2. \quad \dots(11.34)$$

Suppose now somehow we are able to couple the modes so that they have the same relative phase δ

$$\text{i.e.,} \quad \delta_n = \delta. \quad \dots(11.35)$$

The laser is then said to be a *mode-locked laser*.

We have seen in Chapter 8 that the separation between the modes is given by

$$\Delta\omega = \frac{\pi c}{L\eta} \quad \dots(11.36)$$

where L is the cavity length.

For convenience, we represent the angular frequency of the highest frequency mode by ω and the frequency of the n th mode by

$$\omega_n = \omega - n\Delta\omega \quad \dots(11.37)$$

$$\begin{aligned} \therefore E(t) &= A \sum_{N=0}^{N-1} \exp(i\{(\omega - n\Delta\omega)t + \delta\}) \\ &= A \exp(i(\omega t + \delta)) \sum_{n=0}^{N-1} \exp(-in t\Delta\omega) \\ &= A \exp(i(\omega t + \delta)) \sum_{n=0}^{N-1} \exp(-in \phi) \\ &= A \exp(i(\omega t + \delta))[1 + \exp(-i\phi) + \exp(-2i\phi + \dots)] \end{aligned} \quad \dots(11.38)$$

where we have put

$$\phi = t\Delta\omega = \frac{\pi ct}{L\eta} \quad \dots(11.39)$$

Since the terms in the bracket form a geometric series

$$E(t) = A \exp\{(i(\omega t + \delta))\} \left\{ \frac{e^{-Ni\phi} - 1}{e^{-i\phi} - 1} \right\} \quad \dots(11.40)$$

The intensity is given by the square of the amplitude

$$I = A^2 \left\{ \frac{e^{-Ni\phi} - 1}{e^{-i\phi} - 1} \right\}^2 = A^2 \frac{\sin^2(N\phi/2)}{\sin^2(\phi/2)} \quad \dots(11.41)$$

The maximum intensity, therefore, is

$$I = N^2 A^2. \quad \dots(11.42)$$

Thus, the output of a mode-locked laser is N times the power of the same laser with modes uncoupled.

From (11.41) we find that the pulse maxima occur at those times at which the denominator vanishes *i.e.*, when

$$\phi/2 = \frac{\pi c t}{2L\eta} = m\pi \quad \dots(11.43)$$

where m is an integer

$$\therefore t = \frac{2mL\eta}{c} \quad \dots(11.44)$$

Two successive pulses, therefore, are separated by a time

$$t = \frac{2L\eta}{c} \quad \dots(11.45)$$

i.e., by one round trip transit time.

The duration of an individual pulse τ is determined by the linewidth of the gain curve, which, in turn, is related to the number of locked modes m given by (6.28).

$$\text{Thus, } \tau = \frac{1}{\Delta\omega} = \frac{1}{m\Delta\omega'} \quad \dots(11.46)$$

A number of techniques have been developed for achieving mode locking. A review of these techniques can be found in the articles by Harris [168] and Smith [356]. The commonly used methods can be classified into two categories: (i) active mode locking and (ii) passive mode locking.

(i) The first experimental results on active mode locking were obtained by Hargrove *et al.* [166]. A polished quartz block is placed inside the laser cavity and driven into acoustic resonance by a piezoelectric crystal. The standing acoustic wave induces periodic refractive index variations in the quartz block which acts as a diffraction grating. The fixed phase relationship is accomplished by varying the loss of the laser cavity at a frequency equal to the resonator mode spacing *viz.*,

$\Delta\omega = \frac{\pi c}{L\eta}$. When the laser is switched on the mode at the centre at frequency, ω_0 starts oscillating. Since the loss is modulated at frequency $\Delta\omega$ the amplitude of this mode will also oscillate with frequency $\Delta\omega$. The resultant field, therefore, is given by

$$\begin{aligned} E(t) &= (A_0 + A_1 \cos \Delta\omega t) \cos \omega_0 t \\ &= A_0 \cos \omega_0 t + \frac{1}{2} A_1 \{ \cos(\omega_0 + \Delta\omega)t + \cos(\omega_0 - \Delta\omega)t \} \end{aligned} \quad \dots(11.47)$$

This shows that the modes with frequencies $\omega_0 + \Delta\omega$ and $\omega_0 - \Delta\omega$ also oscillate and have perfect phase relationship with the mode ω_0 , which leads to the mode locking.

(ii) In the passive mode locking, a bleachable dye cell described above in connection with the Q -switching, is placed in the laser cavity. When an intense pulse passes through these absorbers, the low power

wings of the pulse are attenuated because of the absorption by dye molecules. The high power pulse is transmitted because the dye is bleached. It is essential in this case, however, that the absorber recovers in a time which is short compared with the duration of the pulse. Hence, absorbers having very small relaxation time are used.

11.5 ULTRA-SHORT LIGHT PULSES

The continuously pumped mode-locked dye lasers developed, in early 1970s made possible for the first time, the production of subpico-second optical pulses in 1974. In 1981, Fork *et al.* [123] of the Bell Laboratories, reported the first production of optical pulses briefer than 100 femtoseconds with a newly developed colliding-pulse ring dye laser. In the same year Nakalnika *et al.* [283] reported a new technique for the compression of picosecond light pulse in a single mode optical fibre. Shank and his colleagues at the Bell Laboratories have now succeeded in bringing these two developments together and compressing the 90-fsec output of their colliding pulse laser by a factor of three *i.e.*, 30 femtoseconds ($= 3 \times 10^{-14}$ sec) long or 14 cycles of 6200 Å red light [342].

Lasers such as above, until very recently, were operated using rhodamine 6G as the gain medium and DODC1 as the saturable absorber. Femtosecond generation in these lasers is restricted to 600–635 nm range. During the past few years rapid progress has been made in extending the wavelength coverage by using different combinations of gain medium and saturable absorber. French and Taylor [129, 130] have demonstrated almost continuous Operation of c.w. Argon laser pumped system across the spectral range 490–780 nm yielding pulses as short as 80 femtoseconds. Dawson *et al.* [90, 91, 92] have demonstrated the operation across the spectral range 560 to 975 nm, under frequency doubled c.w. mode locked Nd : YAG laser pumping. The pulses in this case are reported to be about 85 femtoseconds.

Femtosecond light pulse generation now makes possible “snapshots” of atomic collisions, molecular reactions and fast surface phenomena.

11.6 MODE PULLING

We have shown in Chapter 8 that a number of axial modes, separated by $\Delta\omega = \frac{\pi c}{L}$, resonate within the Doppler broadened line width of a given atomic transition. This was experimentally verified by Herriott [184]. The experiment was repeated by Bennett [36] using a laser specially constructed for the purpose. Bennett's laser had properties similar to those of the laser used by Javan *et al.*, [202], except that the device oscillated only on the strongest of the five transitions, *viz.*, $2s_2 - 2p_4$ transition at 11522.76 Å.

Bennett's experiment revealed some interesting anomalies. He found that the beat frequency is not equal to $\frac{\pi c}{L}$ but is less than $\frac{\pi c}{L}$ by about 1 part in 800. For example, for one of the interferometer lengths, the calculated beat frequency was $161,316 \pm 0.022$ Mc/sec; whereas the measured beat frequency was $161,107 \pm 0.010$ Mc/sec, the fractional difference between these being $(1.3 \pm 0.2) \times 10^{-3}$.

Still more interesting are the two observations Bennett made on increasing the power level: (1) He observed that the frequency of the $c/2L$ beat increases with increasing power. This increase was anomalous. One would expect the pulling towards the line centre to increase with the number of excited atoms and that the pulling would be less for a cavity resonance near the line centre than for one further away from it. Hence, the frequency separation between adjacent cavity resonances should decrease with increasing power. (2) At low powers a single beat was observed at just less than $\frac{\pi c}{L}$; as the laser power was increased, the $\frac{\pi c}{L}$ beat split by ~ 20 kHz and the $\frac{2\pi c}{L}$ beat appeared; when the power was further increased, the $\frac{\pi c}{L}$ beat became triple and the $\frac{2\pi c}{L}$ beat double, and so on.

The 'pulling' of the frequencies towards the centre of the gain curve, can be explained qualitatively by the consideration of the frequency dependence of the refractive index of the amplifying medium. The nature of this dependence is shown in Fig. 11.8. In a passive resonator the separation of adjacent frequencies of the modes is given by $\Delta\omega_q = \frac{\pi c}{L}$. In an amplifying medium the formula changes to

$$\Delta\omega_q = \frac{\pi c}{L\eta} \quad \dots(11.48)$$

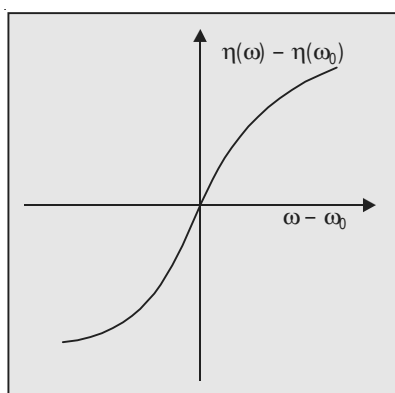


Fig. 11.8 Frequency dependence of the refractive index

where η is the refractive index. Fig. 11.8 shows that for $\omega < \omega_0$, $n(\omega) < n(\omega_0)$ and, hence $\Delta\omega_g$ increases as can be seen from (11.48). That is frequencies on the left of ω_0 move to the right. On the other hand, frequencies on the right of ω_0 shift to the left because for $\omega > \omega_0$, $n(\omega) > n(\omega_0)$. Thus, frequencies on either side of ω_0 are pulled towards the centre of the gain curve.

The other observations suggest that some non-linear frequency-dependent pulling mechanism exists which makes the spacing between adjacent resonant modes different. The following approximate theory based on the assumption that no coupling effects exist between simultaneously oscillating modes through the line-dependent non-linearities in the medium, explains the dominant mode pulling effects.

The phase shift per transit through an evacuated tube of length L is

$$\phi = \frac{\omega L}{c} \quad \dots(11.49)$$

Therefore, the dispersion for the evacuated cavity is

$$\frac{\partial\phi}{\partial\omega} = \frac{L}{c} \quad (\text{constant}) \quad \dots(11.50)$$

For a standing wave to build up, oscillation modes must correspond to a phase shift equal to an integral multiple of π .

Let E be the energy in the mode of interest and f the fractional energy loss per pass. The energy will decay with time at the rate $(c/L)fE$. (Note: $t = L/c$).

The Q of the cavity is

$$Q = \frac{\omega \times \text{Energy stored in the cavity}}{\text{Energy lost per cycle to the walls}}$$

$$\frac{\omega_{\text{osc}} E}{(c/L)f E} = \frac{\omega_{\text{osc}}}{(c/L)f}. \quad \dots(11.51)$$

The quality factor is also defined as

$$Q = -\frac{\omega_{\text{osc}}}{\Delta\omega_{\text{osc}}} \quad \dots(11.52)$$

$$\therefore \frac{\omega_{\text{osc}}}{(c/L)f} = \frac{\omega_{\text{osc}}}{\Delta\omega_{\text{osc}}}$$

$$\text{i.e.,} \quad \Delta\omega_{\text{osc}} = \frac{cf}{L} \quad \dots(11.53)$$

$$\text{Hence,} \quad \frac{\partial\phi}{\partial\omega} = \frac{L}{c} = \frac{f}{\Delta\omega_{\text{osc}}} \quad \dots(11.54)$$

The introduction of the medium changes the refractive index in the system, thereby altering single-pass phase shift from that obtained in the evacuated

case; the mode separation becomes $\frac{\pi c}{L\eta}$. Oscillations now occur at frequency $\bar{\omega}$, different from ω_{osc} , but the single-pass phase shift is still an integral multiple of π . Since the dispersion for the amplifying medium is smaller than that for the cavity, oscillations occur close to ω_{osc} and the pulling is small. If $\Delta\phi_m(\bar{\omega})$ is the total change in the single-pass phase-shift at the actual frequency of oscillation caused by the insertion of the medium, the actual frequency of oscillation $\bar{\omega}$ is given by

$$\frac{\partial\phi}{\partial\omega}(\bar{\omega} - \omega_{osc}) + \Delta\phi_m(\bar{\omega}) = 0 \quad \dots(11.55)$$

$$\therefore \bar{\omega} = \omega_{osc} - \frac{\Delta\phi_m(\bar{\omega})}{\partial\phi/\partial\omega} = \omega_{osc} - \frac{\Delta\omega_{osc}}{f} \Delta\phi_m(\bar{\omega}) \quad \dots(11.56)$$

where we have used (11.54).

Here, $\omega_{osc} - \bar{\omega}$ represents the degree of “pulling” of the mode. The quantity ($\Delta\phi_m(\bar{\omega})$) is a function of the fractional energy gain per pass $g(\bar{\omega})$. Since the latter varies with frequency across the line profile of the transition, so does $\Delta\phi_m(\bar{\omega})$. Generally it is zero at the line centre (ω_m), negative for lower frequencies and positive for higher frequencies. The equation, therefore, predicts a shift in the direction of the line centre.

Obviously the gain at the frequency of oscillation must saturate at

$$g(\bar{\omega}) = f \quad \dots(11.57)$$

In the case of homogeneous or “natural” broadening, the same atoms are responsible for the gain over different regions of the line, so, removal of excited atoms by stimulated emission reduces the number of atoms available for amplification at other frequencies. Hence, gain proportionality is always maintained over the line. In other words, the reduction of the gain at frequency $\bar{\omega}$ necessary to satisfy (11.57) produces a proportionate reduction in gain at all other frequencies. Hence, the oscillation frequency is always given by its value at threshold and there is no direct power-dependent pulling effect.

Using Kramers-Kronig relations, Bennett obtained the following relation for $\Delta\phi_m(\bar{\omega})$.

$$\Delta\phi_m(\bar{\omega}) \sim -g(\bar{\omega}) \frac{\omega_m - \bar{\omega}}{\Delta\omega_m} \quad \dots(11.58)$$

From Eqns. (11.56), (11.57) and (11.58)

$$\bar{\omega} = \frac{\omega_{osc}\Delta\omega_m + \omega_m\Delta\omega_{osc}}{\Delta\omega_m + \Delta\omega_{osc}} \quad \dots(11.59)$$

In the case of inhomogeneous broadening, the relation becomes

$$\Delta\phi_m(\bar{\omega}) = -0.28 g(\bar{\omega}) \exp\left[-\left(\frac{\omega_m - \omega}{0.6 \Delta\omega_m}\right)^2\right] \sin\left(\frac{\omega_m - \omega}{0.3 \Delta\omega_m}\right) \quad \dots(11.60)$$

This ‘mode pulling’ accounts satisfactorily for the observed axial mode beat of just less than $\frac{\pi c}{L}$ and also for the splitting of the beat when other axial modes start to oscillate as the input power is increased. It does not account for the power dependence of the actual frequencies between the beat components at $\sim \frac{\pi c}{L}$ and $\sim \frac{2\pi c}{L}$. This could be accounted for by considering the effect of “hole burning”.

11.7 HOLE BURNING

As pointed out above, in the case of homogeneous broadening, irradiation at any frequency in the line produces a decrease in absorption across the entire width, *i.e.*, it causes “bleaching”. In the case of inhomogeneous broadening such as Doppler broadening, irradiation at a particular frequency causes an absorption decrease only in a range of the order of the homogeneous width centred around the pumping frequency while the rest of the band remains unaffected. This behaviour is often called ‘*hole burning*’.

We give below a simple analysis of this process.

Consider a sample of excited atoms through which an electromagnetic wave of density $p(\omega)$ is propagating. This wave can interact only with a restricted class of atoms whose velocity component v in the direction of the laser beam satisfies the relation

$$\frac{\omega - \omega_0}{\omega_0} = \frac{v}{c} \quad \dots(11.61)$$

where ω_0 is the central frequency of the resonance line.

We first write down the rate equations for the upper and lower laser levels, which we consider, for simplicity, to be non-degenerate. The various parameters that we will be using in these equations are

$N_i(v) \rightarrow$ is the number of atoms in a level i moving with velocity, v

$S_i \rightarrow$ the rate at which level i is populated by collisions and by radiative transfer from other levels,

$P(v) \rightarrow$ is a normalized Maxwell velocity distribution (see Eqn. 5.72)

$\tau_i \rightarrow$ is the effective lifetime of the level i

$A_{21}, B_{21} \rightarrow$ are Einstein’s coefficients.

The rate equation are:

$$\frac{dN_2(v)}{dt} = S_2 P(v) - \frac{N_2(v)}{\tau} - (N_2(v) - N_1(v)) B_{21} p(\omega) g(\omega)$$

$$\frac{dN_1(v)}{dt} = S_1 P(v) - \frac{N_1(v)}{\tau} + (N_2(v)A_{21} + (N_2(v) - N_1(v))B_{21}\rho(\omega)g(\omega)) \quad \dots(11.62)$$

Note: (i) that $\frac{N_2(v)}{\tau}$ gives the total rate of relaxation by radiative and non-radiative processes. That is

$$\frac{N_2(v)}{\tau} = N_2(v) \left(\frac{1}{\tau_{21}} + \frac{1}{\tau_{nr}} \right); \left(\frac{1}{\tau_{21}} = A_{21} \right)$$

and (ii) that $g(\omega)$ is the Lorentzian frequency response of the atoms moving with axial velocity v

$$\text{In the steady state } \frac{dN_2(v)}{dt} = \frac{dN_1(v)}{dt} = 0$$

The solution of these equations gives the value of N_1 and N_2 and a straightforward manipulation leads to the following expression for the population inversion density

$$N_2(v) - N_1(v) = \frac{\{S_2\tau_2 - (S_1 + \tau_2 A_{21} S_2)\tau_1\}P(v)}{1 + \beta B_{21}\rho(\omega)g(\omega)} \quad \dots(11.63)$$

where $\beta = \tau_1 + \tau_2 - \tau_1\tau_2 A_{21}$...(11.64)

Substituting for $g(\omega)$

$$g(\omega) = \frac{\gamma/2\pi}{\left\{ \omega - \omega_0 \left(1 + \frac{v}{c} \right) \right\}^2 + \gamma^2/4}$$

we get

$$N_2(v) - N_1(v) = \frac{\{S_2\tau_2 - (S_1 + \tau_2 A_{21} S_2)\tau_1\}P(v)}{1 + \beta B_{21}\rho(\omega) \frac{\gamma/2\pi}{\left\{ \omega - \omega_0 \left(1 + \frac{v}{c} \right) \right\}^2 + \gamma^2/4}} \quad \dots(11.65)$$

If $\rho(\omega) \rightarrow 0$, the inversion density will have a Gaussian distribution as a function of v given by $P(v)$ and shown in Fig. 11.9 (a). However, at finite values of $\rho(\omega)$, the second term in the denominator has a minimum value when

$\omega = \omega_0 \left(1 + \frac{v}{c} \right)$. This is illustrated by the curve (b). The beam of radiation

of angular frequency ω , thus, burns a ‘hole’ in the velocity distribution. The depth and width of a hole depend upon the power in the mode and the natural line width of the transition involved. Typically, the width appears to be in the range 3–30 MHz.

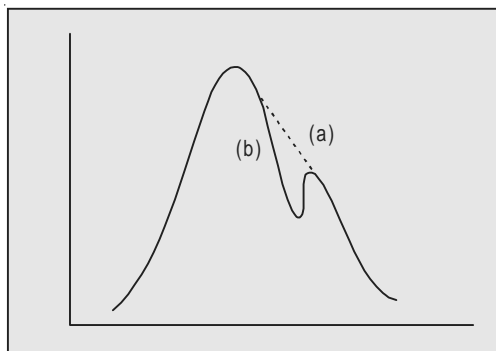


Fig. 11.9 Hole burning

Bennett [38] soon realized that on the basis of this model, there would be two “holes” “burned for each resonance. Imagine a standing wave in the cavity to be made up of a pair of running waves, one in each direction. The running wave in the $+x$ direction will interact primarily with atoms whose Doppler shifted transition frequencies arise from a velocity component $+vx$, where

$$\omega_L = \left(1 + \frac{vx}{c}\right)\omega_0 \quad \dots(11.66)$$

while that in the $-x$ direction interacts mainly with atoms moving with the velocity $-vx$, at a frequency ω'_L given by

$$\omega'_L = \left(1 - \frac{vx}{c}\right)\omega_0 \quad \dots(11.67)$$

Hence, two holes are burned in the profile, one at ω_L and the other at $\omega'_L = 2\omega_0 - \omega_L$ Fig. (11.10). The two holes are symmetrically located about

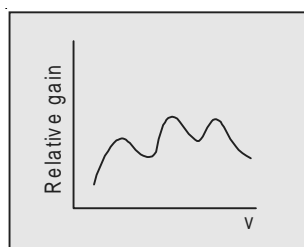


Fig. 11.10 Hole burning

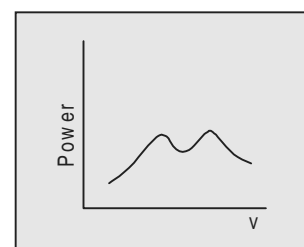


Fig. 11.11 Lamb dip

the line centre. Only when $\omega_L = \omega_0$ will there be a single hole. If the oscillation frequency is varied linearly across the gain profile then, due to the two holes being coincident at ω_0 , there will be a dip in the output intensity at that frequency Fig. (11.11). This is known as *Lamb dip* (after W.E. Lamb Jr. who first predicted the effect theoretically). [229]. It was confirmed experimentally by the observations of McFarlane *et al.* [274] and Szoke and Javan [370].

11.8 DISTRIBUTED FEEDBACK LASER

We have discussed so far lasers with Fabry-Perot type of optical resonators, where the feedback is provided by reflection at the end mirrors. We shall discuss in this section lasers in which amplification occurs without resonating mirrors. The necessary feed back in these lasers is provided by the spatial variation of the refractive index of the laser medium. These lasers are termed as "Distributed Feedback Lasers (DFB)", because the feedback is provided throughout the entire laser medium.

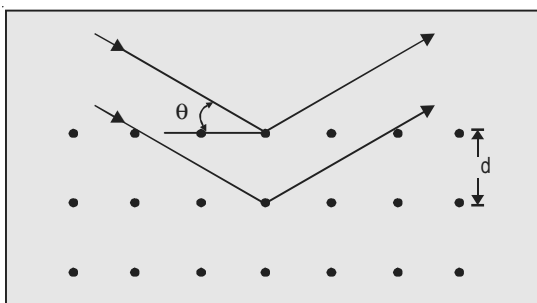


Fig. 11.12 Bragg reflection

The principle of distributed feedback lasers is based on Bragg's law, which states that the light waves reflected from different planes in a crystal (Fig. 11.12) will be in phase if the following condition is satisfied

$$2d \sin \theta = m\lambda \quad \dots(11.68)$$

where θ is the glancing angle,

D is the separation between successive planes,

λ is the wavelength of radiation and m is an integer.

Suppose the refractive index of an active element is spatially modulated along its optical axis. In Fig. 11.13 the dashed lines represent the reflecting planes resulting from the spatial modulation. The normally incident light waves will be reflected back at the planes. If the condition

$$2D\eta = m\lambda \quad \dots(11.69)$$

where D is the separation between the adjacent planes, η the refractive index and m is an integer, is satisfied, the energy of the wave propagated in one direction is continuously fed back in the opposite direction by Bragg scattering, thus producing a highly selective feedback.

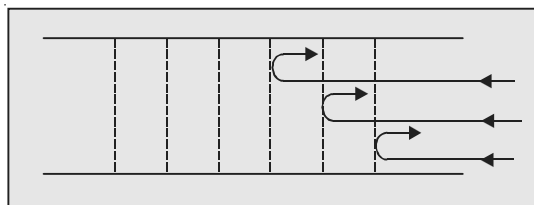


Fig. 11.13 Reflection in a spatially modulated medium

The first DFB laser based on this principle was constructed by Kogelnik and Shank [220].

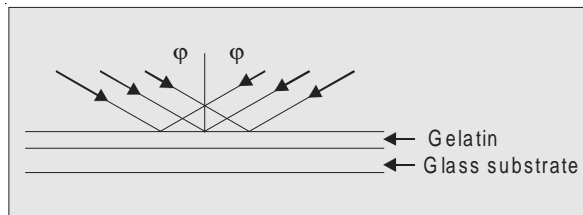


Fig. 11.14 Preparation of a spatially modulated medium

Let us consider the structure of a typical DFB laser. The active element of such a laser is an activated thin film on the surface of a substrate. Usually a thin film of gelatin with a dye incorporated in it is employed in such lasers. A thin gelatin film with dichromate added to it is deposited on a glass substrate. Two ultraviolet beams from a He-Cd laser are allowed to interfere on the surface of the film [Fig. 11.14]. The period of the interference fringes produced on the film is given by

$$2D \sin \varphi = m\lambda \quad \dots(11.70)$$

The modulation period is suitably adjusted by changing the angle of incidence φ . Since dichromated gelatin is a photo-sensitive medium, the gelatin developed after the exposure, contains a spatial modulation of the refractive index which results from the interference pattern produced by the two beams.

The dye material-rhodamine 6G-is added to the gelatin layer. A nitrogen laser is then employed for pumping rhodamine 6G (Fig. 11.15)

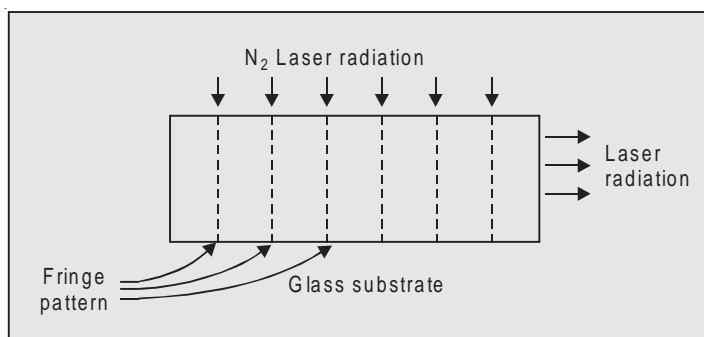


Fig. 11.15 DFB laser

The laser output of a wavelength $\sim 0.63 \mu\text{m}$ is obtained with such a laser.

In a different type of DFB laser a thin film of GaAs is employed. This laser has a corrugated interface between the GaAs active layer and a $\text{Ga}_{1-x}\text{Al}_x\text{As}$ layer that acts as a cladding. The corrugation provides a periodic structure which produces the feedback.

The DFB lasers are significant advances in the field of integrated optics. They provide a means of better restricting the laser operation to a single mode.

11.9 GAMMA-RAY LASER

It is generally believed that levels of nuclear excitation that might be efficiently stimulated in a gamma ray laser are very difficult to pump, because absorption widths in nuclei are too narrow to permit effective pumping with X-rays. Similar fears were expressed in atomic physics before Maiman's discovery of the ruby laser. But exploration of a broad absorption band linked through efficient kinetics to the narrow laser level, led to the development of the ruby laser. Collins *et al.* [82] proposed an analogous effect at the nuclear level for pumping a gamma ray laser.

Samples of ^{79}Br and ^{77}Se , both in natural isotopic abundance, were excited by them with 20 ns pulses of bremsstrahlung radiation produced by an electron beam machine. The spectral energy density developed at the tungsten converter was of the order of 10^{13} keV per pulse. The samples were positioned in a pneumatic shuttle tube directly behind the target foil and were automatically transferred to the counting chamber after each shot. The nuclear fluorescence spectra observed showed that a gamma ray laser is definitely feasible if an appropriate isotope exists.

12

HOLOGRAPHY

The most widespread method of obtaining optical images is the *photographic method*. The image of a three dimensional object is recorded on a two dimensional photographic plate or film. Absorption of light in the light-sensitive layer results into chemical reactions and in formation of a latent image. This is transformed into a visible one by process of developing. When we examine a photograph from various directions, we do not get new angles of approach and we cannot see what is happening on the other side of the object. This is because, in the conventional photography, only the distribution of the square of the amplitude is recorded in a two dimensional projection of the object on the plane of the photograph.

A fundamentally new method of recording optical images is now available. This is known as *holography*. The word “holography” originates from the Greek word “holos” meaning the whole. Holography means “complete recording”. In this technique a light wave is a carrier of information and it is recorded in terms of wave parameters: amplitude and phase components. The technique was first proposed by Gabor [133] in 1949. Note that Gabor did not have a laser when he formulated the idea of holography. It was not extant then. He ran his first experiments with mercury arc lamp as the source of light. The technique became a practical proposition only after the advent of lasers and opened the way to major advances in holography.

The process does not record the image of the object but rather records the reflected light wave. The record is called a “hologram”. It does not bear any resemblance to the original object but possesses a spectacular property. It memorizes, so to say, an encoded image of the object and contains much more information than ordinary photograph can record.

Laser holograms were prepared for the first time by Leith and Upatnick [237, 238]. Denisuk [96, 97], using thick layers of photosensitive material, recorded three dimensional holograms.

12.1 PRINCIPLE OF HOLOGRAPHY

The basic principle of holography can be explained in two steps: (i) recording of the hologram, and (ii) reconstructing the image.

12.1.1 Recording of the Hologram

Holography is in principle an interference based technique and, hence, light waves with a high degree of coherence are required for its realization. The principle is illustrated in Figs. 12.1 and 12.2.

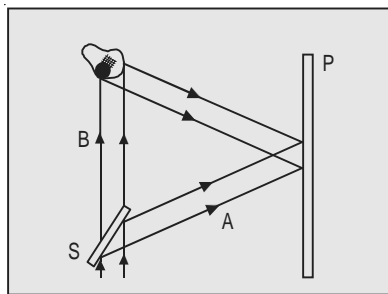


Fig. 12.1 Recording of a hologram

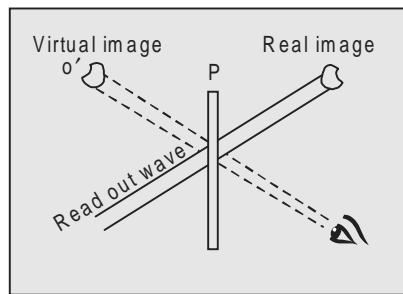


Fig. 12.2 Reconstruction of the image

A laser beam is divided by a beam splitter S into two beams A and B . The transmitted beam B illuminates the object whose hologram is to be recorded and a part of the light scattered by the object impinges on a photographic plate. The reflected beam A , which is called the *reference beam*, also falls onto the photographic plate. The superposition of these two beams produces an interference pattern which is recorded on the plate. The pattern is very fine, the spacing between the fringes being as small as 0.001 mm. The developed plate is known as the *hologram*. The hologram is quite unintelligible and gives no hint of the image embedded in it. It contains, however, enough information to provide a complete reconstruction of the object. The fine structure of interference fringes requires photographic emulsion with a high spatial resolution.

12.1.2 Reconstruction of the Image

If now the object is removed and the hologram is put in the place where it was when formed, the laser beam which is now known as the *readout wave*, interacts with the interference pattern on the plate and two images are produced by the diffracted waves (Fig. 12.2). One of them appears at the original position occupied by the object (virtual image) and the other (real image) which can be photographed directly without using a lens.

The hologram contains in the form of its interference pattern information in all the geometrical characteristics of the object. The virtual image, which is seen, by looking through the hologram as if it were a window, appears in complete three dimensional form. If one moves his eye from the viewing position, the perspective of the picture changes and it is possible to see the other sides of the object. The real image has all the aforementioned properties and is found between the observer and the plate as shown in Fig. 12.2. The real image will appear inverted in depth, *i.e.*, the relief of the object is reversed, with the features of the object farther from the viewer appearing closer; but there will be no lateral inversion. This image is called pseudoscopic image. Since, how-ever, the real image reverses foreground and background, the interest of the observer lies in the virtual image.

Although light is commonly used for holography, holograms have been successfully recorded with acoustic radiation, electron beams, X-rays and microwaves.

12.2 THEORY

To understand the various characteristics of holograms it is necessary to discuss the theory on which holography is based.

Let us first consider the case of a small object P . The source illuminates the object, but most of the light falls undisturbed on a photographic plate (Fig. 12.3). The light scattered or diffracted by the object also falls on the plate where it interferes with the direct beam—the reference beam. To find the intensity at a point O on the plate, we may write the field arriving at O as

$$E = E_r + E_0 \quad \dots(12.1)$$

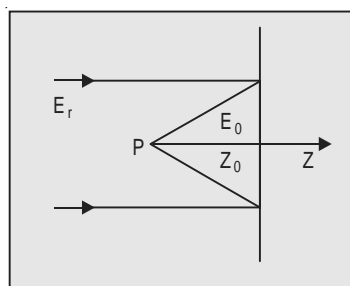


Fig. 12.3 Hologram of a point object

where E_r is the field due to the reference beam and E_0 is the field scattered from the object. The scattered field E_0 is not simple, both amplitude and phase vary greatly with position. The reflected wave-fronts are spherical and concentric around the point of origin. We represent the field of such a wave-front by

$$E_0 = \frac{A_0}{r_0} \exp(i(kr_0 - \omega t)) \quad \dots(12.2)$$

and the field E_r by the plane wave

$$E_r = A_r \exp(i(kz_0 - \omega t)) \quad \dots(12.3)$$

where $r_0 = PO$ and z_0 is the distance from P to the plate.

The intensity at O is

$$\begin{aligned} I &= |E_r + E_0|^2 \\ &= |A_r|^2 + \frac{|A_0|^2}{r_0^2} + \frac{A_0 A_r^*}{r_0} \exp(ik(r_0 - z_0)) \\ &\quad + \frac{A_0^* A_r}{r_0} \exp(ik(z_0 - r_0)) \end{aligned} \quad \dots(12.4)$$

Choosing the constants K and ϕ suitably, we can combine the last two terms from the above relation and write it as

$$I = |A_r|^2 + \frac{|A_0|^2}{r_0^2} + K \frac{\cos[k(r_0 - z_0) + \phi]}{r_0} \quad \dots(12.5)$$

Because of the cosine term, the total intensity I as a function of r_0 shows a series of maxima and minima. The interference of the plane wave E_r with the spherical wave E_0 , thus produces a set of circular interference fringes on the plate which, when developed, forms the hologram. If we assume that the plate response is proportional to the intensity I , the power transmission of the plate, T^2 , is given by

$$T^2 = 1 - \alpha I \quad \dots(12.6)$$

$$\text{or} \quad T \approx 1 - \frac{1}{2}\alpha I \quad \dots(12.7)$$

where α is a constant.

Let us now see what happens when this hologram is illuminated by the reference beam. The field of the transmitted wave is

$$\begin{aligned} E &= TE_r = \left(1 - \frac{\alpha}{2}I\right) A_r \exp(i(kz_0 - \omega t)) \\ &= \left\{1 - \frac{\alpha}{2}|A_r|^2 - \frac{\alpha}{2} \cdot \frac{|A_0|^2}{r_0^2}\right\} A_r \exp(i(kz_0 - \omega t)) \\ &\quad - \frac{\alpha}{2} \cdot \frac{A_0 A_r^*}{r_0} \exp(ik(r_0 - z_0)) A_r \exp(i(z_0 - \omega t)) \\ &\quad - \frac{\alpha}{2} \cdot \frac{A_0^* A_r}{r_0} \exp(ik(z_0 - r_0)) A_r \exp(i(z_0 - \omega t)) \\ &= \left\{1 - \frac{\alpha}{2}|A_r|^2 - \frac{\alpha}{2} \cdot \frac{|A_0|^2}{r_0^2}\right\} A_r \exp(i(kz_0 - \omega t)) \end{aligned}$$

$$\begin{aligned}
 & -\frac{\alpha A_0 |A_r|^2}{2r_0} \exp(i(kr_0 - \omega t)) \\
 & -\frac{\alpha}{2} \cdot \frac{A_0^* A_r^2}{r_0} \exp(i(2kz_0 - kr_0 - \omega t)) \quad \dots(12.8)
 \end{aligned}$$

where we have used (12.4).

The first term of (12.8) represents the same plane wave beyond the plate as the one incident on it, except for the attenuation corresponding to the average blackening of the plate (see 12.3). The second term represents a diverging spherical wave surface identical with the wave surface emitted by the object except for a constant factor (see 12.2). This wave surface when projected back seems to emanate from an apparent object located at the place where the original object was located (Fig. 12.4). This is the virtual image of the object. The third term represents also a spherical wave surface which is a replica of the original wave but has a conjugate or reverse curvature. It converges at a point P' producing a real image at this point which can be photographed without a lens. The hologram thus produces a virtual image P and a real image P' .

The general theory of holography is too cumbersome to pursue further. We can, however, generalize the treatment given above for a point object to an object of finite size. As before the intensity at the point O is

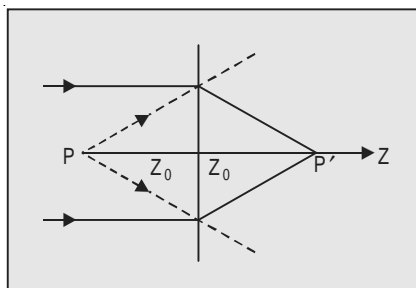


Fig. 12.4 Reconstruction of the image

$$I = |E_r + E_0|^2 = |E_r|^2 + |E_0|^2 + E_0 E_0^* + E_0^* E_r \quad \dots(12.9)$$

When the hologram is illuminated by the reference beam, the field on the other side of the plate is

$$\begin{aligned}
 E = TE_r = & \left\{ 1 - \frac{\alpha}{2} |E_r|^2 - \frac{\alpha}{2} |E_0|^2 \right\} E_r \\
 & - \frac{\alpha}{2} E_0 |E_r|^2 - \frac{\alpha}{2} E_0^* E_r^2 \quad \dots(12.10)
 \end{aligned}$$

As before, the first term gives the attenuated reference wave; the second term produces the virtual image and the third term produces a real image of the object at a position which is the mirror image of the virtual image, with respect to the plate.

Equation (12.10) shows how holography allows us to make a complete record of the wave coming from the object. In the absence of the reference beam the blackening of the plate would be proportional to $|E_0|^2$ i.e., only the modulus of E_0 would be recorded. This means that only the amplitude information would be recorded and the phase information is thereby lost. Because of the presence of the reference wave, the field recorded on the plate is proportional to E_0 as can be seen from the second term of (12.10), i.e., both amplitude and the phase are recorded thus making the complete reconstruction of the object possible.

Gas lasers operating in the continuous wave (cw) mode, are often used for holography because their coherence is high. However, their emitting power being low, time of exposure has to be large, and, hence, moving objects cannot be photographed using gas lasers. Pulsed solid state lasers make it possible to cut down the exposure to about 10^{-3} sec and, hence, can be used to photograph moving objects and to record the development of a process in time.

12.3 SOME DISTINGUISHING CHARACTERISTICS OF HOLOGRAPH

One may prefer, at first glance, a photograph to a hologram because a photograph shows everything ‘clearly’, while a hologram is quite unintelligible. However, holographs have some interesting properties which make it preferable to a photograph.

- (i) The virtual image produced by a hologram appears in complete three dimensional form. The observer sees something looking very much like the object did in the process of hologram recording. If he tilts his head, he notices other objects behind the one in the foreground or new details that were not noticeable before. The image manifests vivid realism.
- (ii) Destruction of a portion of a photographic image results in an irreparable loss of information corresponding to a part of the object. In the case of a hologram the information about a point object is recorded over the whole area of the hologram as can be seen from Fig. 12.3, and each such point of a real object is recorded on the whole hologram and not in one of its points as is the case in a photograph. Each point on the hologram receives light from all parts of the object and, therefore, contains information about the geometrical characteristics of the entire image. Each part of the hologram, no matter how small, can reproduce the entire image. Consequently, destruction of a part of a hologram does not erase a specific portion of the image. It may be noted, however, that the reduction in size worsens the resolution which is a function of the aperture of the imaging system. A hologram, thus, is a reliable method of data storage.

- (iii) Another characteristic which proves the supremacy of a hologram over a photograph is its information capacity. Superposition of several images on a photographic plate is pointless. A hologram, on the other hand, may contain a number of consecutively recorded scenes that can be recorded independently. Different scenes can be recorded on a hologram, each time changing the angle at which the reference wave is incident on the holographic plate, which can be done by rotating the plate. Reconstruction of a specific scene only requires that the hologram be properly oriented with respect to the read out wave. It has been estimated that a single hologram with an area of about 100 square centimeters, may contain at least one volume of Encyclopaedia Britannica. This indicates the extremely high information capacity of holograms.
- (iv) Yet another curious property of the wave-front reconstruction process is that it does not produce negatives. One may consider a hologram itself as a negative. But the image it produces is a positive. A hologram copied from another by contact printing would, no doubt, be reversed in the sense that opaque areas now become transparent and vice-versa; but the image reconstructed from it, would be identical in all respects to that produced by the original. This is because the information is recorded on the plate in the form of a modulated spatial carrier. It may be recalled that the information on the grating carrier is embodied in the fringe contrast and in the fringe spacing; neither of this is altered by the reversal of polarity.

12.4 PRACTICAL APPLICATIONS OF HOLOGRAPHY

Holography has a wide range of applications, particularly in science and technology. Specialists in the field of data processing devote much of their attention to holography. The links between computer science and holography are now well established and are developing fruitfully. An application, remarkable for its simplicity, is found in an experiment of Brian Thompson and his colleagues at Technical Operation, Inc. These workers were faced with the problem of measuring the distribution by size and other properties of floating fog like particles in a sample volume. Such particles generally do not remain stationary long enough for the observer to focus on them. It is also desirable to photograph all the particles in the volume at a given time. The wave-front reconstruction method offers an ideal solution to this problem. A hologram is made by illuminating the volume by a short-pulse laser which "freezes" the motion of the particles. In the reconstruction an image of the entire volume is produced, and the particle size, distribution and cross-sectional geometry can be measured by microscopic examination.

It is not likely that holography will replace photographic methods in everyday situations; its maximum effect is in the scientific and technical domains. Nevertheless, we may expect holography to come into our daily life in the not very distant future. It has been experimentally demonstrated that holographic cinema is a feasible proposition and holographic television is also likely to make its appearance in the near future. Holography can be useful in practically every area of human activity, ranging from linguistics to the investigation of processes occurring in thermonuclear plasma.

12.5 ADVANCES IN HOLOGRAPHY

A major drawback of conventional holographic process is the requirement of coherent illumination in the image reconstruction. The *rainbow* (white light transmission) holography devised by Benton [40] is a major improvement in holography. Rainbow holograms can be viewed with a white light source and the image reconstructed is exceptionally bright. However, because of the complex nature of the two-step process involved, its scientific applications are to some extent limited. A one-step process demonstrated by Chen and Yu [73] greatly simplifies the procedure.

An entirely new method of storing confidential data, based on sandwich holography, has been suggested by Abramson *et al.* [3].

For details of all these methods, one has to refer to the original papers.

13

NON-LINEAR OPTICS

Can the optical properties of a medium depend upon the intensity of radiation? In the pre-laser era, the answer to this question, perhaps, would have been an emphatic “no”. The basis for this conclusion is that the field strengths of the conventional light sources used before the advent of lasers, were much smaller than the field strengths of atomic and inter-atomic fields. The latter are of the order of 10^7 to 10^{10} V/cm; whereas the former would not exceed 10^3 V/cm. It is natural that the light wave with such a low intensity is not able to affect atomic fields to the extent of changing optical parameters. The high degree of coherence of the laser radiation has made it possible to have extremely high spatial concentration of light power. It is now possible to generate 1 MW pulses, lasting a few tenths of nanoseconds, using moderately powerful lasers. The energy current density in a beam of cross-section 1 mm^2 of such a laser is $J_E \approx 10^6 \text{ MW/m}^2$, which corresponds to peak electric field strength $E \approx 3 \times 10^7 \text{ V/m}$. Due to coherence, the beam can be focussed to an area $A \approx \lambda^2$. If the laser wavelength is assumed to be 1μ , then $A = 10^{-12} \text{ m}^2$ and, hence $J_E \approx 10^{18} \text{ MW/m}^2$ giving $E \approx 3 \times 10^{10} \text{ V/m}$, which is within the range of atomic fields. At such high fields, the relationship between the electric polarization P and the field strength E ceases to be linear and some interesting nonlinear effects come to the fore. Bloembergen played an important role in establishing the theoretical framework of nonlinear optics. We deal in this chapter some nonlinear effects describable by semiclassical theory in the electric dipole approximation.

13.1 HARMONIC GENERATION

Non-linear properties in optical region have been strikingly demonstrated by the harmonic generation of light observed for the first time by Franken and coworkers in 1961 [126]. They observed ultraviolet light at twice the frequency of a ruby laser light ($\lambda = 6493 \text{ \AA}$), when the light was made to traverse a quartz

crystal. This experiment attracted widespread attention and marked the beginning of the experimental and theoretical investigation of nonlinear optical properties.

A simplest scheme for this experiment is shown in Fig. 13.1.

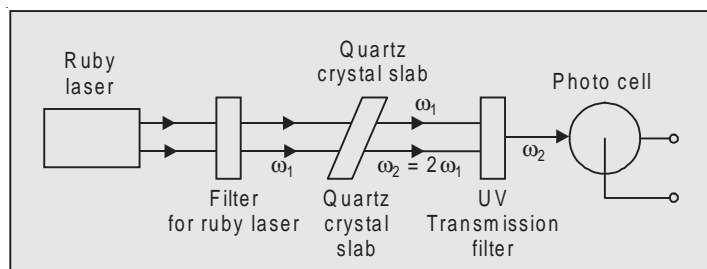


Fig. 13.1 Second harmonic generations

A ruby laser beam ($\lambda = 6493 \text{ \AA}$) with average power of the order of 10 kW is focussed on a quartz slab. The transmitted light then was passed through a filter which cuts off the red light and allows uv light to pass through. The emerging light was incident on a photocell. Radiation with wavelength $\lambda = 3471 \text{ \AA}$ and the power of the order of 1 mW was observed in the transmitted light. How can one account for this change in frequency?

A dielectric medium when placed in an electric field is polarized, if the medium does not have a transition at the frequency of the field. Each constituent molecule acts as a dipole, with a dipole moment \mathbf{P}_i . The dipole moment vector per unit volume \mathbf{P} is given by

$$\mathbf{P} = \sum_i \mathbf{P}_i \quad \dots(13.1)$$

where the summation is over the dipoles in the unit volume. The orienting effect of the external field on the molecular dipoles depends both on the properties of the medium and on the field strength. Thus, we can write [233]

$$\mathbf{P} = \epsilon_0 \chi \mathbf{E} \quad \dots(13.2)$$

where χ is called the *polarizability or dielectric susceptibility* of the medium.

This relation is valid for the field strengths of conventional sources. The quantity χ is a constant only in the sense of being independent of E ; its magnitude is a function of the frequency. With sufficiently intense laser radiation the relation (13.2) does not hold good and has to be generalized to

$$P = \epsilon_0 (\chi^{(1)} E + \chi^{(2)} E^2 + \chi^{(3)} E^3 + \dots) \quad \dots(13.3)$$

where $\chi^{(1)}$ is the same as χ in (13.2); the coefficients $\chi^{(2)}, \chi^{(3)}, \dots$ define the degree of non-linearity and are known as nonlinear susceptibilities. If the field is low, as it is in the case of ordinary light sources, only the first term of (13.3) can be retained. It is for this reason that the prelaser optics is known as *linear optics*. Higher the value of the electric field, more significant become the higher

order terms. It may be noted that optical characteristics of a medium, such as dielectric permittivity, refractive index, *etc.*, which depend upon susceptibility, also become functions of the field strength E , if it is sufficiently high. The medium of which the polarization is described by a nonlinear relation of the type (13.3) is called a “non-linear medium.”

Suppose now that the field incident on a medium has the form

$$E = E_0 \cos \omega t. \quad \dots(13.4)$$

Substituting this in (13.3), we have

$$P = \epsilon_0 \chi^{(1)} E_0 \cos \omega t + \epsilon_0 \chi^{(2)} E_0^2 \cos^2 \omega t + \epsilon_0 \chi^{(3)} E_0^3 \cos^3 \omega t + \dots \quad \dots(13.5)$$

Using the trigonometric relations

$$\cos^2 \theta = \frac{1 + \cos 2\theta}{2}; \quad \cos^3 \theta = \frac{\cos 3\theta + 3 \cos \theta}{4} \quad \dots(13.6)$$

we can transform (13.5) to the form

$$\begin{aligned} P = & \frac{1}{2} \epsilon_0 \chi^{(2)} E_0^2 + \epsilon_0 \left(\chi^{(1)} + \frac{3}{4} \chi^{(3)} E_0^2 \right) E_0 \cos \omega t \\ & + \frac{1}{2} \epsilon_0 \chi^{(2)} E_0^2 \cos 2\omega t + \frac{1}{4} \epsilon_0 \chi^{(3)} E_0^3 \cos 3\omega t + \dots \quad \dots(13.7) \end{aligned}$$

The first term is a constant term. It gives rise to a dc field across the medium, the effect of which is of comparatively little practical importance. The second follows the external polarization and is called the *first or fundamental harmonic of polarization*; the third oscillates at frequency 2ω and is called the *second harmonic of polarization*, the fourth is called the *third harmonic of polarization*, and so on.

13.2 SECOND HARMONIC GENERATION

A polarization oscillating at frequency 2ω radiates an electromagnetic wave of the same frequency, which propagates with the same velocity as that of the incident wave. The wave, thus, produced, has the same characteristics of directionality and monochromacy as the incident wave and is emitted in the same direction. This phenomenon is known as the *Second Harmonic Generation* (SHG).

In most crystalline materials, the nonlinear polarizability $\chi^{(2)}$ depends on the direction of propagation, polarization of the electric field and the orientation of the optic axis of the crystal. Since in such crystalline materials the vectors \mathbf{P} and \mathbf{E} are not necessarily parallel the coefficients χ must be treated as tensors. The second order polarization, therefore, may be represented by the relation of the type

$$P_i^{(2)} = \epsilon_0 \sum_{j,k} \chi_{ijk}^{(2)} E_j E_k \quad \dots(13.8)$$

where i, j, k represent the coordinates x, y, z . Most of the coefficients χ_{ijk} , however, are usually zero and we have to deal only with one or two components.

It must be mentioned here that the second harmonic generation represented by (13.8) occurs only in certain type of crystals. Consider, for example, a crystal that is isotropic. In this case χ_{ijk} is independent of direction and, hence, is a constant. If we now reverse, the direction of the axis ($x \rightarrow -x, y \rightarrow -y, z \rightarrow -z$) leaving electric field and dipole moment unchanged in direction, the sign of these two must change.

$$\therefore -P_i^{(2)} = \epsilon_0 \sum_{j,k} \chi_{ijk}^{(2)} (-E_j) (-E_k) = +P_i^{(2)} \quad \dots(13.9)$$

which means

$$P_i^{(2)} = 0 \text{ and, hence, } \chi_{ijk}^{(2)} = 0.$$

Second harmonic generation, therefore, cannot occur in an isotropic medium such as liquids or gases nor in centro-symmetric crystals (*i.e.*, crystals symmetrical about a point). Only crystals that lack inversion symmetry exhibit SHG.

In the case of non-centro-symmetric materials (*e.g.*, anisotropic crystals, such as uniaxial crystals) both the quadratic and cubic terms are present. However, generally, the cubic term is substantially smaller than the second order term and may be ignored.

For such materials, we can write

$$P = \epsilon_0 \chi^{(1)} E + \epsilon_0 \chi^{(2)} E^2 \quad \dots(13.10)$$

and the medium is said to have second order linearity.

13.3 PHASE MATCHING

The intense development of research on the mechanism of generation of optical harmonics in crystals and media in which such generation is effectively realizable, has indicated the importance of phase relation between the fundamental and generated harmonics, as they propagate in crystals having optical dispersion [Bloembergen 51, Franken and Ward 127]. It was observed that the efficiency of the generation of harmonics depends not only on the intensity of the exciting radiation, but also on its direction of propagation in crystals.

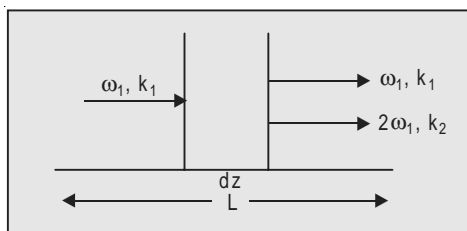


Fig. 13.2 Second harmonic wave propagating through a material of length L

Suppose a plane wave at frequency ω and the second harmonic wave at frequency 2ω driven by it are propagating in the z -direction through a material of length L (Fig. 13.2). Let us find an expression for the intensity of SHG at the exit surface of the material.

The amount of second harmonic radiation produced within a slab of width dz located at z will be proportional to the width and to the second harmonic dipole moment per unit volume induced at frequency 2ω , *i.e.*, $P_{(z)}^2$ which, in turn, is proportional to the square of the electric field E , that is

$$dE_{(z)}^{(2)} \propto P_{(z)}^{(2)} dz \propto \exp(2i(k_1 z - \omega t)) dz \quad (\because E \propto \exp(i(k_1 z - \omega t))) \quad \dots(13.11)$$

where dE_2^2 is the amount of second harmonic radiation within the slab.

We see that the spatial variation of the second harmonic polarization is characterized by a wave member $2k_1$.

The second harmonic radiation produced by this slab at the exit surface of the crystal, *i.e.*, at $z = L$ obviously will be

$$dE_{(L)}^{(2)} \propto dE_{(z)}^{(2)} \exp(ik_2(L - z)) dz \quad \dots(13.12)$$

where $L - z$ is the distance from the slab to the end of the crystal and k_2 is the propagation wave number of the second harmonic radiation. In general, $k_2 \neq k_1$ because of dispersion. (Note $k = 2\pi\eta/\lambda$.)

$$\begin{aligned} \therefore dE_{(L)}^{(2)} &\propto \exp(2i(k_1 z - \omega t)) \exp(ik_2(L - z)) dz \\ &= \exp(i(2k_1 - k_2)z) \exp(i(k_2 L - 2\omega t)) dz \end{aligned} \quad \dots(13.13)$$

We have assumed here that the incident power is nearly unchanged as the beam propagates through the crystal.

Integrating (13.13)

$$\begin{aligned} E_{(L)}^{(2)} &\propto \int_0^L \exp(i(2k_1 - k_2)z) \exp(i(k_2 L - 2\omega t)) dz \\ &= \frac{\exp(i(k_2 L - 2\omega t) [\exp(i(2k_1 - k_2)L) - 1])}{i(2k_1 - k_2)} \end{aligned} \quad \dots(13.14)$$

On simplification and some manipulation, we get

$$E_{(L)}^{(2)} \propto \frac{\sin\left(\frac{2k_1 - k_2}{2}\right)L}{\left(\frac{2k_1 - k_2}{2}\right)} \quad \dots(13.15)$$

where we have taken only the real part of the proportionality factor.

This will be maximum when $\frac{(2k_1 - k_2)L}{2} = \frac{\pi}{2}$, that is, the field of the second harmonic generation will be maximum when

$$L = \frac{\pi}{2k_1 - k_2} = \frac{\lambda}{4(\eta_{\omega} - \eta_{2\omega})} \quad \dots(13.16)$$

where η_{ω} , $\eta_{2\omega}$ are the refractive indices at ω and 2ω respectively.

Increasing L beyond this value will not result into any increase in $E^{(2)}$. The magnitude of L given by (13.16) is called the *coherence length for the second harmonic radiation*.

The expression for intensity, viz.

$$I \propto \frac{\sin^2 \left(\frac{2k_1 - k_2}{2} \right) L}{\left(\frac{2k_1 - k_2}{2} \right)^2} \quad \dots(13.17)$$

is sharply peaked about

$$\left(\frac{2k_1 - k_2}{2} \right) L = 0$$

that is when $k_2 = 2k_1$...(13.18)

For efficient frequency doubling, this relation must be satisfied. This requirement is known as *phase-matching criterion*.

Since

$$k_2 = \frac{2\omega\eta_{2\omega}}{c} \quad \text{and} \quad k_1 = \frac{\omega\eta_{\omega}}{c} \quad \dots(13.19)$$

relation (13.18) reduces to

$$\eta_{2\omega} = \eta_{\omega} \quad \dots(13.20)$$

Thus, the phase matching criterion becomes a refractive-index criterion. It is rather difficult to fulfill this requirement because most materials show some sort of dispersion in the refractive index.

A satisfactory solution to this problem would be to use the dependence of the refractive index on the direction in anisotropic crystals. A birefringent material has different refractive indices for different polarization of light. This occurs generally in crystals of low symmetry. A light wave entering an anisotropic crystal splits into two waves travelling at different velocities. In uniaxial crystals the ray corresponding to the wave whose refractive index is independent of the direction of propagation is called the *ordinary ray*.

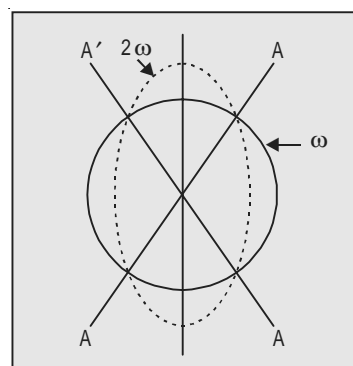


Fig. 13.3 Indicatrix for a negative uniaxial crystal

The ray corresponding to the other light wave whose refractive index depends upon the direction of propagation is called *extraordinary ray*. The behaviour of the refractive index is usually described in terms of refractive index surface, *i.e.*, the *indicatrix* or *index ellipsoid*. In the case of the ordinary ray it is a sphere; for extraordinary ray it is an *ellipsoid*. We, therefore, have to choose a material in which the refractive index for the extraordinary ray at 2ω , is equal to that of the ordinary ray at ω . This points to the fact that effective frequency conversion in the second harmonic is possible only in a limited number of crystals.

Consider a negative uniaxial crystal, *i.e.*, a crystal for which the refractive index for the ordinary ray is greater than that for the extraordinary ray. Fig. 13.3 shows a section through the refractive index surfaces (indicatrix) for one such crystal. The dotted curve represents the surface corresponding to the frequency 2ω and the solid curve for frequency ω . OX is the optic axis of the crystal. The refractive index surface of the ordinary wave and that for the extraordinary wave intersect at A . This means, that for the waves propagating in the direction OA

$$\eta_0(\omega) = \eta_e(2\omega) \quad \dots(13.21)$$

That is, the incident and the second harmonic waves propagating in this direction are *phase matched*. The cone angle θ is the phase matching angle. The phase matching condition is satisfied for all directions lying on the cone.

As stated in Sec. 13.1, SHG was first realized successfully in quartz. It was subsequently generated in many other crystals such as: potassium dihydrophosphate (KDP) [Hagen *et al.*, 157], ammonium dihydrophosphate (ADP), [Dowling 103], barium titanate [Geusie *et al.*, 143], lithium iodate [Chesler *et al.*, 74], *etc.*, A SH peak power of 200 kW has been obtained with only 6 mJ energy in a single pulse [Terhune *et al.*, 375]. Conversion efficiencies of 15 – 20% have been found at input power densities of the order of 100 MW cm⁻².

SHG was also successfully realized in gases [Adams *et al.*, 4, Ashkin *et al.*, 16, White *et al.*, 398] and in semiconductors [Armstrong *et al.*, 14 Garfinkel *et al.*, 135]. It would be interesting to note that SHG has been observed in calcite as a function of dc electric field, although the crystal possesses a centre of inversion. This is because the imposed electric field removes the symmetry [Terhune *et al.*, 374].

The importance of second harmonic generation lies in the fact that it is one of the principal methods of effective conversion of infrared radiation into visible and visible into ultraviolet. The mechanism of the second harmonic generation has been thoroughly investigated theoretically [13, 52, 211, 212, 218, 236, 253].

13.4 THIRD HARMONIC GENERATION

As stated in Sec. 13.2, in the case of centrosymmetric materials, the expression (13.3) will lack terms in even powers of E and it will reduce to

$$P = \epsilon_0 \chi^{(1)} E + \epsilon_0 \chi^{(3)} E^3 + \dots \quad \dots(13.22)$$

Or in vector notation

$$P = \epsilon_0 \chi^{(1)} E + \epsilon_0 \chi^{(3)} E^2 E + \dots \quad \dots(13.23)$$

Third harmonic generation (THG) is, therefore, possible in crystals that exhibit inversion symmetry. The development of Q -switched lasers had made it possible to generate third harmonic in crystals [32, 267]. However, the energy conversion efficiency in such cases is very low. For example, in calcite the maximum energy conversion efficiency in the third harmonic was 0.01%.

Experiments for observation of the third harmonic were also performed by Maker and Terhune [268] using giant pulse lasers. Zwernemann and Beeker [415] have observed experimentally the enhancement of third harmonic generation (THG) at 9.33 μm in CO by having the interaction take place in a waveguide. They have presented a theoretical determination of the most suitable waveguide in which the interaction can take place.

The process of generation of higher order harmonics can be explained on the same lines.

13.5 OPTICAL MIXING

In the equation for nonlinear polarization (13.3), we have assumed that the factor E^2 in the second term, is the product of the electric field strength with itself, $\mathbf{E} \cdot \mathbf{E}$. However, such a nonpolarization term may also result from the interaction of two fields with different frequencies. Suppose two coherent light wave trains of unequal frequencies ω_1 and ω_2 are traversing the material. The effective field in the material is

$$E = E_1 \cos \omega_1 t + E_2 \cos \omega_2 t \quad \dots(13.24)$$

Substituting this in (13.3), the second term becomes

$$\begin{aligned} P^{(2)} &= \epsilon_0 \chi^{(2)} (E_1 \cos \omega_1 t + E_2 \cos \omega_2 t)^2 \\ &= \epsilon_0 \chi^{(2)} (E_1^2 \cos^2 \omega_1 t + E_2^2 \cos^2 \omega_2 t) \\ &\quad + 2\epsilon_0 \chi^{(2)} E_1 E_2 \cos \omega_1 t \cos \omega_2 t \end{aligned} \quad \dots(13.25)$$

Using the trigonometric relation

$$2\cos \alpha \cos \beta = \cos(\alpha + \beta) + \cos(\alpha - \beta)$$

We can express the last term as

$$\begin{aligned} 2\epsilon_0 \chi^{(2)} E_1 E_2 \cos \omega_1 t \cos \omega_2 t \\ = \epsilon_0 \chi^{(2)} E_1 E_2 [\cos(\omega_1 + \omega_2)t + \cos(\omega_1 - \omega_2)t] \end{aligned} \quad \dots(13.26)$$

This shows that the non-linear polarization and, therefore, emitted radiation contains frequencies $\omega_1 + \omega_2$ and $\omega_1 - \omega_2$. The energy conversion between the beams can take place over significant distances only if the beams travel in the same direction and at the same velocity.

The sum and difference frequencies can be observed experimentally. Generation of difference optical frequencies was first observed by mixing a beam from a ruby laser with an incoherent beam of a mercury lamp ($\lambda = 3115 \text{ \AA}$). The efficiency with which the difference frequency was generated was negligible; with the power in the mercury beam amounting to about $2 \times 10^{-4} \text{ W}$, the power radiated at the difference frequency was 10^{-10} W . Optical mixing of the emission, of two ruby lasers with different frequencies was first observed by Franken and coworkers [127].

The first term of (13.25), besides frequency doubling, also leads to a dc term (Sec. 13.7). Bass *et al.*, [33] observed a dc pulse of about $200 \mu\text{V}$ when 1 MW radiation was passed through a KDP crystal. Sum of the frequencies from two ruby lasers held at different temperatures was observed by Bass *et al.*, [32] and from a ruby and a neodymium laser by Miller and Savage [275].

We have considered above only the second order term in (13.3). In a more general case, polarization expression may include terms with E^3 , E^4 , etc., Substitution of (13.24) in (13.3) with higher order terms, results into an expression containing terms with frequencies $\omega = m\omega_1 \pm n\omega_2$, where m and n are integers. This shows that in addition to the sum and difference of frequencies, other type of frequency mixing is possible.

The mixing of optical frequencies in crystals, thus, uncovers additional possibilities for optical frequency conversion. It has provided a source of narrow band coherent radiation in various regions including those in which there are no primary lasers available. Primary laser radiation is available from the IR through the visible and uv down to $\sim 116 \text{ nm}$. Optical frequency mixing has enabled us to extend the range of wavelength to the XUV reaching almost to the soft X-ray range. Currently it is the only source of coherent radiation in XUV.

Incidentally, it may be mentioned here that $\omega_1 - \omega_2$ may fall into the range of acoustic frequencies. In a sense, therefore, frequency mixing is an optical method of generating ultrasonic waves.

As in the case of second harmonic generation, phase-matching condition is also important in frequency mixing. In fact, it is more stringent in the latter case, because of the number of frequencies involved. In the case of second harmonic generation, it is necessary to find a direction in crystals such that $k_1 = k_2$. In the case of sum or difference frequencies, three waves must be matched. If

$$\omega_3 = \omega_1 \pm \omega_2, \quad \dots(13.27)$$

the condition to be satisfied is

$$k_3 = k_1 \pm k_2 \quad \dots(13.28)$$

13.6 PARAMETRIC GENERATION OF LIGHT

Parametric phenomena in electronics are widely known. They occur in circuits involving nonlinear capacitors. Similar processes occur in optics when nonlinear crystals are used as parametric media. The process is known as *parametric generation of light*, and is based on “optical mixing” discussed in the preceding section.

Suppose a powerful signal at frequency ω_p (pump frequency) is applied to a parametric medium and a small signal at frequency ω_s (signal frequency) is introduced at one end. The fields at the original frequencies are regarded as fixed parameters. “Mixing” of the signal and the pump frequency may result into a secondary wave at frequency ω_i given by

$$\omega_i = \omega_p - \omega_s \quad \dots(13.29)$$

which is known as ‘idler’ frequency. The corresponding field strength being proportional to

$$E_p E_s = E_i \quad \dots(13.30)$$

as shown by equation (13.26).

In view of the non-linear properties of the medium, further mixing may occur. In particular, the field generated by the polarization component oscillating at the idler frequency and the original pump field, when mixed, would make a contribution to the signal field. Thus

$$\omega_p - \omega_i = \omega_p - (\omega_p - \omega_s) = \omega_s. \quad \dots(13.31)$$

The strength of the contribution is proportional to

$$E_p E_i = E_p^2 E_s \quad \dots(13.32)$$

where we have used (13.30). This shows that the strength is proportional to E_s , in accordance with the usual requirement for parametric amplification. Thus, the secondary light waves at frequencies ω_s and ω_i can be excited parametrically at the expense of the part of energy of the pumping wave. Initial signals required for triggering the process of parametric generation are always available in any crystal in the form of spontaneous photons.

13.7 SELF-FOCUSSING OF LIGHT

The refractive index of a material is related to the susceptibility by the relation.

$$\eta = \sqrt{1 + \chi} \quad \dots(13.33)$$

Since the susceptibility χ is a function of the field E , η depends on E . This dependence of the refractive index on the field strength gives rise to a non-linear effect: *self-focussing of intense light beams*.

Self-focussing does not alter the frequency of the light waves. We need, therefore, consider only the second term in the relation (13.7) which describes the fundamental harmonic, viz.

$$P^{(1)} = \epsilon_0(\chi^{(1)} + \frac{3}{4}\chi^{(2)}E_0^2)E. \quad \dots(13.34)$$

The expression for the refractive index consequently is

$$\eta = \sqrt{1 + (\chi^{(1)} + \frac{3}{4}\chi^{(2)}E_0^2)} \quad \dots(13.35)$$

We write this as

$$\eta = \sqrt{\epsilon_l + \epsilon_{nl}} \quad \dots(13.36)$$

where we have put

$$\epsilon_l = 1 + \chi^{(1)} \quad \dots(13.37)$$

which gives the dielectric permittivity of the linear medium, and

$$\epsilon_{nl} = \frac{3}{4}\chi^{(2)}E_0^2 \quad \dots(13.38)$$

is a non-linear increment in the expression for dielectric permittivity.

$$\eta = \sqrt{\epsilon_l} \sqrt{1 + \frac{\epsilon_{nl}}{\epsilon_l}} \approx \sqrt{\epsilon_l} \left(1 + \frac{\epsilon_{nl}}{2\epsilon_l}\right) \quad \dots(13.39)$$

$$(\because \epsilon_{nl} \ll \epsilon_l)$$

$$= \eta_l \left(1 + \frac{\epsilon_{nl}}{2\eta_l^2}\right) = \eta_l \left(1 + \frac{3\chi^{(2)}E_0^2}{8\eta_l^2}\right)$$

or

$$\eta = \eta_l (1 + \eta_{nl} E_0^2) \quad \dots(13.40)$$

where $\eta_l = \sqrt{\epsilon_l}$ is the refractive index of the linear medium, and

$$\eta_l \eta_{nl} E_0^2 = \frac{\epsilon_{nl}}{2\sqrt{\epsilon_l}} = \frac{3\chi^{(2)}E_0^2}{8\sqrt{1 + \chi^{(1)}}} \quad \dots(13.41)$$

is the non-linear increment in the expression for the refractive index. We, thus, see that the refractive index of a non-linear medium is proportional to the square of the amplitude of the field, that is, to the intensity. Now the intensity of a laser beam is not constant over its cross-section. It peaks at the axis of the beam and falls off gradually away from the axis. The velocity of the light wave is given by $v = c/\eta$. Since η decreases owing to the falling of the intensity of the light beam, the velocity increases with the distance away from the axis. Consequently, a plane wave-front incident on material becomes concave as it

propagates through the medium and contracts towards the axis (Fig. 13.4). In other words, it self-focusses, after which it propagates as a narrow light fibre.

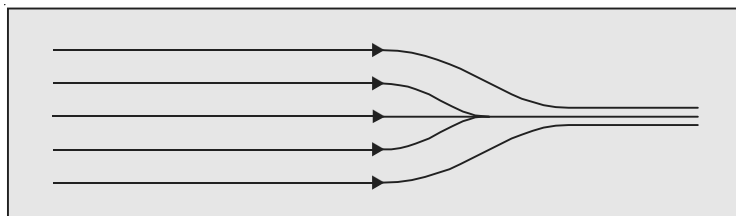


Fig. 13.4 Self-focussing

The distance L_0 over which the beam self-focusses can be approximately estimated using the formula [371],

$$L_0 = \frac{D}{\sqrt{\eta_{nl} E_0^2}} \quad \dots(13.42)$$

where D is the diameter of the beam. Self-focussing occurs when intensity reaches a certain limiting value. This threshold value is estimated from the formula

$$I_{\text{thresh}} = \frac{\lambda^2}{\eta_l^2 \eta_{nl} D^2} \quad \dots(13.43)$$

The formula shows that for higher frequencies and for materials with greater non-linear susceptibilities, the threshold intensity is lower.

Experimental investigations in self-focussing have been carried out in liquids: Carbon disulphide, benzene, acetone, etc., For a beam diameters of $0.5 \mu\text{m}$, the self-focussing distance, is about 10 cm and the observed light fibres were 30 to $50 \mu\text{m}$, in diameter. It has been further established that the observed light fibre has still a finer structure; it consists of a number of still thinner filaments with diameters of about $5 \mu\text{m}$ [371]. Self-focussing, on the whole, is a complicated phenomenon.

14

MULIPHOTON PROCESSES

In the preceding chapter we discussed the problem of non-linear interaction between electromagnetic radiation and matter from semiclassical point of view. We will now reformulate the problem in quantum mechanical terms using the concept of photon stream instead of electromagnetic waves.

By multiphoton process we mean an interaction between radiation and matter accompanied by absorption or emission or both, of not less than two photons per elementary act. Such multiphoton processes were thought of even during the first years of development of quantum mechanics [104,131,149]. However, the experimental techniques available at that time were not adequate to observe the predicted phenomena. Prior to the appearance of lasers, the only two photon processes that could be observed experimentally were Rayleigh and Raman scattering. Multiphoton processes have assumed importance only after the advent of lasers.

14.1 MULTIQUANTUM PHOTOELECTRIC EFFECT

The photoelectric effect consists in ejection of electrons from matter by the action of light. If the energy $\hbar\omega$ of a photon absorbed by an electron inside a material exceeds the work W required to remove an electron from this material (work-function), the electron will leave the material. Its energy after liberation will be

$$\frac{1}{2}mv^2 = \hbar\omega - W. \quad \dots(14.1)$$

The photoelectric effect will, therefore, be observed if

$$\hbar\omega > W. \quad \dots(14.2)$$

The lowest frequency at which the photoelectric effect is observable, viz.

$$\omega_0 = \frac{W}{\hbar} \quad \dots(14.3)$$

is called the *threshold frequency*. The effect has nothing to do with the intensity of the radiation.

Could the photoelectric effect be observed at frequencies lower than the threshold frequency, *i.e.*, for $\omega < \omega_0$? In pre-laser optics the answer to this question would have been in the negative because it was always assumed that electron can absorb only one photon at a time. In the extremely high intensity laser pulses the density of photons is so high that an electron could absorb simultaneously two or more photons—a nonlinear effect. The laws of photoelectric effect, therefore, need reconsideration.

Suppose an electron in a material absorbs N photons at a time. Equation (14.1) then changes to

$$\frac{1}{2}mv^2 = N\hbar\omega - W. \quad \dots(14.4)$$

The photoelectric effect, therefore, can be observed if the condition

$$\omega \geq \frac{W}{N\hbar} \quad \dots(14.5)$$

is satisfied. This gives the threshold frequency

$$\omega_{\text{thresh}} = \frac{W}{N\hbar} \quad \dots(14.6)$$

which is smaller than ω_0 given by (14.3). Thus, higher the light intensity, lower is the threshold frequency. The photoelectric effect, therefore, depends both on the frequency of the radiation as well as on its intensity. It may be called *multiquantum photoelectric effect*.

14.2 TWO-PHOTON PROCESSES

Is it possible to transform a coherent light wave with frequency ω into a coherent light wave with frequency 2ω or 3ω ? Such a conversion, if possible, cannot take place through interaction between photons. There is no direct photon-to-photon interaction. It is indeed true that the general tendency of photons is to occupy a state which is densely populated by other photons. This is the characteristic of all bosonic particles. But it has nothing to do with the concept of direct interaction between photons. A photon cannot absorb or scatter other photons nor does it decay of its own. No known force can mediate interaction between photons. The transformation of photons can be brought about only through an intermediary—a quantum system such as an atom or a molecule characterized by a system of discrete energy levels. An atom or a molecule can absorb or emit photons and in the process may undergo a transition from one energy level to the other.

Consider, for example, a process shown in Fig. 14.1. The atom absorbs energy $\hbar\omega$ and changes from level 1 to level 2. After a shortwhile it returns to level 1 by emitting a photon of the same energy. The state of the atom remains unaltered as far as its energy is concerned; but the emitted photon, although has the same energy as the incident photon, may be in a different state in that it may have a different momentum, direction and polarization. The atom has acted in this transformation as an intermediary.

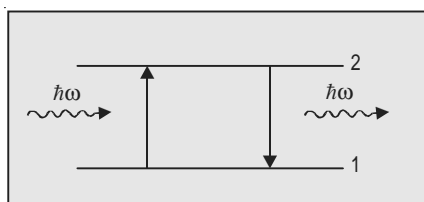


Fig. 14.1 Absorption and emission of a photon—a two level system

Consider now another process (Fig. 14.2). The molecule absorbs a photon of energy $\hbar\omega_{13}$ and shifts from level 1 to level 3 and then emits a photon of energy $\hbar\omega_{32}$ by dropping from level 3 to level 2. In this process photon frequency ω_{13} has been converted into a frequency ω_{32} through the intermediary role played by the molecule; but in this case the state of the intermediary is also changed.

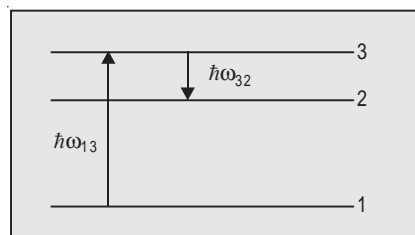


Fig. 14.2 Absorption and emission of a photon—a three

14.3 THEORY OF TWO-PHOTON PROCESSES

In Chapter 3 we used perturbation theory to obtain expression for the rate at which an atom absorbs light. In these calculations we had retained the linear term and neglected the higher order terms on the ground that they are very weak. They are not, however, so weak for light from a laser source. The very high photon flux and the associated high field of radiation enables the atom or molecule to interact with more than one photon at the same time giving rise to a variety of optical processes, such as multiphoton absorption, second harmonic generation, frequency mixing, etc. These multiphoton processes are described by second and higher order approximations of the perturbation theory. We shall illustrate the method by applying it to two-photon absorption. It would be

interesting to note that the possibility of two-photon absorption was first suggested by M. Goeppert-Mayer [149] many years before lasers were thought of.

Let us go all the way back to the perturbation theory of the interaction of radiation with matter, introduced in Chapter 3. We considered there a quantum system described by a time-independent Hamiltonian H_0 , *i.e.*,

$$\hat{H}_0 |\psi, t\rangle = i\hbar \frac{\partial}{\partial t} |\psi, t\rangle \quad \dots(14.7)$$

under the influence of a perturbation whose operator $\hat{H}'(t)$ was of the form

$$\begin{aligned} \hat{H}'(t) &= \hat{H}'^-(t) \text{ if } 0 \leq t \leq \tau \\ &= 0 \text{ if } t < 0 \text{ and } t > \tau \end{aligned} \quad \dots(14.8)$$

The relevant Schrödinger equation was

$$(\hat{H}_0 + \hat{H}'(t)) |\psi, t\rangle = i\hbar \frac{\partial}{\partial t} |\psi, t\rangle \quad \dots(14.9)$$

Assuming the solution of this equation to be a linear combination of basic states $|u_n\rangle$, *i.e.*,

$$|\psi, t\rangle = \sum_n C_n(t) \exp(-i E_n t / \hbar) |u_n\rangle \quad \dots(14.10)$$

and with a few manipulations and calculations we arrived at the equation

$$\frac{d C_m(t)}{dt} = \frac{1}{i\hbar} \sum_{n=0}^{\infty} C_n(t) \langle u_m | \hat{H}'(t) | u_n \rangle \exp(-(i/\hbar)(E_n - E_m)t) \quad \dots(14.11)$$

From this and with the approximation that at $t = 0$, $C_n(t) = 1$ and $C_m(t) = 0$ for all m , we arrived at the relation

$$\frac{d C_m(t)}{dt} = \frac{1}{i\hbar} \langle u_m | \hat{H}'(t) | u_n \rangle \exp(i\omega_{mn}t) \quad \dots(14.12)$$

which, on integration, gave an approximate first-order relation

$$C_m^{(1)}(t) = \frac{1}{i\hbar} \int_0^t \langle u_m | \hat{H}'(t') | u_n \rangle \exp(i\omega_{mn}t') dt' \quad \dots(14.13)$$

The superscript on $C_m(t)$ represents the order of the approximation.

Further, using the fact that the main contribution to the interaction comes from dipole interaction, we put

$$\hat{H}'(t) = \sum_j \mathbf{e} \mathbf{r}_j \cdot \mathbf{E}_0 \cos \omega t \quad \dots(14.14)$$

and obtained the formula

$$C_m^{(1)}(t) = \frac{eE_0 \langle u_m | X | u_n \rangle}{2\hbar}$$

$$\times \left\{ \frac{1 - \exp(i(\omega_{mn} + \omega)t)}{\omega_{mn} + \omega} + \frac{1 - \exp(i(i\omega_{mn} - \omega)t)}{\omega_{mn} - \omega} \right\} \quad \dots(14.15)$$

So far we have recapitulated the treatment given in Chapter 3 for obtaining the first order solution; let us now extend the theory to the second order.

Recall, that equation (14.12) was derived from the general solution (14.11) by putting $C_n(t) = 1$. For extending the theory to the second order, we have to replace $C_n(t)$ by (14.15). Thus

$$\begin{aligned} \frac{dC_l^{(2)}(t)}{dt} &= \frac{1}{l\hbar} \sum_m C_m^{(1)}(t) \langle u_l | \hat{H}'(t) | u_m \rangle \exp(i\omega_{lm} t) \\ &= \frac{1}{i\hbar} \sum_m \frac{eE_0 \langle u_m | X | u_n \rangle}{2\hbar} \\ &\quad \times \left\{ \frac{1 - \exp(i(\omega_{mn} + \omega)t)}{\omega_{mn} + \omega} + \frac{1 - \exp(i(\omega_{mn} - \omega)t)}{\omega_{mn} - \omega} \right\} \\ &\quad \times \langle u_l | \hat{H}'(t) | u_m \rangle \exp(i\omega_{lm} t) \\ &= \frac{1}{i\hbar} \sum_m \frac{e^2 E_0^2 \langle u_l | X | u_m \rangle \langle u_m | X | u_n \rangle}{4\hbar} \\ &\quad \times \left\{ \frac{1 - \exp(i(\omega_{mn} + \omega)t)}{\omega_{mn} + \omega} + \frac{1 - \exp(i(\omega_{mn} - \omega)t)}{\omega_{mn} - \omega} \right\} \times \\ &\quad \times \{ (\exp(i(\omega_{lm} + \omega)t) + \exp(i(\omega_{lm} - \omega)t)) \} \quad \dots(14.16) \end{aligned}$$

where we have put

$$\begin{aligned} \langle u_l | \hat{H}'(t) | u_m \rangle &= \left\langle u_l | \sum_j e\mathbf{r}_j \cdot \mathbf{E}_0 \cos \omega t | u_m \right\rangle \\ &= eE_0 \langle u_l | X | u_m \rangle \left(\frac{e^{i\omega t} + e^{-i\omega t}}{2} \right) \end{aligned}$$

In integrating this equation, we retain only those terms in which the denominator approaches zero; the other terms make no contribution to the accumulating probability. We assume $E_l > E_m > E_n$ which makes ω_{lm}, ω_{mn} , positive. Hence, we retain only the terms in $\omega_{mn} - \omega$ and $\omega_{lm} - \omega$. Thus,

$$\begin{aligned}
C_l^{(2)}(t) &= \frac{1}{i\hbar} \sum_m \frac{e^2 E_0^2 \langle u_l | X | u_m \rangle \langle u_m | X | u_n \rangle}{4\hbar} \\
&\quad \times \int_0^{t'} \left\{ \frac{1 - \exp(i(\omega_{mn} - \omega)t')}{\omega_{mn} - \omega} \right\} \exp(i(\omega_{ln} - \omega)t') dt' \\
&= \frac{1}{4\hbar^2} \sum_m e^2 E_0^2 \langle u_l | X | u_m \rangle \langle u_m | X | u_n \rangle \\
&\quad \times \left[\frac{1 - \exp(i(\omega_{ln} - \omega)t)}{(\omega_{mn} - \omega)(\omega_{ln} - \omega)} - \frac{1 - \exp(i(\omega_{ln} - 2\omega)t)}{(\omega_{mn} - \omega)(\omega_{ln} - 2\omega)} \right] \quad \dots(14.17)
\end{aligned}$$

where we have used the relation $\omega_{ln} = \omega_{mn} + \omega_{lm}$.

We notice that in second order, a resonance appears at $\omega_{ln} = 2\omega$ corresponding to a two-photon absorption process. The probability of the two-photon processes occurring is given by $|C_i^{(2)}(t)|^2$ in which only the second term in the brackets is relevant.

$$\begin{aligned}
\therefore P_{n \rightarrow l}^{(t)} &= |C_l^{(2)}(t)|^2 = \sum_m \frac{e^4 E_0^4 |\langle u_l | X | u_m \rangle \langle u_m | X | u_n \rangle|^2}{16\hbar^4 (\omega_{mn} - \omega)^2} \\
&\quad \times \frac{4t \sin^2(\omega_{ln} - 2\omega)t/2}{(\omega_{ln} - 2\omega)^2 t} \quad \dots(14.18)
\end{aligned}$$

\therefore The rate of two-photon absorption is

$$= \sum_m \frac{\pi e^4 E_0^4 |\langle u_l | X | u_m \rangle \langle u_m | X | u_n \rangle|^2}{8\hbar^4 (\omega_{mn} - \omega)^2} \delta(\omega_{ln} - 2\omega) \quad \dots(14.19)$$

where we have used the relation

$$\delta(\omega_{ln} - 2\omega) = \frac{2}{\pi} \lim_{t \rightarrow \infty} \frac{\sin^2(\omega_{ln} - 2\omega)t/2}{(\omega_{ln} - 2\omega)^2 t}. \quad \dots(14.20)$$

The appearance of the intermediate states in the above formula reflects the possibility of attaining the final state via a series of intermediate states, which are connected with the initial and final states by non-zero matrix elements. In each transition the system absorbs or emits one photon. The transition $n \rightarrow l$ represented by the formula (14.19) is, therefore, a two-photon process (Fig. 14.3). It must be emphasized here, however, that this transition, or for that matter any multiphoton transition, cannot, in principle, be divided into a temporal sequence of events. It should be understood that both photons are absorbed simultaneously. It would be incorrect to assume that first one photon

is absorbed and then the other. In such a case the transition would be equivalent to two single photon transitions and not one two-photon transition.

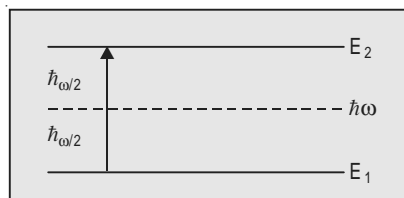


Fig. 14.3 Two-photon absorption

Two important features of two-photon absorption need be mentioned here:

- (i) We know that a single photon absorption occurs between states of opposite parity. In a nonlinear medium a two-photon absorption, such as the one shown in Fig. 14.3, occurs between states of the same parity. That is, a transition that is forbidden for one-photon absorption is allowed for two-photon absorption.
- (ii) Formula (14.19) shows that the probability of two photon absorption is proportional to the fourth power of the electric field, *i.e.*, to the square of the intensity.

14.4 EXPERIMENTS IN TWO-PHOTON PROCESSES

14.4.1 CaF₂: Eu⁺⁺ Crystals

The two-photon absorption was observed for the first time in CaF₂ crystals activated with divalent europium, Eu⁺⁺ replacing Ca⁺⁺ ions [Kaiser *et al.*, 206]. The radiation from a ruby laser was focussed on a thin (0.1 mm) slab of a CaF₂: Eu⁺⁺ crystal, placed in front of the entrance slit of a spectrograph. Two red filters with transmission less than 10⁻⁴ for $\lambda < 6100 \text{ \AA}$ were placed in front of the crystal so as to exclude the possibility of blue or ultraviolet radiation from the pump lamp falling on the crystal. Since the lowest lying energy level in the CaF₂: Eu⁺⁺ crystal corresponds to an energy of 22,000 cm⁻¹, the crystals are transparent to the radiation from a ruby laser which corresponds to 14,400 cm⁻¹.

With the arrangement described above, the spectrographic record showed, besides a line at $\lambda = 6943 \text{ \AA}$ emitted by the ruby laser, a line at $\lambda = 4250 \text{ \AA}$. When inactivated CaF₂ crystal was illuminated with the same laser, no radiation at $\lambda = 4250 \text{ \AA}$ was observed. The line at this wavelength, therefore, must be attributed to the transition of Eu⁺⁺ ions. It was further found that the fluorescence intensity was proportional to the square of the laser emission intensity, thus, suggesting that the line at 4250 Å is, probably, a result of a two-photon process.

It is known that $\text{CaF}_2 : \text{Eu}^{++}$ crystals have an intense absorption band between 30,000 and 25,000 cm^{-1} , corresponding to electron transition $4s \longleftrightarrow 5d$ of Eu^{++} ions. When the crystal is excited with the light in the same wavelength range, a bright blue fluorescence is observed with a band width $\sim 300 \text{ \AA}$ near 4200 \AA . This fluorescence is interpreted as a result of non-radiative transition of Eu^{++} from the upper state into an intermediate lower state with subsequent emission as the ions undergo a transition to the ground state. The observation made in the above experiment was, therefore, interpreted as excitation by two photon absorption to the state $5d$, followed by non-radiative and radiative transitions as above. A simplified analysis of this process was given by Kleinman [217] where it is assumed that the two-photon transition proceeds via an intermediate state connected with the initial and final states.

14.4.2 Cesium Vapour

Two-photon absorption in an atomic system was first observed by Abella [1], on exciting cesium vapour with ruby laser. The two main requirements for the two-photon absorption are: (i) the energy for lifting the atom to the excited level should be double the energy of exciting photon, and (ii) the initial and final states should have the same parity. Both these conditions are satisfied in the case of cesium. The transition to $9D_{5/2}$ and $9D_{3/2}$ levels of cesium correspond to energies 28,836.06 and 28,828.90 cm^{-1} respectively, which is close to double the energy of the ruby laser ($\sim 14,400 \text{ cm}^{-1}$) and their parity is the same as that of the initial state. Figure 14.4 shows the various levels involved in the process.

A very elementary experimental set up was used for this investigation. The radiation from a ruby laser was focussed on a cell containing cesium vapour. The fluorescence light, filtered out with a CuSO_4 solution and with a narrow-band interference filter, was detected by a photomultiplier, at right angles to

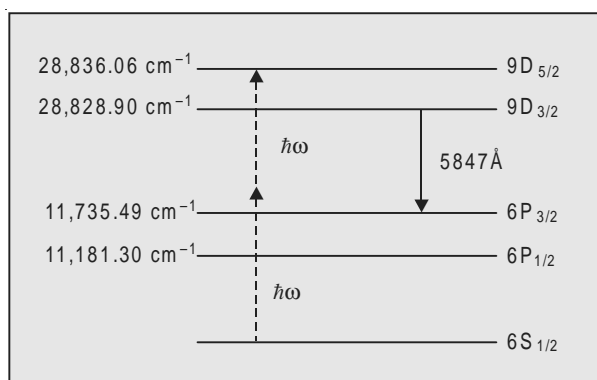


Fig. 14.4 Energy level scheme for Cs atom

the direction of the laser beam. It was established before hand that in the absence of cesium vapour, no fluorescence could be observed in the range of

wavelengths of the laser. With cesium, fluorescence line was observed at $\lambda = 5847 \text{ \AA}$ corresponding to the transition $9D_{3/2} - 6P_{3/2}$. The line appeared only when the central wavelength in the laser emission was equal to $6935.5 \pm 0.05 \text{ \AA}$. This dependence of the fluorescence on the wavelength of the laser emission indicates the occurrence of two-photon absorption.

14.4.3 Anthracene

Two-photon excitation of fluorescence in anthracene single crystals was observed by Peticolas *et al.* [305] and Singh *et al.* [351]. The light beam from a ruby laser was focussed on the slabs of anthracene ranging in thickness from 100μ to 20 m, cut from a single crystal of anthracene. The spectrum observed (Fig. 14.5) on a grating spectrograph was found to be exactly similar to the one obtained when the crystal was excited by radiation of wavelength larger than 3800 \AA and corresponding to the transition from the excited $^1B_{2u}$ state to the ground state 1A_g . The excited $^1B_{2u}$ state lies at about $28,800 \text{ cm}^{-1}$ which is close to double the energy of the ruby laser. The state was not observed in the case of a single-photon excitation because it has the same parity as that of the ground state, but its existence was predicted theoretically. The observed quadratic dependence of the fluorescence intensity on the intensity of the exciting laser radiation can serve as an argument in favour of the two photon mechanism of excitation.

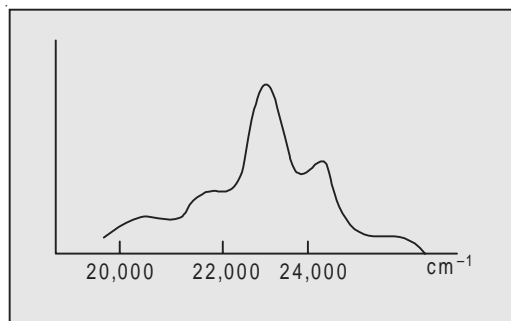


Fig. 14.5 Fluorescence spectrum of anthracene

14.4.4 KI

A different experimental technique was used by Hopfield *et al.* [192] in their study of two photon absorption in KI crystals. The experimental set up is shown in Fig. 14.6. The sample used measured $2 \times 3 \times 25 \text{ mm}$.

As shown in the figure, two light sources were used, a ruby laser with pulsed energy approximately 15 J and a xenon lamp giving continuous spectrum in the ultraviolet. A measure of the two-photon absorption was the decrease in

the xenon lamp radiation transmitted through the sample, under the action of the laser pulse.

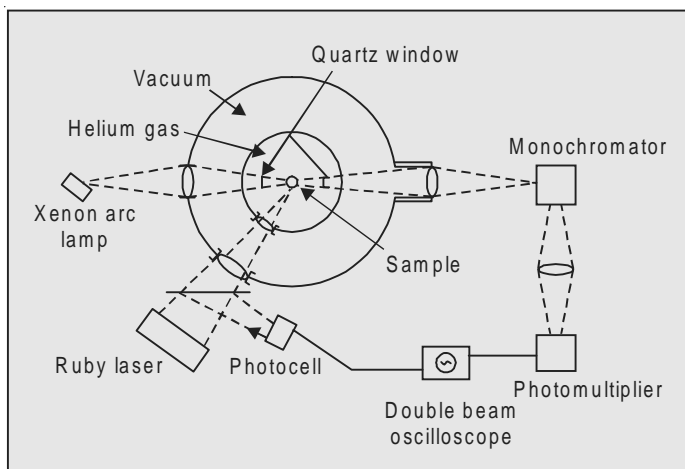


Fig. 14.6 Experimental arrangement for two-photon absorption in KI crystal

14.4.5 Two-Photon Effect in a Semiconductor

The internal two-photon photoeffect in a semiconductor which consists in exciting electrons from the valence band to the conduction band, was observed by Braunstein and Ockman [65] in CdS, using a ruby laser. The energy gap in the semiconductor being 2.4 eV, the energy of a photon of the ruby laser (1.8 eV) is insufficient to excite the electrons in the conduction band. The semiconductor, therefore, is transparent to the source with this wavelength. Two-photon excitation of electrons in the conduction band was detected by observing recombination emission from the excitation and the impurity levels, arising as a result of two-photon excitation. The intensity of the recombination emission has exhibited a quadratic dependence on the excitation intensity and its order of magnitude is close to that predicted theoretically.

14.4.6 Two-Photon Ionization

The possibility of two-photon ionization of atoms is of considerable interest both from the theoretical and experimental points of view. Such an effect can be observed in the negative ions I^- , Br^- and F^- which have an ionization potential sufficiently low for two-photon excitation with the aid of a ruby laser [Coltman, 81].

14.5 VIOLATION OF THE SQUARE LAW DEPENDENCE

Bradley *et al.*, [63, 64] observed that in rhodamine B, at high laser intensities or photon fluxes, the fluorescence intensity does not show the expected square law dependence on the laser intensity. Similar investigations by Eichler *et al.*, [110] in rhodamine G show that up to incident intensities of 6×10^{28} photon $\text{cm}^{-2} \text{ sec}^{-1}$, the two-photon fluorescence intensity showed a quadratic dependence on the photon flux. At higher photon flux it increased less than quadratically with the increase of excitation intensity. The possible mechanism suggested by them for this quenching is stimulated Raman scattering, since it was observed that the two-photon fluorescence quenching and the stimulated anti-Stokes emission had thresholds in the same power range.

14.6 DOPPLER-FREE TWO-PHOTON SPECTROSCOPY

The feasibility of Doppler-free two-photon spectroscopy was shown in 1974, independently, by Bernard Cagnac (France), Bloembergen and Levenson (Harvard) and Hansch, Maisel, Harrey and Schawlow (Stanford). In this form of high resolution non-linear laser spectroscopy, gas atoms in a standing wave field are excited by absorbing two photons from opposite directions. Their first-order Doppler shifts are equal and opposite and, hence, the sum frequency is unchanged. (See Chapter 15, Sec. 15.10).

14.7 MULTIPHOTON PROCESSES

In Section 14.2 we derived an expression for two-photon absorption. The general expression for the transition rate from the initial state $|i\rangle$ to the final state $|f\rangle$ is

$$R_{i \rightarrow f} = \frac{2\pi}{\hbar^2} \left| \langle f | \hat{H}' | i \rangle + \frac{1}{\hbar} \sum_l \frac{\langle f | \hat{H}' | l \rangle \langle l | \hat{H}' | i \rangle}{\omega_i - \omega_l} \dots \right. \\ \left. + \frac{1}{\hbar^{n-1}} \sum_{l_1} \sum_{l_2} \dots \sum_{l_{n-1}} \frac{\left| \langle f | \hat{H}' | l_1 \rangle \langle l_1 | \hat{H}' | l_2 \rangle \dots \langle l_{n-1} | \hat{H}' | i \rangle \right|^2}{(\omega_i - \omega_{l_1})(\omega_i - \omega_{l_2}) \dots (\omega_i - \omega_{l_{n-1}})} \times \delta(\omega_i - \omega_f) \right| \dots \quad (14.21)$$

If we are considering a simple absorption or emission of a photon, only one photon state is changed and only the first order term suffices. It represents the rate of direct transition from state $|i\rangle$ to state $|f\rangle$. For the two-photon

absorption process second order term is required. The higher order terms also represent transition from the initial state $|i\rangle$ to the final state $|f\rangle$; but the transitions are via one or more intermediate states.

It may be noted that the presence of the delta-function ensures conservation of energy between the initial and the final states, but not necessarily in the case of intermediate states. The intermediate states are called *virtual states* of transition. In multiphoton transitions it is necessary to resort to this concept of “virtual levels”. How does a virtual level differ from a real level? A microscopic object can always be observed on any really existing level. A multiphoton transition cannot be separated in time in different stages and, hence, the microscopic object working as an intermediary, cannot be observed on a virtual level. The system passes through the intermediate states only in a virtual sense. There is no need, therefore, for energy to be conserved in the intermediate states since no real transitions are made into them.

14.8 THREE-PHOTON PROCESSES

For a three-photon process we have to consider the third term in (14.21). The matrix elements in this term indicate that the fluorescence resulting from three-photon absorption must be proportional to the cube of the laser output. The simultaneous absorption of three-photons was demonstrated by Singh and Bradley [352]. Substantial ion yields were observed by Harrison *et al.*, [172] when CH_2I_2 was excited by 248 and 193 nm. The yield was found to increase with the third power of the laser intensity, thus suggesting that three-photon excitation is required for ion formation.

14.9 SECOND HARMONIC GENERATION (SHG)

Second harmonic generation is a three-photon process as shown in Fig. 14.7. Two photons, each with energy $\hbar\omega$, are absorbed and one photon with energy $2\hbar\omega$ is emitted. The state of the quantum system remaining unaltered. This gives an impression that two colliding photons merge ‘directly’ into a single one. The levels shown in the figure by dotted lines are the “virtual levels.”

We have shown in the preceding chapter that for efficient transfer of light energy from the pumping wave to the secondary wave the condition of “*wave synchronism*” has to be satisfied. That is, the pumping wave parameters, should match with those of the secondary wave. In photon terms this condition is equivalent to the energy-momentum conservation laws to be satisfied by the photons participating in the process.

$$\hbar\omega + \hbar\omega = 2\hbar\omega \quad \dots(14.22)$$

$$P_1 + P_2 = P \quad \dots(14.23)$$

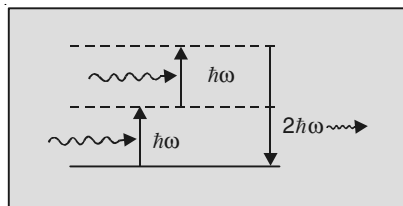


Fig. 14.7 Second harmonic generation

Assuming that the directions of the pumping wave and the secondary wave are the same, we can write (14.23) in the scalar form

$$2p_1 = p. \quad \dots(14.24)$$

Since $p = \frac{h\omega}{c} \eta(\omega)$, the above relation becomes

$$\frac{2h\omega}{c} \eta(\omega) = \frac{h(2\omega)}{c} \eta(2\omega) \quad \dots(14.25)$$

i.e.,

$$\eta(\omega) = \eta(2\omega) \quad (\text{Sec. 13.21}) \quad \dots(14.26)$$

14.10 PARAMETRIC GENERATION OF LIGHT

In terms of photon concepts, the parametric generation of light can be explained with the help of (Fig. 14.8). It shows a three-photon process in which one photon of energy $\hbar\omega$ is absorbed by the microscopic system and two photons, one with energy $\hbar\omega_1$ and the other with energy $\hbar\omega_2$ are emitted, the state of the microscopic system remaining unaltered, indicating, as if, a photon has decayed into two new secondary photons. The energy-momentum conservation laws to be satisfied are

$$\hbar\omega = \hbar\omega_1 + \hbar\omega_2 \quad \dots(14.27)$$

$$\mathbf{p} = \mathbf{p}_1 + \mathbf{p}_2 \quad \dots(14.28)$$

The process describes the “transformation” as we may call it, of a light wave with frequency ω into two new light waves of frequency ω_1 and ω_2 .

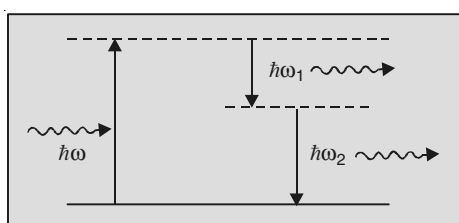


Fig. 14.8 Parametric generation of light

14.11 PARAMETRIC LIGHT OSCILLATOR

To obtain high power by parametric amplification, a uni-axial crystal with relatively high nonlinear susceptibility, cut according to the requirement of the wave-synchronism, is placed inside an optical resonator. A laser is used for pumping the parametric amplifier. The intensity of the pumping wave must be high enough to bring out the nonlinear properties of the crystal and to compensate for the losses that may occur. The mirrors of the resonator must have high reflectances for ω_1 and $\omega_2 = \omega - \omega_1$, but high transmittance for the laser frequency ω . The parametric amplifier, under these conditions, goes into oscillations at both frequencies ω_1 and ω_2 . The process is known as *parametric oscillation*.

The most promising use of a parametric oscillator is that it provides a tunable source of coherent radiation. Parametric processes have been widely used to generate tunable laser light [357]. Tuning of a parametric light oscillator can be effected by controlling the frequency of the secondary waves generated. There are several methods of controlling the frequency. One of these is to rotate the crystal in such a way that different frequencies are phase-matched. The other is to vary the crystal temperature. Since the refractive index is a function of temperature, the change in temperature will affect the shape of the refractive index surfaces corresponding to the ordinary and extraordinary waves and thus, will lead to the change in the direction of wave-synchronism for any fixed combination of frequencies.

A schematic diagram for a typical optical parametric oscillator is shown in (Fig. 14.9).

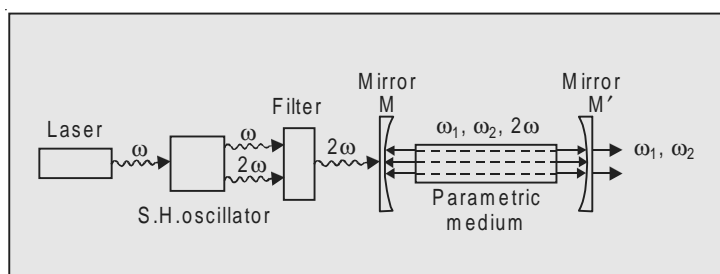


Fig. 14.9 Optical parametric oscillator

Intense pumping light at frequency ω from a *Q*-switched laser passes through a SH oscillator producing a second harmonic radiation at frequency 2ω . A filter F eliminates the fundamental and allows only the second harmonic to pass into the parametric medium P . The radiations at ω_1 and ω_2 build up in P . The mirror M allows radiation at 2ω to pass into the medium, but reflects those at ω_1 and ω_2 , while the mirror M' reflects the pumping light at 2ω back into the medium, but allows a portion of ω_1 and ω_2 to emerge. The medium P is placed in an oven which makes it possible to change the temperature.

In order that it produces only one wave, sometimes a Glan prism is introduced in the cavity between the crystal and the output mirrors. The prism passes one wave but deflects the other.

Parametric oscillations have been tuned across the visible and near infrared region in LiNbO_3 when pumped at the second harmonic of the $1.06 \mu\text{m}$ Nd: YAG laser [Bjorkholm *et al.*, 48, Falk *et al.*, 121].

14.12 FREQUENCY UPCONVERSION

Parametric amplification can also be used to convert from a low frequency to a higher one. Suppose two collinear beams with frequencies ω_1 and ω_2 are incident on a nonlinear crystal. If the crystal is phase matched for these frequencies as well as the sum frequency $\omega = \omega_1 + \omega_2$, this third frequency is generated. This process is known as *frequency upconversion*.

The processes of SHG and frequency mixing can be combined to produce beams of higher frequencies. As an example, consider the scheme shown in Fig. 14.10.

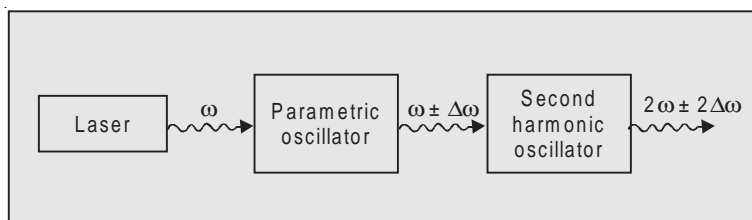


Fig. 14.10 Frequency upconversion

The laser emits a coherent light wave with frequency ω . This wave serves as the pumping wave for the parametric oscillator which emits radiation that can be continuously tuned in the range $\omega_1 - \Delta\omega$ to $\omega_1 + \Delta\omega$. This in turn serves as a pumping wave to SH oscillator. What emerges is a coherent radiation with frequency continuously tunable from

$$2\omega_1 - 2\Delta\omega \text{ to } 2\omega_1 + 2\Delta\omega$$

Consider now another example (Fig. 14.11).

The light at frequency ω from a laser, after passing through two SH oscillators is converted into light with frequency 4ω . Mixing this fourth harmonic with ω with the aid of a parametric oscillator, we get a fifth optical harmonic. It must be noted that at each conversion some portion of the energy is lost.

14.13 PHASE-CONJUGATE OPTICS

One of the new research areas in coherent optics which is receiving increasing attention is what is known as *phase-conjugate optics*. Its main feature is the generation of an electromagnetic wave with a phase distribution, that is, at each point in space, the exact opposite of that of an arbitrary incoming wave and

which propagates in the opposite direction, retracting the original path of the incoming wave.

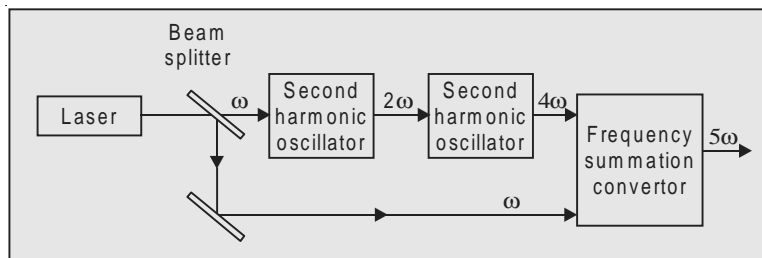


Fig. 14.11 Fifth optical harmonic

Suppose a beam with a plane wavefront emitted by a laser, traverses an active material and then is reflected backwards by a plane mirror. As the beam passes through the material, it undergoes wavefront distortions. The distorted wavefront would be somewhat like the one shown in Fig. 14.12(a) [373]. The

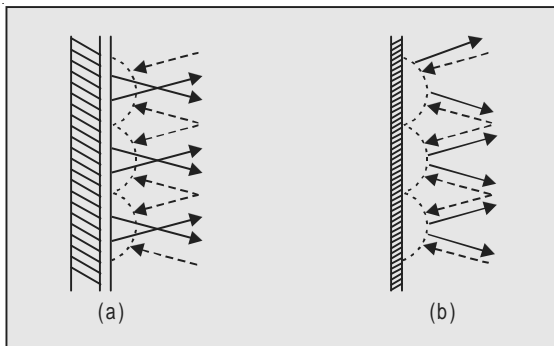


Fig. 14.12 Phase conjugation

rays, normal to the wavefront and incident on the mirror, are shown by dotted lines and those reflected according to the law of reflection by solid lines. If now the plane mirror is replaced by a reflecting surface which has the same shape as the oncoming wavefront, the reflected rays will experience a turn of 180° as shown in Fig. 14.12(b) and, thus, a reversal of the wavefront will occur. That is, the reversed rays acquire the conjugate phases and, hence, the process is known as *phase conjugation*. If such a phase-conjugated reversal is brought about in systems used with lasers, the beam, upon a round trip through the active material, will regain the same wavefront it had in its forward trip, thus resulting into a more powerful beam. The question is how to prepare such an adaptive system?

Let us discuss briefly the basic approaches proposed for phase conjugation. Yariv [409-10] proposed the use of three wave mixing for this purpose.

A wave E_1 at frequency ω and a wave vector \mathbf{k}_1 (ω) and another intense pump wave E_2 at a frequency 2ω and a wave vector \mathbf{k}_2 (2ω) are incident

simultaneously on the crystal. If the crystal is lacking in inversion symmetry, in addition to the linear polarization, a second order nonlinear polarization proportional to $E_1^* E_2$ occurs in it (See Chapter 13), which acts as a source that radiates a third wave E_3 , at the difference frequency $2\omega - \omega = \omega$ with the wavevector $\mathbf{k}_3(\omega)$ and with a spatial amplitude distribution proportional to $E_1^* E_2$. Effective transfer of energy from E_2 to E_3 is possible only if the phase matching condition

$$\mathbf{k}_3(\omega) = \mathbf{k}_2(2\omega) - \mathbf{k}_1(\omega) \quad \dots(14.29)$$

is satisfied. If E_2 is a plane wave, E_3 becomes conjugate replica of E_1 . If (14.29) is not satisfied, the wavefronts of E_3 , at different regions of the crystal, do not add up in phase and the amplitude of E_3 is reduced due to the destructive interference. Phase conjugation using this technique was demonstrated by Avizonis *et al.* [19].

Four wave mixing was first demonstrated experimentally by Terhune and his collaborators. Bloembergen and his collaborators have studied four wave mixing systematically as a function of the three frequencies in many different materials and obtained their dispersive character. Subsequently they used four light beams of almost equal frequency to show the effect of collision-induced coherence—apparently a paradoxical behaviour since collisions are known to destroy coherence.

Hellworth [183] showed that phase-matching condition that is inherent in the three wave mixing is eliminated in the *degenerate four wave mixing*. All the four optical fields involved in this mixing process are of the same frequency ω ; hence the name degenerate. Briefly, the mixing process can be explained as follows: Suppose two intense pump waves E_1 and E_2 , both at frequency ω , illuminate a nonlinear medium. The waves chosen for this purpose are counterpropagating plane waves so that their wavevectors $\mathbf{k}_1(\omega)$ and $\mathbf{k}_2(\omega)$ add up to zero. An arbitrary input wave, also at frequency ω , but with a wavevector $\mathbf{k}_4(\omega)$, is now incident on the medium (Fig. 14.13). Resulting third order nonlinear polarization radiates to give a field E_3 , also at frequency ω but with a wavevector

$$\mathbf{k}_3(\omega) = \mathbf{k}_1(\omega) + \mathbf{k}_2(\omega) - \mathbf{k}_4(\omega) = -\mathbf{k}_4(\omega) \quad \dots(14.30)$$

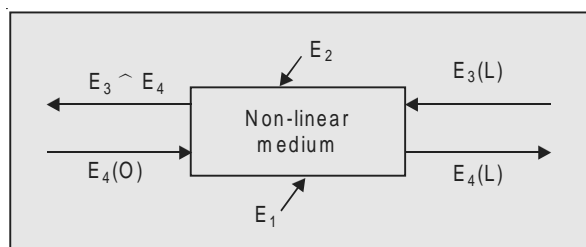


Fig. 14.13 Four wave mixing

The phase matching condition is thus, automatically satisfied.

The backward-going wave E_3 , in turn combines with the two pump wave E_1, E_2 to induce a third order polarization with amplitude distribution proportional to $E_1 E_2 E_3^*$, which radiates into E_4 . The counterpropagating conjugate pair, E_3 and E_4 are thus coupled through the nonlinear polarization and are amplified simultaneously, energy for which is provided by the pump waves E_1 and E_2 .

The nonlinear medium in the case considered may be viewed as a conjugate mirror, reflecting an arbitrary wave E_4 to give backward a wave $E_3 \propto E_4^*$. The reflected wave is a time-reversed replica and retraces the exact path of the incident wave. In a conventional mirror, the reflected wave will take a course dictated by the laws of reflection. The difference between the conjugate mirror and a conventional one, is brought out very clearly in the following illustration given by AuYeung and Yariv [18] (Fig. 14.14 (a), (b)).

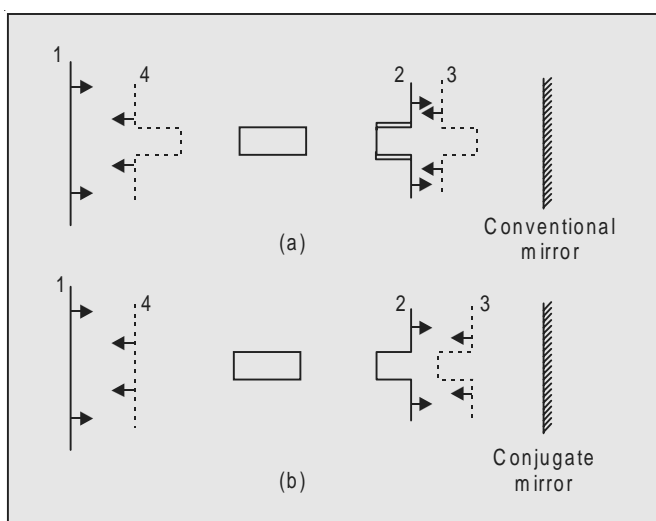


Fig. 14.14 Reflected wave-fronts from the conventional and the conjugate mirror

In Fig. 14.14(a), a plane wave (1) incident upon a distorting medium emerges with a bulge (2). The wave (3) reflected from a conventional mirror traverses the medium in reverse, resulting in a doubling of the bulge depth.

Consider now Fig. 14.14 (b)]. The reflected wave front (3) in this case is identical to the incident wave (2) and when it emerges out of the medium, there is a perfect smoothing of the bulge and the wave front becomes identical with (1).

Considerable amount of work has since been done in the field of phase-conjugation. Amplified phase-conjugation spectrum and parametric oscillation were demonstrated by Bloom *et al.*, [56] and by Pepper *et al.*, [303]. It may be noted that coherent anti-Stokes Raman scattering (CARS), discussed in the next chapter, is an example of four wave mixing.

INDEX

- Absolute rotation of the earth 255
Absorption coefficient 67
Ammonia maser 46
Annihilation operator 26
Anthracene 211
Anti-Stokes lines 224
Argon bomb 105
Argon ion laser 119
Artificial earth satellite 262
Atomic absorption coefficient 67
Atmospheric optics 264
Atomic cross-section 68
Axial modes 85
- Bleachable absorbers 169
Bohr radius 21
Boltzmann distribution 9
Brewster angle 115
Brillouin scattering 233
Bromine laser 159
- C³ laser 147
CaF₂: Eu⁺⁺ Crystals 209
CaF₂: U³⁺ 106
Cesium vapour 210
Charge transfer ionization 122
Chemical laser 154
Chemical pumping 79
- Closure theorem 38
CO chemical laser 158
Coaxial-cable system 261
Coherence 6, 57
longitudinal 59
spatial 58
temporal 58
transverse 59
degree of 59
length 60
time 59
Coherence and the size of the source 60
Coherence Anti-Stokes Raman scattering (CARS) 228
Coherence length for the second harmonic radiation 196
Coherent-state description of the electromagnetic field 34
Collision broadening 72
Communication by lasers 261
Condition for laser action 140
Confocal mirror systems 115
Confocal resonator 88
CO₂ laser 123
Counting of atoms 256
Creation operator 26
Critical inversion 93

- Degree of coherence 59
DF:CO₂ laser 157
Dielectric susceptibility 192
Directionality 3
Distributed feedback laser 180
Doppler broadening 69, 74
Doppler-free two photon spectroscopy 213, 238
Dye lasers 150
- Einstein coefficients 8
Electric dipole interaction 20
Electric pumping 79
Electroionization laser 128
Electromagnetic potentials 29
Electrostatic focuser 48
Ether drift 255
Excimer laser 133
- Fluorescence quantum yield 95
Fock states 29
Four wave mixing 219
Free electron laser 230
Frequency upconversion 217
Fringe visibility 59
Füchbauer Ladenburg formula 67
- Gamma ray laser 182
Gas-dynamic laser 129
Gas-dynamic pumping 79
Gas lasers 111
Gas lens 262
Gaussian lineshape 75
Giant pulse 160
Giant pulse dynamics 165
- Half width 66
Hamiltonian for the total electromagnetic field 33
Harmonic generation 191
HCl laser 155
HCN laser 127
He:Cd laser 121
- He:Ne laser 112
He:Se laser 122
HF laser 156
H₂ laser 132
Hole burning 177
Holography 183
applications of 189
Ho³⁺: YLF laser 110
Homogeneous broadening 69
Hydrogen maser 50
Hyper-Raman effect 225, 226
Hyper Rayleigh scattering 226
- Indicatrix 197
Induced emission 10
Injection laser 143
Injection laser threshold current 144
Interaction of radiation with matter 16, 38
Interaction Hamiltonian 38
Interference and waves 55
Intrinsic broadening 69
Intrinsic semiconductor 137
Intrinsic semiconductor laser 137
Inversion threshold pumping rate 83
Ion lasers 119
Isolators 170
Isotope separation 257
- Kerr effect 161
KI 211
Kinetics of optical absorption 64
Krypton ion laser 121
k-space 85
- Lamb dip 179
Landau levels 229
Landau splitting factor 229
Lasers:
Argon ion 119
Bromine 158

- C³ 147
CaF₂:U³⁺ 106
Chemical 154
CO chemical 154
CO₂ 123
Copper vapour 117
DF:CO₂ 157
Distributed feedback 180
Dye 150
Electroionization 128
Excimer 133
Free electron 230
Gamma ray 182
Gas 111
Gas dynamic 129
HCN 127
HCl 155
He:Cd 121
He:Ne 112
He:Se 122
HF 156
H₂ 132
Ho³⁺:YLF 110
Injection 143
Intrinsic semiconductor 137
Ion 119
Krypton ion 121
Liquid 148
Mercury ion 121
Metal vapour 121
Molecular gas 123
Nd:glass 108
Nd:YAG 107
N₂ 130
Ruby 97
Semiconductor 135
Solid state 97
Spin-flip 229
Superradiant 118, 130
TEA 127
Vibronic 130
Laser action condition for 140
Laser amplifier 169
Laser cooling and trapping of neutral atoms 250
Laser fluorescensors 264
Lasers in:
Astronomy 265
Biology 265
Chemistry 261
Medicine 265
Industry 266
Laser induced collisions 242
Laser induced phenomena 240
Laser pumping 79
Laser ranging 264
Laser ranging retro-reflector 3
Laser spectroscopy 221
Lidar 265
Life-time 13
Line broadening mechanism 69
Line shape function 68
Longitudinal modes 85
Lorentz line shape 70
Losses inside the cavity 90
Magnetic field 53
Masers 45
Ammonia 46
Hydrogen 50
Mechanical shutter 161
Mercury ion laser 121
Metal vapour laser 121
Microwave amplifier 50
Microwave radio relay 262
Microwave spectrometer 50
Mode locking 170
Mode pulling 173
Modulation of an electron wave by a light wave 240
Molecular gas lasers 123
Momentum transfer 12
Monochromacity 5, 64
Multi-photon ionization 247
Multiphoton processes 203, 213
Multiplexing 262

- Multiquantum photoelectric effect 203
- Natural broadening 69
- Nd:Glass laser 108
- Nd: YAG laser 107
- N_2 laser 130
- Noise 54
- Nonhomogeneous broadening 69
- Non-linear medium 193
- Non-linear optics 191
- Non-linear susceptibility 192
- Non reciprocal isolator 169
- Number of modes per unit volume 85
- Number operator 27
- Occupation number state 29
- Open resonator 87
- Optic fibres 263
- Optical mixing 198
- Optical processes, theory of 55
- Optical pumping 79
- Pair excitation 242
- Parametric generation of light 200, 215
- Parametric light oscillator 216
- Peak power emitted during a pulse 164
- Penning ionization 121
- Perturbation theory 17
- Phase coherence factor 63
- Phase conjugate optics 217
- Phase matching 197
- Photo-acoustic Raman spectroscopy (PARS) 232
- Photo-deflection method 257
- Photoelectric effect 203
- Plasma 259
- Planck's formula 5, 10
- Pockell's effect 161
- Polarizability 192
- Population inversion 79
- Principle of superposition 55
- Pulsed maser 52
- Pumping power 101
- Pumping rate 80
- Q-switching 160
- Quality factor 49, 89
- Quantization of the field 29
- Quantum electrodynamics 26
- Quantum noise 14
- Quantum yield 95
- Quasi-fermi level 142
- Raman scattering 221
- Ranging 264
- Rayleigh range 3
- Rayleigh scattering 221
- Reflection coefficient 91
- Resonance frequency 68, 87, 88
- Resonator 83
- active 83
 - confocal 89
 - open 87
 - passive 83
- Ruby laser 97
- Saturation 67, 169
- Saturated absorption spectroscopy 235
- Schawlow-Townes condition 93
- Second harmonic generation 193, 214
- Second quantization 39
- Self-focussing of light 200
- Self-terminating laser pulse 118
- Semiclassical electrodynamics 16
- Semiconductor lasers 135
- Shape of spectral lines 68
- Single atom detection 248
- Solid state lasers 97
- Solid state masers 54

- SONRES 249
Spiking 105
Spin-flip Raman laser 229
Spontaneous emission 10
Stimulated absorption 65
Stimulated Brillouin scattering 229
Stimulated emission 10
Stimulated Raman effect 223
Superradiant 130
Super-radiant lasers 118, 130
- TEA laser 127
Temporal coherence 57, 59
Theory of some optical processes 55
Thermonuclear fusion 259
Third harmonic generation 198
Three level laser system 81
Three level maser system 52
Three wave mixing 218
Three-photon processes 214
Threshold condition 90
Threshold condition for oscillation 49
Threshold current 144
Threshold frequency 204
Transverse coherence 59
Transverse electromagnetic modes 84
Two level laser system 79
Two level maser system 46
- Two photon effect in a semiconductor 212
Two photon ionization 212
Two photon processes 204 experiments with 209 anthracene 211 $\text{CaF}_2:\text{Eu}^{++}$ 209 Ce 210 KI 211 semiconductor 212
- Ultra-short light pulses 173
Unsaturated gain coefficient 92
- Vacuum state 33
Vibrational modes of a resonator 83
Vibronic lasers 130
Violation of the square law dependence 213
Virtual states 214
Visibility and the size of the source 62
- Waves and interference 55
Wave-guide 262
Wave synchronism 214
Width of a spectral line 68
Wien's radiation law 11
- Zero point energy 33

APPENDIX B

CONVERSION FACTORS FOR ENERGY UNITS

Unit	erg	eV	cal/mole	cm^{-1}
erg	1	6.2418×10^{11}	1.4395×10^{16}	5.0346×10^{15}
eV	1.6021×10^{-12}	1	2.3063×10^4	8.0660×10^3
cal/mole	6.9466×10^{-17}	4.3359×10^{-5}	1	0.34973
cm^{-1}	1.9862×10^{-16}	1.2398×10^{-4}	2.8592	1

APPENDIX A

PHYSICAL CONSTANTS

Velocity of light	2.99792×10^8 m/sec
Planck's constant	6.62619×10^{-34} J sec
Electron charge	1.602×10^{-19} coul
Electron mass	9.1095×10^{-31} kg
Proton mass	1.6726×10^{-27} kg
Atomic mass unit (amu)	1.6605×10^{-27} kg
Boltzmann constant	1.381×10^{-23} J/K
Bohr radius	5.292×10^{-11} m
Avogadro number	6.0235×10^{22} mole ⁻¹
Permittivity of free space	8.85418×10^{-12} farads/m

15

LASER SPECTROSCOPY

It is not possible to cover all the fields of spectroscopy in a chapter of a limited size. We, therefore, intend to restrict our discussion to light scattering and saturation-spectroscopy, since the introduction of laser as a source of excitation has revolutionized these fields.

15.1 RAYLEIGH AND RAMAN SCATTERING

When a monochromatic radiation of frequency ν_0 is passed through a non-absorbing medium, it is found that most of it is transmitted without any change, and some of it is scattered. If the scattered energy is analysed by means of a spectrometer, the bulk of the energy is found at the frequency of the incident beam ν_0 , but a small portion of the scattered energy will be found at frequencies $\nu' = \nu_0 \pm \nu_M$. The displaced frequencies are associated with transitions between rotational, vibrational and electronic levels of the molecular systems. For example, when a material containing a carbonyl group is exposed to a light beam of frequency $19,436 \text{ cm}^{-1}$, the scattered radiation is found to contain besides the frequency $19,436 \text{ cm}^{-1}$, also frequencies near $17,786 \text{ cm}^{-1}$ and $21,086 \text{ cm}^{-1}$.

The scattering of radiation without change of frequency arising from scattering centres, like molecules, which are much smaller than the wavelength of the incident radiation, is called *Rayleigh scattering*, after Lord Rayleigh who studied its various features in terms of classical theory [323]. The scattering of radiation with change of frequency is called *Raman scattering*, after C.V. Raman who along with K.S. Krishnan observed it for the first time in 1928 [319]. Shortly after Raman published his results, Landsberg and Mandelstam [230] reported their observations on the light scattering with change of frequency in quartz. The effect, however, had been predicted earlier by Smekal [354].

Raman scattering is always accompanied by Rayleigh scattering. The spectrum of the scattered radiation, thus, consists of the original line and

Raman lines. Raman lines at wave-numbers less than the incident wave-numbers ($\nu_0 - \nu_M$), are known as Stokes lines and those with wave numbers greater than ν_0 , ($\nu_0 + \nu_M$), as anti-Stokes lines. For example, the spectrum of the light scattered by the liquid carbon tetrachloride when illuminated by monochromatic radiation from mercury at $\nu_0 = 22938 \text{ cm}^{-1}$ ($\lambda = 4358.3\text{\AA}$), as recorded by Raman and Krishnan [320], showed a strong band $\nu_0 = 22938 \text{ cm}^{-1}$, due to Rayleigh scattering and weaker bands at $\nu_0 \pm 218$, $\nu_0 \pm 314$, $\nu_0 \pm 459$, $\nu_0 - 762$ and $\nu_0 - 790 \text{ cm}^{-1}$. The first three pairs are the Stokes and anti-Stokes Raman lines corresponding to the rotational transitions and the last two are associated with the vibrational transitions in the carbon tetrachloride molecule, corresponding anti-Stokes lines of which were not recorded. These lines, however, were observed after the advent of lasers by other workers when carbon tetrachloride was excited by $\nu_0 = 20487 \text{ cm}^{-1}$ ($\lambda = 4879.9 \text{ \AA}$) line from an argon ion laser.

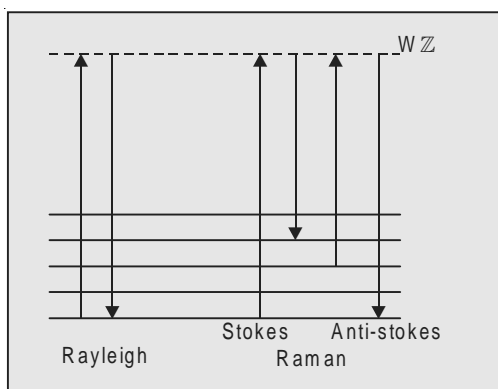


Fig. 15.1 Rayleigh and Raman scattering

The frequency shifts of the Raman lines, their intensity and polarization are characteristic of the scattering substance. According to the classical theory, Stokes and anti-Stokes lines should appear with equal intensity. Experiments, however, show that Stokes lines are far more intense. Figure 15.1 shows the levels involved in the Raman spectra. The level w' shown in the figure does not, in general, correspond to a stationary state. It is a virtual level. Since energy is not preserved in a transition to a virtual level, the molecule will immediately return to a stationary state under emission of a photon. The principal difference between fluorescence and Raman effect is that in fluorescence there is always a transition to a stationary upper level, whereas in Raman effect there is no such state.

The high intensity and narrow linewidth of the laser radiation have made it possible to measure the Raman scattering properties of materials under high resolution and, have, thus propelled Raman spectroscopy into its present popularity. The first Raman spectra using pulsed ruby laser as a source, were

photographed by Porto and Wood [315] and by Stoicheff [367]. The argon ion laser with its output of the order of a few watts and with its radiation falling in the blue-green region has been the most commonly used source for Raman spectra studies. The development of tunable dye lasers and the frequency doubling techniques which give an access to the ultraviolet region, have added a new dimension to the studies in Raman effect.

The use of lasers for exciting Raman scattering has made it possible to observe some new Raman scattering phenomena, of considerable fundamental interest. We will consider briefly in this Chapter three relatively new phenomena which are variants of the Raman effect and which arise from the nonlinear interaction of a system with intense monochromatic radiation. These are: (i) the stimulated Raman effect, (ii) the hyper-Raman effect, and (iii) coherent anti-Stokes Raman scattering (CARS). The giant-pulse or Q -switched laser systems commonly used for such investigations are ruby laser emitting at $\lambda = 6943.3 \text{ \AA}$ and neodymium-glass laser with an output at $\lambda = 10600 \text{ \AA}$. The outputs of these lasers are of short duration and of very high powers. The pulses extend over about 10 to 100 nanoseconds. Using a frequency doubling crystal like KDP, output at twice the frequency can be produced.

15.2 STIMULATED RAMAN EFFECT

Investigations of Raman scattering with the aid of lasers, led in early sixties to the discovery of *stimulated Raman scattering*.

While experimenting with a Q -switched giant pulse ruby laser provided with a nitrobenzene-filled Kerr cell as a shutter, Woodbury and Ng [406] observed, besides the stimulated emission at $\lambda = 6943.3 \text{ \AA}$, an additional intense radiation at $\lambda = 7670 \text{ \AA}$. This additional emission also displayed several characteristic properties of stimulated emission such as: (i) a marked threshold occurred both when the ruby laser power and the length of the liquid column were varied, (ii) the linewidth was found to decrease with increasing input intensity; (iii) emission showed sharp directionality. The line $\lambda = 7670 \text{ \AA}$ was later identified by Eckardt *et al.*, [106] as a line of the Raman spectrum of nitrobenzene. In subsequent investigation it was observed that when a Raman active material is placed inside the cavity of a Q -switched ruby laser, the high power pulse induces gain in the medium at Stokes frequencies $v_0 - nv_M$ ($n = 1, 2, 3, \dots$) shifted from the laser frequency v_0 by multiples of the various Raman frequencies v_M of the medium. If the gain is high enough to compensate for the cavity losses at $v_0 - nv_M$, a strong built up of coherent light at the shifted frequency can occur. The process being analogous to normal stimulated emission is called Stimulated Raman Scattering (SRS).

Subsequently Terhune [376] observed that if an external beam from a giant pulse ruby laser is focussed into cells containing Raman active liquids,

anti-stokes radiation at frequencies $v_0 + nv_R$ ($n = 1, 2, 3, \dots$) is also generated which emanates from the region of high focus in cones which make small angles with the normal to the cell.

The mechanism of stimulated Raman scattering has been explained by a number of workers on the basis of quantum and semiclassical theory of multiphoton processes [136, 181, 182, 254]. Garmire's theory [136] in particular, is very simple, involves classical arguments and accounts for certain observations made in the careful work of Chiao and Stoicheff [73]. Bloembergen and Shen [53] introduced a number of refinements in the theory. The theory thus refined has been useful in explaining the observed forward-backward asymmetry of the intensity of the Stokes radiation.

A typical arrangement for detection of stimulated Raman effect is shown in Fig. 15.2.

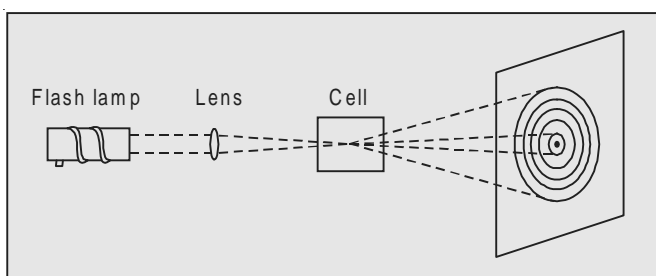


Fig. 15.2 Stimulated Raman effect

A giant pulse laser radiation is focussed into the sample and the scattering is observed along the laser beam direction and at small angles to this direction. If the forward scattered radiation is dispersed and photographically recorded, it is found to consist of the incident wave number v_0 and the Stokes and anti-Stokes lines at $v_0 \pm nv_M$ where v_M corresponds to just *one* Raman active vibration of the scattering molecule and n takes integral values 1, 2, 3,... etc. For example, the radiation scattered by liquid benzene, when illuminated with the focussed output of a giant pulsed ruby laser, shows Stokes and anti-Stokes shifts which are exact multiples of the wave number of the strongest vibrational band in the normal Raman spectrum of benzene, viz., 992 cm^{-1} .

If the forward scattered radiation is photographed on a coloursensitive film, a striking pattern of concentric coloured rings is obtained (Fig. 15.3), which reveals that stimulated Raman scattering has a spectral angular dependence. These additional wavelengths are as coherent and as well collimated as the main beam. The red spot at the centre corresponds to the ruby laser wavelength and also to the Stokes bands which lie at lower wavenumbers and are emitted essentially along the laser beam direction. The coloured rings correspond to successive anti-Stokes lines at higher wavenumbers which are emitted only along directions which make specific small angles with the laser beam direction.

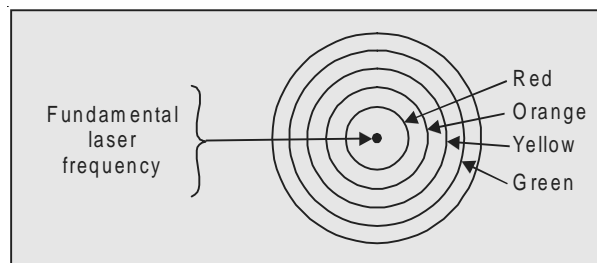


Fig. 15.3 Stimulated Raman effect on a colour sensitive film

Investigations have revealed that the mechanism responsible for the enhancement of the stimulated Raman Stokes lines is that of parametric amplification. The power transferred to the first Stokes line at $v_0 - v_M$ is related exponentially to the power in the laser at v_0 . The first Stokes line rapidly becomes intense enough to act as a powerful source at wave numbers $v_0 - v_M$, and another Stokes line at

$$(v_0 - v_M) - v_M = v_0 - 2v_M \quad \dots(15.1)$$

is generated. As this line gains in intensity, it acts as another source giving rise to a third line and so on.

The generation of the anti-Stokes wavenumbers does not arise as a result of downward transitions from a populated upper state. The essential difference between stimulated Raman scattering and stimulated emission in lasers is that in Raman scattering there is no need for inverting the population of the states. The generation of anti-Stokes lines corresponds to the frequency conversion process. One may, formally regard the anti-Stokes photons to be created at the expense of two laser photons. Conversion of energy demands that the following relation be satisfied

$$2hv_0 = (hv_0 + hv_M) + (hv_0 - hv_M) \quad \dots(15.2)$$

which dictates that a Stokes line is also generated along with the anti-Stokes line. Thus two incident photons are destructed and two photons with frequencies $v_0 - v_M$ and $v_0 + v_M$ are created so that conservation of energy is achieved. Conservation of momentum leads to the anti-Stokes photons being restricted to a particular angle with the laser beam direction and consequently the emitted radiation occurs in rings around the forward scattered laser beam.

15.3 HYPER-RAMAN EFFECT

It has been found that when a system is illuminated with radiation of wave number v_0 from a focussed giant-pulse laser, it gives rise to a scattered radiation at twice the incident frequency $2v_0$ (elastic scattering) and at displaced frequencies $2v_0 \pm v_M$ (inelastic scattering). Terhune *et al.*, [377] found that when a beam of a giant-pulse ruby laser, at $v_0 = 14,402 \text{ cm}^{-1}$ was brought to a focus inside liquids or fused quartz, a fraction of incident energy emerged

as scattered radiation around 28804 cm^{-1} . The scattered radiation was found to vary as the square of the laser intensity and occurred only in the focal region. These elastic and inelastic scatterings are now referred to as *hyper-Rayleigh* and *hyper-Raman* scatterings respectively. Detailed theoretical treatments of the hyper-Raman effect have since been developed [89, 255, 326–329].

15.3.1 Classical Treatment

Let us first consider a simplified classical treatment to explain the occurrence of hyper-Rayleigh and hyper-Raman effect.

We have seen in Chapter 13 that the second order induced dipole is given by

$$P^{(2)} = \epsilon_0 X^{(2)} \mathbf{E} \cdot \mathbf{E} \quad \dots(15.3)$$

Following the same treatment, we assume

$$\mathbf{E} = \mathbf{E}_0 \cos \omega t \quad \dots(15.4)$$

For a molecule oscillating with frequency ω_M in the simple harmonic approximation, we write

$$Q = Q_0 \cos \omega_M t \quad \dots(15.5)$$

where Q is the displacement. The dependence of $X^{(2)}$ on Q , to a first approximation, is given by

$$X^{(2)} = X_0^{(2)} + \frac{\partial X^{(2)}}{\partial Q} Q \quad \dots(15.6)$$

Substituting (15.4), (15.5) and (15.6) in (15.3), we have

$$\begin{aligned} P^{(2)} &= \epsilon_0 \left\{ X_0^{(2)} + \frac{\partial X^{(2)}}{\partial Q} Q_0 \cos \omega_M t \right\} E_0^2 \cos^2 \omega t \\ &= \epsilon_0 \left\{ X_0^{(2)} + \frac{\partial X^{(2)}}{\partial Q} Q_0 \cos \omega_M t \right\} E_0^2 \left(\frac{1 + \cos 2\omega t}{2} \right) \\ &= \frac{1}{2} \epsilon_0 X_0^{(2)} E_0^2 + \frac{1}{2} \epsilon_0 Q_0 \left(\frac{\partial X^{(2)}}{\partial Q} \right) E_0^2 \cos \omega_M t \\ &\quad + \frac{1}{2} \epsilon_0 X_0^{(2)} E_0^2 \cos 2\omega t + \frac{1}{2} \epsilon_0 Q_0 \left(\frac{\partial X^{(2)}}{\partial Q} \right) E_0^2 \cos \omega_M t \cos 2\omega t \\ &= \frac{1}{2} \epsilon_0 X_0^{(2)} E_0^2 + \frac{1}{2} \epsilon_0 Q_0 \left(\frac{\partial X^{(2)}}{\partial Q} \right) E_0^2 \cos \omega_M t \\ &\quad + \frac{1}{2} \epsilon_0 X_0^{(2)} E_0^2 \cos 2\omega t + \frac{1}{4} \epsilon_0 Q_0 \left(\frac{\partial X^{(2)}}{\partial Q} \right) E_0^2 \end{aligned}$$

$$\times [\cos(2\omega + \omega_M)t + \cos(2\omega - \omega_M)t] \quad \dots(15.7)$$

$$= P_{(\omega=0)}^{(2)} + P_{(\omega_M)}^{(2)} + P_{(2\omega)}^2 + P_{(2\omega \pm \omega_M)}^{(2)} \quad \dots(15.8)$$

The first term gives a static field; the second produces radiation at the molecular frequency ω_M ; the third gives rise to a radiation at 2ω (hyper-Rayleigh scattering) and the last generates radiation at $2\omega \pm \omega_M$ —Stokes and anti-Stokes hyper-Raman scattering.

15.3.2 Quantum Mechanical Treatment

The perturbation theory developed in Chapters 3 and 14, can be applied to obtain the transition rate for hyper-Rayleigh/Raman processes.

The transition rate for a transition from an initial state $|i\rangle$ to the final state $|f\rangle$, in the case of a “three photon process” is given by the third term of equation (14.21), viz.

$$R_{i \rightarrow f} = \frac{2\pi}{\hbar^2} \sum_f \frac{1}{\hbar^2} \sum_{l,m} \frac{\langle f | \hat{H}' | l \rangle \langle l | \hat{H}' | m \rangle \langle m | \hat{H}' | i \rangle}{(\omega_i - \omega_l)(\omega_i - \omega_m)} \delta(\omega_i - \omega_f) \quad \dots(15.9)$$

This term describes a process in which a single photon is absorbed and two photons are emitted, or a process in which two photons are absorbed and a single photon is emitted. This latter process corresponds to hyper Raman scattering. For the case of hyper-Raman scattering, equation (15.9) generates three contributions which differ in the type of intermediate states, depending upon the different possible order of events, which lead ultimately to absorption of two photons and emission of a single photon. The three possibilities involve the operator contributions: $a_s^* a a$; $a a_s^* a$ and $a a a_s^*$ (see Chapter 3).

Evaluating the matrix elements corresponding to the three cases, by the method illustrated in Chapter 3, and adding, we get for the transition rate [326].

$$R_{i \rightarrow f} = \sum_f \sum_{k_s} \frac{2\pi e^6}{\hbar^6} \left(\frac{\hbar^3 \omega^3 \omega_s}{8 \epsilon_0^3 V^3} \right) n^2 \times \left| \sum_{l,m} \left\{ \frac{(\epsilon_s \cdot \mathbf{D}_{fl})(\epsilon \cdot \mathbf{D}_{lm})(\epsilon \cdot \mathbf{D}_{mi})}{(\omega_{il} + 2\omega)(\omega_{im} + \omega)} \right. \right. \\ \left. \left. + \frac{(\epsilon \cdot \mathbf{D}_{fl})(\epsilon_s \cdot \mathbf{D}_{lm})(\epsilon \cdot \mathbf{D}_{mi})}{(\omega_{il} + \omega - \omega_s)(\omega_{im} + \omega)} + \frac{(\epsilon \cdot \mathbf{D}_{fl})(\epsilon \cdot \mathbf{D}_{lm})(\epsilon_s \cdot \mathbf{D}_{mi})}{(\omega_{il} + \omega - \omega_s)(\omega_{im} + \omega)} \right\} \right|^2 \\ \times \delta(\omega_{if} + 2\omega - \omega_s) \quad \dots(15.10)$$

where ϵ , ϵ_s are the unit polarization vectors of the incident and scattered photons and other symbols have the same meaning as in Chapter 3.

The formula shows that we have hyper-Stokes Raman scattering, hyper anti-Stokes Raman scattering, or hyper-Rayleigh scattering, according as ω_{if} is

less than zero, greater than zero or equal to zero respectively. In each case the intensity of scattered radiation is proportional to the square of the incident intensity, in agreement with experimental observations of Terhune *et al.*, [377].

Usually a *Q*-switched ruby laser ($\lambda = 6943\text{\AA}$) is used as the excitation source. The radiation emerging from the Raman cell is focussed on the slit of a monochromator and the dispersed light is detected with a photomultiplier. The monochromator is set at fixed frequencies and the number of photoelectrons from the photocathode is counted with a photon counting system.

The vibrational selection rules for hyper-Raman scattering are different from those for linear Raman scattering and for infrared absorption. Some vibrations which are both infrared and Raman inactive and were so far considered spectroscopically inaccessible, are hyper-Raman active; whereas some Raman active bands are not hyper-Raman active. *All infrared active bands are also hyper-Raman active.* Hyper-Raman active vibrations, which are also infrared active, can be distinguished in a hyper-Raman spectra by the fact that they are always polarized.

Hyper-Raman spectra have been observed in a number of molecules such as water, carbon tetrachloride [128], methane [386], etc.

15.4 COHERENT ANTI-STOKES RAMAN SCATTERING (CARS)

Of the three nonlinear Raman scattering phenomena mentioned in Section 15.1, the last, viz. CARS, holds greater promise for future development. The technique involves two powerful collinear laser beams. If a coherent radiation of wave-number v_1 is mixed in a molecular medium with coherent radiation of wave-number v_2 and their irradiances are sufficiently high, then a new coherent radiation of wavenumber v_3 is generated, where

$$v_3 = v_1 + (v_1 - v_2) \quad \dots(15.11)$$

If, further, v_1 is so adjusted that $v_1 - v_2 = v_M$ where v_M is a molecular wave number of the medium, then

$$v_3 = v_1 + v_M \quad \dots(15.12)$$

In this case v_3 is coincident in wavenumber with anti-Stokes Raman scattering associated with the molecular wave-number v_M . Radiation produced in this way is termed *Coherent Anti-Stokes Raman Scattering (CARS)*. A nonlinear mixing of this kind was first discovered by Maker and Terhune [268].

CARS is superior to normal Raman scattering, firstly, because conversion efficiency to v_3 in CARS is several orders of magnitude greater than the conversion efficiency in the normal Raman effect; and secondly, because the radiation v_3 is highly coherent and confined to a small solid angle; whereas, normal Raman scattering is incoherent and extends over a solid angle 4π .

The technique of CARS is being widely used. It is found to be the best tool for high resolution spectroscopy. The technique offers advantages of

spectral and spatial discrimination against fluorescence and does not require a spectrometer. The technique has been successfully used as an effective spatial probe of concentration of gases in flames. Regnier and Taran [324] used this technique to find the distribution of hydrogen in a hydrogen gas flame. The technique permits powerful fluorescence-free analysis of biological samples [288].

A comprehensive review of coherent Raman spectroscopy is given by Eesley [109].

15.5 SPIN-FLIP RAMAN LASER

Another phenomenon leading to laser action is what is known as “spin-flip” Raman scattering. This scattering has been characterized as “spin-flip”, because in the process of scattering of light from a conduction band electron, the spin of the electron is reversed.

It has been shown [Landau, 229] that energy levels of electrons in a semiconductor placed in a strong magnetic field of induction B are given by

$$E = \frac{\hbar^2 k^2}{2m} + \left(n + \frac{1}{2}\right) \hbar\omega_c, \quad \dots(15.13)$$

where m is the effective mass of the electron, $\omega_c = eB/m$ is the cyclotron frequency and n is an integer. The discrete levels given by different values of n are known as *Landau levels*. The specification of energy levels as given by (15.13) does not take into account the interaction between the magnetic field and the electron spin. When a free electron is placed in a magnetic field of induction B , it has energy $\pm \beta B$ where $\beta = e\hbar/2m$ is the Bohr magneton. The energy of electrons in solids placed in a magnetic field is $\pm \frac{1}{2}g\beta B$ where ‘ g ’ is a number known as *Landau splitting factor*. It has the value 2 for free electrons; but takes a different value in a semiconductor because of the strong spin-orbit coupling.

The expression for the total energy, therefore, is

$$E = \frac{\hbar k^2}{2m} + \left(n + \frac{1}{2}\right) \frac{\hbar e B}{m} \pm \frac{1}{2} g \beta B \quad \dots(15.14)$$

The expression shows that each Landau level is doubled. The transition between two states with the same value of n is, thus, possible if the spin is reversed. If the electron is in a magnetic field, the spin energy $g\beta B$ is either taken from or given to the energy of the scattered quantum, resulting in decrease or increase in frequency of an amount $g\beta B/\hbar$, thus producing Stokes and anti-Stokes shifts.

The simplified energy diagram of electrons in a semiconductor with and without an applied magnetic field is given in Fig. 15.4 [279]. Electrons in the

lowest orbital energy state can flip their spin and reduce the energy of the pump photon by an amount $g\beta B$.

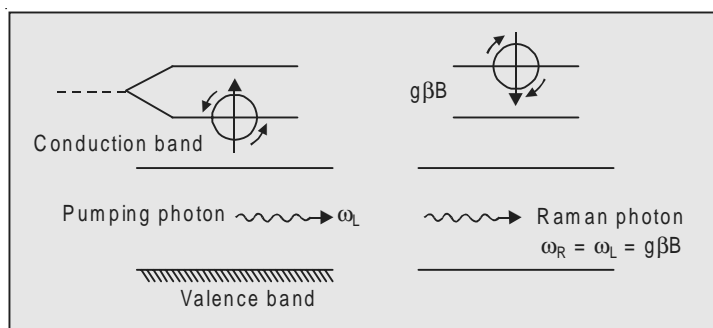


Fig. 15.4 Spin-flip Raman laser

Indium antimonide is found to be very suitable for this kind of scattering, which is so strong that the scattered radiation may readily be made to show laser action. Laser action with the spin-flip scattered radiation was observed by Mooradian *et al.*, [280], and Patel and Shaw [301-2] using transverse scattering and by Allwood [10], using forward scattering. A high intensity infrared laser such as CO or CO₂ is focussed into the crystal. Stimulated Raman scattering occurs from the Zeeman split levels of the electrons in the semiconductor. Since the frequency shift is proportional to the magnetic induction B , the laser wavelength is varied by varying the magnetic field. The spin-flip laser, thus, provides a continuously tunable source of radiation. These lasers are usually operated at cryogenic temperatures simply to remove the heat generated by the pumping source. Recently, however, there is a radical change in its design, which has made it possible to run the laser continuously at room temperature [173]. High power CO₂ pumped spin-flip Raman lasers have been investigated by Agarwal *et al.*, [5].

Besides InSb, many other materials have been tried as a basis for spin-flip laser; but apart from Hg_xCl_{1-x}Te, none other has given such intense spin-flip scattering.

15.6 FREE-ELECTRON LASER (FEL)

We have discussed in Chapters 7–10, the various types of lasers. The operating frequencies of these lasers are determined by energy levels in atoms or molecules. Is it possible to design a laser in which energy levels of atoms or molecules are not involved? Stimulated scattering from free electrons passing through spatially varying magnetic field, has made such a laser possible. Free electron lasers are high power tunable lasers in which the kinetic energy of a beam of

electrons is converted into light. The feasibility of at least two varieties of *free-electron laser* (FEL) have so far been demonstrated.

In one variety reported by Deacon *et al.*, [93], the coherent radiation arises in a stimulating scattering process in which a free electron moving at relativistic velocity is scattered by a spatially varying magnetic field. The upper laser state consists of a fast electron together with a virtual photon from a rippled magnetic field; the lower state has a scattered photon together with a low energy electron. With enough scattering events, the scattered radiation can build up to such a high level as to raise the intensity above the threshold.

In the other variety, reported by McDermott *et al.*, [273], an electron beam emerging from an accelerator, passes through a region in which a strong longitudinal field has a spatially periodic ripple imposed on it. The ripple is produced by inserting within the solenoid, a set of aluminium rings that carry currents in alternate directions. Light emitted, while the electrons are in this region, is reflected by annular mirrors, which define the optical cavity.

The successful operation of FEL requires the maintenance of a very precise relationship between the phase of the radiation field and the position of the electron relative to the periodic magnetic field of the wiggler. The wavelength of peak gain is determined by the electron beam's energy, the strength of the magnetic field and the period over which the magnetic field reverses. These parameters are design variables and, hence, the laser can be operated at any chosen wavelength. The FEL, thus, has a broad range of application.

Accelerators and storage rings generally used for high energy physics, have provided electron beams of sufficient energy to yield laser output in the near infrared at 1.6 μm [Neil *et al.*, 286] and even in the visible at 6500 Å [Billardin *et al.*, 45].

The non-linear interaction of the signal wave in the electron plasma and the rippled field produces a disturbance that propagates as a wave along the beam and reinforces the scattering into the laser mode. The process is essentially stimulated Raman scattering from the electron beam and the laser is analogous to a parametric amplifier with virtual photons of the magnetic field serving as the high energy "pump" mode; the plasma wave as the "idler" mode and the scattered light as the "signal" mode.

Some of the important characteristics of free electron lasers are:

1. Their operating frequencies do not depend upon bound energy levels of atoms or molecules;
2. Their frequency is tunable by variation of electron energy;
3. Their high average output power is greater than 10 kW;
4. Their high efficiency is greater than 10%; and
5. The radiation generated by them spreads over the electromagnetic spectrum from 1000 Å to \sim 1 mm.

15.7 PHOTO-ACOUSTIC RAMAN SPECTROSCOPY (PARS)

The potential of acoustic techniques for detecting laser absorption was first explored by Kerr and Atwood [214]. Photo-acoustic spectroscopy has proved to be an exceptionally versatile spectroscopy tool. The photo-acoustic technique is based on the direct absorption of light in the sample. In general terms, the technique is a three-step sequence involving (i) intermittent absorption of light in a sample from a periodically modulated beam, (ii) heat production by the absorbed energy, and (iii) generation of acoustic pressure oscillations.

Photo-acoustic Raman Spectroscopy (PARS) is a new nonlinear spectroscopic technique which is fundamentally different from the technique described above, because in this case the light is not absorbed by the sample. The theory underlying the photo-acoustic Raman effect is described by Barrett and Heller [26].

Population of the upper energy level of a transition is accomplished in PARS by a stimulated Raman process rather than by a direct absorption. This requires simultaneous illumination of the sample by two laser beams whose frequencies differ by a Raman transition frequency. The process is shown schematically in Fig. 15.5.

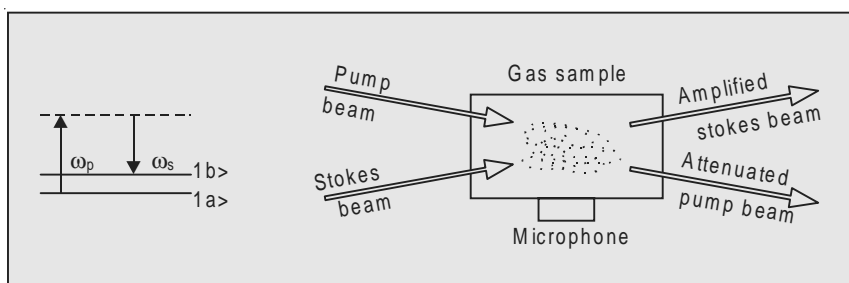


Fig. 15.5 Photo-acoustic Raman process

Two incident laser beams with frequencies ω_p (pump frequency) and ω_s (Stokes frequency), such that $\omega_p - \omega_s = \omega_0$ (Raman transition frequency), interact with two energy states $|a\rangle$ and $|b\rangle$ of a molecule. A nonlinear interaction between ω_p and ω_s results in the amplification of the Stokes beam and the attenuation of the pump beam. One molecule is transferred from level $|a\rangle$ to level $|b\rangle$ for each Stokes photon that is generated by the interaction, thus producing excess population in the level $|b\rangle$. Collisional relaxation following SRS, produces a pressure change in the sample which is detected by a microphone. The first experimental demonstration of the PARS technique was accomplished by Barrett and Berry [25] using low power cw laser excitation of a gaseous sample.

Raman active transitions can occur in molecules that have no infrared spectrum, since the occurrence of Raman spectrum depends on the change in polarizability of the molecule and not on a transition dipole moment, which is a prerequisite for infrared transition. PARS, therefore, is a particularly attractive technique for studying such molecules.

The technique has been successfully used by West and Barrett [395] to study pure rotational Raman transition in gases. In pure rotational Raman spectra recorded by conventional techniques, Rayleigh component, at zero frequency shift, is always more intense than Raman scattering and sometimes interferes with observation of low-lying rotational levels. One of the characteristic features of pure rotational PARS spectra is the absence of the Rayleigh component.

15.8 BRILLOUIN SCATTERING

When an acoustic wave traverses an elastic medium, it changes locally the dielectric constant and, consequently the index of refraction of the medium. In the presence of an electromagnetic wave such acoustic vibrations cause a scattering known as Brillouin scattering. There is a close analogy between the Raman scattering and the Brillouin scattering. The former is caused by optical vibrations, while the latter by acoustic waves. Brillouin scattering is always accompanied by the emission or absorption of a photon [76, 282].

Consider a photon of energy $\hbar\omega_1$ interacting with a photon of energy $\hbar\omega_a$, where $\omega_1 \gg \omega_a$. Conservation of energy and linear momentum demands that the following relationships be satisfied:

$$\hbar\omega_1 + \hbar\omega_a = \hbar\omega_2^+ \quad \dots(15.15)$$

$$\hbar\omega_1 - \hbar\omega_a = \hbar\omega_2^- \quad \dots(15.16)$$

$$\hbar\mathbf{k}_1 + \hbar\mathbf{k}_a = \hbar\mathbf{k}_2^+ \quad \dots(15.17)$$

$$\hbar\mathbf{k}_1 - \hbar\mathbf{k}_a = \hbar\mathbf{k}_2^- \quad \dots(15.18)$$

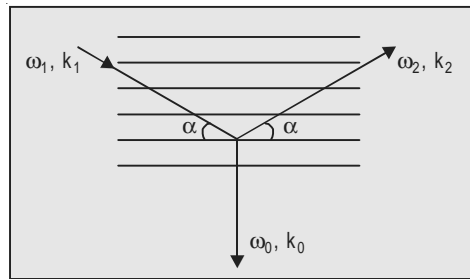
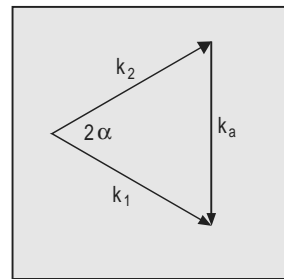
where ω^+ and ω^- are the sum and difference frequencies and \mathbf{k}_i are the propagation vectors.

Geometrical representation of the wavevectors is given in Fig. 15.7. Remember $k_1 \approx k_2$.

Figure 15.6 shows an acoustic wave set up in a small crystal. The straight lines represent the crests of the wave, *i.e.*, planes of highest refractive index. An electromagnetic wave (ω_1 , \mathbf{k}_1) incident on one such plane generates a new wave (ω_2 , \mathbf{k}_2) travelling in the direction shown. Because k_a is very small, we find that

$$k_a \approx 2k_1 \sin \alpha \\ i.e., \quad \lambda_1 = 2\lambda_a \sin \alpha \quad \dots(15.19)$$

where 2α is the scattering angle.

**Fig. 15.6** Brillouin scattering**Fig. 15.7** Geometrical representation of Eqn. (15.18)

One may consider this to be a special case of the Bragg's X-ray diffraction condition

$$2d \sin \alpha = 2\lambda_a \sin \alpha = n\lambda_1 \quad \dots(15.20)$$

where d is the separation between reflecting planes and the integer n gives the order of diffraction.

The change in frequencies between the incident and the reflected wave is, obviously, due to the movement of the "diffraction grating" formed by the acoustic wave and travelling through the crystal with the phase velocity v_{pa} .

According to the Doppler principle, the frequency measured in a frame of reference moving with a velocity v away from the source is given by

The change in frequency is

$$\omega' = \omega \left(\frac{1-v/c}{1+v/c} \right)^{1/2} \quad \dots(15.21)$$

\therefore The change in frequency is

$$\omega - \omega' = \omega \left[1 - \left(\frac{1-v/c}{1+v/c} \right)^{1/2} \right] \approx \omega v/c \quad \dots(15.22)$$

assuming $v < < c$.

In the case under consideration, $\omega = \omega_1$, $\omega' = \omega_2$, $c = v_{p1}$. (velocity of light in the crystal) and taking into account the total change in the direction of the reflected wave $v = 2v_{pa} \sin \alpha$ (see Fig. 15.7).

$$\begin{aligned} \therefore \omega_1 - \omega_2 &= \frac{2\omega_1 v_{pa} \sin \alpha}{v_{p1}} \\ &= \frac{2\omega_a \lambda_a \sin \alpha}{\lambda_1} = \omega_a \end{aligned} \quad \dots(15.23)$$

where we have used (15.19).

For the acoustic waves travelling in the opposite direction

$$\omega_1 - \omega_2 = -\omega_a \quad \dots(15.24)$$

Thus, phonon frequencies can be found from the study of Brillouin scattering. The frequency shifts observed are usually less than ~ 10 GHz and vary with the scattering angle. By varying the angle α from the forward to the backward direction, one can study ‘phonon spectroscopy’ by light scattering [167].

It has been found that if the incident radiation is very intense, a parametric amplification process may be set up giving rise to the so-called *stimulated Brillouin scattering* [207, 54].

A new method for the accurate measurements of Brillouin line shifts is presented by Sussans and Vacher [368]. By modulating a reference beam at a microwave frequency corresponding exactly to the shift of a Brillouin line, the Brillouin scattering frequency is obtained by direct comparison. The errors which usually creep in due to imperfect calibration and nonlinearity of the Fabry-Perot interferometer are, thus, eliminated.

An elementary classical derivation of the Brillouin scattering conditions has been given by Heald [174].

15.9 SATURATION-ABSORPTION SPECTROSCOPY

The ways in which the saturation absorption can be used in optical spectroscopy are many and wide ranging. One of the important uses is in overcoming the Doppler broadening which so often obscures finer details of the spectra of free atoms and molecules. Much information, therefore, can be gained if Doppler broadening can be eliminated.

Dye lasers typically give a line width of about 0.03 Å, which one could further refine to 0.004 Å, by placing an etalon inside the laser resonator. These lasers can without great difficulty be monochromatic to one part in 10^8 or less. The narrowness of the lines from the tunable dye lasers together with the other properties of the laser light provided just what was needed to display spectral lines without Doppler broadening.

Christian Borde in Paris and independently Hansch and his colleagues at Stanford developed a new technique known as *saturation-spectroscopy* which is becoming an increasingly useful tool in optical spectroscopy.

Essentially the method consists in subjecting the sample to be investigated to two light waves of the same frequency but propagating in the opposite directions through the sample. If the light is sufficiently intense, it will burn a hole in the absorption profile of the gas by saturating the molecules lying within a homogeneous line width ω . If the light travelling in the positive direction saturates the gas at $\omega = \omega_0 - \delta$, this saturation will affect the transmission of light at negative direction at $\omega' = \omega_0 + \delta$ by the Doppler effect. If the applied

frequency is set to the exact peak of the line, *i.e.*, $\omega = \omega' = \omega_0$, the same set of molecules having zero velocity along the direction of propagation will interact with both light waves simultaneously producing a sharp dip—Lamb dip—in the absorption of light through the sample. The net effect is to produce a very narrow line right at the centre position of a molecular transition. The technique, thus, provides a useful method for resolving the transition blended into an inhomogeneously broadened line.

The experimental arrangement for the studies in saturation spectroscopy is shown schematically in Fig. 15.8.

The absorbing gas sample is kept in a cell outside the laser resonator. A beam from a laser is split into two parts: a strong saturating beam and a weaker probe beam. These are sent by mirrors in nearly opposite directions through the sample.

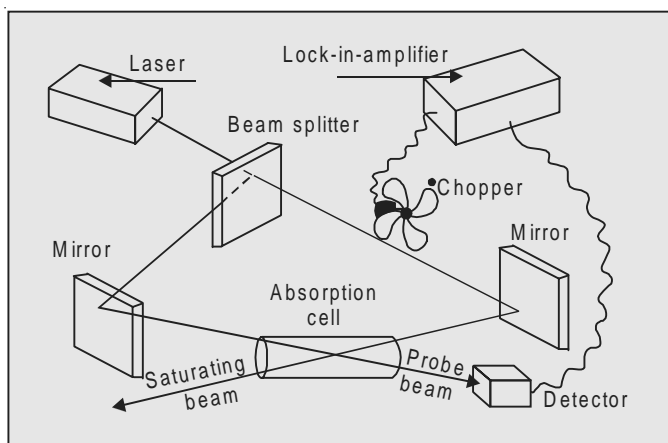


Fig. 15.8 Experimental arrangement for the study of Doppler-free spectra

The saturating beam is chopped at an audio frequency. When it is on, it bleaches a path through the sample, so that less of the probe beam is absorbed allowing the probe signal to be received at the detector. As the saturating beam is chopped on and off, the probe beam is modulated. However, this happens only when the laser is tuned near the centre of the Doppler broadened absorption line, so that both beams interact with the same atoms or molecules, those with the zero velocity component, along the direction of the oppositely directed beams. This approach eliminates Doppler broadening due to motion of the atoms.

With the saturation method and the broadly tunable lasers, Hansch *et al.*, [161] were able to study the fine structure of the well-known red line of atomic hydrogen H_{α} . The hydrogen atoms have an exceptionally large Doppler broadening

as a result of which in the conventional spectrum most of the fine structure is obscured. The Doppler-free laser technique reveals details, including the Lamb shift, which had not been previously resolved optically in hydrogen. In 1976, Wieman and Hansch [403] introduced a polarization technique which made the Doppler-free laser spectroscopy still more sensitive.

Saturation absorption spectroscopy has been proved to be extremely useful in determining a very accurate value of the velocity of light. Using the fact that $3.39\text{ }\mu\text{m}$ He:Ne laser can be locked very accurately with the methane saturation absorption resonance, Barger *et al.*, [22] have found the velocity of light to be equal to $299,792,4574 \pm 11.1\text{ ms}^{-1}$, which is 100 times better than the value found earlier by Froome [132] viz., $299,792,500 \pm 100\text{ ms}^{-1}$.

The fine structure components of the hydrogen Balmer α line corresponding to the transition $n = 3 \rightarrow n = 2$ at $6563\text{ }\text{\AA}$, consists of seven closely spaced components shown in Fig. 15.9. Dirac theory predicts that the levels with same j but different l will be degenerate. This conclusion, however, is at variance with experiment. Lamb and Rutherford [225] have shown by means of an

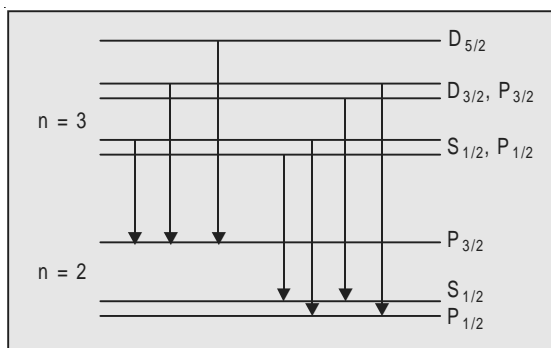


Fig. 15.9 Hydrogen α line

atomic beam radio-frequency resonance experiment that the $^2S_{1/2}$ and $^2P_{1/2}$ levels corresponding to $n = 2$ state in atomic hydrogen are separated by about 1058 MHz. The components have been found to be well resolved by the technique of saturation spectroscopy and the study has shown that the value of Lamb-shift between $^2P_{1/2}$ and $^2S_{1/2}$ is 1052.7 MHz in good agreement with theory based on quantum electrodynamics.

Saturation absorption spectroscopy has been proved to be extremely useful in determining accurate value of the velocity of light. Using the fact that $3.39\text{ }\mu\text{m}$ He : Ne laser can be locked very accurately with the methane saturation-absorption resonance, Barger *et al.*, [22] have found the velocity of light to be equal to $299,792,4574 \pm 11.1\text{ ms}^{-1}$, which is 100 times better than the value found earlier by Froome [132] viz., $299,792,500 \pm 100\text{ ms}^{-1}$.

15.10 DOPPLER-FREE TWO PHOTON SPECTROSCOPY

Consider an atom moving through the standing wave radiation field of a tunable laser. In its own rest frame the atom with velocity component v_x along the beam axis “sees” photons of frequency $\omega(1 - v_x/c)$ travelling one direction and of frequency $\omega(1 + v_x/c)$ in the opposite direction where ω is the frequency of the laser beam. If the frequency of the laser is such that the atom in the state E_1 can reach an excited state E_2 , by absorbing simultaneously one photon from each of the oppositely directed beams, then

$$E_2 - E_1 = \hbar \left\{ \omega \left(1 - \frac{v_x}{c} \right) + \omega \left(1 + \frac{v_x}{c} \right) \right\} = 2\hbar\omega \quad \dots(15.25)$$

The expression is independent of velocity, since the absorption of a photon from each of the beams leaves the linear momentum of the atom unchanged and, hence, the Doppler broadening of the two-photon absorption line is completely eliminated. An advantage of two-photon absorption over saturation-absorption experiment is that in the former case, since the effect is independent of the velocity of the atoms, every atom in the laser beam may take part in the process and not only those atoms having zero axial velocity as is the case in the latter technique.

Doppler-free two-photon spectra have been obtained experimentally in sodium vapour by Biraben *et al.*, [46], Levenson and Bloembergen [248] and Hansch *et al.*, [163], using pulsed, tunable and cw dye lasers. The schematic diagram for the study of two photon absorption is shown in Fig. 15.10.

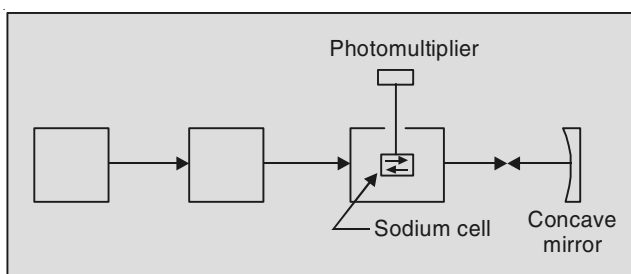


Fig. 15.10 Two-photon absorption

A cw dye laser is pumped by an Argon ion laser. The dye laser radiation is focussed into a sodium vapour cell and the transmitted light is then refocussed into the cell by means of a concave mirror, thus producing a standing wave field in the cell. The energy level diagram of sodium, showing relevant transitions, is given in Fig. 15.11. When the dye laser is tuned through the region 6022 Å, sodium atoms in the ground state $3s$ absorb simultaneously two photons and make a transition to the $5s$ state from where they decay spontaneously to the

$3^2P_{1/2}$ and $3^2P_{3/2}$ levels emitting radiation at 6154 Å and 6160 Å. The observation of radiation at these two wavelengths is a measure of the two photon absorption to the $5s$ state.

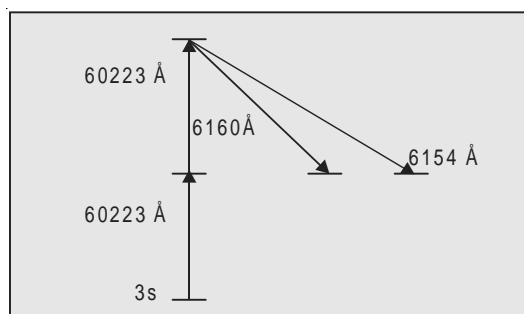


Fig. 15.11 Energy level diagram of sodium showing two-photon absorption

Since two-photon absorption permits us to detect transitions between levels having the same parity, it can be used for observing $1^2S_{1/2} \rightarrow 2^2S_{1/2}$ transition in hydrogen and deuterium. This transition lies in the region close to 1215 Å and, hence, a radiation at 2430 Å is necessary for two-photon absorption. Hansch *et al.*, [164] have been able to make measurements on these lines using the second harmonic of a pulsed dye laser. The Lamb-shifts of the 1s state determined from these measurements are:

$$\begin{aligned}\text{Hydrogen: } & 8.6 \pm 0.8 \text{ GHz} \\ \text{Deuterium: } & 8.3 \pm 0.3 \text{ GHz.}\end{aligned}$$

16

SOME LASER INDUCED PHENOMENA

We present in this chapter some very interesting laser-induced phenomena recently discovered. Explanations for their occurrence have been offered by the investigators; but some of these are of tentative nature and may need further scrutiny.

16.1 MODULATION OF AN ELECTRON WAVE BY A LIGHT WAVE

An experiment reported by Schwarz and Hora [339] shows that a free electron beam passing through a thin crystal illuminated by a monochromatic coherent polarized intense light source, may acquire a quantum state of oscillations of a frequency apparently equal to the light frequency.

Thin films of SiO_2 and Al_2O_3 were epitaxially vacuum-deposited to different thicknesses, varying from 600 to 2000 Å. An electron beam of 50 keV energy and a beam current of the order of a microampere was directed through a spot of few microns diameter. A diffraction pattern on a luminescent screen indicated that the beam passed through the monocrystal structure. When the fluorescent screen was replaced by a nonfluorescent screen—a smooth flat sheet of polycrystalline alumina—the diffraction pattern produced by the electrons became invisible, as expected. When with this set up, a parallel light beam of the width of 10 to 100 µm from an argon ion laser ($\lambda = 4880 \text{ \AA}$) of 10 W output was directed symmetrically lengthwise through the solid optically transparent films and perpendicular to the electron beam, with the electric vector of light polarized parallel to the electron beam (Fig. 16.1), diffraction pattern became visible again on the non-luminescent screen with the same spot position as on the fluorescent screen. The only difference was that this time the spots emitted light of approximately the same wavelength as that of the blue argon laser.

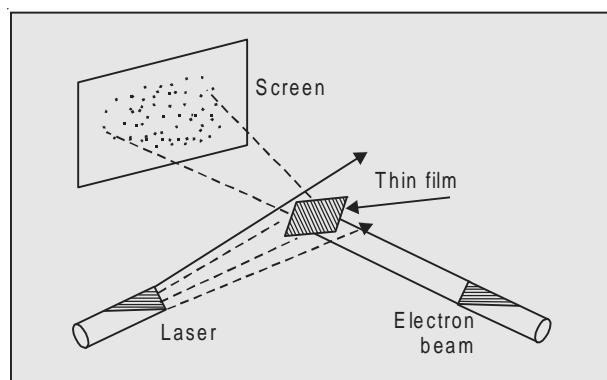


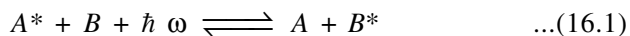
Fig. 16.1 Schwarz-Hora experiment

When the polarization was rotated, so as to make the electric vector parallel to the plate, the light spots on the non-luminescent screen disappeared completely. This shows that the electrons remain in the state of oscillation of the light frequency ω picked up from the photon-electron interaction within the crystal. The fact that the light spots on the nonluminescent screen were really due to the electrons, was proved by applying a magnetic field of about 300 Gauss which could displace the spots. The experiment shows that electrons, by some unknown mechanism, pick up the laser light and subsequently deposit it on the non-fluorescent screen. The effect was reproducible; but the authors had no substantial explanation for the observation.

A theory, however, has been proposed by Favro *et al.*, [122] to explain the observations of Schwarz and Hora. They suggest that laser light somehow superimposes its properties upon those of individual electrons. The intense laser fields modulate the “wave-packets” associated with the electrons and these modulated electrons, after passing through the thin crystal, relinquish the information they have acquired by radiating light at the laser frequency when they strike the screen. Actually, in order to modulate a simple electron the wavelength of the modulating radiation must be smaller than the width of the electron’s wave-packet. In conventional klystrons, the wavelength of klystron is not short enough to penetrate into a wavepacket, but electromagnetic radiation is used to modulate bunches of electrons, which subsequently radiate at microwave frequencies. According to Favro *et al.*, no bunching can take place at the usual laser power levels, so the individual particles themselves become modulated. However, Olicer and Cutler [289] have proposed an alternative explanation of the Schwarz-Hora experiment based essentially upon the concept of electron bunching.

16.2 LASER INDUCED COLLISION PROCESSES—PAIR EXCITATION

Laser induced collision processes in which elementary excitation transfer events, involving simultaneous quantum emission and absorption by colliding atoms, occurs in the presence of a strong electromagnetic field with a frequency close to resonance, were first considered by Gudzenko and Yakovlenko [155]. The typical reaction they considered was of the type



in which the energy of the colliding atom A^* is transferred to the atom B , in the presence of a photon field at frequency, ω , which is supposed to be close to the frequency

$$\omega = \omega_- = \frac{E_B^* - E_A^*}{\hbar} \quad \dots(16.2)$$

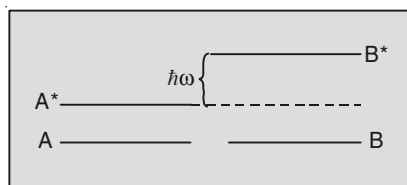


Fig. 16.2 Laser induced collision process

Assuming dipole-dipole interaction and using second order perturbation theory, they derived an expression for the cross-section for such a radiative collision. They also suggested that Cs atom in $6p\ 2P_{1/2}$ state (A^*) and potassium in $5s\ ^2S_{1/2}$ state (B), would be a suitable pair for observing the reaction discussed.

Subsequently the same authors [156] considered the kind of radiative collision in which two atoms are simultaneously excited by one photon, and after the collision each atom carries away its own share of energy. The relevant reaction is (Fig. 16.3)

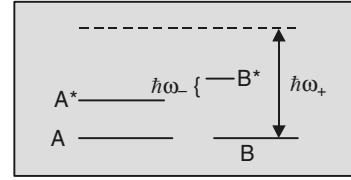
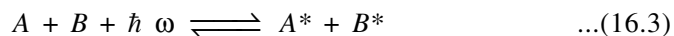


Fig. 16.3 Pair excitation



$$\text{where } \omega = \omega_+ = \frac{E_A^* + E_B^*}{\hbar} \quad \dots(16.4)$$

The theory for this process is identical to that for (16.1). However, for the observation of the process (16.1) one requires a powerful laser at frequency $\omega = \omega_-$, and also optical pumping of state A^* ; whereas, in the case of process (16.3), since the atoms are in the ground state, ordinary radiation source may

give reliable results. For example, in the case of Rb and Cs, one can observe the reaction (Fig. 16.4)

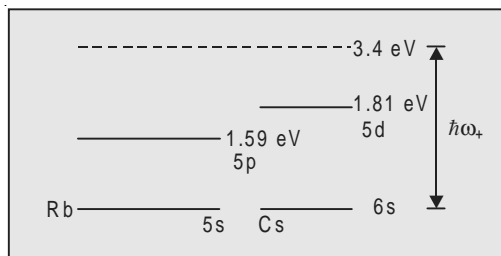
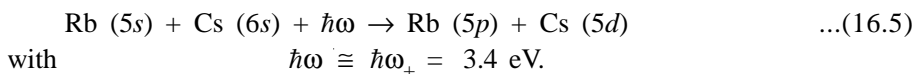


Fig. 16.4 Rb-Cs pair excitation



This absorption process was termed by them as a *pair excitation*.

It must be noted that in the case of dipole-dipole interaction between atoms, the transition to the excited state must be optically allowed for one atom, while for the other, it must be allowed for a two-photon process.

The dynamics of such (dipole-dipole) laser induced inelastic collisions was also studied later by Harris *et al.*, [169–71].

(i) The observation of a spontaneous radiative de-excitation process, in which, during the collision of two excited atoms, a photon is spontaneously emitted at their sum energy, was first reported by White *et al.* [399]. They studied the process



where the fluorescence occurs at the sum energy of two excited Ba atoms (Fig. 16.5). The process may be viewed as a virtual collision followed by a real emission. During the collision of a Ba ($6p' \ ^1P_1^0$) atom with a Ba ($5d \ ^1D_2$) atom, the dipole-dipole coupling causes the two atoms to make transitions to the ground level and to a virtual level at $29,455 \text{ cm}^{-1}$ with $6P' \ ^1P_1^0$ character respectively. While in this virtual level, the $6p' \ ^1P_1^0$ like atom may spontaneously emit a photon. Pumping of the Ba $6p' \ ^1P_1^0$ and $5d \ ^1D_2$ levels, in the above experiment, was achieved by two-photon excitation at $\lambda = 6144 \text{ Å}$ of the Ba $6p \ ^1D_2$ level followed by cascade radiative decay to $6p' \ ^1P_1^0$ and $5d \ ^1D_2$ levels.

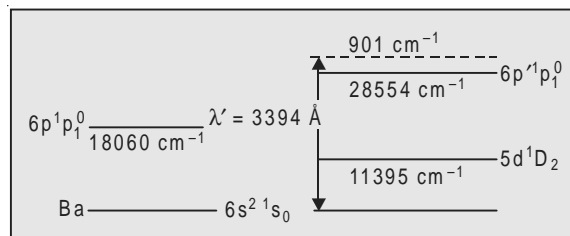
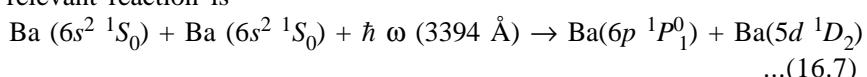
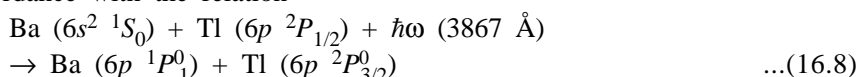


Fig. 16.5 Spontaneous emission at the sum energy of two colliding excited atoms

(ii) The absorption analogue of the Ba-Ba radiative collisional fluorescence described above was reported later by the same authors [400]. The experimental set up consisted of a metal vapour oven capable of operating at temperatures of the order of 1600 °C with a hot-zone length of 10 cm. The cell was filled with 500 Torr of argon buffer gas, to prevent the metal vapours from condensing on the cold cell windows. A high pressure Hg-Xe arc lamp was used as the white light source. Absorption was observed at 3394 Å corresponding to the absorption energy equal to the sum of the barium $6p' \ ^1P_1^0$ and $5d \ ^1D_2$ levels. The relevant reaction is



(iii) Similar observations were made by these authors in a mixture of Ba and Tl vapour, in which Ba-Tl pair absorption at 3867 Å was observed in accordance with the relation



The energy levels involved are shown in Fig. 16.6.

Such a pair absorption had been observed earlier in molecular systems in the infrared by Welsh *et al.*, [394].

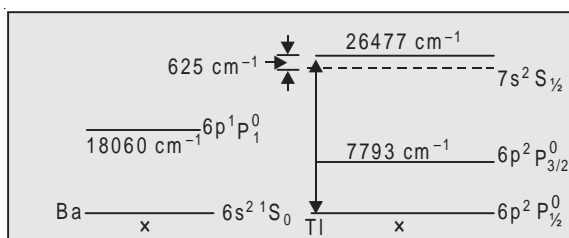
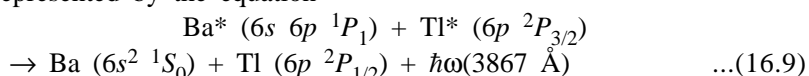


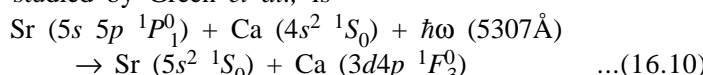
Fig. 16.6 Pair absorption : Ba-Tl system

(iv) The emission, which is the reverse of the pair absorption discussed above, was observed by Falcone and Zdziuk [120]. They observed radiative collisional fluorescence at a wavelength corresponding to the sum of the energies of the thermally excited electronic states of the colliding Ba and Tl atoms. The emission was observed in a hot cell containing Ba and Tl metal vapours at 1700 °C, using a 1m spectrometer and a GaAs photomultiplier. The process can be represented by the equation



(v) Observations of laser-induced dipole-quadrupole inelastic collision process was reported by Green *et al.*, [153]. In the dipole-dipole processes described so far, one species makes a parity allowed transition, while the other makes a parity-non-allowed transition [156]. In a dipole-quadrupole process, both species make parity-allowed or non-allowed transitions.

The process studied by Green *et al.*, is



The energy level diagram is given in Fig. (16.7). Energy is initially stored in the Sr ($5s 5p \ ^1P_1^0$) level. As the atoms collide, the Sr atom makes a dipole transition to the ground state, while the Ca atom undergoes a quadrupole transition to a virtual level of $4s 3d \ ^1D_2$ character. The applied laser field then induces a dipole transition from the virtual level to the Ca ($3d 4p \ ^1F_3^0$) target state.

The experimental investigation employed two synchronously pumped dye lasers. The output of one dye laser, the pump laser ($\lambda = 4607 \text{ \AA}$) was used

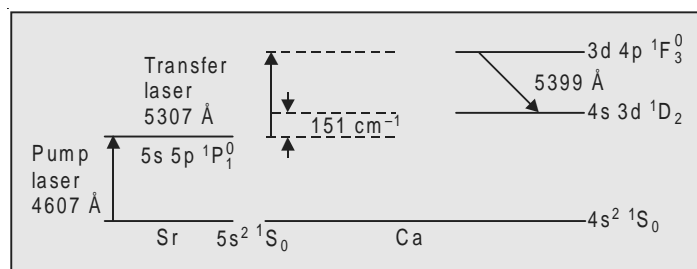
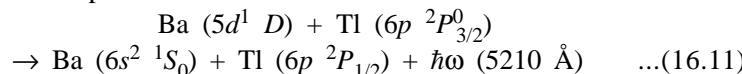


Fig. 16.7 Dipole-quadrupole process

to prepare the Sr ($5s 5p \ ^1P_1^0$) state; while the output of the second laser, the transfer laser, was used to induce the collision process. The fluorescence was observed at 5349 \AA , corresponding to the transition from the target state to the $4s 3d \ ^1D_2$ state. Two additional measurements were made to confirm this interpretation: (1) The pump laser was detuned 5 \AA from the Sr ($5s^2 \ ^1S_0$)—Sr ($5s 5p \ ^1P_1^0$) transition, to eliminate the Sr ($5s 5p \ ^1P_1^0$) population. The signal at 5307 \AA did not appear, (2). The pump laser was tuned to the Ca ($4s^2 \ ^1S_0$)—Ca ($4s 3d \ ^1D_2$) transition, thereby creating a large Ca ($4s 3d \ ^1D_2$) population. The signal at 5307 \AA was absent.

(vi) The observation of a spontaneous radiative de-excitation process, in which the long range dipole-quadrupole interaction between two excited species causes the emission of a photon at their sum energy, was reported by White [401]. The collision process studied was



where the fluorescence occurs at the sum energy of the excited Ba ($5d \ ^1D_2$) atom and the Tl ($6p \ ^2P_{3/2}^0$) atom (Fig. 16.8). Pumping of the Ba ($5d \ ^1D_2$) level was achieved through stimulated Raman scattering of 3547 \AA radiation in the Ba vapour itself. When this radiation was focussed at the centre of the metal vapour oven, strong stimulated Raman scattering at the first Stokes frequency (5955 \AA) was observed in Ba vapour. No such stimulated Raman scattering

occurred in the Tl vapour. The Tl ($6p\ ^2P_{3/2}^0$) storage density was, therefore, assumed to be due solely to thermal excitation ($T = 1410^\circ\text{C}$). The process may be viewed as follows: During the collision of the excited Ba and Tl atoms, the long-range dipole-quadrupole coupling causes the Tl atoms to be de-excited to the ground state, and the Ba atoms to be excited to a virtual level with $6p\ ^1P_1^0$ character at $19188\ \text{cm}^{-1}$, from where they spontaneously radiate a photon.

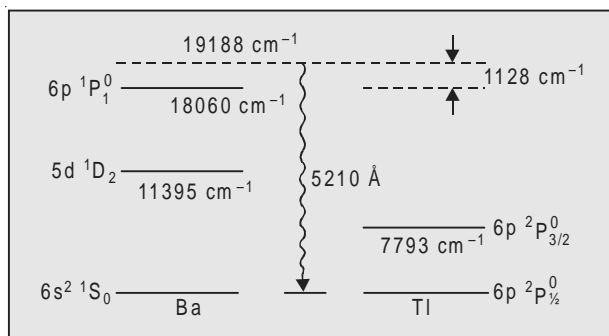
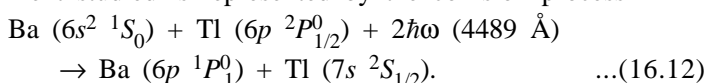


Fig. 16.8 Dipole-quadrupole interaction emission at sum energy

(vii) The laser induced collision processes discussed so far, have all involved single photon interactions. The observation of a multiphoton laser-induced collision was reported by White [402], who observed that during the long-range collisions of a ground state Ba-atom and a ground state Tl-atom, two laser photons, which are non-resonant with either of the isolated species, are absorbed resulting in the simultaneous excitation of both atoms to excited states. The experiment studied is represented by the collision process



This interaction is a two-photon laser induced pair absorption and according to the authors, may be visualised by the following perturbation sequence (Fig. 16.9):

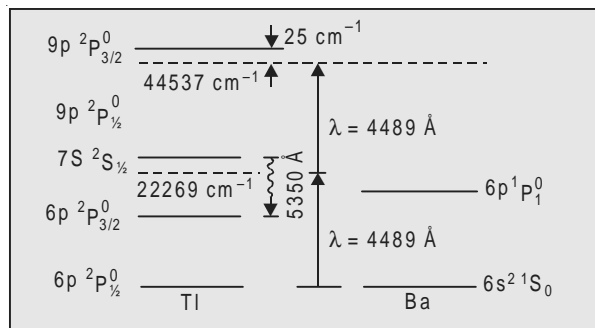


Fig. 16.9 Two-photon laser-induced collision

During the collision of Ba and Tl atoms, the Tl ($6p\ ^2P_{1/2}^0$) atom may absorb a laser photon, resulting in its excitation to a virtual level with

$7s\ ^2S_{1/2}$ character at 22269 cm^{-1} . Absorption of a second laser photon, may further excite the Tl atom to a virtual level at 44537 cm^{-1} coupled to the Tl ($9p\ ^2P^0_{3/2}$) state. The collisional interaction is completed through the long-range dipole-dipole coupling between the excited Tl and the ground state Ba atom, resulting in the de-excitation of the Tl-atom from the virtual level at 44537 cm^{-1} to the Tl ($7s\ ^2S_{1/2}$) state and the excitation of Ba atom to the Ba ($6p\ ^1P^0_1$) state.

Generation of the tunable laser light in the vicinity of 4489 \AA was accomplished by using a Nd : YAG laser pumped coumarin 450 dye laser system. Observation of the two-photon laser induced collisional excitation was carried out by monitoring the fluorescence from the Tl ($7s\ ^2S_{1/2}$) – ($6p\ ^2P^0_{3/2}$) transition at 5350 \AA , as a function of the two-photon excitation laser wavelength.

16.3 MULTI-PHOTON IONIZATION

One of the most rapidly growing field of laser spectroscopy is the *multi-photon ionization spectroscopy* (MPI) [203]. In fact, the concept of multiphoton ionization was commonly used even before the advent of lasers. Ionization of molecules, in those days, was considered to be a two- or more steps process. In certain molecules, where radiationless transition could populate long-lived triplet states, sequential absorption of two or more photons could cause ionization. The primary interest in these investigations, however, was in the spectroscopy of ions and not in the rate of production of ions. With the advent of lasers, it was realized that the rate of production of ions could be used as a measure of the oscillator strength in absorption processes.

Multi-photon transitions to the ionization continuum can be explained by the treatment of multiple resonances in one-atom systems interacting with external radiation. The probability of ionization can be calculated theoretically and the results compared with those of experiments, in which ions obtained from the ionization processes are collected. Details about the ionization mechanism can be obtained by measuring the energy spectrum of electrons emitted.

The sixth order ionization of oxygen molecules by a ruby laser with photons of 1.785 eV energy has been reported by Martin and Mandel [270]. The energy spectrum of the emitted electrons obtained by them shows two separate groups of electrons: one group consists of fast electrons with energies of the order of 10 eV and the other group of slow electrons with energies of the order of 1 eV or less. The slow electrons have been explained, by the authors, as due to the excitation of the O_2 molecules to an intermediate level by six-photon absorption, followed by ionization by the absorption of one additional photon, in a transition that is effectively saturated. This explanation is supported by the fact that the oxygen spectrum shows a resonance at the

six-photon excitation level. No explanation was available for the occurrence of fast electrons.

As pointed out by Ben-Aryeh [35], if one pursues the idea that the fast electrons are the result of individual molecules interacting with the ruby laser beam, it is found that the energy of the fast electrons corresponds with twelve-photon ionization, which, after subtracting the ionization potential of 12.01 eV, gives out approximately the energy of the fast electrons. It is possible to explain the absorption of twelve photons in the ionization continuum by taking into account the coupling mechanism between the ionization continuum and the discrete state O_2^+ in the continuum. However, Ben-Aryeh has pointed out another possibility, namely, that the twelve-photon ionization is due to resonance interaction between molecules excited to an intermediate level corresponding to six-photon excitation and the spontaneous ultraviolet radiation emitted by the collection of excited molecules in this level. He has treated the problem theoretically, has given a general formalism for ionization of a molecule by radiation at two frequencies and has obtained the expression for the probability for ionization. An experimental study of the oxygen ionization from the point of view suggested by Ben-Aryeh may, perhaps, throw some light on the exact ionization mechanism responsible for the energy spectrum observed.

16.4 SINGLE ATOM DETECTION WITH LASERS

The development of broadly tunable dye lasers has made it possible to detect a single atom. Various single-atom detection schemes have been proposed and demonstrated during the last ten years. The different methods suggested can broadly be classified into two groups: (i) Fluorescence methods, and (ii) Ionization methods. Both these groups involve the same first step, viz. excitation of the atom to a low-lying excited state by a dye laser beam tuned to the resonant wave-length of the atom (see Fig. 16.10 large arrow). The dashed lines indicate non-radiative transition. A few milliwatts dye laser is usually sufficient to saturate the transition, thus, creating a high probability that the atom is in excited state. The excited atom can then be detected by any method of either group.

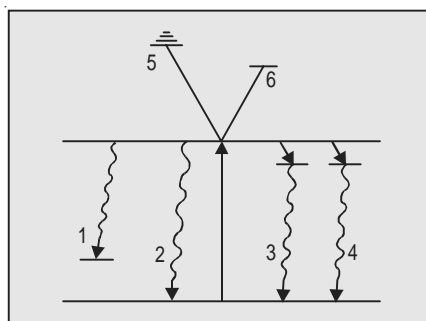


Fig. 16.10 Single atom detection

16.4.1 Fluorescence Methods

The atom can be detected through the spontaneous emission that the atom radiates in all directions when it decays from the excited to the ground state via one of the four pathways shown in Fig. (16.10 wavy lines). The atoms can be re-excited soon after they reach the ground state. The delays before the emission are of the order 10^{-7} to 10^{-8} sec, which means 10^7 to 10^8 photons of spontaneous emission may be emitted per second. Even with a moderate collection efficiency, of the order of 10^5 counts/sec of signal can be recorded each time a single atom passes into the laser beam and this single atom fluorescence signal is detectable provided no stray laser light reaches the detector.

The experiments in detection at the single-atom level were made for the first time by Fairbank *et al.*, [88] using the emission followed by path 1. They measured the vapour density of sodium using this method. The signal photons had approximately the same wavelength as the laser, except for a small Doppler shift. It was not possible, therefore, to distinguish the signal and the stray-light photons.

In 1977 Gelbwachs *et al.*, [139] showed a way out of the problem. They used path 3 of Fig. 16.10 and called their methods SONRES (Saturated Optical Non Resonant Emission Spectroscopy). In this scheme, they used a buffer gas, argon, at atmosphere pressure. The collision of the excited atom with the buffer gas atom transfers the former to a nearby state for which it undergoes a radiative transition to the ground state. The emitted photon is thus shifted from the laser light by 6 Å. Thus, using a monochromator, they could reject all stray light and pass only the desired spontaneous emission.

Similar measurements, using different techniques, were made by other workers also [20,154]. It should also be possible to do single atom detection by photoacoustic spectroscopy. Often the energy liberated in the collisions is converted directly into kinetic energy of the buffer gas. The local temperature and pressure rise propagates outwards as an acoustic wave from the atom which can be detected by a sensitive microphone. The technique has not yet been used on the single-atom scale [118].

16.4.2 Ionization Methods

In these methods laser-induced ionization of the atom produces a free electron and an ion, which can be detected by placing electrodes near the interaction region. Hurst *et al.*, [197] used resonance ionization spectroscopy [RIS] (path 5), for single-atom detection. In their experiment cesium atoms were ionized directly by the same high intensity laser beam that provided the first step of excitation.

However, since the photoionization cross-sections are small, high-power pulsed laser is required. Bekov *et al.*, [34] used a slightly different technique

for detecting single sodium and ytterbium atoms in which the laser power requirement was considerably reduced. They used a second laser beam to excite the atoms to a high-lying state near the ionization limit (path 6). A subsequent application of a pulsed electric field of the order of 10 kV/cm was sufficient to cause spontaneous ionization of the excited atoms.

The technique of single-atom detection may have a wide range of applications [118], such as: high resolution spectroscopy of rare isotopic species, detection of solar neutrinos and super-heavy elements, search for quarks, the fundamental sub-units of elementary particles, etc.

16.5 LASER COOLING AND TRAPPING OF NEUTRAL ATOMS

The trapping of ions, electrons and neutrons by various electromagnetic field configurations, is now well known. But the prospect of trapping electrically neutral atoms was not realized until recently. This is because the electromagnetic forces which can be applied to atoms are so small that only very slow atoms can be held by such forces. One of the rapidly developing field now-a-days is the mechanical effects of light, and it has been shown recently that using mechanical forces exerted by laser light, one can trap neutral atoms and cool them to a very low temperature. For ultra-high resolution spectroscopic study, it is necessary to eliminate Doppler broadening and, hence, the importance of stopping and cooling atoms.

Laser cooling of atomic gases was originally proposed by Hansch and Schawlow [165], and independently by Wineland and Dehmelt [404]. The basic technique is that a laser beam tuned slightly to the red of a principal excitation frequency opposes an atomic beam. Beam atoms of the correct velocity which “see” the photons “blue-shifted” due to the Doppler effect towards resonance with excitation frequency, may absorb them. The absorption of such a head-on colliding photon results into losing some of their forward momentum. By the principle of conservation of momentum, this causes a decrease in velocity given by

$$\Delta v = \frac{hv}{mc} \quad \dots(16.13)$$

where v = laser frequency; m = atomic mass.

The slowing effect caused by such absorption is proportional to the number of photons absorbed. Thus, in the case of sodium beam excited by 5890 Å radiation corresponding to its “yellow” transition, each absorbed laser photon reduces the longitudinal velocity by $\Delta v = -\frac{hv}{mc} = 3$ cm/s. Hence, stopping of sodium atom moving with a velocity 1000 m/s, requires absorption of about 30,000 photons.

The excited atoms will emit photons and in turn will experience recoil momentum kicks; but these will be in random directions. The net force acts in the direction of the incident light beam. Cooling is brought about by decelerating atoms in this manner.

The main problem in this technique, however, is to maintain the proper relation between the laser wavelength and the beam velocity as the atoms slow down and are, thus, shifted out of resonance. An atomic beam emerging from an oven with a broad velocity distribution peaking near a certain velocity, will pass through the observation region in a few milliseconds. Hence, only a small number of atoms will have just the right velocity to be Doppler shifted into resonance and even these will go out of resonance when photon absorption slows them down. One way to overcome this difficulty is to use a laser that can be swept rapidly from lower to higher frequency, keeping the laser light in resonance with the atomic excitation as the atoms slow down. Alternatively, one can use a laser of fixed frequency and vary the transition frequency to compensate the changing Doppler shift by passing the atomic beam through a varying magnetic field.

Prodan *et al.*, [317] adopted the latter technique to bring an atomic beam of sodium from 1000 m/s to rest within a few metres. The technique, briefly, is as follows.

An atomic beam emerging from an oven is surrounded with a solenoid whose winding density decreases gradually in the downstream direction (Fig. 16.11). The atoms, therefore, will be moving in a continuously varying axial magnetic field that gets weaker as the atoms slow down. With a fixed frequency laser tuned in such a way that an atom moving with a velocity of 1000 m/s sees the oncoming photons Doppler shifted into resonance with the

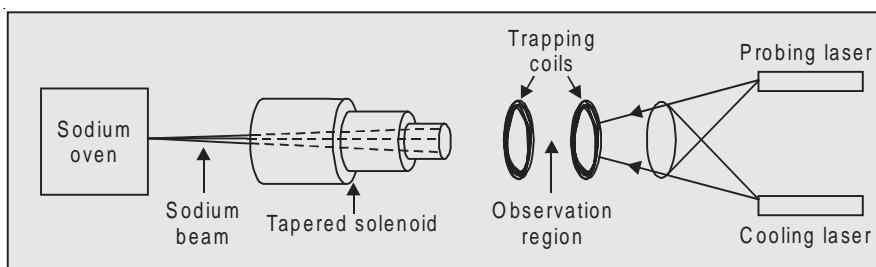


Fig. 16.11 Trapping of sodium beam

Zeeman-shifted transitions the magnetic field variation is so arranged that as the atoms move downstream and decelerate, Zeeman splitting of the upper and lower states decreases at just the right rate to compensate for the decrease in the Doppler shift. In this way, one can decrease the mean velocity of the beam and cool it, that is, compress the longitudinal velocity distribution.

We have seen above that about 30000 photon absorptions are required to bring 1000 m/s sodium atoms to rest. The atoms must have some time to return to the ground state before it can absorb another photon. Since the lifetime of excited sodium atoms is about 16 ns, the distance required to stop the beam is about half a metre. This is a value predicted theoretically for an ideal apparatus. Actually, Prodan *et al.*, built a 1.1 metre solenoid and with it, were able to bring the beam to rest in the downstream end of the solenoid.

It was, however, necessary to get the atoms outside the solenoid for observation and trapping. This was done by shutting off the cooling laser for a while, allowing a moderately slow (~ 100 m/s) sample of atoms to drift from the solenoid to the observation region and bringing them abruptly to a halt, with a very short final pulse from the cooling laser. The technique has produced samples of sodium atoms with a velocity distribution centred at zero and having a spread of 15 m/s corresponding to a temperature below 100 millikelvin. The final velocity distribution is determined by observing the fluorescence, induced by a small probing laser as a function of its frequency, essentially measuring the population at various Doppler shifts.

For trapping the stopped atoms, a magnetic trap which avails itself of atom's magnetic moment, was used. This consists of a pair of current coils separated by a distance of 3 cm and looping the beam axis. The upstream coil is turned on before the 100 m/s sample traverses it, thus providing an inhomogeneous magnetic field which increases the efficiency of the final stopping burst from the laser. Soon after, the second coil, farther downstream is turned on with its current in the opposite direction, thus springing the magnetic trap.

Ertmar *et al.*, [115] opted for the first method stated above, viz. bringing the atom beam to rest by sweeping the cooling laser frequency in synchrony with its decreased Doppler shift. This was accomplished by passing the light from a fixed frequency dye laser through a Pockel's effect crystal subjected to a frequency swept r.f. voltage. Chu *et al.*, [79] adopted the same technique as Ertmar's with some changes. They used optical-dipole trap instead of a magnetic trap. The optical dipole trap avails of the electric dipole force exerted by the intensity gradient of the focussed laser beam on the oscillating electric dipole induced in the atom by the same laser field. They managed to hold the stopped beam temporarily in a 'molasses trap' at the intersection of six laser beams (Fig. 16.12), and, thus, cool it in only a millisecond to about 240 microkelvin. The system could hold 10^6 atoms/cm³ in the cooling region for more than a tenth of a second. The swarm of photons traversing the intersection region in all directions produces, in effect, a viscous medium with the atoms experiencing a damping force proportional to their velocity. This viscous 'medium' of photons is called 'optical molasses'.

In 1986, Chu *et al.*, [80] demonstrated the optical trapping of the atoms for the first time. The optical trap itself comprises a single strongly focussed

Gaussian beam tuned about 10^4 natural linewidths below the atomic resonance. The trap relies on the dipole force of resonance radiation pressure. This single beam gradient force trap was first proposed by Ashkin [17]. In the experiment the trap laser beam was focussed into a collection of atoms, confined and cooled by optical molasses. The trapped atoms were observed as an intense small spot of fluorescence within the much more diffused light scattered from atoms in molasses.

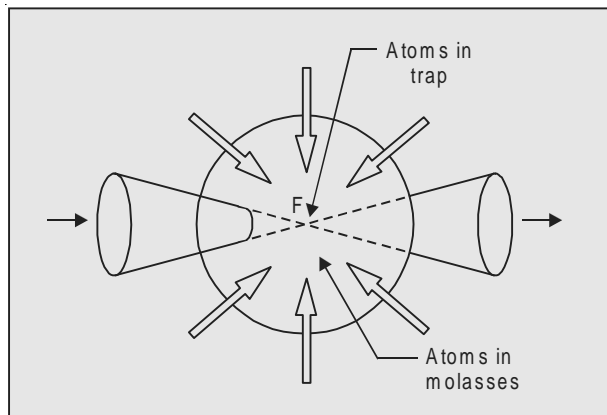


Fig. 16.12 Trapping of sodium atoms

Using 200 mW of trap laser power, about 500 atoms were trapped in a volume of about 10^{-4} cm³. The atomic density of the trap $\sim 5 \times 10^{11}$ atoms/cm³ was about 10^5 times the molasses density. The temperature of the trap was about 350 mk, slightly higher than that of atoms in optical molasses.

17

APPLICATIONS OF LASERS

The applications of lasers are widespread and range over various scientific disciplines, such as Physics, Chemistry, Biology, Medicine, etc. They have exciting potential applications in the realms of industry, communications and warfare. The applications are far too many to describe even in a book several times the length of this one. The examples that are considered in this chapter are selected just to illustrate the wide applicability of lasers.

17.1 SOME EXPERIMENTS OF FUNDAMENTAL IMPORTANCE

Certain elementary experiments of pedagogical value and of fundamental interest and importance, can be performed with considerable ease and greater precision using laser as a light source [68, 231, 306, 407]. An advanced laboratory experiment for the study of Brownian motion using light scattering with laser as the incident light source has been described by Clark *et al.*, [78]

Light from a He-Ne laser producing at least 1 mW of power is focussed onto a cell containing a dilute aqueous solution of polystyrene spheres of uniform diameter (Fig. 17.1). The light scattered by each illuminated particle into a small range of angles about some angle θ is collected onto the photosurface of an RCA 931 photomultiplier tube. The photomultiplier output current is proportional to the intensity of the light falling on the photo-cathode. Because the phase of the field scattered by each particle relative to that of the other particles changes in time as the particles move, the intensity is constantly fluctuating around its average values. The frequency spectrum of the scattered light provides the conditional probability which has the form [232]

$$P(\mathbf{r}, t) = (4 \pi D t)^{-3/2} \exp(-r^2/4Dt). \quad \dots(17.1)$$

It is thus possible to determine accurately the diffusion constant D and to obtain quantitative information about the motion of the particles.

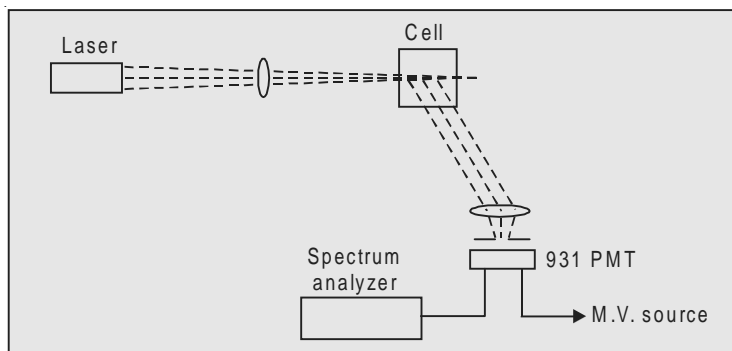


Fig. 17.1 Block diagram of the apparatus for the study of Brownian motion

17.2 ETHER DRIFT

Lasers help exploration of some basic questions of physics. In the late 19th century and early 20th century it was not really accepted that an electromagnetic wave could be propagated in empty space. The medium of light propagation was supposed to be the all-pervading 'ether'. Michelson and Morley had shown in 1881 that the velocity of light is unaffected by the motion of the earth through space, which would not have been constant if ether were present. Jaseja *et al.*, [200] performed an improved version of the Michelson-Morley experiment. In this new experiment two He-Ne lasers were installed in a wine cellar far removed from automobile traffic. The lasers were mounted at right angles on an extremely rigid support. The experiment was repeated by turning the lasers in different directions with respect to the earth's motion. The apparatus was sensitive enough to detect a change in the velocity of light as small as three millimetres per second. The accuracy attained by Michelson and Morley was about 150 millimetres per second. Even with this high precision, no anisotropy in the velocity of light associated with the motion of the earth was detected.

17.3 ABSOLUTE ROTATION OF THE EARTH

In 1904 Michelson suggested the following experiment to detect the absolute rotation of the earth: By placing mirrors at the four corners of a square, the light can be made to circulate in both directions around the four sides of the square. As long as the square is at rest, the time taken for a complete circuit is the same in either direction. But, if the square is made to rotate about an axis perpendicular to its plane, a ray travelling in the direction of rotation will take longer to complete the trip than one travelling in the opposite direction. This fact could be used to detect the earth's rotation. However, the speed of the light being much higher than that of the mirrors, the effect produced by the earth's

rotation would be too small to be measured. In 1925 Michelson and Gale used evacuated pipes forming a square 450 metres on a side and found that the earth's rotation caused a shift of a quarter of a wavelength.

The experiment can now be done in a more sensitive way using lasers. Four He-Ne lasers form the sides of a square (Fig. 17.2). Mirrors are so placed at the four corners that light leaving one end of a laser, goes round the circuit and returns to its starting point. If the square is rotating in the clockwise direction, the clockwise beam will travel farther to make a complete circuit and its frequency falls. The counter-clockwise beam correspondingly rises in frequency. The difference between these frequencies can be measured with the help of a photodetector and, hence, the rate of the rotation of the square (*i.e.*, the earth) can be calculated.

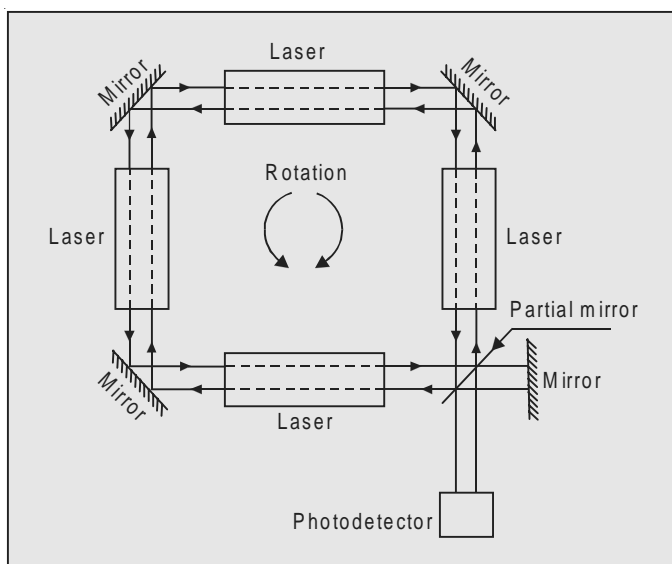


Fig. 17.2 Operation of the ring laser

17.4 COUNTING OF ATOMS

The monochromacy, directionality and intensity of laser light have made possible a wide range of scientific investigations which would not have been possible without lasers. With the modern pulsed laser, Rutherford's idea of "counting atoms", becomes entirely practicable, and individual atoms can now be counted by several different methods. Pulsed lasers can be used to remove one electron from each atom in a population of atoms of a selected type through a variety of photoionization schemes which form a part of what is known as 'resonance ionization spectroscopy'. Once an atom is ionized, it can be directed into detectors and stored there for almost any desired time.

17.5 ISOTOPE SEPARATION

Lasers have been successfully used to separate the isotopic species of an element present in an isotopic mixture. The technique of isotopic separation is of immense importance for nuclear power engineering. Natural uranium ore, used to fuel nuclear stations, contains mainly the isotope ^{238}U and only 0.7% of ^{235}U , which, in fact, fires nuclear plants and, hence, it is essential that it be separated from the ore. The technique is based on the fact that different isotopes absorb light at different frequencies. A particular species is selectively excited by means of a highly monochromatic laser, properly tuned to specific resonance, and then separated from the mixture by one of the several processes available. For example, Fig. 17.3 shows two isotopes, A and B, their excitation and ionization levels and the isotopic shift. The isotope A is selectively excited

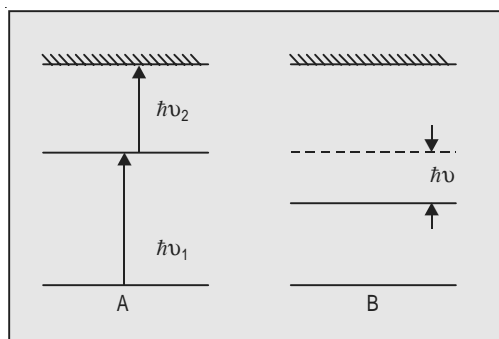


Fig. 17.3 Two-step photoionization

by absorption of photon $\hbar\nu_1$, from a tunable laser. The excited atom is subsequently ionized by another photon $\hbar\nu_2$ and then removed. The method is known as *two-step photoionization methods*. The diagram of a system for uranium isotope separation using this principle is given in Fig. 17.4. The frequency separation between the absorption bands of ^{238}U and ^{235}U is more than ~ 5 GHz. The dye laser has a bandwidth of ~ 0.1 GHz and, hence, it can be tuned to pump the required isotope. The beam of uranium atoms emerging from a heated furnace is pumped by a continuous dye laser tuned to a desired wavelength, viz. $\lambda = 5915.4$ Å. Atoms are then ionized by exciting them by ultraviolet radiation from a mercury lamp. The isotopes are separated in a mass spectrometer.

The isotopes can also be separated by what is known as *photon-deflection* method. An atom absorbing a photon of energy $\hbar\nu$ acquires a momentum $\hbar\nu$ in the direction of propagation of the photon. When it emits a photon, it acquires the same amount of momentum in the opposite direction. If it is made

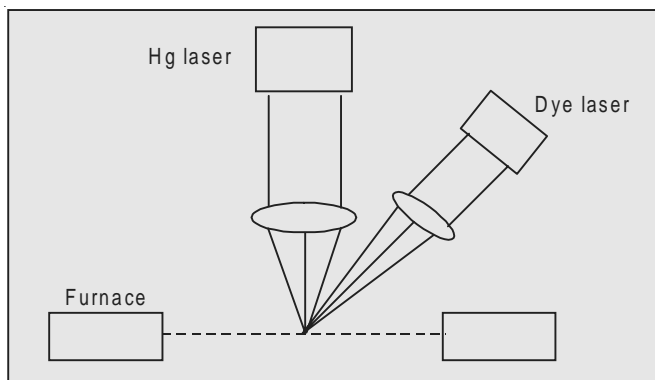


Fig. 17.4 Isotope separation

to absorb and emit the photon repeatedly a large number of times, it may acquire momentum sufficient to deflect away from the main stream. The atoms, physically deflected in this way, are then easily removed. There are various processes available for the removal of isotopic species. For example, isotopes of

1. hydrogen and boron were separated by photodissociation [413]
2. boron and chlorine by photochemical method [11]
3. calcium by two-step photoionization [67]
4. barium and calcium by photodeflection [41]
5. chromium by photoionization [383].

Jesey Nuclear-Avco Isotopes Inc [JNAI] have recently developed a laser isotope separation process [307] for separating uranium isotopes. The process exploits the fact that the absorption lines of ^{235}U and ^{238}U atoms have very small shifts—of the order of one-fourth of a wave number or 3×10^{-5} eV—in some transitions in the visible range. These shifts, though small, are larger than the bandwidths of individual transitions for each isotope. A collection of lasers tuned to the proper transition wavelengths can make the shifted absorption wavelengths accessible to selective excitation and ionization. JNAI used four different wavelength dye lasers. Three of these were for excitation and one for ionization (Fig. 17.5). This three-step process allows the use of lasers in the red-orange portion of the spectrum, where dyes are more efficient. The laser system sends properly tuned and timed pulses into a vacuum chamber, which contain both a uranium vapour source and an electromagnetic or plasma type of ion separator to remove ^{235}U ion from the neutral ^{238}U background vapours. The module is surrounded by a 100–200 gauss magnetic field parallel to the laser beam, which focusses a high-energy electron beam along a narrow line on the surface of molten uranium contained in a water-cooled crucible. The electron beam heats the uranium to 3000°K , producing a vapour which is allowed to expand radially to speeds comparable to that of sound. The vapour,

thus, enters the ion extraction structure, where it is illuminated by the laser beams. Once the ^{235}U atoms are selectively ionized, an electric pulse is applied to the ion deflector plates. The resulting electric field produces electron currents within the vapour which, together with the magnetic field, deflect ions out of the main stream onto to the product collection surfaces. For a high ionization probability, an average power of several kilowatts for the laser system is required.

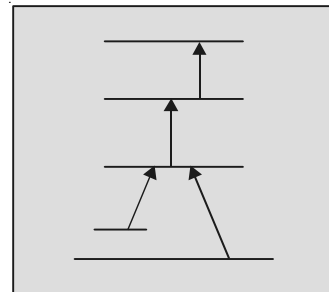


Fig. 17.5 Three-step photo-ionization

17.6 PLASMA

A plasma with very high electron density, 10^{20} cm^{-3} or more, may be produced by focussing a Q -spoiled giant pulse ruby or neodymium laser on a solid target with a peak laser power of the order of 100 megawatts. Stages of ionization in the range ~ 12 to 15 are attained despite the short lifetime of plasma, because of the very high electron density.

Laser methods have been devised to determine electron densities and temperatures of gas discharge plasmas by measuring either the refractive index or the spectral linewidth. The useful formulae are

$$\eta^2 = 1 - \left(\frac{\omega_p}{\omega} \right)^2 \quad \dots(17.2)$$

where ω is the angular frequency of the radiation for which the refractive index is determined and ω_p is the plasma angular frequency given by [232]

$$\omega_p = \left(\frac{n_e e^2}{m \epsilon_0} \right)^{1/2} \quad \dots(17.3)$$

where n_e is the electron density and m is the mass of the electron.

17.7 THERMONUCLEAR FUSION

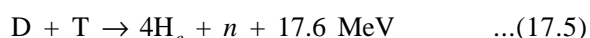
Fusion is a process in which atoms of two elements are compressed to such an extent that their nuclei fuse together and a new element is produced, whose mass is less than the sum of the masses of the two elements. The difference in mass is converted into energy in accordance with Einstein's equation

$$E = mc^2 \quad \dots(17.4)$$

For example, if one gram of mass is converted into energy, 9×10^{13} Joules of energy will be released, which is equal to the energy generated by 1000 MW power station run continuously for 25 hours. It is now known that the enormous amount of energy released from the sun is due to fusion of hydrogen brought about by gravitational forces. The sun produces energy of the order of 3×10^{26} Joules/sec. Fusion also is a source of energy in stars. The potential of controlled thermonuclear fusion, as an inexhaustible source of energy, is now well established. Fusion, therefore, is receiving increasing attention from the scientists.

For the nuclei to fuse together, a way must be found to overcome the mutual electrostatic repulsion or Coulomb repulsive barrier between the proton clouds of the two nuclei. This could be done by heating the matter to such a high temperature (~ 10 K) that the thermal velocity imparted to the nuclei is sufficient to overcome the mutual electrostatic repulsion. Matter at such high temperature comprises a mixture of electrons and ions—a plasma. The fusion power released at such a high temperature is much greater than the energy lost by radiation. However, for the release of a sufficient amount of thermonuclear energy and to sustain fusion reaction, it is necessary to confine the hot plasma, so that the fusion reaction continues for a long time. The laser has the potential to generate very high temperature and pressure required to initiate a fusion reaction and to concentrate large amount of energy in a small volume and, hence, can be an extremely useful tool in bringing about a fusion reaction.

In a typical scheme, a pea-sized target pellet, a fraction of a millimetre in diameter containing fusion fuel—usually a deuterium-tritium mixture—is projected into a reaction chamber, where it is suddenly irradiated with intense, high-energy laser beam. A pulse of 1 ns duration develops a power density of $\sim 10^{16}$ cm² at the pellet surface. As the surface of the target blasts away, the rocket like reaction forces implode the target's interior to densities ($\sim 1,000$ times liquid density) and temperature ($\sim 100,000,000$ °C) sufficient to cause the nuclei to fuse, releasing a large amount of thermonuclear energy in accordance with the equation



where n represents a neutron.

For both inertial and magnetic fusion, burn efficiency—the percentage of nuclei that fuse—is proportional to the product of density and confinement time. In magnetic fusion, the fuel density is limited by material properties, so the efficiency of the burn is increased by extending the duration of confinement. In inertial fusion, Newton's laws and thermal velocity limit the confinement time, so the fuel is compressed to higher densities.

17.8 LASERS IN CHEMISTRY

After the rapid progress in the area of isotope separation, several new areas in which lasers can be used to study chemical processes, are receiving much attention. One of the most important questions in chemistry is the study of the nature of chemical bonds. Laser light provides the most precise and controllable means for this purpose. With a sufficiently intense laser radiation, properly tuned to specific resonance, it is possible to break the molecules where we want to break them.

Photoacoustic spectroscopy (PAS) has become an invaluable experimental technique with weakly absorbing gases [219, 334]. A new method for trace analysis of gases has been developed by Siebert *et al.*, [346]. The technique is based on the pulsed photoacoustic Raman spectroscopy (PARS) which uses highly acoustic methods to detect the energy deposited in a gas sample by the process of stimulated Raman scattering. The analysis of mixtures of CH₄ in N₂, CO₂ in N₂ and N₂O in N₂ has been carried out using this method.

Some ingeneous radiochemical methods have recently been suggested [247] that might make it possible to detect the small number of atoms produced by interaction of low-energy solar neutrinos.

Another research direction that has risen in importance is the study and modification of surfaces using lasers. A group at the MIT Lincoln Laboratory has recently demonstrated the ability of ultraviolet lasers to deposit metallic films and introduce dopants in semiconductor substrates with a spatial resolution of about a micron. Infrared CO₂ lasers have also been used to deposit metal structures about 50 microns wide by laser-induced chemical vapour depositions [309]. These techniques hold a great promise for dealing with the present difficulties and future needs of microelectronic design and fabrication.

17.9 COMMUNICATION BY LASER

The four techniques commonly used for transmitting a large volume of messages over a long distance, are:

1. Coaxial-cable System

The cable consists of a copper tube about 3/8 inch in diameter with a single copper-wire-conductor in the centre. The cables carry radio waves with frequencies from 500,000 to 20,000,000 cycles per second. Amplifying equipment is located every two to four miles along the cable.

2. Microwave-radio Relay

The relay towers are located some 20 to 30 miles apart. The system employs microwave radiation in the frequency band between 1 billion to 10 billion cycles per second.

3. Wave-guide

A simple hollow tube about two inches in diameter is used as a waveguide to transmit millimetre waves with frequencies between 30 billion to 90 billion cycles per second.

4. Artificial Earth Satellite

This broad band communication operates within the microwave-radio band.

The main principle involved in these long distance communication systems is the principle of “multiplexing”, *i.e.*, the simultaneous transmission of different messages over the same path ways. The frequency band required for a channel for transmitting an individual human voice extends from 200 to 4,000 cycles per second. The information contained in this frequency band can be transmitted in any band that is 3,800 cycles per second wide, regardless of the region of the spectrum in which it is located. Higher frequency regions have far more room for communication channels and, hence, have a much greater potential capacity than the lower frequencies. For example, the frequency in the visible region at 6000 \AA is 5×10^{14} cycles per second; while that at $\lambda = 6 \text{ cm}$, it is 5×10^9 cycles per second. Thus, the communication capacity of a typical light wave is about 100,000 times greater than that of a typical microwave.

For modulation—the act of transferring a signal from one frequency band to another—to be effective without any interference to the signal, the system requires an oscillator capable of producing a carrier wave with a narrow spectral width. The unique properties of laser light, viz. coherence and monochromacy, meet these requirements. However, one has to get over some difficulties before the lasers are exploited for this purpose. Even when a highly directed laser beam is used, factors such as rain, snow and fog can cause heavy power losses. Laser transmission can be shielded from the atmosphere by putting lenses in an air tight pipe spaced 300 feet or more apart (Fig. 17.6). However, to allow the beam to follow a curved path, a large number of lenses would be necessary which would cause considerable transmission loss. This difficulty could be overcome by using a “gas lens” in which a gas, for example, carbon dioxide, is passed through a heated tube. Because the gas travels faster in the centre of the tube, it is cooler and, hence, denser there than at the walls, thus establishing a refractive index gradient which makes the gas to act as a converging lens. In this lens the losses are limited only to the slight scattering by the gas molecules.

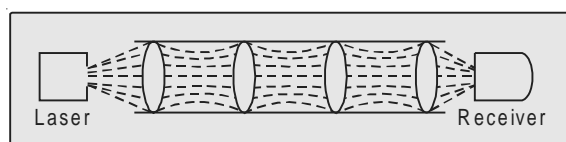


Fig. 17.6 Series of lenses to confine the laser beam and guide it to the receiver

Attention was subsequently directed to the possibility of using glass fibres as the medium for transmission of light waves employing the phenomenon of total internal reflection. Optical communication systems based on lasers and low-loss optical fibres are now being developed rapidly. Historically, multimode fibres were developed first. However, single-mode fibres are now more in use since they offer much more capacity.

On casual inspection multimode and single-mode fibres look identical. They both have outer diameter of the order of 125 microns. It is the internal optical design of the fibre that is different in the two cases (Fig. 17.7) [322]. The main difference is that the diameter of the single mode fibre's core is only 5 to 10 microns, while that of the multimode fibre's core varies from 50 to 200 microns. In the large cores, light can propagate in many modes, most of them involving repeated reflections at the core cladding interface. The diameters of the small cores are only a few times the wavelength of the light to be transmitted and only one mode, called fundamental mode, can propagate and it travels directly down the centre of the core. Bell Labs have recently announced [291] that they have transmitted light 119 km without the use of repeaters. The signal, in this case, was sent by the new C³ laser.

Optical fibres carry not only time-variable waveforms as described above but also spatial signals. A two dimensional picture can be conveyed to an appropriate place by means of optical fibres. For this purpose the fibres are stranded into cables. A cable may include over a hundred thousand fibres, each

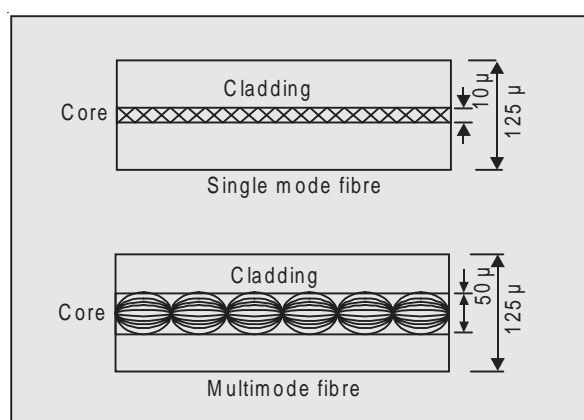


Fig. 17.7 Single and multimode fibres

of which has a cladding preventing its light energy from entering the adjacent fibres. The relative arrangement of the fibres is kept the same at the input and the output. Light reflected from each element of the picture enters into the respective fibre and produces this element at the output.

Laser communication lines based on fibre optics have been extremely useful in the modern computer networks.

17.10 RANGING

The position of a distant object can be determined with the help of a range finder, in which a signal from a laser switches on a counting circuit and the signal returned from the target terminates the count. The result is a digital count that can be calibrated directly in distance.

Optical range finders not only afford accurate ranging, but also make possible the determination of the size and shape of the object and its orientation.

The velocity of a moving object can be measured by comparing the frequency of the signal reflected from the object with the emitted frequency. The frequency shift is given by the formula

$$\Delta v = 2vu/c \quad \dots(17.6)$$

where u is the radial velocity of the target and v is the frequency of the signal.

Laser fluorescensors are used for remote environmental monitoring. The basic concept of a laser fluorescensor is as follows: A laser and a receiver are installed on a remote sensing platform such as an aircraft. The laser beam illuminates a small area at the surface of the target. Any fluorescence induced by the absorption of the laser light is detected and analysed by the receiver. The nature of the target is judged from the strength and spectral distribution of the fluorescence signal.

17.11 ATMOSPHERIC OPTICS

Atmospheric optics uses lasers for the remote probing of the atmosphere, including the measurement of traces of pollutant gases, temperature, water vapour concentration, sometimes at ranges greater than five to ten miles away. The first precision measurement of ozone in the atmosphere was made using laser remote sensing [322].

The pollutants in the atmosphere include oxides of nitrogen, carbon monoxide, sulphur dioxide and other matter. The chemical analysis of the sample collected from the atmosphere does not give real time data. The laser technique does not require any sample collection. The method consists of sending a laser beam through the atmosphere and carrying out measurements on the transmitted or scattered light. The results are available immediately and there is no distortion of the quantities measured.

Laser radar or “lidar” as it is known, has proved to be a powerful tool for investigation of a variety of atmospheric features. It employs a pulsed laser as a source of light energy. Light that is backscattered by the congestion of matter is detected by a photodetector. The distance of the scattering matter is calculated from the time the pulse takes to go to the matter and return back to the system. Lidar thus, provides the distribution of atmospheric pollutants in different vertical sections.

Measurements with lidar described above are useful in determining the concentration of matter at different heights, but does not give any information about the nature of scattering particles. This can be obtained from the measurements of Raman shifts. Because Raman shifts are characteristic of each species, analysis of backscattered light reveals the nature of the constituents by their shifts.

17.12 LASERS IN ASTRONOMY

Radio telescopes have now an additional accessory—a ruby laser, with the help of which the astronomers have been able to extend their range of observation. Radio astronomers have found lasers extremely valuable for amplifying very faint radio signals from space.

With the help of lasers it is possible to hear the bursts of light and radiation waves from stars which emitted them over a millions of years ago.

17.13 LASERS IN BIOLOGY

The ability of laser beams to concentrate high power density of light at a focal point has opened a new vista of micro Raman spectroscopic analysis, which enables one to extend such studies to biological and biomedical samples available only in very small quantities.

The measurements of Brillouin spectra can be related to the intrinsic molecular properties. Using a single-mode argon-ion laser and triple-pass Fabry-Perot interferometer, Brillouin scattering spectra of a wide range of biological materials were obtained by Vaughan and Randall [385]. From the Brillouin spectra measurements of the biological fibres collagen and keratin, synthetic polypeptides and material from the lens and cornea of the eye, coupled with density measurements, values of elastic moduli were deduced.

17.14 LASERS IN MEDICINE

Laser radiation is often used in controlling haemorrhage. Argon ion and CO₂ lasers are common sources in the treatment of lever and lungs, and for elimination of moles and tumors developing on the skin tissues.

Laser technology has made many surgical procedures less painful for the patient. Still more important are the prospects for treating conditions that cannot be dealt with effectively by other means. Laser's exquisite precision, spatial and temporal, not to mention precision of delivery through fibre-optic endoscopes, has been the principal attraction for surgeons.

Lasers are used in ophthalmology to reattach a detached retina. The green beam of the Ar⁺ laser is focussed on a certain point of the retina. The beam passes through the lens of the eye and the vitrious chamber without being absorbed, but is strongly absorbed by the red blood cells of the retina and the resulting thermal effect leads to reattachment of retina. The duration of the laser pulse is ~ 0.01 s and this being very short, the operation is virtually painless. Penetration of blood vessels in the eye for treating glaucoma is another area where lasers are found to be useful.

Lasers are now increasingly used in therapy and also in stomatology. They can selectively destroy tissues of the tooth affected by ovaries.

New types of surgery with ultraviolet excimer lasers and high powered pulsed neodymium laser energy transmitted through an optical fibre is now used in the treatment of liver cancer.

17.15 LASERS IN INDUSTRY

The precision properties of laser light have been of immense help in industry, particularly in testing the quality of optical components: lenses, prisms, etc. Accuracy in the measurement of the sizes of physical quantities is considerably increased. The length of a metre bar can now be measured by an automatic fringe counting method.

The ability of the laser beam to concentrate large-power in a small volume is easily utilised for the drilling of small holes and for the welding of small metal parts.

Lasers are found to be very effective in cutting different types of material. A CO₂ laser of 100 W continuous output can cut a cloth at a speed of 1 m/s. Thus it can prepare cut-pieces for about 50 suits in an hour. Laser cutting technology is widely used in the fabrication of space craft. A CO₂ laser of 3 kW continuous output cuts titanium sheets of 50 mm thickness at a velocity of 0.5 m/minute.

Lasers have been used as light sources for telephoto pictures. Pulsed Q-switched lasers are suitable for technical motion picture photography. Ellis and Fourney obtained pictures of bubble formation at the rate of 200,000 frames per second with a Q-switched ruby laser. The spiky output from a normal ruby laser has been found to be useful in high speed photography. The intensity of individual spikes is high enough for the light reflected from a

moving object to be recorded on a photographic plate. The successive positions of a bullet travelling at a speed of $20,000 \text{ cm sec}^{-1}$ have been photographed using a ruby laser [176].

One obvious use of a high-power source of relatively narrow-band radiation, such as free electron laser, is in industrial chemistry, to supply energy to specific reactions. For example, one could use such a source to clean the exhaust gases from combustion by selectively decomposing noxious substances. Similarly one could purify the feedstocks for chemical processes by selective destruction of contaminants.

It has been observed that finger-prints can be detected under laser light where the normal method of obtaining finger prints through dusting powder is ineffective. It is likely that people carry some kind of fluorescent contaminant on hands, picked up from minute traces of ink, paints, etc. If the blue light of an argon-ion laser is directed at suspected finger prints. Latent finger prints emit a part of the beam energy as yellow-light fluorescence. The laser technique can also be used for detection and analysis of older finger prints on, say, documents currency bills, cloth, etc. This is possible because finger prints contain ultraminiute quantities of stable amino acids, which when treated with certain chemicals become fluorescent.

**This page
intentionally left
blank**

14

MULIPHOTON PROCESSES

In the preceding chapter we discussed the problem of non-linear interaction between electromagnetic radiation and matter from semiclassical point of view. We will now reformulate the problem in quantum mechanical terms using the concept of photon stream instead of electromagnetic waves.

By multiphoton process we mean an interaction between radiation and matter accompanied by absorption or emission or both, of not less than two photons per elementary act. Such multiphoton processes were thought of even during the first years of development of quantum mechanics [104,131,149]. However, the experimental techniques available at that time were not adequate to observe the predicted phenomena. Prior to the appearance of lasers, the only two photon processes that could be observed experimentally were Rayleigh and Raman scattering. Multiphoton processes have assumed importance only after the advent of lasers.

14.1 MULTIQUANTUM PHOTOELECTRIC EFFECT

The photoelectric effect consists in ejection of electrons from matter by the action of light. If the energy $\hbar\omega$ of a photon absorbed by an electron inside a material exceeds the work W required to remove an electron from this material (work-function), the electron will leave the material. Its energy after liberation will be

$$\frac{1}{2}mv^2 = \hbar\omega - W. \quad \dots(14.1)$$

The photoelectric effect will, therefore, be observed if

$$\hbar\omega > W. \quad \dots(14.2)$$

The lowest frequency at which the photoelectric effect is observable, viz.

$$\omega_0 = \frac{W}{\hbar} \quad \dots(14.3)$$

is called the *threshold frequency*. The effect has nothing to do with the intensity of the radiation.

Could the photoelectric effect be observed at frequencies lower than the threshold frequency, *i.e.*, for $\omega < \omega_0$? In pre-laser optics the answer to this question would have been in the negative because it was always assumed that electron can absorb only one photon at a time. In the extremely high intensity laser pulses the density of photons is so high that an electron could absorb simultaneously two or more photons—a nonlinear effect. The laws of photoelectric effect, therefore, need reconsideration.

Suppose an electron in a material absorbs N photons at a time. Equation (14.1) then changes to

$$\frac{1}{2}mv^2 = N\hbar\omega - W. \quad \dots(14.4)$$

The photoelectric effect, therefore, can be observed if the condition

$$\omega \geq \frac{W}{N\hbar} \quad \dots(14.5)$$

is satisfied. This gives the threshold frequency

$$\omega_{\text{thresh}} = \frac{W}{N\hbar} \quad \dots(14.6)$$

which is smaller than ω_0 given by (14.3). Thus, higher the light intensity, lower is the threshold frequency. The photoelectric effect, therefore, depends both on the frequency of the radiation as well as on its intensity. It may be called *multiquantum photoelectric effect*.

14.2 TWO-PHOTON PROCESSES

Is it possible to transform a coherent light wave with frequency ω into a coherent light wave with frequency 2ω or 3ω ? Such a conversion, if possible, cannot take place through interaction between photons. There is no direct photon-to-photon interaction. It is indeed true that the general tendency of photons is to occupy a state which is densely populated by other photons. This is the characteristic of all bosonic particles. But it has nothing to do with the concept of direct interaction between photons. A photon cannot absorb or scatter other photons nor does it decay of its own. No known force can mediate interaction between photons. The transformation of photons can be brought about only through an intermediary—a quantum system such as an atom or a molecule characterized by a system of discrete energy levels. An atom or a molecule can absorb or emit photons and in the process may undergo a transition from one energy level to the other.

Consider, for example, a process shown in Fig. 14.1. The atom absorbs energy $\hbar\omega$ and changes from level 1 to level 2. After a shortwhile it returns to level 1 by emitting a photon of the same energy. The state of the atom remains unaltered as far as its energy is concerned; but the emitted photon, although has the same energy as the incident photon, may be in a different state in that it may have a different momentum, direction and polarization. The atom has acted in this transformation as an intermediary.

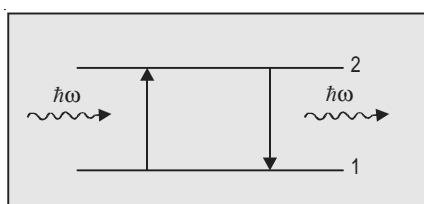


Fig. 14.1 Absorption and emission of a photon—a two level system

Consider now another process (Fig. 14.2). The molecule absorbs a photon of energy $\hbar\omega_{13}$ and shifts from level 1 to level 3 and then emits a photon of energy $\hbar\omega_{32}$ by dropping from level 3 to level 2. In this process photon frequency ω_{13} has been converted into a frequency ω_{32} through the intermediary role played by the molecule; but in this case the state of the intermediary is also changed.

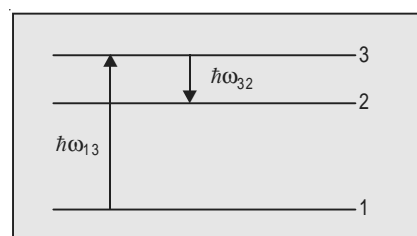


Fig. 14.2 Absorption and emission of a photon—a three

14.3 THEORY OF TWO-PHOTON PROCESSES

In Chapter 3 we used perturbation theory to obtain expression for the rate at which an atom absorbs light. In these calculations we had retained the linear term and neglected the higher order terms on the ground that they are very weak. They are not, however, so weak for light from a laser source. The very high photon flux and the associated high field of radiation enables the atom or molecule to interact with more than one photon at the same time giving rise to a variety of optical processes, such as multiphoton absorption, second harmonic generation, frequency mixing, etc. These multiphoton processes are described by second and higher order approximations of the perturbation theory. We shall illustrate the method by applying it to two-photon absorption. It would be

interesting to note that the possibility of two-photon absorption was first suggested by M. Goeppert-Mayer [149] many years before lasers were thought of.

Let us go all the way back to the perturbation theory of the interaction of radiation with matter, introduced in Chapter 3. We considered there a quantum system described by a time-independent Hamiltonian H_0 , *i.e.*,

$$\hat{H}_0 |\psi, t\rangle = i\hbar \frac{\partial}{\partial t} |\psi, t\rangle \quad \dots(14.7)$$

under the influence of a perturbation whose operator $\hat{H}'(t)$ was of the form

$$\begin{aligned} \hat{H}'(t) &= \hat{H}'(t) \text{ if } 0 \leq t \leq \tau \\ &= 0 \text{ if } t < 0 \text{ and } t > \tau \end{aligned} \quad \dots(14.8)$$

The relevant Schrödinger equation was

$$(\hat{H}_0 + \hat{H}'(t)) |\psi, t\rangle = i\hbar \frac{\partial}{\partial t} |\psi, t\rangle \quad \dots(14.9)$$

Assuming the solution of this equation to be a linear combination of basic states $|u_n\rangle$, *i.e.*,

$$|\psi, t\rangle = \sum_n C_n(t) \exp(-i E_n t / \hbar) |u_n\rangle \quad \dots(14.10)$$

and with a few manipulations and calculations we arrived at the equation

$$\frac{d C_m(t)}{dt} = \frac{1}{i\hbar} \sum_{n=0}^{\infty} C_n(t) \langle u_m | \hat{H}'(t) | u_n \rangle \exp(-(i/\hbar)(E_n - E_m)t) \quad \dots(14.11)$$

From this and with the approximation that at $t = 0$, $C_n(t) = 1$ and $C_m(t) = 0$ for all m , we arrived at the relation

$$\frac{d C_m(t)}{dt} = \frac{1}{i\hbar} \langle u_m | \hat{H}'(t) | u_n \rangle \exp(i\omega_{mn}t) \quad \dots(14.12)$$

which, on integration, gave an approximate first-order relation

$$C_m^{(1)}(t) = \frac{1}{i\hbar} \int_0^t \langle u_m | \hat{H}'(t') | u_n \rangle \exp(i\omega_{mn}t') dt' \quad \dots(14.13)$$

The superscript on $C_m(t)$ represents the order of the approximation.

Further, using the fact that the main contribution to the interaction comes from dipole interaction, we put

$$\hat{H}'(t) = \sum_j \mathbf{e} \mathbf{r}_j \cdot \mathbf{E}_0 \cos \omega t \quad \dots(14.14)$$

and obtained the formula

$$C_m^{(1)}(t) = \frac{eE_0 \langle u_m | X | u_n \rangle}{2\hbar}$$

$$\times \left\{ \frac{1 - \exp(i(\omega_{mn} + \omega)t)}{\omega_{mn} + \omega} + \frac{1 - \exp(i(i\omega_{mn} - \omega)t)}{\omega_{mn} - \omega} \right\} \quad \dots(14.15)$$

So far we have recapitulated the treatment given in Chapter 3 for obtaining the first order solution; let us now extend the theory to the second order.

Recall, that equation (14.12) was derived from the general solution (14.11) by putting $C_n(t) = 1$. For extending the theory to the second order, we have to replace $C_n(t)$ by (14.15). Thus

$$\begin{aligned} \frac{dC_l^{(2)}(t)}{dt} &= \frac{1}{l\hbar} \sum_m C_m^{(1)}(t) \langle u_l | \hat{H}'(t) | u_m \rangle \exp(i\omega_{lm} t) \\ &= \frac{1}{i\hbar} \sum_m \frac{eE_0 \langle u_m | X | u_n \rangle}{2\hbar} \\ &\quad \times \left\{ \frac{1 - \exp(i(\omega_{mn} + \omega)t)}{\omega_{mn} + \omega} + \frac{1 - \exp(i(\omega_{mn} - \omega)t)}{\omega_{mn} - \omega} \right\} \\ &\quad \times \langle u_l | \hat{H}'(t) | u_m \rangle \exp(i\omega_{lm} t) \\ &= \frac{1}{i\hbar} \sum_m \frac{e^2 E_0^2 \langle u_l | X | u_m \rangle \langle u_m | X | u_n \rangle}{4\hbar} \\ &\quad \times \left\{ \frac{1 - \exp(i(\omega_{mn} + \omega)t)}{\omega_{mn} + \omega} + \frac{1 - \exp(i(\omega_{mn} - \omega)t)}{\omega_{mn} - \omega} \right\} \times \\ &\quad \times \{ (\exp(i(\omega_{lm} + \omega)t) + \exp(i(\omega_{lm} - \omega)t)) \} \quad \dots(14.16) \end{aligned}$$

where we have put

$$\begin{aligned} \langle u_l | \hat{H}'(t) | u_m \rangle &= \left\langle u_l | \sum_j e \mathbf{r}_j \cdot \mathbf{E}_0 \cos \omega t | u_m \right\rangle \\ &= eE_0 \langle u_l | X | u_m \rangle \left(\frac{e^{i\omega t} + e^{-i\omega t}}{2} \right) \end{aligned}$$

In integrating this equation, we retain only those terms in which the denominator approaches zero; the other terms make no contribution to the accumulating probability. We assume $E_l > E_m > E_n$ which makes ω_{lm}, ω_{mn} , positive. Hence, we retain only the terms in $\omega_{mn} - \omega$ and $\omega_{lm} - \omega$. Thus,

$$\begin{aligned}
C_l^{(2)}(t) &= \frac{1}{i\hbar} \sum_m \frac{e^2 E_0^2 \langle u_l | X | u_m \rangle \langle u_m | X | u_n \rangle}{4\hbar} \\
&\quad \times \int_0^{t'} \left\{ \frac{1 - \exp(i(\omega_{mn} - \omega)t')}{\omega_{mn} - \omega} \right\} \exp(i(\omega_{ln} - \omega)t') dt' \\
&= \frac{1}{4\hbar^2} \sum_m e^2 E_0^2 \langle u_l | X | u_m \rangle \langle u_m | X | u_n \rangle \\
&\quad \times \left[\frac{1 - \exp(i(\omega_{ln} - \omega)t)}{(\omega_{mn} - \omega)(\omega_{ln} - \omega)} - \frac{1 - \exp(i(\omega_{ln} - 2\omega)t)}{(\omega_{mn} - \omega)(\omega_{ln} - 2\omega)} \right] \quad \dots(14.17)
\end{aligned}$$

where we have used the relation $\omega_{ln} = \omega_{mn} + \omega_{lm}$.

We notice that in second order, a resonance appears at $\omega_{ln} = 2\omega$ corresponding to a two-photon absorption process. The probability of the two-photon processes occurring is given by $|C_i^{(2)}(t)|^2$ in which only the second term in the brackets is relevant.

$$\begin{aligned}
\therefore P_{n \rightarrow l}^{(t)} &= |C_l^{(2)}(t)|^2 = \sum_m \frac{e^4 E_0^4 |\langle u_l | X | u_m \rangle \langle u_m | X | u_n \rangle|^2}{16\hbar^4 (\omega_{mn} - \omega)^2} \\
&\quad \times \frac{4t \sin^2(\omega_{ln} - 2\omega)t/2}{(\omega_{ln} - 2\omega)^2 t} \quad \dots(14.18)
\end{aligned}$$

\therefore The rate of two-photon absorption is

$$= \sum_m \frac{\pi e^4 E_0^4 |\langle u_l | X | u_m \rangle \langle u_m | X | u_n \rangle|^2}{8\hbar^4 (\omega_{mn} - \omega)^2} \delta(\omega_{ln} - 2\omega) \quad \dots(14.19)$$

where we have used the relation

$$\delta(\omega_{ln} - 2\omega) = \frac{2}{\pi} \lim_{t \rightarrow \infty} \frac{\sin^2(\omega_{ln} - 2\omega)t/2}{(\omega_{ln} - 2\omega)^2 t}. \quad \dots(14.20)$$

The appearance of the intermediate states in the above formula reflects the possibility of attaining the final state via a series of intermediate states, which are connected with the initial and final states by non-zero matrix elements. In each transition the system absorbs or emits one photon. The transition $n \rightarrow l$ represented by the formula (14.19) is, therefore, a two-photon process (Fig. 14.3). It must be emphasized here, however, that this transition, or for that matter any multiphoton transition, cannot, in principle, be divided into a temporal sequence of events. It should be understood that both photons are absorbed simultaneously. It would be incorrect to assume that first one photon

is absorbed and then the other. In such a case the transition would be equivalent to two single photon transitions and not one two-photon transition.

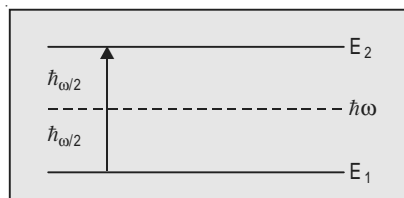


Fig. 14.3 Two-photon absorption

Two important features of two-photon absorption need be mentioned here:

- (i) We know that a single photon absorption occurs between states of opposite parity. In a nonlinear medium a two-photon absorption, such as the one shown in Fig. 14.3, occurs between states of the same parity. That is, a transition that is forbidden for one-photon absorption is allowed for two-photon absorption.
- (ii) Formula (14.19) shows that the probability of two photon absorption is proportional to the fourth power of the electric field, *i.e.*, to the square of the intensity.

14.4 EXPERIMENTS IN TWO-PHOTON PROCESSES

14.4.1 CaF₂: Eu⁺⁺ Crystals

The two-photon absorption was observed for the first time in CaF₂ crystals activated with divalent europium, Eu⁺⁺ replacing Ca⁺⁺ ions [Kaiser *et al.*, 206]. The radiation from a ruby laser was focussed on a thin (0.1 mm) slab of a CaF₂: Eu⁺⁺ crystal, placed in front of the entrance slit of a spectrograph. Two red filters with transmission less than 10⁻⁴ for $\lambda < 6100 \text{ \AA}$ were placed in front of the crystal so as to exclude the possibility of blue or ultraviolet radiation from the pump lamp falling on the crystal. Since the lowest lying energy level in the CaF₂: Eu⁺⁺ crystal corresponds to an energy of 22,000 cm⁻¹, the crystals are transparent to the radiation from a ruby laser which corresponds to 14,400 cm⁻¹.

With the arrangement described above, the spectrographic record showed, besides a line at $\lambda = 6943 \text{ \AA}$ emitted by the ruby laser, a line at $\lambda = 4250 \text{ \AA}$. When inactivated CaF₂ crystal was illuminated with the same laser, no radiation at $\lambda = 4250 \text{ \AA}$ was observed. The line at this wavelength, therefore, must be attributed to the transition of Eu⁺⁺ ions. It was further found that the fluorescence intensity was proportional to the square of the laser emission intensity, thus, suggesting that the line at 4250 Å is, probably, a result of a two-photon process.

It is known that $\text{CaF}_2 : \text{Eu}^{++}$ crystals have an intense absorption band between 30,000 and 25,000 cm^{-1} , corresponding to electron transition $4s \longleftrightarrow 5d$ of Eu^{++} ions. When the crystal is excited with the light in the same wavelength range, a bright blue fluorescence is observed with a band width $\sim 300 \text{ \AA}$ near 4200 \AA . This fluorescence is interpreted as a result of non-radiative transition of Eu^{++} from the upper state into an intermediate lower state with subsequent emission as the ions undergo a transition to the ground state. The observation made in the above experiment was, therefore, interpreted as excitation by two photon absorption to the state $5d$, followed by non-radiative and radiative transitions as above. A simplified analysis of this process was given by Kleinman [217] where it is assumed that the two-photon transition proceeds via an intermediate state connected with the initial and final states.

14.4.2 Cesium Vapour

Two-photon absorption in an atomic system was first observed by Abella [1], on exciting cesium vapour with ruby laser. The two main requirements for the two-photon absorption are: (i) the energy for lifting the atom to the excited level should be double the energy of exciting photon, and (ii) the initial and final states should have the same parity. Both these conditions are satisfied in the case of cesium. The transition to $9D_{5/2}$ and $9D_{3/2}$ levels of cesium correspond to energies 28,836.06 and 28,828.90 cm^{-1} respectively, which is close to double the energy of the ruby laser ($\sim 14,400 \text{ cm}^{-1}$) and their parity is the same as that of the initial state. Figure 14.4 shows the various levels involved in the process.

A very elementary experimental set up was used for this investigation. The radiation from a ruby laser was focussed on a cell containing cesium vapour. The fluorescence light, filtered out with a CuSO_4 solution and with a narrow-band interference filter, was detected by a photomultiplier, at right angles to

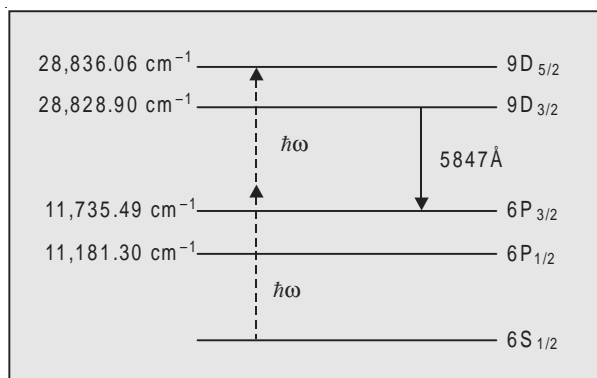


Fig. 14.4 Energy level scheme for Cs atom

the direction of the laser beam. It was established before hand that in the absence of cesium vapour, no fluorescence could be observed in the range of

wavelengths of the laser. With cesium, fluorescence line was observed at $\lambda = 5847 \text{ \AA}$ corresponding to the transition $9D_{3/2} - 6P_{3/2}$. The line appeared only when the central wavelength in the laser emission was equal to $6935.5 \pm 0.05 \text{ \AA}$. This dependence of the fluorescence on the wavelength of the laser emission indicates the occurrence of two-photon absorption.

14.4.3 Anthracene

Two-photon excitation of fluorescence in anthracene single crystals was observed by Peticolas *et al.* [305] and Singh *et al.* [351]. The light beam from a ruby laser was focussed on the slabs of anthracene ranging in thickness from $100 \mu\text{m}$ to 20 m , cut from a single crystal of anthracene. The spectrum observed (Fig. 14.5) on a grating spectrograph was found to be exactly similar to the one obtained when the crystal was excited by radiation of wavelength larger than 3800 \AA and corresponding to the transition from the excited $^1B_{2u}$ state to the ground state 1A_g . The excited $^1B_{2u}$ state lies at about $28,800 \text{ cm}^{-1}$ which is close to double the energy of the ruby laser. The state was not observed in the case of a single-photon excitation because it has the same parity as that of the ground state, but its existence was predicted theoretically. The observed quadratic dependence of the fluorescence intensity on the intensity of the exciting laser radiation can serve as an argument in favour of the two photon mechanism of excitation.

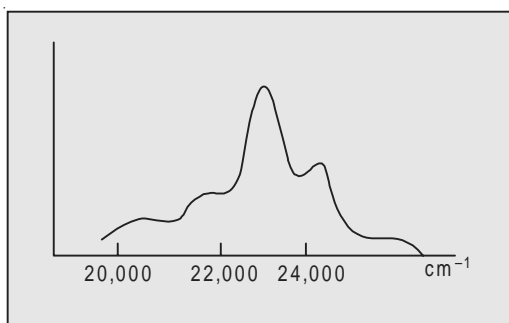


Fig. 14.5 Fluorescence spectrum of anthracene

14.4.4 KI

A different experimental technique was used by Hopfield *et al.* [192] in their study of two photon absorption in KI crystals. The experimental set up is shown in Fig. 14.6. The sample used measured $2 \times 3 \times 25 \text{ mm}$.

As shown in the figure, two light sources were used, a ruby laser with pulsed energy approximately 15 J and a xenon lamp giving continuous spectrum in the ultraviolet. A measure of the two-photon absorption was the decrease in

the xenon lamp radiation transmitted through the sample, under the action of the laser pulse.

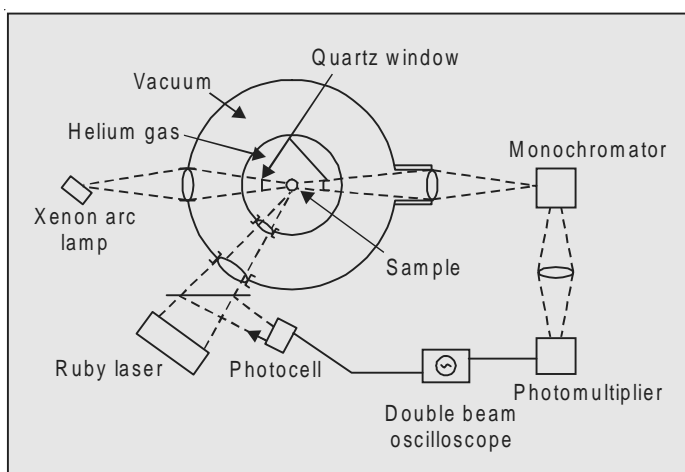


Fig. 14.6 Experimental arrangement for two-photon absorption in KI crystal

14.4.5 Two-Photon Effect in a Semiconductor

The internal two-photon photoeffect in a semiconductor which consists in exciting electrons from the valence band to the conduction band, was observed by Braunstein and Ockman [65] in CdS, using a ruby laser. The energy gap in the semiconductor being 2.4 eV, the energy of a photon of the ruby laser (1.8 eV) is insufficient to excite the electrons in the conduction band. The semiconductor, therefore, is transparent to the source with this wavelength. Two-photon excitation of electrons in the conduction band was detected by observing recombination emission from the excitation and the impurity levels, arising as a result of two-photon excitation. The intensity of the recombination emission has exhibited a quadratic dependence on the excitation intensity and its order of magnitude is close to that predicted theoretically.

14.4.6 Two-Photon Ionization

The possibility of two-photon ionization of atoms is of considerable interest both from the theoretical and experimental points of view. Such an effect can be observed in the negative ions I^- , Br^- and F^- which have an ionization potential sufficiently low for two-photon excitation with the aid of a ruby laser [Coltman, 81].

14.5 VIOLATION OF THE SQUARE LAW DEPENDENCE

Bradley *et al.*, [63, 64] observed that in rhodamine B, at high laser intensities or photon fluxes, the fluorescence intensity does not show the expected square law dependence on the laser intensity. Similar investigations by Eichler *et al.*, [110] in rhodamine G show that up to incident intensities of 6×10^{28} photon $\text{cm}^{-2} \text{ sec}^{-1}$, the two-photon fluorescence intensity showed a quadratic dependence on the photon flux. At higher photon flux it increased less than quadratically with the increase of excitation intensity. The possible mechanism suggested by them for this quenching is stimulated Raman scattering, since it was observed that the two-photon fluorescence quenching and the stimulated anti-Stokes emission had thresholds in the same power range.

14.6 DOPPLER-FREE TWO-PHOTON SPECTROSCOPY

The feasibility of Doppler-free two-photon spectroscopy was shown in 1974, independently, by Bernard Cagnac (France), Bloembergen and Levenson (Harvard) and Hansch, Maisel, Harrey and Schawlow (Stanford). In this form of high resolution non-linear laser spectroscopy, gas atoms in a standing wave field are excited by absorbing two photons from opposite directions. Their first-order Doppler shifts are equal and opposite and, hence, the sum frequency is unchanged. (See Chapter 15, Sec. 15.10).

14.7 MULTIPHOTON PROCESSES

In Section 14.2 we derived an expression for two-photon absorption. The general expression for the transition rate from the initial state $|i\rangle$ to the final state $|f\rangle$ is

$$R_{i \rightarrow f} = \frac{2\pi}{\hbar^2} \left| \langle f | \hat{H}' | i \rangle + \frac{1}{\hbar} \sum_l \frac{\langle f | \hat{H}' | l \rangle \langle l | \hat{H}' | i \rangle}{\omega_i - \omega_l} \dots \right. \\ \left. + \frac{1}{\hbar^{n-1}} \sum_{l_1} \sum_{l_2} \dots \sum_{l_{n-1}} \frac{\left| \langle f | \hat{H}' | l_1 \rangle \langle l_1 | \hat{H}' | l_2 \rangle \dots \langle l_{n-1} | \hat{H}' | i \rangle \right|^2}{(\omega_i - \omega_{l_1})(\omega_i - \omega_{l_2}) \dots (\omega_i - \omega_{l_{n-1}})} \times \delta(\omega_i - \omega_f) \right| \dots \quad (14.21)$$

If we are considering a simple absorption or emission of a photon, only one photon state is changed and only the first order term suffices. It represents the rate of direct transition from state $|i\rangle$ to state $|f\rangle$. For the two-photon

absorption process second order term is required. The higher order terms also represent transition from the initial state $|i\rangle$ to the final state $|f\rangle$; but the transitions are via one or more intermediate states.

It may be noted that the presence of the delta-function ensures conservation of energy between the initial and the final states, but not necessarily in the case of intermediate states. The intermediate states are called *virtual states* of transition. In multiphoton transitions it is necessary to resort to this concept of “virtual levels”. How does a virtual level differ from a real level? A microscopic object can always be observed on any really existing level. A multiphoton transition cannot be separated in time in different stages and, hence, the microscopic object working as an intermediary, cannot be observed on a virtual level. The system passes through the intermediate states only in a virtual sense. There is no need, therefore, for energy to be conserved in the intermediate states since no real transitions are made into them.

14.8 THREE-PHOTON PROCESSES

For a three-photon process we have to consider the third term in (14.21). The matrix elements in this term indicate that the fluorescence resulting from three-photon absorption must be proportional to the cube of the laser output. The simultaneous absorption of three-photons was demonstrated by Singh and Bradley [352]. Substantial ion yields were observed by Harrison *et al.*, [172] when CH_2I_2 was excited by 248 and 193 nm. The yield was found to increase with the third power of the laser intensity, thus suggesting that three-photon excitation is required for ion formation.

14.9 SECOND HARMONIC GENERATION (SHG)

Second harmonic generation is a three-photon process as shown in Fig. 14.7. Two photons, each with energy $\hbar\omega$, are absorbed and one photon with energy $2\hbar\omega$ is emitted. The state of the quantum system remaining unaltered. This gives an impression that two colliding photons merge ‘directly’ into a single one. The levels shown in the figure by dotted lines are the “virtual levels.”

We have shown in the preceding chapter that for efficient transfer of light energy from the pumping wave to the secondary wave the condition of “*wave synchronism*” has to be satisfied. That is, the pumping wave parameters, should match with those of the secondary wave. In photon terms this condition is equivalent to the energy-momentum conservation laws to be satisfied by the photons participating in the process.

$$\hbar\omega + \hbar\omega = 2\hbar\omega \quad \dots(14.22)$$

$$P_1 + P_2 = P \quad \dots(14.23)$$

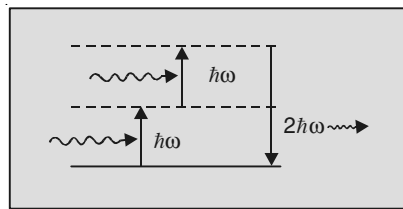


Fig. 14.7 Second harmonic generation

Assuming that the directions of the pumping wave and the secondary wave are the same, we can write (14.23) in the scalar form

$$2p_1 = p. \quad \dots(14.24)$$

Since $p = \frac{h\omega}{c} \eta(\omega)$, the above relation becomes

$$\frac{2h\omega}{c} \eta(\omega) = \frac{h(2\omega)}{c} \eta(2\omega) \quad \dots(14.25)$$

i.e.,

$$\eta(\omega) = \eta(2\omega) \quad (\text{Sec. 13.21}) \quad \dots(14.26)$$

14.10 PARAMETRIC GENERATION OF LIGHT

In terms of photon concepts, the parametric generation of light can be explained with the help of (Fig. 14.8). It shows a three-photon process in which one photon of energy $\hbar\omega$ is absorbed by the microscopic system and two photons, one with energy $\hbar\omega_1$ and the other with energy $\hbar\omega_2$ are emitted, the state of the microscopic system remaining unaltered, indicating, as if, a photon has decayed into two new secondary photons. The energy-momentum conservation laws to be satisfied are

$$\hbar\omega = \hbar\omega_1 + \hbar\omega_2 \quad \dots(14.27)$$

$$\mathbf{p} = \mathbf{p}_1 + \mathbf{p}_2 \quad \dots(14.28)$$

The process describes the “transformation” as we may call it, of a light wave with frequency ω into two new light waves of frequency ω_1 and ω_2 .

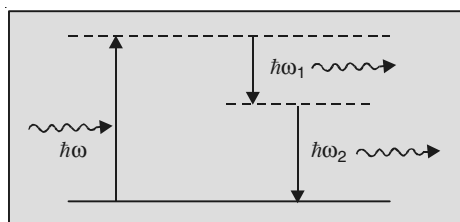


Fig. 14.8 Parametric generation of light

14.11 PARAMETRIC LIGHT OSCILLATOR

To obtain high power by parametric amplification, a uni-axial crystal with relatively high nonlinear susceptibility, cut according to the requirement of the wave-synchronism, is placed inside an optical resonator. A laser is used for pumping the parametric amplifier. The intensity of the pumping wave must be high enough to bring out the nonlinear properties of the crystal and to compensate for the losses that may occur. The mirrors of the resonator must have high reflectances for ω_1 and $\omega_2 = \omega - \omega_1$, but high transmittance for the laser frequency ω . The parametric amplifier, under these conditions, goes into oscillations at both frequencies ω_1 and ω_2 . The process is known as *parametric oscillation*.

The most promising use of a parametric oscillator is that it provides a tunable source of coherent radiation. Parametric processes have been widely used to generate tunable laser light [357]. Tuning of a parametric light oscillator can be effected by controlling the frequency of the secondary waves generated. There are several methods of controlling the frequency. One of these is to rotate the crystal in such a way that different frequencies are phase-matched. The other is to vary the crystal temperature. Since the refractive index is a function of temperature, the change in temperature will affect the shape of the refractive index surfaces corresponding to the ordinary and extraordinary waves and thus, will lead to the change in the direction of wave-synchronism for any fixed combination of frequencies.

A schematic diagram for a typical optical parametric oscillator is shown in (Fig. 14.9).

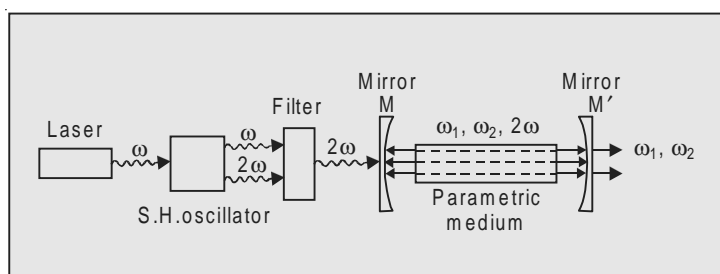


Fig. 14.9 Optical parametric oscillator

Intense pumping light at frequency ω from a *Q*-switched laser passes through a SH oscillator producing a second harmonic radiation at frequency 2ω . A filter F eliminates the fundamental and allows only the second harmonic to pass into the parametric medium P . The radiations at ω_1 and ω_2 build up in P . The mirror M allows radiation at 2ω to pass into the medium, but reflects those at ω_1 and ω_2 , while the mirror M' reflects the pumping light at 2ω back into the medium, but allows a portion of ω_1 and ω_2 to emerge. The medium P is placed in an oven which makes it possible to change the temperature.

In order that it produces only one wave, sometimes a Glan prism is introduced in the cavity between the crystal and the output mirrors. The prism passes one wave but deflects the other.

Parametric oscillations have been tuned across the visible and near infrared region in LiNbO_3 when pumped at the second harmonic of the $1.06 \mu\text{m}$ Nd: YAG laser [Bjorkholm *et al.*, 48, Falk *et al.*, 121].

14.12 FREQUENCY UPCONVERSION

Parametric amplification can also be used to convert from a low frequency to a higher one. Suppose two collinear beams with frequencies ω_1 and ω_2 are incident on a nonlinear crystal. If the crystal is phase matched for these frequencies as well as the sum frequency $\omega = \omega_1 + \omega_2$, this third frequency is generated. This process is known as *frequency upconversion*.

The processes of SHG and frequency mixing can be combined to produce beams of higher frequencies. As an example, consider the scheme shown in Fig. 14.10.

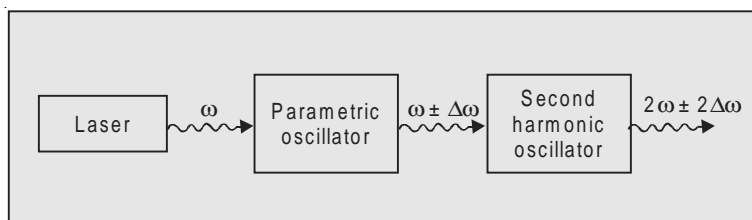


Fig. 14.10 Frequency upconversion

The laser emits a coherent light wave with frequency ω . This wave serves as the pumping wave for the parametric oscillator which emits radiation that can be continuously tuned in the range $\omega_1 - \Delta\omega$ to $\omega_1 + \Delta\omega$. This in turn serves as a pumping wave to SH oscillator. What emerges is a coherent radiation with frequency continuously tunable from

$$2\omega_1 - 2\Delta\omega \text{ to } 2\omega_1 + 2\Delta\omega$$

Consider now another example (Fig. 14.11).

The light at frequency ω from a laser, after passing through two SH oscillators is converted into light with frequency 4ω . Mixing this fourth harmonic with ω with the aid of a parametric oscillator, we get a fifth optical harmonic. It must be noted that at each conversion some portion of the energy is lost.

14.13 PHASE-CONJUGATE OPTICS

One of the new research areas in coherent optics which is receiving increasing attention is what is known as *phase-conjugate optics*. Its main feature is the generation of an electromagnetic wave with a phase distribution, that is, at each point in space, the exact opposite of that of an arbitrary incoming wave and

which propagates in the opposite direction, retracting the original path of the incoming wave.

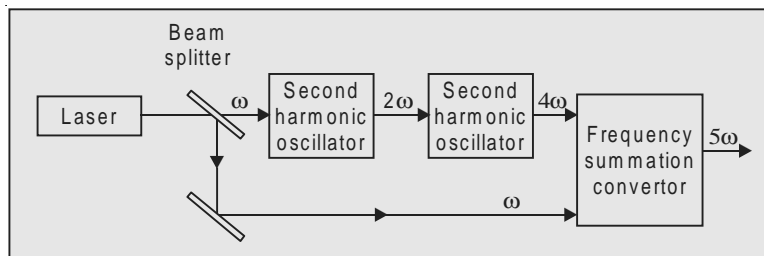


Fig. 14.11 Fifth optical harmonic

Suppose a beam with a plane wavefront emitted by a laser, traverses an active material and then is reflected backwards by a plane mirror. As the beam passes through the material, it undergoes wavefront distortions. The distorted wavefront would be somewhat like the one shown in Fig. 14.12(a) [373]. The

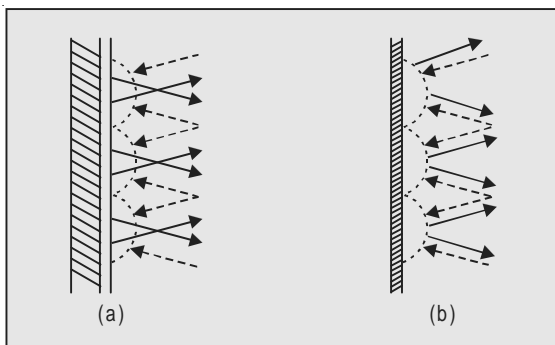


Fig. 14.12 Phase conjugation

rays, normal to the wavefront and incident on the mirror, are shown by dotted lines and those reflected according to the law of reflection by solid lines. If now the plane mirror is replaced by a reflecting surface which has the same shape as the oncoming wavefront, the reflected rays will experience a turn of 180° as shown in Fig. 14.12(b) and, thus, a reversal of the wavefront will occur. That is, the reversed rays acquire the conjugate phases and, hence, the process is known as *phase conjugation*. If such a phase-conjugated reversal is brought about in systems used with lasers, the beam, upon a round trip through the active material, will regain the same wavefront it had in its forward trip, thus resulting into a more powerful beam. The question is how to prepare such an adaptive system?

Let us discuss briefly the basic approaches proposed for phase conjugation. Yariv [409-10] proposed the use of three wave mixing for this purpose.

A wave E_1 at frequency ω and a wave vector \mathbf{k}_1 (ω) and another intense pump wave E_2 at a frequency 2ω and a wave vector \mathbf{k}_2 (2ω) are incident

simultaneously on the crystal. If the crystal is lacking in inversion symmetry, in addition to the linear polarization, a second order nonlinear polarization proportional to $E_1^* E_2$ occurs in it (See Chapter 13), which acts as a source that radiates a third wave E_3 , at the difference frequency $2\omega - \omega = \omega$ with the wavevector $\mathbf{k}_3(\omega)$ and with a spatial amplitude distribution proportional to $E_1^* E_2$. Effective transfer of energy from E_2 to E_3 is possible only if the phase matching condition

$$\mathbf{k}_3(\omega) = \mathbf{k}_2(2\omega) - \mathbf{k}_1(\omega) \quad \dots(14.29)$$

is satisfied. If E_2 is a plane wave, E_3 becomes conjugate replica of E_1 . If (14.29) is not satisfied, the wavefronts of E_3 , at different regions of the crystal, do not add up in phase and the amplitude of E_3 is reduced due to the destructive interference. Phase conjugation using this technique was demonstrated by Avizonis *et al.* [19].

Four wave mixing was first demonstrated experimentally by Terhune and his collaborators. Bloembergen and his collaborators have studied four wave mixing systematically as a function of the three frequencies in many different materials and obtained their dispersive character. Subsequently they used four light beams of almost equal frequency to show the effect of collision-induced coherence—apparently a paradoxical behaviour since collisions are known to destroy coherence.

Hellworth [183] showed that phase-matching condition that is inherent in the three wave mixing is eliminated in the *degenerate four wave mixing*. All the four optical fields involved in this mixing process are of the same frequency ω ; hence the name degenerate. Briefly, the mixing process can be explained as follows: Suppose two intense pump waves E_1 and E_2 , both at frequency ω , illuminate a nonlinear medium. The waves chosen for this purpose are counterpropagating plane waves so that their wavevectors $\mathbf{k}_1(\omega)$ and $\mathbf{k}_2(\omega)$ add up to zero. An arbitrary input wave, also at frequency ω , but with a wavevector $\mathbf{k}_4(\omega)$, is now incident on the medium (Fig. 14.13). Resulting third order nonlinear polarization radiates to give a field E_3 , also at frequency ω but with a wavevector

$$\mathbf{k}_3(\omega) = \mathbf{k}_1(\omega) + \mathbf{k}_2(\omega) - \mathbf{k}_4(\omega) = -\mathbf{k}_4(\omega) \quad \dots(14.30)$$

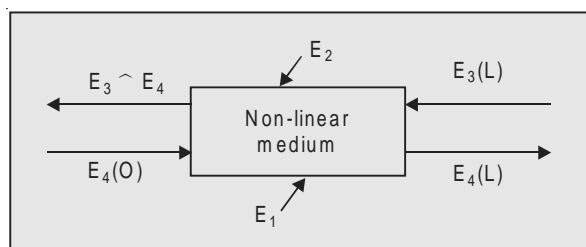


Fig. 14.13 Four wave mixing

The phase matching condition is thus, automatically satisfied.

The backward-going wave E_3 , in turn combines with the two pump wave E_1, E_2 to induce a third order polarization with amplitude distribution proportional to $E_1 E_2 E_3^*$, which radiates into E_4 . The counterpropagating conjugate pair, E_3 and E_4 are thus coupled through the nonlinear polarization and are amplified simultaneously, energy for which is provided by the pump waves E_1 and E_2 .

The nonlinear medium in the case considered may be viewed as a conjugate mirror, reflecting an arbitrary wave E_4 to give backward a wave $E_3 \propto E_4^*$. The reflected wave is a time-reversed replica and retraces the exact path of the incident wave. In a conventional mirror, the reflected wave will take a course dictated by the laws of reflection. The difference between the conjugate mirror and a conventional one, is brought out very clearly in the following illustration given by AuYeung and Yariv [18] (Fig. 14.14 (a), (b)).

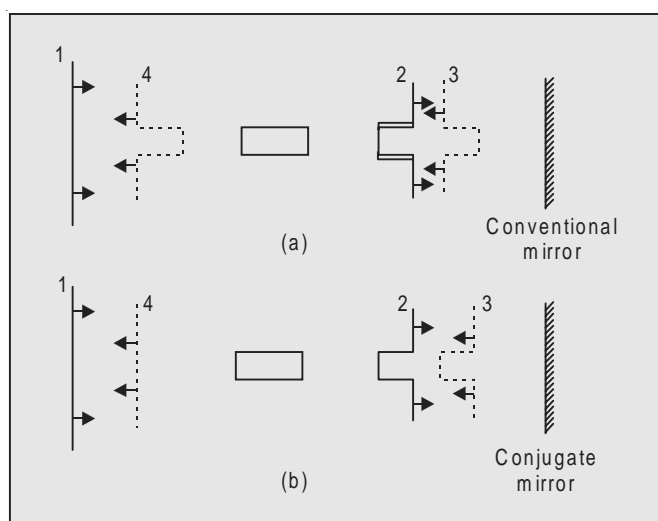


Fig. 14.14 Reflected wave-fronts from the conventional and the conjugate mirror

In Fig. 14.14(a), a plane wave (1) incident upon a distorting medium emerges with a bulge (2). The wave (3) reflected from a conventional mirror traverses the medium in reverse, resulting in a doubling of the bulge depth.

Consider now Fig. [14.14 (b)]. The reflected wave front (3) in this case is identical to the incident wave (2) and when it emerges out of the medium, there is a perfect smoothing of the bulge and the wave front becomes identical with (1).

Considerable amount of work has since been done in the field of phase-conjugation. Amplified phase-conjugation spectrum and parametric oscillation were demonstrated by Bloom *et al.*, [56] and by Pepper *et al.*, [303]. It may be noted that coherent anti-Stokes Raman scattering (CARS), discussed in the next chapter, is an example of four wave mixing.

REFERENCES

1. Abella, I.D., Phys. Rev. Lett. **9**, 453 (1962).
2. Abella, I.D., Kurnit, N.A. and Hartmann, S.Rr., Phys. Rev. **141**, 391 (1966).
3. Abramson, N., Bjelkhagen, H. and Skande, P., App. Opt. **18**, 2017 (1979).
4. Adams, N.L. and Schofer, P.B., App. Phys. Lett. **3**, 19 (1963).
5. Aggarwal, R.L., Lax, B. Chase, C.E. Pidgeon, C.R., Lambert, D., App. Phys. Lett. **18**, 383, (1971).
6. Alferov, Zh. I., Sov. Phys. Solid State **9**, 208 (1967).
7. Alferov, Zh. I., Andreev, V.M., Korolkov, V.I., Portonoi, E.L. and Tretyakov, D.N., Soviet Phys. Semicond. **2**, 843 (1969).
8. Ali, A.W., Koll, A.C. and Shipma, J.D., App. Opt. **6**, 2115 (1967).
9. Allen, L., *Essentials of Lasers*, Pergamon Press (1969).
10. Allwood, R.L., J. Phys. C, Solid State Phys. **3**, L186 (1970).
11. Ambartsumian, R.V., Ambartsumian, V.S., Letokhov, V.S., Ryabov, E.A. and Chekalov, N.C.V., JETP Lett. **20**, 273 (1974).
12. Analau, K.G., Maylotti, D.H., Pacey, P.D. and Polanyi, S.C., Phys. Lett. **24A**, 208 (1967).
13. Armstrong, J.A., Bloembergen, N., Ducuing, J. and Pershan, P.S., Phys. Rev. **127**, 1918 (1962).
14. Armstrong, J.A., Nathan, M.I. and Smith, A.W., App. Phys. Lett. **3**, 68 (1963).
15. Ashby, D.E.T.F. and Jephcott, D.F., App. Phys. Lett. **3**, 13 (1963).
16. Ashkin, A., Boyd, G.D. and Dziedzio, J.M., Phys. Rev. Lett. **11**, 14 (1963).
17. Ashkin, A., Phys. Rev. Lett. **40**, 729 (1978).
18. AuYeung, J. and Yariv, A., Optic News 5, No. **2**, 13 (1979).
19. Avizonis, P.V., Hopf, F.A., Bamberger, W.D., Jacobs, S.F., Tonula, A. and Womach, K.A., App. Phys. Lett. **31**, 435 (1977).
20. Balykin, V.I., Letokhov, V.S., Mishin, V.I. and Semohisen, V.A., JETP Lett. **26**, 492 (1977).
21. Barger, B.L. and Hall, J.L., Phys. Rev. Lett. **22**, 4 (196).
22. Barger, R.L., and Hall, J.L., App. Phys. Lett. **22**, 196 (1973).

23. Barnes, F.S. (Ed.,) *Laser Theory* IEEE Press (1972).
24. Barrett, A.H., Sc. Am. **219**, N. 6, 36 (1968).
25. Barrett, J.T. and Berry, M.J., App. Phys. Lett. **34**, 144 (1979).
26. Barrett, J.T. and Heller, D.F. J.O.S.A. **71**, 1299 (1981).
27. Basov, N.G. and Prokhorov, A.M., J. Expt. Th. Phys. (USSR) **27**, 431 (1954).
28. Basov, N.G. and Prokhorov, A.M., J. Expt. Th. Phys. (USSR) **28**, 249 (1955).
29. Basov, N.G., Kroklin, O.N. and Popov, Y.N. JETP **13**, 1320 (1961).
30. Basov, N.G., Danilychev, V.A., Propov, Y.N. and Khodkevich, D.D. JETP Lett. **12**, 1329 (1970).
31. Basov, N.G. (Ed.), *Lasers and Holography Data Processing*, Mir Publishers (1984).
32. Bass, M., Franken, P.A., Hill, A.E., Peters, C.W. and Weinreich, G. Phys. Rev. Lett. **8**, 18 (1962).
33. Bass, M., Franken, P.A., Ward, J.F. and Weinrich, G. Phys. Rev. Lett. **9**, 446 (1962).
34. Bekov, G.I., Letokhov, V.S., Matveen, O.I. and Mishin, V.I. Opt. Lett. **3**, 159 (1978).
35. Ben-Aryeh, Y. Opt. Lett. **2**, 154 (1978).
36. Bennett Jr., W.R. Phys. Rev. **126**, 580 (1962).
37. Bennett Jr., W.R. and Knutson, J.W. Proc. JEEE **52**, 864 (1964).
38. Bennett Jr., W.R. *Quantum Electronics*, Ed. Grivet and Bloembergen, N. Dunod, Paris, 711 (1964).
39. Bennett Jr., W.R. and Kindlmann, P.J., Phys. Rev. **149**, 38 (1966).
40. Benton, S.A.J.O.S.A. **54**, 1545 (A) (1969).
41. Bernard, M.G.A. and Duraffourg, G. Phys. Stat. Solidi **1**, 699 (1961).
42. Bernhardt, A., Duerre, D.E., Simpson, J.R. and Wood, L.L. Appl. Phys. Lett. **25**, 617 (1974).
43. Bertolotti, M. *Masers and Lasers*, Adam Hilger Ltd., Bristol (1983).
44. Bethe, H.A., and Salpeter, E.E. *Quantum Mechanics of One- and Two-Electron Atoms*, Springer-Verlag, Berlin (1957).
45. Billardon, M., Elleaume, P. Ortega, J.M., Bazin, C., Velghe, M., Petroff, Y., Deacon, D., Robinson, K. and Madey, J., Phys. Rev. Lett. **51**, 1652 (1983).
46. Biraben, F., Cagnac, B. and Crynberg, G., Phys. Rev. Lett., **32**, 643 (1974).
47. Birks, J.B. Rep. Prog. Phys. **38**, 903 (1975).
48. Bjorkholm, J.E., App. Phys. Lett. **13**, 53 (1968).
49. Bloembergen, N. Phys. Rev. **104**, 324 (1956).
50. Bloembergen, N. and Peshan, R.S. Phys. Rev. **128**, 606 (1962).
51. Bloembergen, N. Proc. IEEE **51**, 124 (1963).
52. Bloembergen, N. and Shen, Y.R. Phys. Rev. **133**, A 37 (1964).
53. Bloembergen, N. and Shen, Y.R. Phys. Rev. Lett. **12**, 504 (1964).
54. Bloembergen, N., Am. J. Phys. **35**, 989 (1967).
55. Bloembergen, N. *Nonlinear Optics*, Benjamin W.A. INC N.Y. (1977).
56. Bloom, AL. Sc. Am. **203**, N. 4, 72 (1960).

57. Bloom, D.M., Liao, P.F. and Economou, N.P. Opt. Lett. **2**, 58 (1978).
58. Bonch-Bruevich, A.M. and Khodovo, N.A. Soviet Phys. **85**, 1 (1965).
59. Born, M. and Wolf, E., *Principles of Optics*, Pergamon Press (1986).
60. Bose, S.N.Z. Phys. **26**, 178 (1924).
61. Boyd, G.D. and Gordon, J.P. Bell. Syst. Tech. J. **40**, 489 (1961).
62. Bradley, D.J., Hutchinson, M.H.R. and Koester, H. Proc. Roy. Soc. (London) A **328**, 97 (1972).
63. Bradley, D.J., Hutchinson, M.H.R. and Koester, H. Proc. Roy. Soc. (London) **329**, 105 (1972).
64. Bradley, D.J., Porter, G. and Key, M.H. (Ed.) *Ultra-short Laser Pulses*, The Roy. Soc. (London) (1980).
65. Braunstein, R. and Ockman, N. Phys. Rev. A **134**, 499 (1964).
66. Bridges, W.B., Chester, A.N. Halstead, A.S. and Parker, J.V. Proc. IEEE **59**, 724 (1971).
67. Brinkman, V., Hartig, W., Jelle, H. and Wather, H. App. Phys. **5**, 109 (1974).
68. Brown, D.C. and Rome, J.L. Am. J. Phys. **40**, 470 (1972).
69. Brown, P.F. Proc. Phys. Soc. **86**, 1323 (1965).
70. Butler, J.F., Calawa, A.R. and Rediker, R.H. IEEE J. Quantum Elec. QE **1**, 4 (1965).
71. Butler, J.K., (Ed.) *Semiconductor Injection Lasers*, IEEE Press (1980).
72. Chebotayev, V.P. 3rd Varilov Conference on Nonlinear Optics. Nousibirsk, U.S.S.R. (1973).
73. Chen, H. and Yu, F.T.S. Opt. Lett. **2**, 85 (1973).
74. Chesler, R.B. Karr, M.A. and Geusie, J.E. J. App. Phys., **41**, 4125 (1970).
75. Chiao, R.Y. and Stoicheff, B.P. Phys. Rev. Lett. **12**, 290 (1964).
76. Chiao, R.Y. and Stoicheff, B.P. J.O.S.A. **54**, 1286 (1964).
77. Chicklis, E.P., Nasman, C.S. Folweiler, R.C., Gubbe, D.R., Jensson, H.P. and Linz, A. App. Phys. Lett. **19**, 119 (1971).
78. Clark, N.A., Lunacek, H.H. and Benedik, G.B. Am. J. Phys. **38**, 575 (1970).
79. Chu, S., Hollberg, L. Bjorkholm, J., Cable, A. and Ashkin, A. Phys. Rev. Lett. **55**, 48 (1985).
80. Chu, S., Bjorkholm, J.E., Ashkin, A. and Cable, A. Phys. Rev. Lett. **57**, 314 (1988).
81. Collins, R., Nelson D., Schawlow, A., Bond, W., Garrett, C.G.B., and Kaiser, W. Phys. Rev. Lett., **5**, 7, 303 (1960).
82. Collins, C.B., Lee, F.W. Shenwell, D.M. and DePaola, B.D. J. App. Phys., **53**, 4645 (1982).
83. Coltman, S. Phys. Lett. **4**, 168 (1963).
84. Cook, A.N. New Scientist, 6th April, **26** (1967).
85. Cool, T.A., Falk, F.J. and Stephen, R.R., App. Phys. Lett., **15**, 318 (1969).
86. Cool, T.A. and Stephen R.R., J. Chem. Phys., **51**, 5175 (1969).
87. Cool, T.A. and Stephen, R.R., App. Phys. Lett., **16**, 55 (1970).
88. Corney, A., *Atomic and Laser Spectroscopy*, Clarendon Press Oxford (1977).

89. Cyvin, S.T., Rauch, J.E. and Decius, J.C.J. Chem. Phys. **43**, 4083 (1965).
90. Dawson, M.D., Bogess, T.F., and Smirl, A.L., Opt. Lett., **12**, 254 (1987).
91. Dawson, M.D., Bogess, T.F., and Smirl, A.L., Opt. Lett., **12**, 590 (1987).
92. Dawson, M.D., Bogess, T.F., Garrey, D.W., and Smirl, A.L. IEEJ. Quantum Electronics Lett. QE-23, 290 (1987).
93. Deacon, D.A.G., Elias, L.R., Modey, M.J. Ramian, G.T., Schwettman, H.A. and Smith, T.I., Phys. Rev. Lett. **38**, 892 (1977).
94. De Maria, A.J. Proc. IEEE **61**, 731 (1973).
95. Demtroder, W. *High Resolution Spectroscopy with Lasers*, Physics Reports **7C**, 223 (1973).
96. Denisyuk, Yu.N., Opt. I Spectr., **15**, 523 (1963).
97. Denisyuk, Yu.N., Opt. I Spectr., **18**, 275 (1965).
98. Denisyuk, Yu.N., *Fundamentals of Holography*, Mir Publishers (1984).
99. Deutsch, T.F. App. Phys. Lett., **10**, 234 (1967).
100. Dicke, R.H. Phys. Rev. **93**, 99 (1954).
101. Dirac, P.A.M. *The Principles of Quantum Mechanics*, Oxford (1958).
102. Ditchburn, R.W. Light, Blackie and Sons Ltd. (1963).
103. Dowley, M.W., App. Phys. Lett., **13**, 395 (1968).
104. Eberley, J.H. and Rehler, N.E. Phys. Lett. **29A**, 142 (1969).
105. Eberley, J.H. Am. J. Phys. **40**, 1374 (1972).
106. Echardt, G., Hellwarth, R.W., McClung F.J. Schwartz, S.E., Weiner, D. and Woodbury, E.J. Phys. Rev. Lett. **9**, 455 (1962).
107. Eddington, A. Phil. Mag. **50**, 803 (1925).
108. Edwards, D.F. and She, C.Y. Am. J. Phys., **40**, 1389 (1972).
109. Eesley, G.L. *Coherent Raman Spectroscopy* Pergamon Press (1981).
110. Eichler, H.J., Laughans, D. and Klein, U. App. Opt. **18**, 1383 (1979).
111. Einstein, A. Phys. Z. **18**, 121 (1917).
112. Elias, L.R., Fairbank., W.M., Madey, J.M.J., Schwettmann, H.A. and Smith, J. Phys. Rev. Lett., **36**, 712 (1976).
113. Erbit A. and Jenssen, H.P. App. Optics, **19**, 1729 (1980).
114. Ericsson, G. and Lidholt, L.R. App. Opt. **7**, 211 (1968).
115. Ertmar, W., Blatt, R., Hall, J. and Zhu, M., Phys. Rev. Lett., **54**, 996 (1985).
116. Fabelinskii, I.L. in *Quantum Electronics* Vol. 1 (Nonlinear Optics) Ed. Rabin. H. and Tang, C.L. Academic Press (1975).
117. Fairbank, W.M. Jr., Hansch, T.W. and Schawlow, A.L.J.O.S.A. **65**, 199 (1975).
118. Fairbank, W.M. and She, C.Y. Optics News **5**, No. 2, 4 (1979).
119. Falcone, R.W. and Zdasiuk, G.A. Opt. Lett. **5**, 155 (1980).
120. Falcone, R.W. and Zdasiuk, G.A. Opt. Lett. **5**, 365 (1980).
121. Falk, J., and Murray, J.E., App. Phys. Lett. **14**, 245 (1969).
122. Favro, L.D., Fraddkin, D.M. and Kuo, P.K. Phys. Rev. Lett. **25**, 202 (1970).
123. Fishlock, D. (Ed.) *A Guide to the Laser*, Macdonald, London (1968).
124. Fork, R.L., Greene, B.L. and Shank, C.V. App. Phys. Lett. **38**, 671 (1981).
125. Fox, A.G. and Li, T. Bell Syst. Tech. Journ. **40**, 453 (1965).

126. Franken, P.A., Hill, A.E., Peters, C.W. and Weinreich, G. Phys. Rev. Lett. **7**, 118 (1961).
127. Franken, P.A. and Ward, J.F. Rev. Mod. Phys. **35**, 23 (1963).
- 127A. French, B., *The Moon Book*, Penguin Book, (1977).
128. French, M.J. and Long, D.A.J. Raman Spectroscopy **1**, 53 (1973).
129. French, P.H.W. and Taylor, J.R., Proc. of the 5th OSA Topical meeting Springer Verlag Series in Chemical Physics (1986).
130. French, P.M.W. and Taylor, J.R., Technical Digest on Conference on Lasers and Electro-optica, **14**, 150 (1987).
131. Frenkel, J. *Wave-mechanics* Dover, N.Y. (1950).
132. Froome, K.D., Proc. R. Soc., **247A**, 107 (1958).
133. Gabor, D. Proc. Roy. Soc. London A **197**, 454 (1949).
134. Gabor, D., Kock, W.E. and Stroke, G.W. Science, **173**, 11 (1971).
135. Garfinkel, M. and Engeler, W.E. Appl. Phys. Lett., **3**, 178 (1963).
136. Garmire, E., Pandarese, F. and Townes, C.H. Phys. Rev. Lett. **11**, 160 (1963).
137. Gaydon, A.G. and Wolfhard, H.G. *Flames*, 3rd Ed. Chapman & Hall (1970).
138. Gaydon, A.G. *The Spectroscopy of Flames*, 2nd Ed. Chapman & Hall (1974).
139. Gelbwachs, J.A., Klein, C.F. and Wessel, J.E. App. Phys. Lett. **30**, 489 (1977).
140. Gerardo, J.B. and Verdelyen, J.T. App. Phys. Lett. **3**, 121 (1963).
141. Gerry, E.T., App. Phys. Lett., **7**, 6 (1965).
142. Gerry, E.T. IEEE Spectra **7**, 51 (1970).
143. Geusie, J.E., Levinstein, M. J., Rubin, J.J., Singh, S. and van Uitert, L.G., App. Phys. Lett., **11**, 269 (1968).
144. Giordmaine, J.A., Sc. Am. **210**, N. 4, 38 (1964).
145. Givens, M.P. Am. J. Phys. **35**, 1056 (1967).
146. Glauber, R., Phys. Rev., **130**, 2529 (1963).
147. Glauber, R., Phys. Rev., **131**, 2766 (1963).
148. Glauber, R., Phys. Rev. Lett. **10**, 84 (1963).
149. Goeppert-Mayer, M. Ann. Physik **9**, 273 (1931).
150. Gordon, J.P., Zeiger, H.J. and Townes, C.H. Phys. Rev. **95**, 259 (1954).
151. Gordon, J.P., Zeiger, H.J. and Townes, C.H. Phys. Rev. **99**, 1264 (1955).
152. Gordon, J.P. Sc. Am. **199**, No. 6, 42 (1958).
153. Green, W.R., Wright, M.D., Lukasik, J., Young, J.F. and Harris, S.E. Opt. Lett. **4**, 265 (1979).
154. Greenless, G.W., Clark, D.L., Kaufman, S.I., Lewis, D.A., Jonn., J.F. and Broadhurst, J.H., Opt. Commun. **23**, 236 (1977).
155. Gudzenko, L.I. and Yakovlenko, S.I. Soviet Phys. JETP **35**, 877 (1972).
156. Gudzenko, L.I. and Yakovlenko, S.I. Phys. Lett., **46A**, 475 (1974).
157. Hagen, W.F. and Magnante, P.C., J. App. Phys., **40**, 219 (1969).
158. Hall, R.N., Fenner, G.E., Kingsley, J.D., Soltys, T.J. and Carlson, R.O. Phys. Rev. Lett., **9**, 366 (1962).

159. Hancock, G., Ridley, B.A. and Smith, I.W.H.J.C.S. Faraday **11**, 68, 2117 (1972).
160. Hänsch, T.W., Permier, M. and Schawlow, A.L. IEEE J. Quantum Electronics **QE-8**, 45 (1971).
161. Hänsch, T.W., Shatrin, I. and Schawlow, A.L. Nature, **235**, 63 (1972).
162. Hänsch, T.W., App. Opt., **11**, 895 (1972).
163. Hänsch, T.W., Harvey, K.C., Meisiel, G. and Schawlow, A.L. Opt. Comm. **11**, 50 (1974).
164. Hänsch, T.W., Lee, S.A., Wallenstein, R. and Wieman, C. Phys. Rev. Lett., **34**, 307 (1975).
165. Hänsch, T.W., and Schawlow, A.L., Opt. Commun. **13**, 68 (1975).
166. Hargrove, L.E., Fork, R.L. and Pollock, M.A., App. Phys. Lett. **5**, 4 (1964).
167. Harper, P.G. and Wherrett, B.S. (Ed.) *Nonlinear Optics*, Academic Press (1977).
168. Harris, S.E., App. Opt. **5**, 1639 (1966).
169. Harris, S.E. and Lidow, D.B. Phys. Rev. Lett. **33**, 674 (1974).
170. Harris, S.E. and Lidow, D.B. Phys. Rev. Lett. **34**, 172 (E) (1975).
171. Harris, S.E. and White, J.C. IEEE, J. Quantum Electronics, **QE-13**, 972 (1977).
172. Harrison, R.G., Hawkins, H.L. John P. and Leo, R. *Laser advances and applications*, Proc. of the Fourth Quantum electronics Conference, John Wiley and Sons (1980).
173. Hayashi, I., Panish, M.B., Foy, P.W. and Sumski, S. App. Phys. Lett. **17**, 109 (1970).
174. Heald, M.A. Am. J. Phys. **39**, 684(1971).
175. Heard, Nature **200**, 167 (1963).
176. Heavens, O.S. *Optical Lasers*, Methuen & Co. (London) (1964).
177. Heavens, O.S. *Lasers*, Duckworth (1971).
178. Hoer, C.V. and Settles, R.A. J. Mol. Spec. **23**, 448 (1967).
179. Heitler, W. *The Quantum Theory of Radiation*, Oxford University Press, 2nd Ed. (1947).
180. Hellworth, R.W. in *Advances in Quantum Electronics* Ed. Singer, J.R. Columbia Univ. Press, N.Y. 334 (1961).
181. Hellworth, R.W. Phys. Rev. **130**, 1850 (1963).
182. Hellworth, R.W. App. Opt. **2**, 847 (1963).
183. Hellworth, R.W.J.O.S.A. **67**, 1 (1977).
184. Herriot, D.R. in *Advances in Quantum Electronics*, Ed. Singer, J.R. Columbia Univ. Press, N.Y. (1961).
185. Herriot, D.R.J.O.S.A. **52**, 31 (1962).
186. Herriot, D.R. Sc. Am. **219**, N. 3, 140 (1968).
- 186A. Herzberg, G., *Spectra of Diatomic Molecules*, van Nostrand (1950).
187. Hindmarsh, W.R., *Atomic Spectra*, Pergamon Press (1967).
188. Hodgson, R.T. Phys. Rev. Lett. **25**, 494 (1970).

189. Honkley, E.D., Harman, T.C. and Freed, C. App. Phys. Lett. **13**, 49 (1968).
190. Honkley, E.D. and Freed, C. Phys. Rev. Lett. **23**, 277 (1969).
191. Honkley, E.D. and Kelly, P.L., Science **177**, 635 (1971).
192. Hopfield, J.J., Worlock, J.M. and Park K. Phys. Rev. Lett. **11**, 414 (1963).
193. Houslon, P.L. Chem. Phys. Lett. **47**, 1 (1977).
194. Houtermans, F.G. Helv. Phys. Acta **33**, 933 (1960).
195. Hughes, T.P. in *Nonlinear Optics* (Ed: Harper, P.G and Wherret, B.S) Academic Press (1977).
196. Hung, Cheng and Miller, P.B. Phys. Rev. A **134**, 683 (1964).
197. Hurst, G.S., Nayfesh, M.H. and Young, J.P. App. Phys. Lett. **30**, 229 (1977).
198. Hutchinson, M.H.R. App. Opt. **19**, 3883 (1980).
199. Jacobs, S., Gould, G. and Rabinowitz, P. Phys. Rev. Lett., **7**, 415 (1961).
200. Jaseja, T.S., Javan, A., Murray, J. and Townes, C.H. Phys. Rev. **133**, A1221 (1964).
201. Javan, A. Phys. Rev. Lett. **3**, 187 (1959).
202. Javan, A., Bennett. Jr., W.R. and Herriott, D.P. Phys. Rev. Lett. **6**, 106 (1961).
203. Johnson, P.M. App. Opt. **19**, 3920 (1980).
204. Jones, W.J. and Stoicheff, B.P. Phys. Rev. Lett. **13**, 657 (1964).
205. Jonnathan, N., Mellor-Smith, C.M. and Slater, D.H.J.C.P. **53**, 4396 (1970).
206. Kaiser, W. and Garrett, C.G.B. Phys. Rev. Lett. **7**, 229 (1961).
207. Kaiser, W. and Maier M. in *Laser Handbook* (Ed: Arecchi, F.T. and SchulzDuBois, E.O.) North Holland (1972).
208. Kasper, J.V.V. and Pimental, G.C. App. Phys. Lett. **5**, 231 (1964).
209. Kasper, J.V.V. and Pimental, G.C. Phys. Rev. Lett. **14**, 352 (1965).
210. Kay, S.H. and Maitland, A. Ed. *Quantum Optics*, Academic Press, London (1970).
211. Kelly, P.L.J. Phys. Chem. Solids **24**, 607 (1963).
212. Kelly, P.L.J. Phys. Chem. Solids **24**, 1113 (1963).
213. Kelly, P.L., Phys. Rev. Lett. **15**, 1005 (1965).
214. Kerr, E.L. and Atwood, J.G. App. Opt. **7**, 915 (1968).
215. Kingsley, J.D. and Fenner, G.E. *Quantum Electronics III*, 1884 (1964).
216. Klauder, J.R., Ann. Phys. **11**, 123 (1960).
217. Kleinman, D.A. Phys. Rev. **125**, 87 (1962).
218. Kleinman, D.A. Phys. Rev. **128**, 1761 (1962).
219. Kleppner, D., Goldenberg, H.M. and Ramsen, N.P. Phys. Rev. **126**, 603 (1962).
220. Kogelnik, H. and Shank, C.V. App. Phys. Lett. **18**, 152 (1971).
221. Kogelnik, H., Dienes, A. Ippen, E.P. and Shank, C.V. I.E.E.E. J. Quantum Electronics **QE-8**, 375 (1972).
222. Komringstein, J.A. *Introduction to the Theory of Raman Effect* D. Reidel Publishing Company (1972).
223. Krenser, L.B. and Patel, C.K.N., Science, **173**, 45 (1971).

224. Kubo, R. and Kamimura, H. Ed. *Dynamical Processes in Solid State Optics*, W.A. Benjamin INC. N.Y. (1967).
225. Lamb, Jr., W.E. and Rutherford, R.C., Phys. Rev., **72**, 241 (1947).
226. Lamb Jr., W.E. and Rutherford, R.C., Phys. Rev., **79**, 549 (1950).
227. Lamb Jr., W.E. Phys. Rev. **134**, 1429(1964).
228. Lambropoulos, P. App. Opt. **19**, 3926 (1980).
229. Landau, L.Z. Phys. **64**, 629 (1950).
230. Landsberg, G. and Mandelstam, L. Naturwiss **16**, 557, 772 (1928).
231. Laud, B.B., Sardesai, P.L. and Behere, S.H., Am. J. Phys. **41**, 720 (1973).
232. Laud, B.B. *Introduction to Statistical Mechanics*, Macmillan India (1981).
233. Laud, B.B. *Electromagnetics*, 2nd (Ed.) Wiley Eastern Ltd. (1987).
234. Lawande, S.V. and Lal, B. Physics News, **10**, 2, 41 (1979).
235. Lawrence, G.M. and Liszt, H.S., Phys. Rev., **178**, 122 (1969)
236. Lax, M. and Edwards. Phys. Rev. Lett. **8**, 166 (1962).
237. Leith, E.N. and Upatnicks, J., J.O.S.A. **53**, 1377 (1963).
238. Leith, E.N. and Upatnicks, J., J.O.S.A. **54**, 1295 (1964).
239. Leith, E.N. and Upatnicks, J., Sc. Am. **212**, 24 (1965).
240. Lempicki, A., Samelson, H. and Brecher, C. App. Opt. (Supp. 2) 205, (1965).
241. Lempicki, A. and Samelson, H.Sc. Am. 108 (1969).
242. Lengyl, B.A. *Introduction to Laser Physics*, John Wiley & Sons INC, N. Y. (1966).
243. Lengyl, B.A., *Lasers*, Wiley-Interscience (1971).
244. Leonard, D.A. App. Phys. Lett. **7**, 4 (1965).
245. Leonard, D.A., Lasers Focus, **3**, 26 (1967).
246. Letokhov, V.S., JETP Lett. **7**, 272 (1968).
247. Letokhov, V.S., Mishin, V.I., Esokobilov, M. and Tursunov, A.T. Opt. Common. **41**, 331 (1982).
248. Levenson, M.D. and Bloembergen, N., Phys. Rev. Lett. **32**, 645 (1974).
249. Levenson, M.D. *Introduction to Nonlinear Laser Spectroscopy*, Academic Press (1982).
250. Lindmayer. J. and Wrigley, C.Y. *Fundamentals of Semiconductor Devices*. Affiliated East-West Press, New Delhi (1965).
251. Lindsay, P.A. *Quantum Electronics*, Pitman Publishing (1975).
252. Lipson, S.G. and Lipson, H. *Optical Physics*, Cambridge University Press (1969).
253. Long, D.A. and Stanton, L. Proc. Roy. Soc. A **318**, 441 (1970).
254. Long, D.A. *Raman Spectroscopy* McGraw-Hill Inc. (1977).
255. Loudon, R. Proc. Phys. Soc. **80**, 952 (1962).
256. Loudon, R. Proc. Phys. Soc. **82**, 393 (1963).
257. Loudon, R. *The Quantum Theory of Light*, Clarendon Press (1981).
258. Lumb, M.D. *Luminescence Spectroscopy*, Academic Press (1978).
259. Lyubavsky, Yu. and Ovchinnikov, V. *Solid State Laser Technology*, Mir Publishers (1975).

260. Lyons, H.Sc. Am. **196**, 71 (1957).
261. Mahr, H. in *Quantum Electronics*, Vol. I (Nonlinear Optics) Ed Rabin H. and Tang C.L. Academic Press (1975).
262. Maiman, T.H. Phys. Rev. Lett. **4**, 564 (1960).
263. Maiman, T.H. Nature, **187**, 493 (1960).
264. Maiman, T.H. Phys. Rev. **123**, 1145 (1961).
265. Maiman, T.H. Phys. Rev. **123**, 1151 (1961).
266. Maitland, A. and Dunn, M.H. *Laser Physics*, American Elsevier (1970).
267. Maker, P.D., Terhune, R.W. and Savage, A. Proc. Third Quantum Electronics Conference, Paris 1559 (1963).
268. Maker, P.D. and Terhune, R.W. Phys. Rev. **137 A**, 801 (1965). .
269. Mandl, F. and Shaw, G., *Quantum Field Theory*, John Wiley & Sons (1986).
270. Martin, E.A. and Mandel, L. App. Opt. **15**, 2378 (1976).
271. Mathias, and Parker App. Phys. Lett. **3**, 16 (1963).
272. McAlecse and Franck. G. *The Laser Experimenter's Hand Book*, TAB Books Inc. (1980).
273. McDermott, D.B., Marshall, T.C., Schlesinger, S.P., Parker, R.K. and Granatstein, V.L. Phys. Rev. Lett. **41**, 1368 (1978).
274. McFarlane, R.A., Bennett, W.R. Jr. and Lamb, W.E. Jr. App. Phys. Lett. **2**, 189 (1963).
275. Miller, R.C. and Savage, A. Phys. Rev. **128**, 2175 (1962).
276. Miller, S.E., Sc. Am. **214**, 19 (1966).
277. Minck, R.W., Terhune, R.W. and Wang, C.C., App. Opt. **5**, 1595 (1966).
278. Mitchell, A.G.G. and Zemansky, H.W. *Resonance Radiation and Excited States*, Cambridge Univ. Press (1961).
279. Mooradian, A. in *Nonlinear Opticas*, (Ed : Harper, P.C. and Wherrett B.S.) Academic Press (1977).
280. Mooradian, A., Brueck, S.R.J. and Blum, F.A. App. Phys. Lett. **17**, 481 (1971).
281. Morehead, F.A. Sc. Am. 108 (1969).
282. Mountain, R.D. Rev. Mod. Phys. **38**, 205 (1966).
283. Nakatnika, H., Grischkowsky, D. and Balant, A.C. Phys. Rev. Lett. **47**, 910 (1981).
284. Nakamura, M., Yariv, A., Yen, H.W., Somekh, S. and Garvin, H.L., App. Phys. Lett. **22**, 515 (1973).
285. Nathan, M.I., Dumke, W.P., Burns, G., Dill, F.H. and Lasher, G. App. Phys. Lett. **1**, 62 (1962).
286. Neil, G., Edighoffer, J. Hess, C., Smith, T. and Fornaca, F. Phys. Rev. Lett. **52**, 344 (1984).
287. Nelson, D.F. and Boyle, W. App. Opt. **1**, 181 (1962).
288. Nestor, J.R., Spiro, T.G. and Klauminzer, G.C. *Proc. Fifth International Conf. on Raman Spectroscopy* Ed. Schmid, E.D. 738 (1976).

289. Oliver, B.M. and Cutler, L.S. Phys. Rev. Lett. **25**, 273 (1970).
290. Optic News, **9**, 2, 13 (1983).
291. Optic News, **9**, 5, 10 (1983).
292. O'Shea, D.C., Callen, W.R. and Rhodes, W.T. *Introduction to Lasers and their Applications*, Addison-Wesley (1978).
293. Ostrovsky, Yu. I. *Holography and its Applications*, Mir Publishers, Moscow (1977).
294. Pantell, R.A., Sonem, G. Puthoff, H.E., IEEEJ, *Quantum Electronic* **4**, 965 (1968).
295. Parks, J.H., Ramchandra Rao, D. and Javan, A., App. Phys. Lett. **13**, 142 (1968).
296. Patel, C.K.N. Phys. Rev. **136A**, 1187 (1964).
297. Patel, C.K.N. and Kerl, R.J. App. Phys. Rev. **5**, 81 (1964).
298. Patel, C.K.N. Phys. Rev. Lett. **13**, 617 (1964).
299. Patel, C.K.N. App. Phys. Lett. **7**, 15 (1965).
300. Patel, C.K.N. Sc. Am. 219, N. 2, 22 (1968).
301. Patel, C.K.N. and Shaw, E.D. Phys. Rev. Lett. **24**, 251 (1970).
302. Patel, C.K.N. and Shaw, E.D. Phys. Rev. **33**, 1279 (1971).
303. Pepper, D.M., Fekeli, D. and Yariv, A. App. Phys. Lett. **33**, 41 (1978).
304. Perina, J. *Quantum Statistics of Linear and Nonlinear Optics*, D. Reidel Publishing Company (1984).
305. Petricolas, W.L., Goldsborough, J.P. and Rieckhoff, K.E., Phys. Rev. Lett. **10**, 43 (1963).
306. Phillips, R.A. and Gehrg, R.D. Am. J. Phys. **38**, 429 (1970).
307. Physics To-day, **32**, 7, 17 (1979).
308. Physics To-day, **32**, 7, 19 (1979).
309. Physics To-day, **32**, 11, 20 (1979).
310. Physics To-day, **33**, 10, 21 (1980).
311. Physics To-day, **34**, 12, 19 (1981).
312. Pimentel, G.C., Sc. Am. **214**, 32 (1966).
313. Piper, J.A. and Webb, C.E., J. Phys. D **6**, 400 (1973).
314. Pollock, M.A., App. Phys. Lett. **8**, 237 (1966).
315. Porto, S.P.S. and Wood, D.L., J.O.S.A. **52**, 251 (1962).
316. Powell, H.T. and Ewing, J.J. App. Phys. Lett. **33**, 165 (1978).
317. Prodan, J. Migdall, A., Phillips, W., So, I., Metcalf, H. and Dalibard, Phys. Rev. Lett. **54**, 992 (1985).
318. Prokhorov, A.M., Soviet Phys. JETP **7**, 1140 (1958).
319. Raman, C.V. and Krishnan, K.S. Nature, **121**, 501 (1928).
320. Raman, C.V. and Krishnan, K.S. Proc. Roy. Soc. Lond. **122**, 23 (1929).
321. Ramsey, N.F. *Quantum Electronics III*, Columbia Univ. Press (1964).
322. Ransch, H. Optic News, **10**, 3, 22 (1984).
323. Rayleigh (Lord), Phil. Mag. XLI, 274 (1971).
324. Regnier, P.R. and Taran, J.P. E.A.I.A.A. Journal **12**, 826 (1974).
325. Rhodes, C.H. IEEEJ. Quantum Electronics **QE-10**, 153 (1974).

326. Sardesai, P.L. and Laud, B.B., Jour. Sc. Res. **3**, 129 (1981).
327. Sardesai, P.L. and Laud, B.B., Jour. Sc. Res. **3**, 147 (1981).
328. Sardesai, P.L. and Laud, B.B., Jour. Sc. Res. **4**, 17 (1982).
329. Sardesai, P.L. and Laud, B.B., Jour. Sc. Res. **4**, 65 (1982).
330. Schäfer, P.P. (Ed.) *Dye Lasers*, Topics in Applied Physics, Vol. I, Springer-Verlag, Berlin (1973).
331. Schawlow, A.L. and Townes, C.H. Phys. Rev. **112**, 1940 (1958).
332. Schawlow, A.L. Sc. Am. **204**, 52 (1961).
333. Schawlow, A.L. Sc. Am. **209**, 34 (1963).
334. Schawlow, A.L. Sc. Am. **219**, 3, 20 (1968).
335. Schawlow, A.L. J.O.S.A. **67**, 140 (1977).
336. Schawlow, A.L. Physics To-day **35**, 12,46 (1982).
337. Schiff, L.I. *Quantum Mechanics*, McGraw-Hill (1955).
338. Schnell, W. and Fischer, G. App. Opt. **14**, 2058 (1975).
- 338A. Schrödinger, E., Naturwiss. **19**, 644 (1927).
339. Schwarz, H. and Hora, H. App. Phys. Lett. **15**, 349 (1969).
340. Science, **159**, 699 (1968).
341. Scully, M.D. and Lamb, Jr. W.E. Phys. Rev. **159**, 208 (1967).
342. Shank, C.V., Fork, R.L., Yen, R.T., Stolen, R.K. and Tomlinson, W.J. App. Phys. Lett. **41**, 761 (1982).
343. Shapero, S. and Bloembergen, N. Phys. Rev. **116**, 1453 (1959).
344. Shimoda, K. and Shimuzi, T. *Nonlinear Spectroscopy of Molecules* Progress-Quantum Electronics, Pergamon Press, 2(2), 45 (1972).
345. Shimoda, K. (Ed.), *High-resolution Laser Spectroscopy*, Springer-Verlag (1976).
346. Siebert, D.H., West, G.A. and Barrett, J.J., App. Cpt. **19**, 53 (1980).
347. Siegmann, A.E. *An Introduction to Lasers and Masers*, McGraw-Hill (1971).
348. Silfvast, W.T. and Klein, M.B. App. Phys. Lett., **17**, 400 (1970).
349. Silfvast, W.T., Science Am. **226**, 88 (1973).
350. Silleto, R.M. in *Quantum Optics*, Ed. Kay, J.M. and Maitland, A. Academic Press (1970).
351. Singh, S. and Stoicheff, B.P., J. Chem-Phys. **36**, 2082 (1963).
352. Singh, S. and Bradley, L.T. Phys. Rev. Lett. **12**, 612 (1964).
353. Skribanovitz, N., Herman, I.P., MacGilliray, J.C. and Feld, M.S. Phys. Rev. Lett. **30**, 309 (1973).
354. Smekal, A., Naturwiss. **11**, 873 (1923).
355. Smith, W.V. and Sorokin, P.P. *The Laser* McGraw-Hill (1966).
356. Smith, P.W., Proc. Inst. Elec. and Electronic Engineering, **58**, 1342 (1970).
357. Smith, R.G. in *Lasers* Ed. Levin, A.K. and De Maria, A.J., Mareil Dekho, Inc. N.Y. (1976).
358. Smith, R.A. *Semi-conductors*, 2nd Ed. Cambridge Univ. Press (1979).
359. Snitzer, E. Phys. Rev. Lett. **7**, 444 (1961).
360. Sorokin, P.P. and Stevenson, M. J. Phys. Rev. Lett. **5**, 557 (1960).

361. Sorokin, P.P. and Lankard, J.R. IBMJ Res. Development **10**, 162 (1966).
362. Sorokin, P.P., Lankard, J.R., Hammond, E.C. and Moruzzi, V.L.? IBMJ, Res. Development **11**, 130 (1967).
363. Sorokin, P.P., Sc. Am. **220**, 2,30 (1969).
364. Spencer, D.J. and Wittig, C. Opt. Lett. **4**, 1 (1979).
365. Steinfeld, J.I. *Molecules and Radiation*, Harper and Row (1974).
366. Stevens, B. and Hutton, E. Nature, **186**, 1045 (1960).
367. Stoicheff, B.P. in *Molecular Physics* Ed. Williams, D. Academic Press (1962).
368. Sussans, H. and Vacher, R. App. Opt. **18**, 3815 (1979).
369. Svelto, O. *Principles of Lasers*, Plenum Press, N.Y. (1976).
370. Szoke, A. and Jauan, A., Phys. Rev. Lett. **10**, 521 (1963).
- 370A. Tamir, T. (Ed). *Integrated Optics*, Spring-Verlag (1975).
371. Tarasov, L.V., *Laser Age in Optics*, Mir Publishers (1981).
372. Tarasov, L.V. *Laser Physics*, Mir Publishers (1983).
373. Tarasov, L., *Laser Physics and Applications*, Mir Publishers (1986).
374. Terhune, R.W., Maker, P.D. and Savage, C.M. Phys. Rev. Lett. **8**, 404 (1962).
375. Terhune, R.W., Maker, P.D. and Savage, C.M. App. Phys. Lett. **2**, 54 (1963).
376. Terhune, R.W. Bull. Am. Phys. Soc. **8**, 359 (1963).
377. Terhune, R.W., Maker, P.D. and Savage, C.M. Phys. Rev. Lett. **14**, 681 (1965).
378. Thompson, G.H.B. *Physics of Semiconductor Laser Devices*, John Wiley & Sons (1980).
379. Thorne, A.P., *Spectrophysics*, Chapman and Hall, London (1974).
380. Thorp, J.S., *Masers and Lasers*, MacMillan (1967).
- 380A. Thyagarajan K., and Ghalak, A.K. *Lasers*, MacMillan India (1984).
381. Tobin, M.C. *Laser Roman Spectroscopy*, Wiley Interscience (1971).
382. Tsang W.T., Olsson. N.A. and Logan, R.A. App. Phys. Lett. **42**, 650 (1983).
383. Tuccio, S.A., Dubrin, J.E., Peterson, D.G. and Snavely, B.B., IEEE J, Quantum Electronics, **QE-10**, 790 (1974).
384. Varsanyi, F., Wood, D.L. and Schawlow, A.L. Phys. Rev. Lett. **3**, 544 (1959).
385. Vaughan, J.M. and Randall, J.T. in *Laser Advances and Applications* (Proc. Fifth National Quantum Electronic Conference) Ed. Wherrett, B.S. (1980).
386. Verdiech, J.F., Peterson, S.H., Savage, C.M. and Maker, P.D. Chem. Phys. Lett. **7**, 219 (1970).
387. Walther, H. (Ed). *Laser Spectroscopy of Atoms and Molecules*, Springer-Verlag Berlin (1976).
388. Wang, Chen-show in *Quantum Electronics Vol. I (Nonlinear optics)* Ed. Rabin, H. and Tang, C., Academic Press (1975).

389. Ward, J.F. and Franken, P.D., Phys. Rev. **A 133**, 183 (1964).
390. Webb, J.H., Am. J. Phys. **40**, 850 (1972).
391. Weber, J., IRE Trans. **3**, 10 (1953).
392. Weinberg, D.L. Laser Focus, **5** (4), 34 (1969).
393. Weisskopf, V. and Wigner, E., Z. Phys. **63**, 54 (1930).
394. Welsh, H.L., Crawford, H.F., MacDonald, J.C.F. and Chisholm, O.A., Phys. Rev. **83**, 1264 (1951).
395. West, G.A. and Barrett, J. J., Opt. Lett. **4**, 395 (1979).
396. Wever, H., Nature, **208**, 29 (1965).
397. Wever, H., Astro Phys. J. Supplement, **16**, 10, 146, 214 (1968).
398. White, A.D. and Rigden, J.D. Proc. IRE **50**, 169 (1962).
399. White, J.C., Zdasiuk, G.A., Young, J.F. and Harris, S.E. Phys. Rev. Lett. **41**, 1709 (1978).
400. White, J.C., Zdasiuk, G.A., Young, J.F. and Harris, S.E. Opt. Lett. **4**, 137 (1979).
401. White, J.C. Opt. Lett. **5**, 239 (1980).
402. White, J.C. Opt. Lett. **6**, 242 (1981).
403. Wieman, C. and Hänsch, T.W. Phys. Rev. Lett, **36**, 1170 (1976).
404. Wineland, D.J. and Dehmelt, H., Bull. Am. Phys. Soc. **20**, 637 (1975).
405. Wineland, D.J. and Itano, W.M., Phys. Today **40**, 34 (1987).
406. Woodbury, E.J. and Ng, W.K. Proc. IRE **50**, 2367 (1962).
407. Yap, F.Y. Am. J. Phys. **37**, 1204 (1969).
408. Yariv, A. *Quantum Electronics* 2nd Ed. John Wiley & Sons (1975).
409. Yariv, A. App. Phys. Lett. **28**, 88 (1976).
410. Yariv, A. J.O.S.A. **66**, 301 (1976).
411. Yariv, A. IEEE J. Quantum Electronics, **QE-14**, 650 (1978).
412. Yariv, A. IEEE J. Quantum Electronics, **QE-15**, 524 (1979).
413. Young, E.S. and Moore, C.B. J. Chem. Phys. **59**, 9 (1973).
414. Young, M., *Optics and Lasers*, Springer-Verlag (1977).
415. Zwernemann, S.M. and Becker, M.E., App. Opt. **18**, 728 (1979).

**This page
intentionally left
blank**